



A Computational Approach to the Sizing of Heat Pump Integrated Thermal Energy Storage Systems for Wet Central Heating

Umar Alhaji Mukhtar, B.Eng. M.Sc.

A thesis submitted in fulfilment of the requirements for the degree of
Doctor of Philosophy

Energy System Research Unit
Department of Mechanical and Aerospace Engineering
University of Strathclyde

March 2024

Declaration

This thesis is the result of the author's original research. It has been composed by the author and has not been previously submitted for examination which has led to the award of degree.

The copyright of this thesis belongs to the author under the terms of the United Kingdom copyright Acts as qualified by the University of Strathclyde Regulations 3.50. Due acknowledgment must always be made of the use of any material contained in or derived from this thesis.

Signed:

Date:

Abstract

Integrating heat pumps with a TES system provides a suitable and efficient solution for replacing a gas-fired boiler within a wet central heating system for residential buildings. This approach addresses the growing demand for energy-efficient and low-carbon technologies. The system enhances the efficacy of residential heating by shifting energy consumption to off-peak periods and improving heat distribution during peak demand. This study assesses the feasibility of a phase change-based TES system for load-shifting capabilities in residential heating. The study explores the application of CFD and building simulation models to evaluate the performance of a heat pump-integrated TES system in meeting the full space heating needs of a detached dwelling. The engineering modelling method was employed to estimate the next-day heat demand for a dwelling using the ESP-r tool. This approach facilitates comprehensive simulations that considers the building's physical and thermal characteristics, construction materials, occupancy patterns and weather data to predict the next-day space heat demand of the dwelling. This predictive capability provides a robust foundation for sizing a TES system.

A phase change TES model was developed using the enthalpy formulation method, with the thermal store modelled in the Fluent CFD tool. This involved a single shell-and-tube heat exchanger, comprising PCM in the annular-gap and HTF flowing through the tube. The TES model was validated by comparing its simulated fluid outlet temperature and temperature profiles at different positions with the results reported by Longeon et al. [186]. The results showed that the simulated data closely agreed with the experimental and numerical findings. This demonstrated that the CFD model can reliably predict the heat transfer characteristics and thermal behaviour of the TES system during the charging and discharging phases.

The TES system sizing was demonstrated by utilising the dwelling's peak day heat demand profile to determine the maximum storage capacity, which is then sufficient to meet any daily heat demand throughout the heating season. The thermal behaviour and characteristics of the TES system were evaluated by simulating the charging process of the thermal store using mass flow rates and temperature conditions repre-

sentative of a typical ASHP. The results indicate that system efficiency depends on the type of PCM used, the heat pump's mass flow rate, and the charging strategies employed. A linkage between the dwelling and TES system model was established using a rudimentary model to determine radiator return temperatures during TES utilisation (discharge). Simulating the discharge of the TES system using the radiator fluid outlet temperature at variable inlet mass flow rates provides the heat output, necessary to fulfil the space heating needs of the dwelling.

The results obtained from discharging the TES system indicate a total heat output of 37.44 kWh, with peak and average discharge rates of 1.73 kW and 1.56 kW respectively used to match the detached dwelling's peak day heat demand profile. A statistical analysis using the Pearson correlation coefficient shows a 94% match rate between the TES discharge rate and the dwelling heat demand profiles, indicating that they are in close agreement. The TES system discharge achieved a fluid output temperature of 60–40°C. The fluid output temperature obtained, can effectively meets the space heating needs of the dwelling when larger radiators are used. However, the result of the analysis further indicates that this fluid output temperature is well-suited for underfloor heating systems or radiators designed for low-output temperature applications, particularly when advanced control systems are employed to ensure thermal comfort in buildings.

The study contributes to knowledge by developing a detailed procedure for sizing a heat pump-integrated TES system for wet central heating. The developed methodology was proved by assessing the load-shifting capability of the TES system in meeting the continuous full day space heating needs of the detached dwelling. The study further contributes to knowledge by developing the control procedure for charging and discharging the TES system.

Acknowledgements

Glory be to the Almighty the most exalted for the gift of life, privilege, and strength to conduct this work assiduously. I thank Him for his infinite blessings and guidance that enabled me to complete this project successfully.

I would like to extend special gratitude to my supervisor Emeritus Professor Joe Clarke for his continuous support and guidance throughout this study. His positive attitude and mentorship style have encouraged and challenged me to learn and carry out my PhD research diligently. Special thanks for the mentoring and thorough editing of manuscripts and my PhD thesis. Special appreciation also goes to my second supervisor, Dr Daniel Costola for his valuable thoughts, support, and guidance.

I would like to thank Dr William Dempster, Dr Nick Kelly, Dr Nabila Mohammed, and Hassan Mohammed Sheik for their immense support and assistance rendered during this study. I would also like to thank my colleagues for their prayers and support, and all the ESRU staff for providing the enabling environment to carry out this work.

Special appreciation goes to my parents, brothers, sisters, wife, and children for their unconditional support, patience, encouragement, and prayers during this study. I want to thank all my friends for their support and encouragement.

I am indeed grateful to the Federal Government of Nigeria for the scholarship offered to me through the Tertiary Education Trust Fund (TET-Fund) and the University of Strathclyde for the FEES-only studentship provided, which enabled me to study a PhD.

Finally, this thesis is dedicated to my beloved parents, wife Adama, and children Hauwa and Mukhtar.

Nomenclature

Abbreviations

ASHP	Air Source Heat Pump
ASHPWH	Air Source Heat Pump Water Heater
BEIS	Department for Business, Energy, and Industrial Strategy
BER	Building Energy Rating
CCC	Committee on Climate Change
CFD	Computational Fluid Dynamics
COP	Coefficient of Performance
DHW	Domestic Hot water
ESP-r	Environmental System Performance Research
EU	European Union
HVAC	Heating Ventilation and Air Conditioning
IDEAS	Integrated District Energy Assessment Simulation
IEA	International Energy Agency
HTF	Heat Transfer Fluid
LHS	Latent Heat Storage
NEPCM	Nano-Enhanced Phase Change Material
PCM	Phase Change Material
PRESTO	Pressure Staggering Option
PV	Photovoltaic
RT	Rubitherm Technologies
SHCS	Scottish House Condition Survey
SHS	Sensible Heat Storage
SIMPLE	Semi-Implicit Pressure Linked Equation
TES	Thermal Energy Storage
THS	Thermochemical Heat Storage
TRNSYS	Transient System Simulation
UDF	User-Defined Function

Symbols

C_{eff}	Effective heat capacity	J/kg K
C_p	Specific heat capacity	J/kg K
d_i	Storage element tube diameter	m
d_o	Storage element shell diameter	m
$E_{Dem}[i]$	Dwelling heat demand	kWh
$E_{Loss}[i]$	Thermal storage energy loss	kWh
H	PCM-specific enthalpy	J/kg
h	PCM sensible enthalpy	J/kg
h_m	Heat of melting	J/kg
i	Time step	s
k	Thermal conductivity	W/mK
L	Length of PCM element	m
m	Mass	kg
\dot{m}	Mass flow rate	kg/s
n	Number of PCM elements	-
P	Power output	W
\dot{Q}	Heat transfer rate	W
Q_{HP}	Heat pump power rating	W
Q_{liquid}	Total heat in liquid PCM	J
Q_{PCM}	Total heat in PCM element	J
$Q_{tes,q}$	TES capacity	kWh
Q_{Total}	Total heat stored in PCM	J
q_{total}	Total heat stored per unit mass	J/kg
$Q_{sensible}$	Sensible heat	J
Q_{solid}	Total heat in solid PCM	J
q	Time segment	s
r_i	Storage element tube radius	m
r_o	Storage element shell radius	m
S	Source term	-
t	Time	s

T	Average temperature	K
T_1	PCM temperature after melting	K
T_m	Phase change temperature	K
T_s	PCM temperature before melting	K
T_f	Radiator flow temperature	K
T_r	Radiator fluid outlet temperature	K
x_{seg}	Number of segments	-
β	Volumetric thermal expansion coefficient	K^{-1}
ρ	Density	kg/m^3
λ	Latent heat of fusion	J/kg
f	Liquid fraction	-

Table of Contents

Abstract	ii
Acknowledgements	iv
Nomenclature	v
Table of Contents	viii
List of Figures	xiii
List of Tables	xvii
1 Introduction	1
1.1 General Context	1
1.2 Aims and Objectives	4
1.3 Methodology and Research Tool	5
1.4 Scope of the Study	8
1.5 Research Contributions	8
1.6 Thesis Structure.....	9
2 Literature Review	11
2.1 Introduction	11
2.2 Wet Central Heating.....	11
2.2.1 Background	11
2.2.1.1 Government Policy on Replacing Gas Boilers with Heat Pumps	14
2.2.1.2 Problems of Boiler Replacement with Heat Pump	16
2.2.2 Heat Pumps Wet Central Heating	18
2.2.3 Reviews in Applications of Heat Pump Wet Central Heating	20
2.3 Thermal Energy Storage	25
2.3.1 Introduction	25
2.3.2 Thermal Storage Material Types.....	26
2.3.2.1 Sensible Heat Storage	27

2.3.2.2 Latent Heat Storage.....	31
2.3.3 TES Material Selection Criteria.....	41
2.3.3.1 Operating Temperature and Enthalpy	42
2.3.3.2 Commercial Availability.....	42
2.3.3.3 Heat Exchanger Design Requirements.....	43
2.4 Heat pump Integrated TES Wet Central Heating.....	45
2.4.1 Potentials in Application of TES System.....	46
2.4.2 Challenges in Application of TES System.....	47
2.4.3 Reviews in Applications of Heat Pump TES Wet Central Heating	47
2.5 Next-day Heat Demand Profile Estimation	55
2.5.1 Introduction.....	55
2.5.2 Estimation Approaches	55
2.5.3 The Engineering Modelling Methods	58
2.5.3.1 Development of a Dwelling Model.....	59
2.6 Chapter Summary.....	63
3 Research Procedure	66
3.1 Introduction.....	66
3.2 Determine the TES System Requirement Specification	69
3.3 Determine the TES System Size and Capacity	70
3.4 Develop the TES Model and Computational Procedure	70
3.4.1 Analyse TES Components	70
3.4.2 Set out the HTF and TES Material Section.....	71
3.4.3 Validate the TES System Model	71
3.4.4 Discretise the TES System CFD Domain	72
3.5 Assess the Heat pump-integrated TES System’s Performance.....	72
3.5.1 Set-up Simulation.....	72

3.5.1.1 Boundary and Initial Conditions	73
3.5.2 Charge TES System	73
3.5.3 Discharge TES System.....	74
3.5.4 Match Heat Demand and Power Output Profiles	74
3.6 Chapter Summary.....	75
4 Generation of a Test Heat Demand Profile.....	77
4.1 Introduction	77
4.2 Determination of Dwelling Heat Demand Profile	79
4.2.1 ESP-r Building Energy Simulation	80
4.2.1.1 Weather data.....	80
4.2.1.2 Occupancy Characteristics	81
4.2.1.3 Control and Operational Schedules.....	81
4.3 Chapter Summary.....	85
5 Numerical Modelling and Simulation of LHS System.....	86
5.1 Introduction	86
5.2 Phase Change Heat Transfer Modelling	88
5.2.1 Numerical Modelling	88
5.2.1.1 Variable Grid Method	89
5.2.1.2 Fixed Grid Method.....	89
5.3 CFD Modelling, Verification and Validation	92
5.3.1 The CFD Model	92
5.3.1.1 Boussinesq Approximation	93
5.3.2 Experimental Set-up.....	94
5.3.3 Numerical Procedure and Verification.....	95
5.3.3.1 Grid and Time Step Dependency Study.....	97
5.3.4 Validation of the Numerical Methodology	99

5.3.4.1 Validation with Experimental Results	99
5.3.4.2 Comparison of the CFD Solution with Numerical Results	105
5.4 Chapter Summary	109
6 Thermal Energy Storage System	111
6.1 Introduction	111
6.2 Determination of the TES System Capacity	111
6.3 The TES System Size and Configuration	113
6.4 TES System Sizing	117
6.5 CFD Modelling of the TES System	119
6.6 Chapter Summary	120
7 Thermal Energy Storage System Performance Evaluation	121
7.1 Introduction	121
7.2 TES System Charging	122
7.2.1 TES System Charging Control Procedure	126
7.3 TES system Discharging	133
7.3.1 Determination of Radiator Fluid Outlet Temperature	134
7.3.2 TES System Discharging Control Procedure	138
7.4 Analysis of TES System Output	143
7.4.1 TES Power Output	143
7.4.2 TES System Output Temperature	144
7.5 Chapter Summary	146
8 Conclusions, Limitations of the Study and Future Work	148
8.1 Introduction	148
8.2 Conclusions	148
8.3 Contributions to Knowledge	152
8.4 Limitations of the Study	153

8.5 Recommendations for Future Work.....	154
References	156
Appendices	181
Appendix I: Analysis of the Building Simulation Model Results.	181
Appendix II: Input Data for CFD Simulation	183
Appendix IIA Input Data for CFD Model Validation.....	183
Appendix IIB: Input Data for CFD Simulation of the TES System	184
Appendix III: CFD Code for Variant Inlet HTF Mass Flow Rate	185

List of Figures

Figure 1.1: Building-related energy demand for heating and share by fuel in a net zero scenario 2021-2030 IEA [2].	1
Figure 1.2: Percentage distribution of various heat sources in a surveyed sample of dwellings with wet central heating in the UK housing stock [9].	3
Figure 1.3: Flow chart summary of the project methodology.	7
Figure 2.1: Schematic of the working principle and operation of (a) a gas-fired boiler [31] and (b) a heat pump system within a wet central heating system [32].	12
Figure 2.2: Global heat pump sales within the IEA's net zero emission scenario [40].	15
Figure 2.3: Share of heat pump penetration in some countries in 2021 [40].	16
Figure 2.4: A heat pump directly supplying a wet central heating system.	19
Figure 2.5: Schematic of heat pump integrated TES system.	19
Figure 2.6: Schematic diagram of the solar-assisted ASHP heating system proposed by Liang. [58].	22
Figure 2.7: Schematic of the operation of the ASHP used by Zhang et al. [54].	24
Figure 2.8: Categories of thermal energy storage materials [67].	27
Figure 2.9: Schematic of wet central heating with SHS utilising (a) single tank [74] and (b) two-tank system [45].	30
Figure 2.10: Phase transition as a function of heat addition [79].	33
Figure 2.11: Classification of PCM (a) material type [82] and (b) melting enthalpy and temperature [83].	34
Figure 2.12: PCM-Based hot water storage system [106].	40
Figure 2.13: Schematic of PCM-based solar heating system [107].	41
Figure 2.14: Schematic of PCM-based heat exchanger designs [134,138,139].	44
Figure 2.15: Schematic of a heat pump-integrated TES wet central heating system.	46
Figure 2.16: Schematic of heat pump-integrated TES wet central heating operating in different heating modes [155].	51
Figure 2.17: Model diagram of ASHP and TES tank with resistive backup heater for domestic wet central heating presented by Renaldi et al. [15].	53

Figure 2.18: Schematic diagram of a high-temperature heat pump-integrated TES in various operating modes during the field trial test presented by Shah et al. [16].	54
Figure 2.19: Typical detached dwellings [176].	61
Figure 2.20: The thermal zone geometry of the detached dwelling model.	61
Figure 3.1: Procedure flow chart.	67
Figure 4.1: Determination of heat demand profile using ESP-r.	78
Figure 4.2: Variation of dry-bulb temperature during a typical winter scenario (November to March).	82
Figure 4.3: Seasonal heat demand profile of the detached dwelling for the typical winter scenario (November to March).	83
Figure 4.4: Peak day heat demand profile of the detached dwelling.	84
Figure 5.1: Schematic diagram of a vertical shell-and-tube heat exchanger	86
Figure 5.2: Heat transfer characteristics in the vertical and horizontal heat exchangers during charging and discharging of LHS materials [121].	87
Figure 5.3: The experimental set-up for melting and solidification of the annular PCM conducted by Longeon et al. [186].	94
Figure 5.4: Geometry and boundary condition of the test section.	95
Figure 5.5: Schematic diagram of the axisymmetric geometry and computational domain applied in the Fluent model for validation.	96
Figure 5.6: Average PCM temperature against time for (a) different meshes and (b) convergence time steps.	98
Figure 5.7: Contour of PCM liquid fraction for the CFD solution (left) and the experimental results of Longeon et al. [186] (right) during charging with top HTF injection.	100
Figure 5.8: Temperature variations of the radial points a, b, and c, at axial position D of the CFD solution and the experimental results of Longeon et al. [186] during charging with top HTF injection.	101
Figure 5.9: Variation of the HTF outlet temperature of the CFD solution and the experimental results of Longeon et al. [186] during charging process.	101
Figure 5.10: Temperature variations of the radial points a, b, and c, at axial position D of the CFD solution and the experimental results of Longeon et al. [186] during discharging with bottom HTF injection.	102

Figure 5.11: Variation of the HTF outlet temperature of the CFD solution and the experimental results of Longeon et al. [186] during the discharging process.	103
Figure 5.12: Variation of heat transfer rates at the tube and shell wall during charging process.....	104
Figure 5.13: Temperature contours of the CFD solution (left) and the numerical results of Longeon et al. [186] (right) during charging with top HTF injection.....	106
Figure 5.14: Temperature variations of the radial points a, b, and c, at axial position D for the CFD solution and the numerical results of Longeon et al. [186] during (a) charging and (b) discharging process.....	107
Figure 6.1: Discretised segmented diagram of a dwelling peak day heat demand profile.	112
Figure 6.2: Schematic diagram of the TES system with symmetric PCM element domain.....	114
Figure 6.3: Characteristics of the TES system sizing.	118
Figure 6.4: The axisymmetric geometry and part of the discretised mesh domain of the storage element.....	119
Figure 7.1: Schematic diagram of heat pump charging a TES system.	122
Figure 7.2: Schematic diagram of the single storage element.	123
Figure 7.3: Variation of temperature contour of the storage element during charging with top (left) and bottom (right) HTF flow of 0.33 kg/s at 60°C.	124
Figure 7.4: Variation of average PCM temperature during charging with top and bottom HTF flow of 0.33 kg/s at 60°C.....	125
Figure 7.5: Schematic of a day-to-day TES system charging control.....	126
Figure 7.6: State of charge of the TES system at different mass flow rates for the charging process.....	128
Figure 7.7: Variation of TES system: (a) temperature at points A, B, C and outlet and (b) temperature contour of the storage element over time during the charging process for an HTF flow of 0.25 kg/s at 60°C.	130
Figure 7.8: Variation of TES system: (a) temperature at points A, B, C and outlet and (b) temperature contour of the storage element over time during the charging process for an HTF flow of 0.29 kg/s at 60°C.	131

Figure 7.9: Variation of TES system: (a) temperature at points A, B, C and outlet and (b) temperature contour of the storage element over time during the charging process for an HTF flow of 0.33 kg/s at 60°C.	132
Figure 7.10: Schematic of TES system discharging heat to a dwelling.....	133
Figure 7.11: Variation in the detached dwelling’s heating load over time.....	135
Figure 7.12: Variation of (a) radiator fluid return temperature and (b) mass flow rate during discharging of the TES system.	137
Figure 7.13: Schematic of a day-to-day TES system discharging control.....	139
Figure 7.14: Variation of TES: (a) power output and (b) state of discharge over time during discharging with water flow of 0.02–0.12 kg/s at 36–40°C.	140
Figure 7.15: Variation of TES (a) temperature at points A, B, C and (b) temperature contour of the storage element over time during discharging with water flow of 0.02–0.12 kg/s at 36–40°C.	142
Figure 7.16: Comparison of the TES power output and the detached dwelling’s peak day heat demand profile.....	143
Figure 7.17: Variation of TES system fluid output temperature during discharging with water flow of 0.02–0.12 kg/s at 36–40°C.	145
Figure AI.1: Occupant casual gain profile of the detached dwelling estimated over a 24-hour period.....	182

List of Tables

Table 2.1: Problems associated with heat pumps in wet central heating.	17
Table 2.2: Summary of studies utilising heat pumps for dwelling wet central heating.	21
Table 2.3: Thermo-physical properties of potential SHS materials [70].	29
Table 2.4: Thermophysical properties of LHS materials against operating temperature for wet central heating applications.	39
Table 2.5: Advantages and disadvantages of SHS and LHS materials [20,95,122]. .	40
Table 2.6: Commercial manufacturers of PCM around the world.	43
Table 2.7: Summary of studies utilising the application of heat pump-integrated TES technology for residential wet central heating.	49
Table 2.8: Studies involving prediction of next-day heat demand profiles.	56
Table 2.9: Scottish housing types SHCS [175].	60
Table 2.10: Number of occupied dwellings (in thousands) and their percentage distribution by age band and type SHCS [174].	60
Table 2.11: Representative dwelling design parameter [177].	62
Table 2.12: Scottish construction categories [177,178].	63
Table 4.1: Characteristics of the building construction.	79
Table 5.1: Specification for the point D thermocouple positions a, b and c.	94
Table 5.2: Thermophysical properties of paraffin RT35 [186].	97
Table 5.3: Calculated statistical parameters at the selected points (validation).	103
Table 5.4: Calculated statistical parameters at the selected points.	108
Table 6.1: Geometric characteristics and configuration of the dwelling's TES system.	114
Table 6.2: Thermophysical properties of the PCMs.	115

1 Introduction

1.1 General Context

Energy use in buildings forms a greater part of energy demand globally. One-third of the global energy is consumed in buildings, and this equates to one-quarter of carbon dioxide emissions [1]. Most of the building energy consumption is related to heating and cooling [1]. It has been estimated that globally fossil fuel accounts for around 64% of energy use for building heating, with a decrease of only 3% from 2010 as illustrated in Figure 1.1 [2].

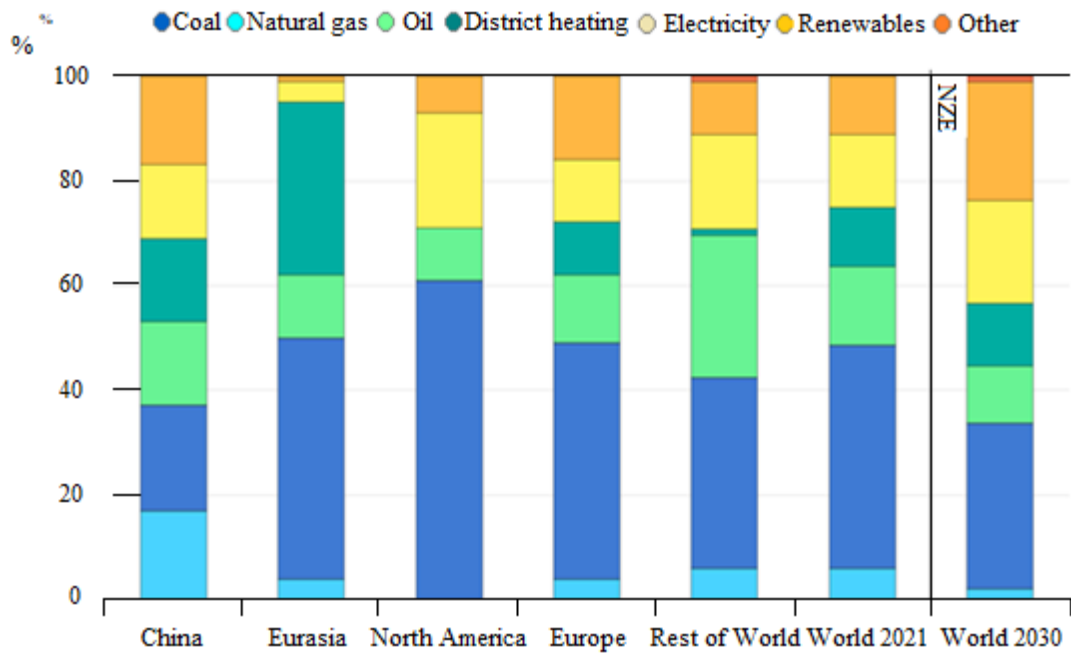


Figure 1.1: Building-related energy demand for heating and share by fuel in a net zero scenario 2021-2030 IEA [2].

In the UK and other countries at the present time, a strong policy push is driving industries towards the electrification of building heating. For example, the EU's energy directives require the energy consumption associated with heating and cooling to emanate from renewable energy sources and stimulate heat pump application for domestic heating [3]. This is in line with the policy of the UK government, targeting a reduction of greenhouse gas emissions by 80% [4]. This target is backed by a spe-

cific plan, which includes the widespread decarbonisation of heating systems through the deployment of heat pumps [5,6].

Focusing on the UK, the larger part of the domestic building stock (~25 million dwellings) uses natural gas for heating [7]. Because of the current energy crisis, policies that favour clean heating solutions are being boosted. To reduce the emissions from domestic heating systems, improvements have been made through more stringent building codes and the use of heat pumps and renewable energy technology. The intention is to replace relatively polluting fossil fuel boilers [2]. However, the decarbonisation of domestic heating faces many challenges, not least the ability of the consumers to switch to a low-carbon heat source and improve their building's energy efficiency [7].

BEIS [7] has identified domestic heating as the most challenging energy-consuming sector to decarbonise. This is due to the cost, complexity, and scale of transitioning to low-carbon residential heating. Among the challenges, is the phasing out of the fossil-fuel based heating systems. It is also important to stress that net zero targets affect some sectors of the economy; this indicates that sectors such as manufacturing or oil and gas are vulnerable to such targets [7].

The adequate implementation of incentives and workforce training is needed to speed up the rate of penetration for decarbonising building heating. As an example, in 2017 there were 29 million dwellings in the UK [7,8], with most residential buildings (~85% in 2019) reliant on gas central heating systems [6,7]

Figure 1.2 depicts the various heat sources used within the UK housing stock. It is evident that the majority (89%) of UK dwellings use a wet central heating system (boiler and radiators). However, an increasing number of UK dwellings are adopting for underfloor heating systems [9].

An analysis by the CCC on the policy to achieve the 2050 net-zero carbon emission target suggests decarbonising all building heating systems [10,11]. This could support the adoption of renewable heating systems such as heat pumps, biomass, and district heating networks.

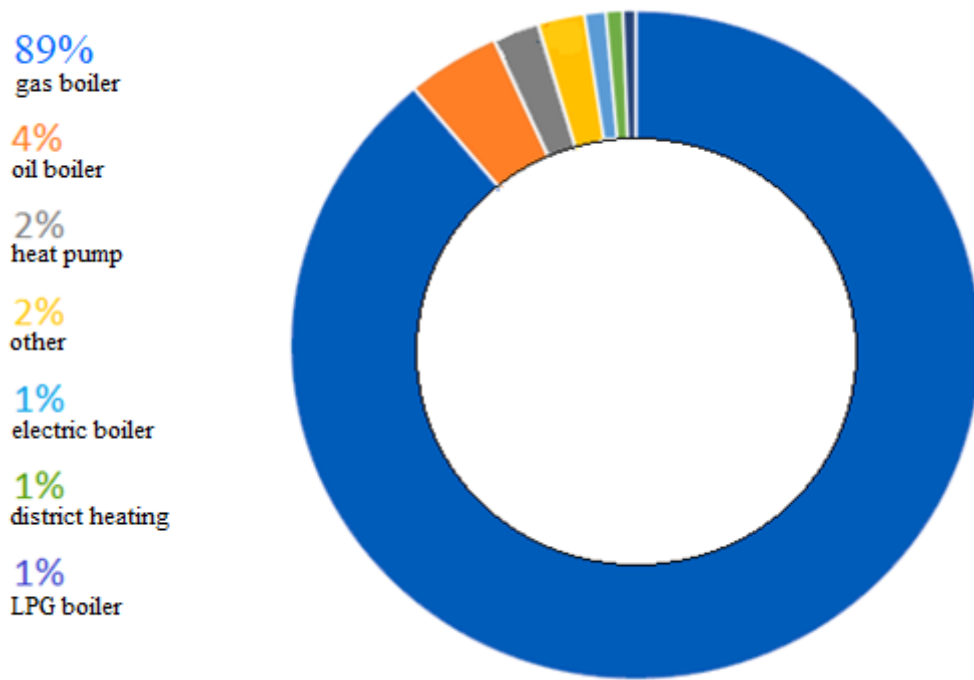


Figure 1.2: Percentage distribution of various heat sources in a surveyed sample of dwellings with wet central heating in the UK housing stock [9].

The present work focuses on the heat pump adaptation of gas-fired, wet central heating systems within existing dwellings. In this work, a TES system pre-charged by a heat pump is virtually applied to provide a dwelling's heating requirement without replacement of the existing pipe network and radiators to save cost. However, heat pumps are associated with operational control challenges in specific cases, such as requiring frequently on-off cycling and modulating the heat pump capacity by varying the compressor speed to match dwelling's heat demand over time [12]. This can lead to system performance degradation and variation in the COP to match varying thermal loads [12]. To mitigate the heat pump operational condition that is associated with such control and avoid the operation of heat pump during times of high electricity tariff, a TES system is introduced in the heating network. The heat pump is applied independent of a dwelling to charge the TES system to meet the heating requirements of dwellings.

1.2 Aims and Objectives

In this work, a study has been undertaken to research the feasibility of adding a phase change TES device to a dwelling's wet central heating system to facilitate day-ahead load shifting. In this mode of operation, the heat pump is activated especially at times of low electricity tariff to charge the thermal store. The stored heat is then accessed as required to meet the dwelling's load profile. An analysis of a likely TES system configuration was undertaken through the modelling and simulation of the combined heat pump and TES under various charge/discharge operating regimes.

The project has the following objectives:

- i. Determination of the requirement specification for the TES system based on specific dwelling characteristic.
- ii. Design of the TES system and consideration of how it can be effectively integrated within an existing wet central heating system.
- iii. Determination of the TES system's size and control to meet a specific dwelling's heat demand and development of the TES model.
- iv. Development of a computational procedure for the TES system model validation to ascertain its performance accuracy for the needs of any dwelling.
- v. Demonstration of using this procedure for performance evaluation.

Numerical modelling of the TES system is carried out using the CFD Fluent phase change model, as described in [13]. This approach simulates the melting and solidification of the storage medium: PCM in a vertical cylindrical enclosure accounting for heat transfer dynamics in the system. The dynamic performance of the TES system is analysed through charging and discharging of the PCM to determine the thermal behaviour and characteristics of the storage system in a realistic manner.

Research Questions

In relation to heat pump/TES system design, the principal issues addressed include the selection of a storage medium and heat exchanger design configuration to enable TES system charging within the shortest possible time. Further, determining the TES

system's capacity needed to meet the next-day dwelling heating requirements. The following specific research questions are considered.

- i. Can a domestic heat pump charge a TES system in day-ahead mode to meet a dwelling's next-day heat demand?
- ii. How can a TES system be sized for a particular dwelling to meet its unique and variable heating energy demand?
- iii. Can a domestic heat pump fully charge a TES system in a reasonable time to meet a dwelling's heat demand throughout the year?
- iv. Can a pre-charged TES system be discharged in a manner that matches a dwelling's heat demand profile over 24 hours?

Numerous studies [14–17] have explored the potential of heat pumps and TES systems for load-shifting applications, with many utilizing the TES over a period within the day or as buffers to assist heat pumps in managing building thermal loads. This study differs in its approach because the TES system is pre-charged by a heat pump for use next-day as the primary heat source, thus achieving day-ahead load-shifting in existing or new dwellings. Using building energy simulation and CFD techniques, this study investigates the dynamic performance of the TES system, with the intended goal of determining its potential to fulfil the next-day's space heating needs of dwellings (but not hot water needs in the present context).

1.3 Methodology and Research Tool

Most dwellings use gas-fired boilers or heat pump systems for wet central heating. A study on the operational principle of a gas fired boiler and heat pump was carried out to investigate their performance within a wet central heating system. The performance of heat pump/TES systems was analysed to determine how best to implement such a system to match a dwelling's heating requirement.

A literature review was conducted to determine the possible forms of thermal storage materials for applications in wet central heating systems. Thermochemical heat storage systems that involve reactors are not commonly used because they are still in the

research and development stage [18,19]. Most thermochemical heat storage materials face technical challenges and barriers, and their complexity limits their application in wet central heating systems [19]. Sensible storage materials especially solid require a large storage volume and the energy stored and released by the storage materials occurs at a temperature change [20]. The low enthalpy and low energy density characteristics of sensible storage materials restrict their ability for numerous applications [20,21]. The latent storage material: PCM, has the best potential to overcome the problems associated with sensible and thermochemical storage. PCM is the most promising thermal storage material for wet central heating applications [22,23].

Candidate PCMs were screened and obtained for use within the operating temperature range applicable for domestic wet central heating. The PCMs considered are commercially available and obtainable in different forms. Two PCMs, paraffin and inorganic salt were eventually selected for use in a vertical shell-and-tube heat exchanger to assess the thermal performance of a single storage element under charging and discharging regimes to evaluate the overall performance of the storage system. It is envisaged that this store can be discretised to accommodate variable requirements throughout the year. That said the present work considers the store capacity to satisfy the peak demand.

Each country has its dwelling characteristics while each dwelling is unique, certain characteristics are specific to each dwelling type. The important requirement in this work is to obtain a day-ahead heat demand profile of a given dwelling to direct TES sizing and charging/discharging. There are various existing approaches [24–27] for the estimation of day-ahead heat demand profiles of dwellings. In this work, an engineering modelling method was used through the application of the ESP-r building performance simulation program. ESP-r can be used to obtain a day-ahead heat demand profile for any target dwelling under typical and extreme weather conditions for use in a TES system design context. The simplified method could then be used to estimate the next-day heat demand of any given dwelling throughout the heating season to govern a day-ahead TES system charging. In addition, the Fluent CFD program was applied for the detailed analysis of a single storage element as a proxy for the thermal performance of the complete TES system. This required the discretisa-

tion of the storage element geometry for numerical simulation. Simulations were conducted for the charging and discharging of the storage system to determine its capability to provide dwelling heating requirements and the degree of match over time with a dwelling's heat demand profile. Fluent was used initially to develop and validate the storage model using the experimental and numerical results from other published work. Figure 1.3 presents a flow chart that summarises the methods applied to achieve the objectives of this work.

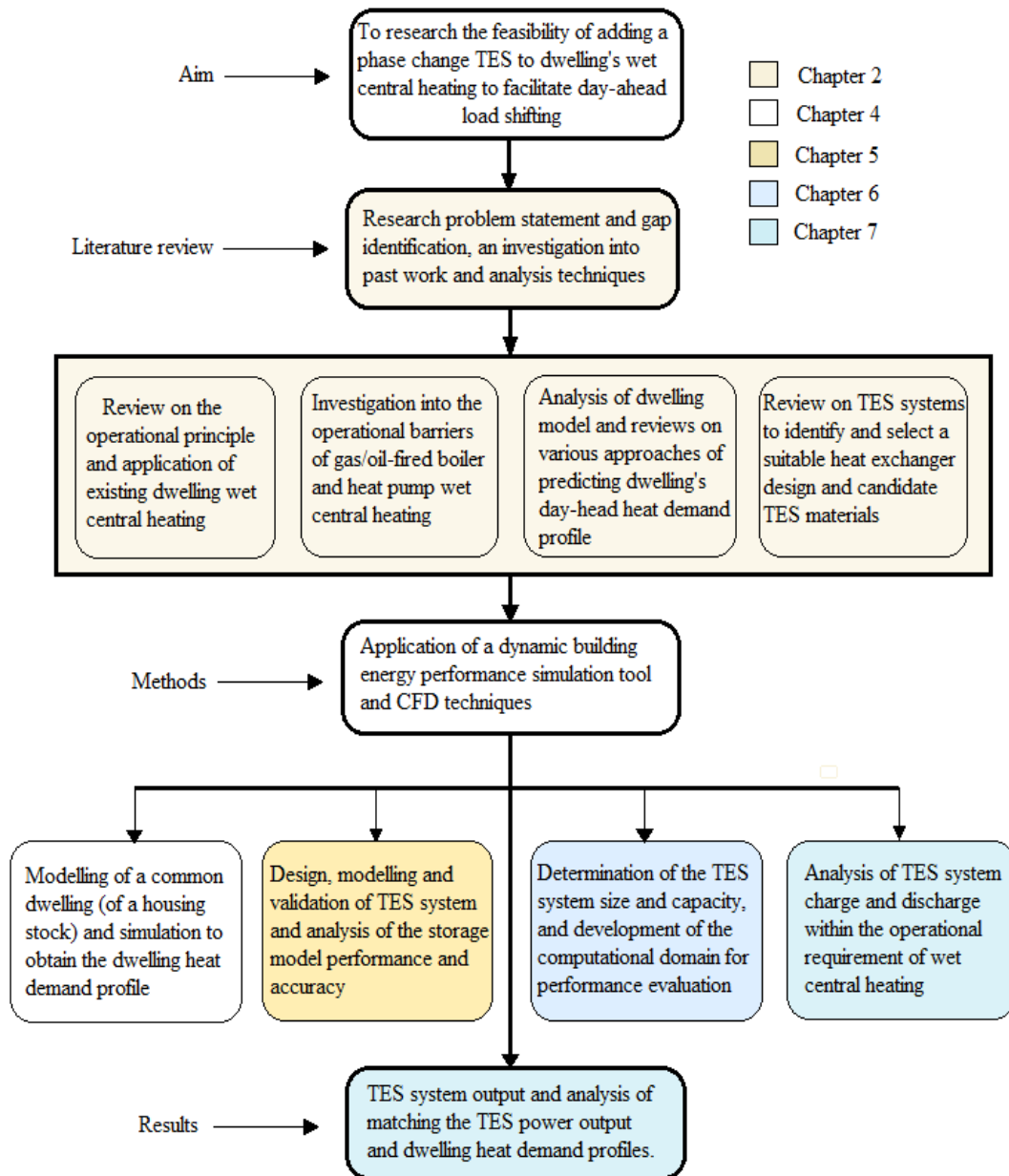


Figure 1.3: Flow chart summary of the project methodology.

1.4 Scope of the Study

The study assesses the feasibility of using a phase change thermal store for load-shifting capabilities in a detached dwelling. It focuses on the application of building simulation and CFD model of a shell-and-tube heat exchanger to evaluate the performance of the TES system, using inorganic hydrated salt as the storage medium and water as the HTF to meet the space heating requirements of the dwelling.

1.5 Research Contributions

This study involves developing a procedure to size heat pump integrated TES systems for wet central heating. The methodology is applied to virtually assess the capability of a domestic heat pump to pre-charge a TES to satisfy next-day dwelling heating demand. The approach improves the efficacy of wet central heating systems by using energy resources during off-peak periods to charge the TES system for next-day discharge. The procedure serves as guidance for sizing heat pumps and TES systems, and the methodology adopted can be used to assess the load-shifting capability of TES systems to meet the space heating needs of a dwelling where its heat demand profile can be estimated in advance.

The contributions of the present research are as follows:

- Design and development of a TES system model for wet central heating in dwellings.
- Analysis and application of the storage system model enabling dwelling wet central heating operations.
- Validation of the TES system model against experimental and numerical results from the literature.
- Development of control procedure for day-to-day charging and discharging of the TES system for wet central heating.
- Application of CFD techniques to charge and discharge the TES system for performance evaluation.
- Analysis of TES system performance using the fluid output temperature and comparison of the storage power output and dwelling heat demand profiles.

1.6 Thesis Structure

The thesis is divided into eight chapters as follows.

- **Chapter 1** presents the general research context and outlines the aims of the study, research questions, methodology used in the research, and the research contributions.
- **Chapter 2** presents the literature review outcome that describes the operational principle of domestic wet central heating, involving the use of a gas-fired boiler or heat pump. A study is undertaken to analyse related past work on the applications of heat pumps and heat pump-integrated TES systems for residential wet central heating. The potential and challenges of using a TES system with a heat pump are identified. The chapter further reviews the literature of related work involving various types of thermal storage materials and their advantages and disadvantages. State-of-the-art thermal storage materials are screened based on their commercial availability and operating characteristics as required for domestic wet central heating. A study is conducted to select an appropriate heat exchanger configuration.
- **Chapter 3** outlines the analysis procedure applied to carry out the research work, indicating the steps undertaken to achieve the objectives of the project.
- **Chapter 4** describes the processes and approaches for the estimation of a day-ahead heat demand profiles for dwellings.
- **Chapter 5** presents a study on a phase change model numerical formulation and the validation of the Fluent model for the melting and solidification of the storage material against experimental results and numerical solutions from the literature.
- **Chapter 6** investigates the TES system sizing and the configuration of the PCM storage to produce the best performance during the charging and discharging processes. The chapter also includes an analysis of the use of the storage model to conduct simulations for the charging and discharging processes.
- **Chapter 7** reports an investigation to analyse the capacity and operation of a domestic heat pump as required to provide the heat transfer fluid (HTF) mass flow rate and temperature suitable for charging the storage system. The chap-

ter also presents the approach involved in discharging the storage system to extract the next-day heating power profile and output temperature to fulfil the space heating needs of a dwelling.

- **Chapter 8** concludes the main research outcomes and outlines the limitations of the study and recommendations for future work.

2 Literature Review

2.1 Introduction

A study is conducted to explore the use of a heat pump and TES system for a dwelling's wet central heating. In the UK and other temperate climate regions, dwelling wet central heating operates using an oil- or gas-fired boiler. This work supports the implementation of policies to electrify heating in buildings by replacing boilers with a heat pump/TES system. This chapter reports a study to investigate the feasibility of applying the TES system to facilitate the operation of dwelling heating by examining the operational characteristics of the boilers and heat pumps used in wet central heating systems. To conduct a study on the application of TES systems for wet central heating, it is necessary to review previous research. This review identifies the different categories of TES and selects the most suitable storage material and heat exchanger design for the present purpose. In addition, the study also requires an investigation into an approach for estimating the heat demand of dwellings. This involves developing a dwelling model to predict, by simulation, the next-day heat demand profile. The purpose of this investigation is to determine the requirement specification of the TES system. While most past work has used TES systems as buffers [14,16,28] supporting a heat pump operation and auxiliary systems in dwelling wet central heating, this study assesses the feasibility of using a TES system for load-shifting capability to provide sufficient heat output needed to meet a continuous full-day space heating requirement of a dwelling as opposed to the fraction of a day as demonstrated in most of the studies.

2.2 Wet Central Heating

2.2.1 Background

With wet central heating, a central heat source is applied to generate hot water that is distributed around a building and becomes available for use for heating and domestic hot water [29]. The main component of such a system is a boiler (or heat pump charged thermal store in the work reported here) and heat emitters that involve multiple radiators and/or underfloor heat exchangers. Other essential components include the pipe network, expansion vessel, relief valves, pump, and motorised valves to iso-

late circuits. The hot water from the boiler circulates through the pipe network that connects the heat emitters throughout the building [30]. The flow of hot water is controlled by a motorised valve, which is responsible for the flow to either the heat emitters for immediate use or the hot water storage tank for DHW. Figure 2.1 illustrates the working principle of a gas-fired boiler and heat pump system.

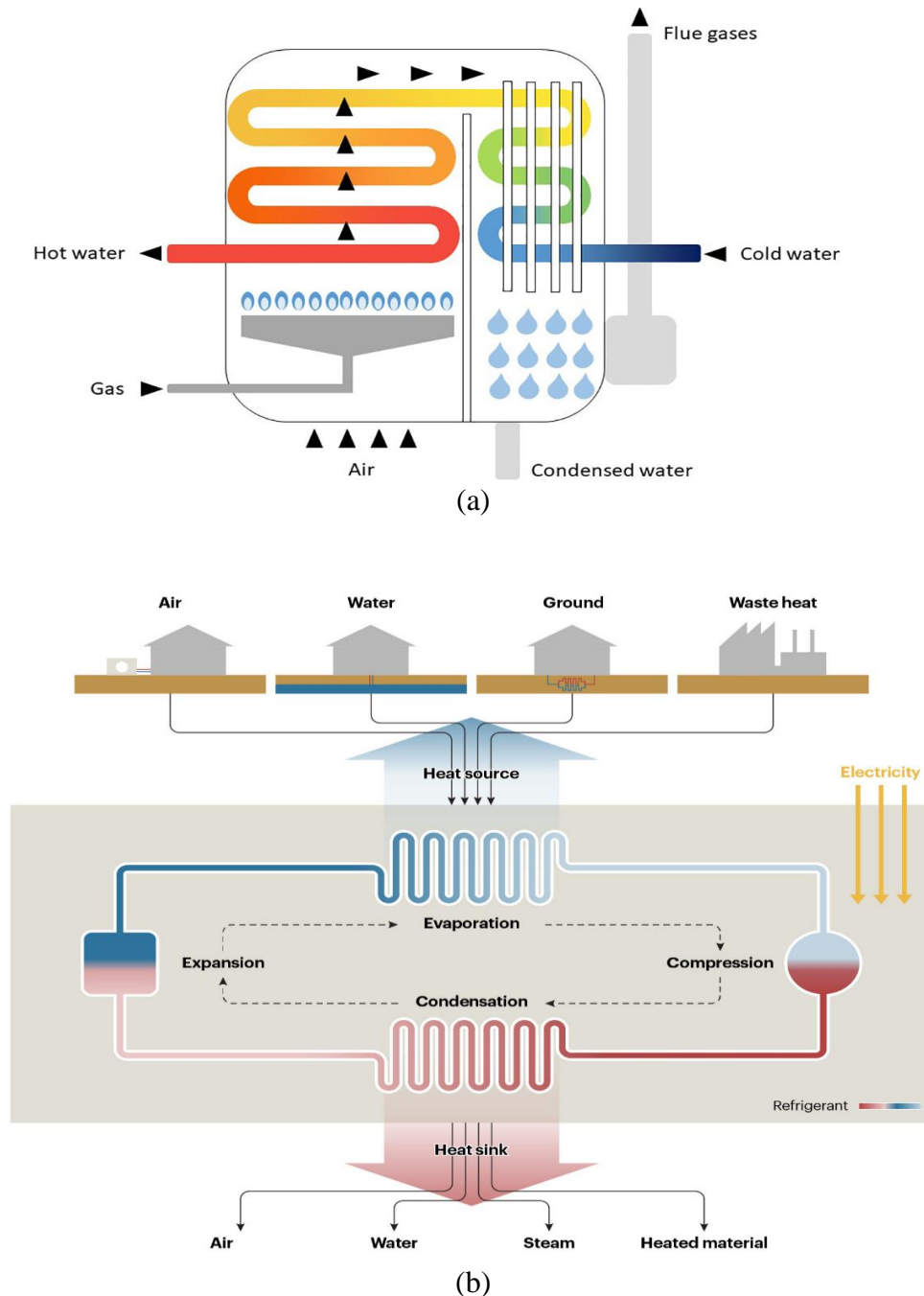


Figure 2.1: Schematic of the working principle and operation of (a) a gas-fired boiler [31] and (b) a heat pump system within a wet central heating system [32].

Wet central heating systems are available in three types: open-vented, sealed, and sealed combi-boiler systems [33]. In the first case, the system is open to the atmosphere with a header tank for top-up due to water loss and to relieve the pressure of the heated water. The sealed system does not have a header tank and is closed to the atmosphere. There is no water loss due to evaporation, and a dedicated expansion vessel is installed to accommodate the expansion and contraction of the heated fluid [34]. The sealed combi-boiler system has advantages over the other two systems as it is easier to install, cheaper to operate and hot water is made available, instantaneously, with no energy cost for storing hot water. However, its drawback is that the system can struggle to cope with high hot water demand with no heating, and no hot water available if the boiler stops (i.e., no storage). Due to its cost-effectiveness and efficiency, the sealed combi-boiler system is the most common form of domestic heating in UK homes, with over 90% of households using the approach [35].

Combi-boiler systems are popular due to their versatility in providing hot water on demand without the need of a hot water tank. Combi-boiler systems, therefore, save space in a building, unlike the standard boiler types that require a cylinder for storing hot water [36]. Further, for enhanced energy efficiency, condensing boilers are applied as they capture and reuse the latent heat from water vapour in the flue waste. Condensing boilers are considered first in any application as they meet best practice requirements [31,36].

A conventional heat pump-based wet central heating system operates by utilising energy from the environment and increasing its temperature to make it suitable for heating buildings. The operation of the system is like the gas boiler type except the boiler is replaced by either an air source or water source heat pump. The heat pump extracts heat from the environment without burning fuel (oil/gas) locally and delivers the heat through a heat exchanger as illustrated in Figure 2.1(b). This requires an electricity supply to compress a refrigerant to raise its temperature [32,37]. In this condition, the pressure of the refrigerant is increased. The refrigerant is condensed to release the heat to a hydronic system such as underfloor heating pipes or radiators to provide room heating. The refrigerant is further expanded by lowering the pressure in the expansion valve to reduce its temperature for a continuous cycle [6].

In most temperate climate regions, a dwelling's wet central heating system operates using a gas-fired boiler or a heat pump employed in direct mode. This contrasts with the aim of this work where a heat pump-integrated TES system is utilised without the need to replace existing system components. The TES system is charged in an offline mode by the heat pump and the stored thermal energy is subsequently discharged to meet a dwelling's next-day heat demand. BEIS [9] provides a detailed description of the operational characteristics of a dwelling's wet central heating components and systems.

2.2.1.1 Government Policy on Replacing Gas Boilers with Heat Pumps

In many countries, there is a policy push driving the industry toward the decarbonisation of heating in buildings and transportation. For example, the European Parliament has issued the 2030 renewable energy directive [38], which requires 32% of all EU energy consumption to emanate from renewable sources. Of this, 40% of the energy is associated with the heating and cooling of buildings. The decarbonisation of heating in dwellings has been reported as the biggest challenge [2]. Electrification of heating through the application of heat pumps is one of the options described in a CCC report for decarbonisation of the sectors requiring heating [39].

Over the last decade, many countries in cold and temperate climate zones have seen an increase in the deployment of heat pumps. Of the 177 million heat pumps installed globally in 2020 (Figure 2.2), 33% were in China, 23% in North America and 12% in Europe [40]. The IEA's net zero pathway estimates that 600 million heat pumps are to be installed globally by 2030. However, the trend from 2010-2020, indicates that 253 million heat pump units are projected to be installed in 2030, as shown in Figure 2.2. This implies that further policy measures are required to accelerate heat pump deployment to align with the IEA's net zero emission scenario targets. The policy strategy implemented by Scandinavian countries such as Norway, Sweden, Denmark, Finland, and Estonia has resulted in the highest adoption rates of heat pumps for heating systems [40,41]. These countries have effectively promoted heat pumps through incentives, regulations and a strong focus on energy efficiency and sustainability. Despite having the coldest winters in Europe, these countries have shown that heat pumps are suitable for cold climate regions contrary to common belief.



Figure 2.2: Global heat pump sales within the IEA's net zero emission scenario [40].

Figure 2.3 shows the rate of heat pump penetration based on the number of heat pumps installed per 100 households in selected countries. This is based on the number of degree days, which is a temperature-weighted average with a reference temperature of 18°C. The market trend indicates a significant global increase in heat pump sales, with a 15% growth in 2021, which is double the growth rate seen over the previous decade [32]. In Europe, the heat pump market experienced a 35% growth in 2021, with higher sales in the Netherlands, France, Italy, and Germany. The surge in demand in the region has been driven by the global energy crisis. The largest market for ASHP sales is in China, with a 7% growth. A larger growth in the sales of ASHP was achieved in the USA with a market growth of 15% in 2021 [40]. These regions, as well as Japan and Korea, are major players in heat pump manufacture. The significant heat pump deployment rate in these countries indicates that the adopted policy strategies have been particularly effective.

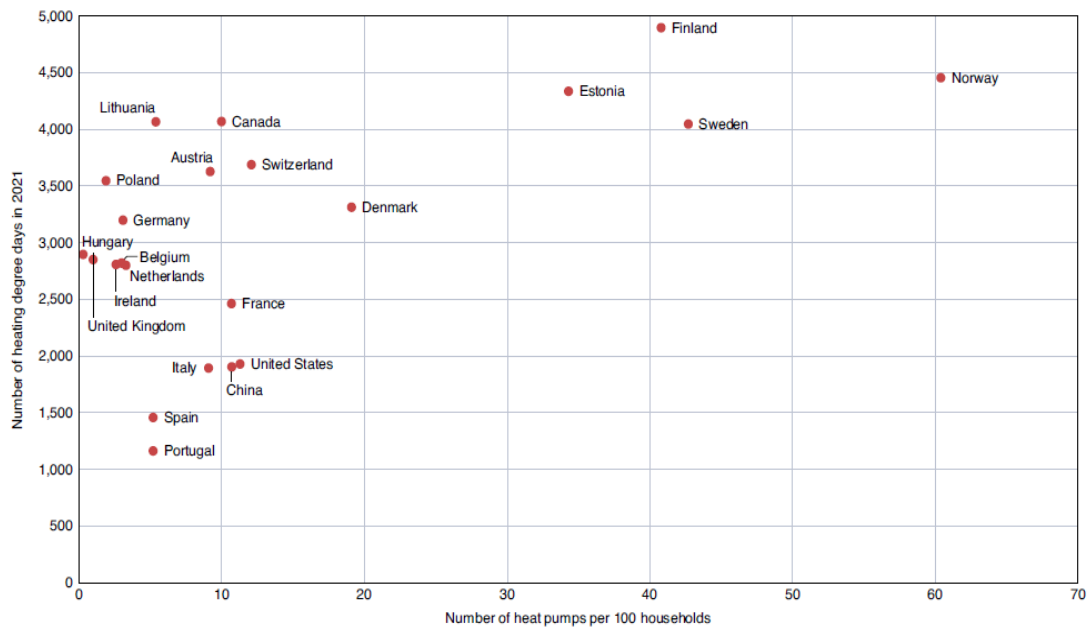


Figure 2.3: Share of heat pump penetration in some countries in 2021 [40].

The use of oil/gas in dwellings for space heating, hot water and cooking has contributed to a fifth of the UK's carbon emissions, making it one of the most targeted sectors of the economy. For the UK to meet its climate target, more effort is required to bring forward low-carbon alternatives such as heat pumps or hydrogen gas systems [42]. The policy for the electrification of building heating is critical to reducing the UK's dependence on fossil fuels. The implementation of this policy would prevent the use of expensive fossil fuels and reduce carbon emissions to the atmosphere [43]. However, the capital, maintenance and running cost of a heat pump system is a barrier to uptake [43]. One UK government initiative is the boiler upgrade scheme which offers grants to consumers for the installation of heat pumps. Up to £5,000 is available for an air source heat pump upgrade and up to £6,000 for a ground source heat pump [44]. However, the grant is not available to those with working boilers who wish to switch [42]. This incentive from the UK Government towards heat pump applications is intended to stimulate the heat pump market in the UK.

2.2.1.2 Problems of Boiler Replacement with Heat Pump

The use of heat pumps for heating may not be suitable for all building types. A heat pump system may not operate efficiently at higher output temperatures in buildings [45], especially during peak electricity demand. High costs will be incurred to im-

prove the building's energy efficiency to mitigate the heat pump operation at low output temperatures before deployment. To ensure effective operation of heat pumps, it is essential a to improve the insulation, use draught-proof doors and windows, increase the size of radiators (to compensate for lower flow temperatures), and potentially install a heat storage device. A change in user behaviour is also required for optimum efficiency [46], as heat pumps operate at relatively low temperatures. The capital, maintenance, and installation costs currently deter customers from purchasing a heat pump [45]. Some of these problems are summarised in Table 2.1.

Table 2.1: Problems associated with heat pumps in wet central heating.

Operational principle	Parameter	Characteristics
<ul style="list-style-type: none"> • The main components of the heating system are a heat pump, pipe networks, radiators, control device valves, and sensors. • Replacement of boilers with a heat pumps requires change in occupant behaviour in terms of heat pump operation control and usage. • The heat pump is connected to the existing pipe networks, radiators, and control systems and sensors. • Requirement for electricity to provide the energy required by the heat pump to heat water and deliver it to the systems. • The heated water flows through the piping network to the radiator system and hot water storage tank. • Hot water from the radiators returns to the heat pump for a continuous cycle of operation. 	Electricity consumption	Increase in electricity demand. Disparity in electricity used by heat pumps and gas boilers. With high electricity tariffs at peak periods (morning and evening), how can the system be feasible regarding electricity usage.
	Operational requirement	Domestic heat pumps usually operate at a lower temperature compared to gas boilers, could heat pumps provide enough heat output during winter? permission is required for installations.
	Cost and price of electricity	High cost of electricity in the operation of the system to provide required heat. The average price of electricity in 2020 was £0.3 per kWh [47].
	CO ₂ emission	e.g. 65g of CO ₂ /kWh is released (UK average September 25, 2023) when a ground source heat pump operates with a COP of 3.2. The lower the COP the higher CO ₂ emissions [48].
	Capital and running costs	A heat pump is associated with high capital, installation, and maintenance cost. This is dependent on the dwelling size. A high cost of electricity is incurred in the operation of the system.

The industry needs to find technical solutions that reduce the upfront cost of procuring, installing, maintaining, and running a heat pump. Higher electricity demand will arise where the deployment rate is excessive and the roll-out extensive. This may lead to an excessively high demand for electricity during peak periods. In addition, many heat pumps use refrigerants that are harmful to the environment [9]. Emissions of refrigerants such as hydrofluorocarbon and hydrofluoro-oleifins due to heat pump scrappage contrasts with the 2050 net zero emissions target. Element Energy [49] have indicated that the possibility to decarbonise the UK's existing housing stock requires an average net projected investment of approximately £10,000 per dwelling. This applies to most of the UK dwellings, amounting to 85% of the total housing stock. This is a substantial capital investment, requiring stakeholder and government interventions. One major challenge is the use of heat pumps at lower output temperatures under extreme weather conditions. In this case, the low heat output may require upgrading or building-side improvements may be necessary (e.g. insulation upgrades, larger radiators or control system timing adjustments) for effective system operation [41].

2.2.2 Heat Pumps Wet Central Heating

The characteristics of heat pump wet central heating systems are similar to the gas-fired boiler type. The only difference is the operational temperature, and the heat output delivered. For the system to work efficiently, the heat output in a heat pump system will be comparably lower. One response to this issue is to refurbish the building to reduce the heat demand by introducing energy efficiency measures and/or increasing radiator surface areas. In the present work, these actions are avoided by introducing heat storage to enable 'off-line' operation in which the heat pump to charges a thermal store in day-ahead mode. Figure 2.4 presents a schematic diagram of a conventional heat pump wet central heating system. In this system, the heat pump delivers the dwelling's heating and hot water requirements.

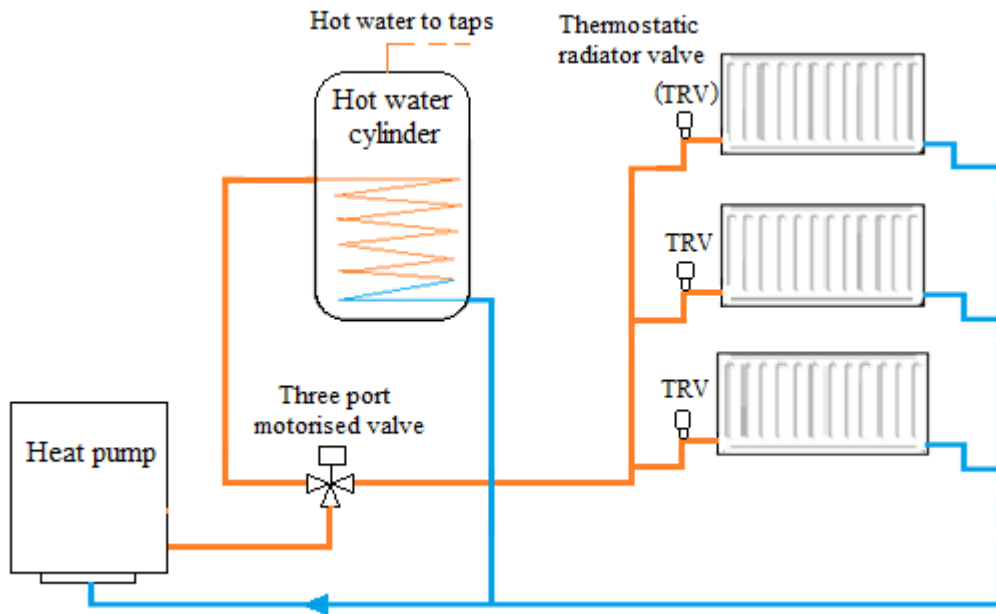


Figure 2.4: A heat pump directly supplying a wet central heating system.

An alternative solution, as considered in the present work, is to integrate the heat pump with a TES system as summarised in Figure 2.5.

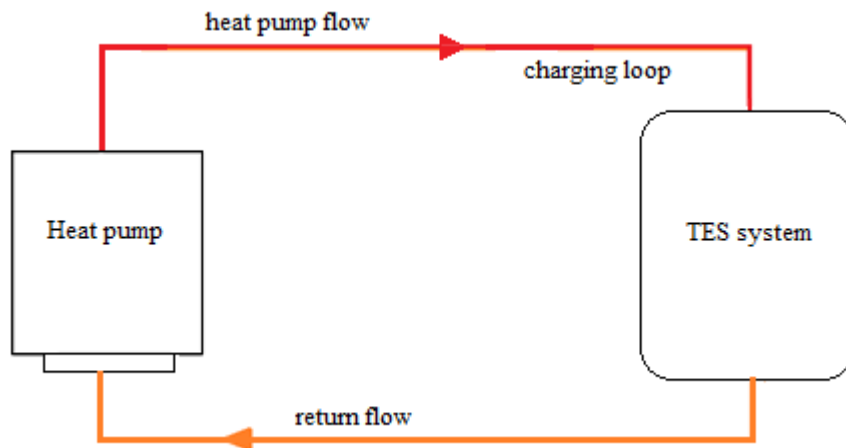


Figure 2.5: Schematic of heat pump integrated TES system.

The application of a heat pump-integrated TES system for dwelling heating has been lacking because of the scarcity of scientific investigation into its use for domestic applications [16]. The technology of the heat pump integrated TES system is promising for delivering an efficient dwelling heating system at low electricity cost [14].

2.2.3 Reviews in Applications of Heat Pump Wet Central Heating

The low carbon footprint characteristics of heat pumps and their potentially higher COP (if well sized and controlled) compared to other heating devices, make heat pumps attractive, particularly for the electrification of heating in buildings. However, the performance operation of heat pumps is strongly affected by its installations, building characteristics, and ambient conditions where they are used [50]. These heat pump characteristics limit their performance in real-life situations as compared to the performance observed under effective environmental conditions.

The use of heat pumps for space heating will be more efficient in a well-insulated building. Around 80% of UK buildings are existing, limiting the deployment potential of heat pumps. ASHP remains the most common type of heat pump found in Europe. However, in some cases, ground and water source heat pumps have been applied to buildings [51]. Researchers have conducted studies to demonstrate the performance of various heat pump deployments. Table 2.2 summarises studies conducted to determine heat pump performance in terms of efficiency rating, management, and control in real-world settings, through carrying out field trials, tests, and experiments. The review also involved the use of statistical data and numerical models with the application of various analyses to assess the performance of heat pumps with the provision of heat for residential buildings. The application of heat pumps to provide dwelling heating has attracted researchers to examine how heat pumps can effectively be managed and controlled.

Zhang et al. [52] established a mathematical model applied to a low-temperature ASHP operating in different heating modes. The model was used to compare the impact of different parameters, including the initial investment, running cost, emissions, and primary energy consumption of the ASHP and other heating systems including electric heaters, gas-fired and coal-fired boilers. The result of the analysis indicated that the ASHP is the most economic, with relatively low emissions in comparison with the other heating systems. The ASHP was able to meet the space heating requirements in the residential buildings operating at an ambient temperature of -15°C . The ASHP operated at lower COP compared to other heating systems.

Table 2.2: Summary of studies utilising heat pumps for dwelling wet central heating.

Authors	Study location	Heat pump capacity	Methodology	Summary of activity
Amirirad et al. [53]	Canada		Experimental investigation and numerical validation using TRN-SYS.	The performance of ASHP and ASHPWH in residential house was experimentally investigated and numerically validated. The overall house energy consumption was evaluated.
Zhang et al. [54]	Harbin, China		Experimental investigation of ASHP performance in the cold region.	The performance of ASHP operating in cold regions of China was investigated. Low COP was achieved. However, high indoor temperature was recorded.
Touche & Prenail, [55]	Toronto, US	1.3 to 3.5 kW	Laboratory test and simulation in an enclosed balcony space thermal buffer zone.	An improvement in the performance of ASHP was achieved when heat gain to the thermal buffer zone was increased. Seasonal prediction of ASHP performance below 10°C was provided.
Stamatelos et al. [56]	Climatic data of Volos City, Greece	10.5 kW cooling and 11 kW heating	Modelling and simulation of a three-zone residential house using TRNSYS.	A typical day simulation involving a roof-top PV panel and HVAC control system was conducted. Holistic appraisal of the building energy performance and optimisation of the top-roof PV panel to increase electricity production to energise the heat pump.
Zhang et al. [52]	Residential building in Beijing	ASHP operating at -15°C	Mathematical modelling and simulation of a residential building.	The comparison was made on the different heating systems based on investment and annual running cost, emission, and primary energy consumption.
Kelly & Cockroft [24]	Westfield. UK	8 kW ASHP retrofitted in dwelling	ESP-r building performance simulation tool and field trial data utilised.	Assessment of the performance of ASHP retrofitted into a dwelling in comparison with the boiler. Performance analysis for the two heating systems was presented.
Kelly et al. [57]	Data set for BER certificate of Ireland, UK	Variable capacity of 8 kW, 12 kW, and 16 kW	Economic analysis based on the heating residential market using the BER data set.	Study on the performance of various heating technologies about efficiency, economy, and environmental issues. Dwelling energy consumption: emissions, pollution, and running costs of ASHP and other heating systems were compared.
Liang et al. [58]	Nanjing, China	10 kW	Established mathematical modelling for building heating.	Improvement in the performance of solar-assisted ASHP. The study findings indicated that the system performance is proportional to the area of the solar collector.

Kelly and Cockroft [24] used monitored data and a simulation model (ESP-r) to assess ASHP performance when retrofitted into dwellings that use a gas boiler for space heating and domestic hot water. The result obtained from a field trial was applied to verify the simulation model. On comparing the ASHP and gas-fired boiler performance, a 12% energy saving, and 10% higher running cost was recorded with the ASHP operating at 2.7 COP calculated from the simulation.

Liang et al. [58] proposed a solar-assisted ASHP with a flexible operational mode to improve the performance of building heating systems for typical sunny and cold days in the winter heating season. An established mathematical model of a solar-assisted ASHP having a capacity of 10 kW was validated against a monitored ASHP. Figure 2.6 illustrates the proposed model of the solar-assisted ASHP. The result of the analysis indicated that the system performance is directly related to the solar collector area. During a typical sunny day, an increase in the solar collector area increases the

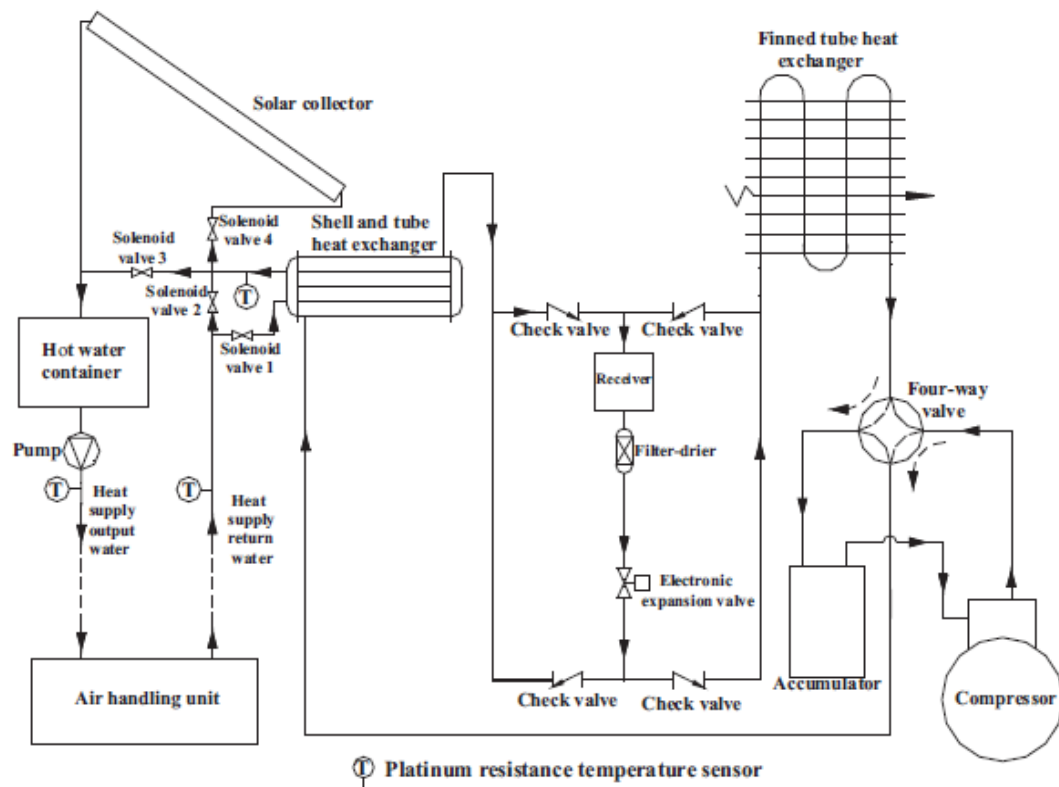


Figure 2.6: Schematic diagram of the solar-assisted ASHP heating system proposed by Liang. [58].

COP of the heat pump system, which leads to a marked energy saving. The performance results for the winter heating season are consistent with the typical sunny days although absolute values differ due to the heating system being affected by weather.

Kelly et al. [57] conducted an economic analysis to estimate the ASHP potential market. The analysis was based on a residential heating market in Ireland, where the performance of different technologies regarding efficiency, economics and environmental issues were employed. BER data, which provides information on the characteristics and energy consumption of HVAC systems and lighting for all Ireland houses with BER certificates, was used for the analysis. The influence of capital grants and higher oil prices on ASHP market potential was assessed by assessing a number of alternative scenarios. The results indicated that about 8 kilotons of PM_{2.5} and 11 kilotons NO_x were mitigated as well as approximately 4.3 million tonnes of CO₂ emissions reduction achieved annually. The combination of the effect of high oil prices, the running cost of existing heating systems and government grants, provides a greater potential market share for the ASHP.

Amirirad et al. [53] conducted a numerical and experimental study for a year-round application of ASHP and electric water heaters in Canada. Their method involved the installation of an ASHPWH in an archetype sustainable house that was reconfigured with bespoke piping networks. Six temperature sensors were installed in a tank and the experimental data was collected in real-time using a data acquisition system. The experimental data was compared with the output from a TRNSYS model. A previously developed model of ASHP was linked to the ASHPWH to evaluate the energy performance of the house. The heating and cooling house was supplied by the ASHP. The overall energy consumption of the house was evaluated during the operation of the ASHP, ASHPWH and water heater. It was found that a net reduction of 21.3% was possible for the house heating, cooling, and water heating electricity consumption about the operation of the ASHPWH. The COP of the system fluctuated between 1.5 and 5 with an outlet water temperature range of about 50°C to 56°C [53].

Touchie and Presnial [55] conducted detailed laboratory testing and simulations of a low-temperature ASHP that operates in a thermal buffer zone. An energy model was developed and calibrated using the data collected from the laboratory apparatus to

appraise the performance of the ASHP system. An improved performance was achieved when heat gain to the thermal buffer zone was increased.

Zhang et al. [54] carried out a study to investigate experimentally the application of ASHP for heating in Harbin, the coldest provincial capital of China. The purpose of the study was to determine whether ASHP can be applied in severely cold regions of China. The experimental set-up comprised an evaporator located in outdoors and a compressor, condenser and expansion valve located indoors. The settings of the ASHP components applied for the heating in the indoor and outdoor conditions are shown in Figure 2.7. Thermocouples were attached at different positions of the inlet and outlet of the evaporator and the condenser to determine the heating temperature of the system under different indoor and outdoor temperature combinations. The thermocouples were connected to a data acquisition system with the temperature recorded at intervals of one minute. Three days of the cold heating period were selected for the experiment. The result of the experiment showed that the heating temperature of the ASHP fluctuates between 21.6°C and 27.3°C maximum. The high temperature obtained was a result of high indoor temperatures recorded between 19.8°C to 24.2°C within the three selected days. The COP of the system showed low values in the range of 1.04 to 2.44. There was no obvious frost observed because of the low relative humidity of the outdoor air throughout the three days.

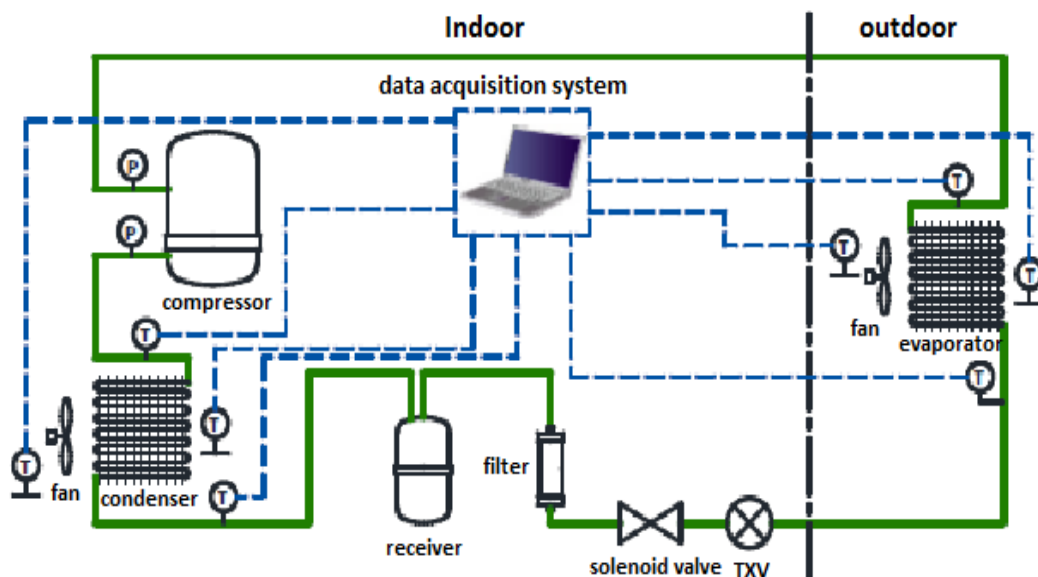


Figure 2.7: Schematic of the operation of the ASHP used by Zhang et al. [54].

Stamatellos et al. [56] used TRNSYS to evaluate the performance of an ASHP energised by a roof-top PV-panels to provide the heating requirements for a two-story building with a basement. A simulation of a typical day heating operation was conducted with a detailed HVAC control system model. The TRNSYS model included components of the HVAC system to holistic performance appraisals. A three-zone residential building in Volos, Greece was modelled with the ASHP and roof-top PV installation. The results of the simulations demonstrated that the heating and cooling of the house would be met by the ASHP over a 10-day period in mid-October (the neutral season). The roof-top PV-panels was optimised to increase the production of electricity to match the peak period of the Greek electricity market.

The review studies have shown that heat pumps are effective in providing dwelling wet central heating. This method of heating is known for its low greenhouse gas emissions. However, the running costs can be high, especially when the heat pump is operated at low COP values, as noted in most of the cases studied. This necessitates the use of a TES system for load-shifting to provide efficient heating. This study investigates the feasibility of utilizing a TES system for load-shifting purposes by charging the storage system using a heat pump operated in day-ahead mode to improve the overall efficiency of the system.

2.3 Thermal Energy Storage

2.3.1 Introduction

To bridge a temporal gap between energy demand and supply, which can occur due to the stochastic nature of renewable energy sources or variations in electricity pricing in a volatile market, a TES system can be used to store energy in the form of heat (or cold) for later use under varying load condition. The operation of a TES system involves a cycle comprising charging from a heat source, storing the energy, and discharging the stored energy at some later time [20].

A TES system comprises a storage medium, a heat exchanger, and a connecting heat transfer fluid. The TES operational charging and discharging cycle is achieved using active or passive technologies [59]. The purpose of the application of the TES system is to accumulate energy for later use. The high cost during times of peak electricity

demand has incentivised stakeholders to search for an alternative solution to provide energy savings and overcome the mismatch between energy demand and supply in buildings [20,60]. Space and water heating in the UK and other cold climate countries in Europe accounts for around 80% of the domestic final energy consumption [61]. The application of a TES system to provide heating in a residential building can reduce the energy cost and the high energy demand during peak times [62,63]. The goal of achieving energy efficiency in buildings using TES technologies has been pursued by many researchers [20,59,64]. The application of TES as an active system requires the HTF to provide the charging and discharging of some storage material.

The operation of an active TES system sometimes requires the support of an HVAC system [65]. Active systems work directly or indirectly. In a direct system, the HTF acts directly on the storage medium whereas an indirect system requires a secondary medium to store heat [66]. A passive system uses a secondary fluid to charge and discharge the storage medium. The passive system operates without the support of an HVAC system [64]. The most important design criterion in the present work is the requirement specification for a TES system applicable to domestic wet central heating. The requirement is to determine the maximum load to be met to determine the capacity of the storage system, and the required delivery temperature to determine the heat exchanger configuration. To ensure efficient operation of the TES system, an active system is employed in the present project. In this case, the heat pump is applied to charge the TES system, which can operate as a sensible or latent heat store.

2.3.2 Thermal Storage Material Types

There are various types of thermal storage material. The main types are classified as sensible, latent, and thermochemical heat storage (THS) systems [66,67]. Due to the health risks involved in the use of various chemicals, the risk of fire hazards during chemical reactions, and the complexity associated with most THS systems, they are not commonly applied for wet central heating. Because of the health risk characteristics of THS systems, this study focuses only on the application of sensible and latent heat storage systems for wet central heating operations. Figure 2.8 summarises the classification of thermal storage materials.

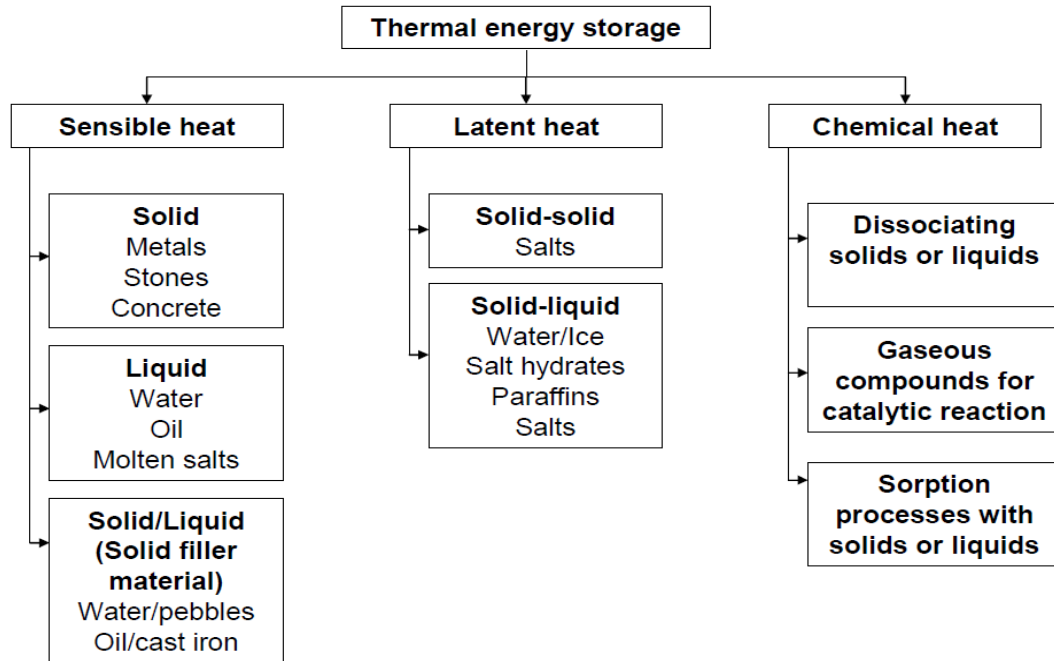


Figure 2.8: Categories of thermal energy storage materials [67].

2.3.2.1 Sensible Heat Storage

The sensible storage of heat occurs when the temperature of a storage material increases or decreases relative to a reference point. The specific heat capacity of sensible storage materials determines the amount of heat energy that can be stored. The energy stored in an SHS material is calculated as the product of mass, specific heat capacity and temperature difference as shown in Equation (2.1).

$$Q_{sensible} = m \cdot C_p \cdot \Delta T \quad (2.1)$$

where, $Q_{sensible}$ is the amount of heat stored in the material, m mass, C_p specific heat capacity of the material at constant pressure and ΔT the change in temperature during heat addition or reduction [67].

With SHS there is no change in phase of the material, it only changes temperature with an increase or decrease in heat absorption or release. Examples of SHS materials are bricks, oils, sand, soil, rocks or packed beds, water, and many more that absorb and release heat with change in temperature [21,67]. The rate at which heat is transferred to the storage medium is determined by its thermal conductivity. A SHS

material is selected based on its thermal capacity factor [21]. This indicated that storage materials with higher specific heat capacity and thermal conductivity possess good sensible storage properties. The material of an SHS system can be solid or liquid [21,68], or dual media [69]

Solid Storage Media

Solid storage media are natural and low-cost materials such as sand, sandstone, granites, bricks, broken rocks, and concrete [20]. These material types are generally preferred for application as SHS medium for cooling and heating buildings. A solid storage medium is charged and discharged by an HTF that flows directly or indirectly to contact the storage material [67]. A preliminary study is required to determine the compatibility of storage material and HTF for a direct contact application. However, indirect contact requires the use of a heat exchanger with high thermal conductivity. The heat exchanger is designed in such a way as to increase contact with the storage material for effective charging and discharging [70].

Solid storage media are usually applied within the building fabric to provide thermal comfort in buildings. Researchers have demonstrated the effects of incorporating Trombe wall, concrete, sandstone, and bricks [21,71,72]. Such materials are commonly applied as SHS in passive systems within buildings. Some technologies apply solid storage media actively operating as sensible storage modules, with time-shifted charge, and later discharge to provide cooling and heating requirements in buildings [21,73].

Liquid Storage Media

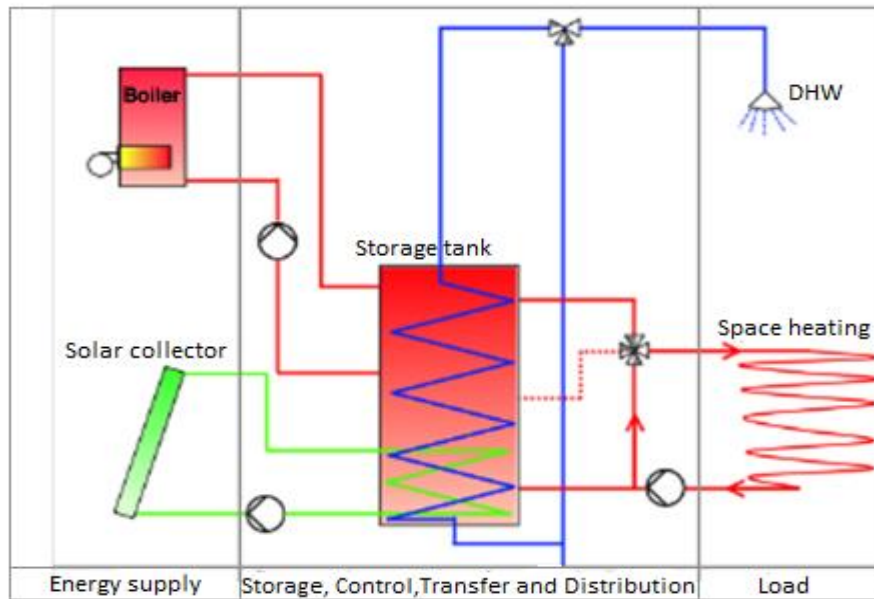
The most common sensible liquid storage media applied in wet central heating is water because of the numerous advantages it offers [74]. These include high specific heat capacity, low cost, ready availability, and non-toxicity [72]. Liquids such as thermal oil are used in some storage applications. In these cases, thermal oil is preferred to water for its high-temperature performance, high heat transfer capability, and the ability to remain in a liquid state when subjected to high temperatures [75]. In addition, because of the dynamic nature of thermal oil, it possesses the advantage of being applied as both the HTF and storage medium [75].

Table 2.3 presents the various potential SHS media with thermo-physical properties characterised in the operating temperature range suitable for wet central heating applications. Storage approaches that involve liquid media are applicable using single or two-tank storage techniques. In a single storage tank, liquid (usually water) is thermally stratified for system operation at high and low temperatures. This is contrary to using a two-tank storage system in which two tanks are maintained at different temperatures with one containing hot and the other cold [45].

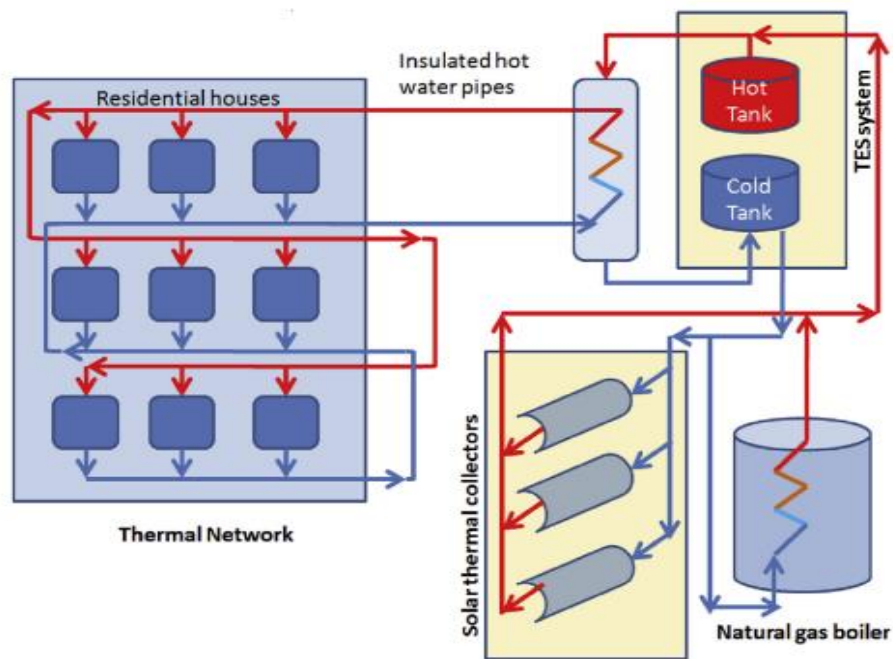
Table 2.3: Thermo-physical properties of potential SHS materials [70].

Phase type	Storage material	Temperature range (°C)	Density (kg/m ³)	Specific heat (J/kg K)
Solid	Rock	20	2560	879
	Sand	200 - 300		1.3
	Bricks	200 - 800	1600	840
	Granite	-	2400	790
	Pebble stone	-	1920	835
	Concrete	200 - 400	1900-2300	850
Liquid	Water	0 - 100	1000	4190
	Caloria HT43	12 - 260	867	2200
	Glycerine	17 - 290	1260	2420
	Liquid Paraffin	0 - 200	900	2130
	Molten salt	0 - 400	1950	1570
	Engine oil	0 - 160	888	1880
Organic liquid	Ethanol	0 - 78	790	2400
	Propanol	0 - 97	800	2500
	Butanol	0 - 118	809	2400
	Isobutanol	0 - 100	808	3000
	Isopentanol	0 - 148	831	2200
	Octane	0 - 126	704	2400

The use of a hot water tank for dwelling heating is not new. Energy saving can be achieved using hot water tank heating systems through the application of solar energy and other heat energy supply systems. Figure 2.9 shows a schematic diagram of a wet central heating system with single and two-tank SHS systems [45,68]. The boiler and solar collector transfer heat to the TES system and later discharge the TES to provide space heating in dwellings.



(a)



(b)

Figure 2.9: Schematic of wet central heating with SHS utilising (a) single tank [74] and (b) two-tank system [45].

In a dual storage medium, solid and liquid media are fused in an insulated storage tank. In this type of storage medium, the combination of two or more HTFs, concrete fillers, blocks and/or rods is often used as dual storage media [76]. However, applications of dual media involve water fused with solid modules in a storage tank charged by a heat generator such as a solar collector or electric heater. The operation of such a system is achieved using water often applied as the HTF with storage material contained in the tank [77]. Single and dual storage media are thermally stratified with hot and cold sections separated by a thermocline. In this technique, the storage system operates with a fluid density applied to separate the hot and cold sections. The cold water settles at the bottom of the tank with the hot water at the top [78].

2.3.2.2 Latent Heat Storage

Phase transition of a material is used to describe a LHS system. The phase change usually occurs from solid to solid, solid to gas, solid to liquid or liquid to gas phase and vice-versa. In a solid-to-liquid transformation, melting and solidification of the material occur. During melting, PCM absorbs heat at an almost constant temperature and thus stores a larger amount of heat. The heat stored in the material is released during solidification. This operation is directly related to the enthalpy of the material.

The high energy storage density of PCM makes it an advantageous TES medium compared to SHS [21,79]. Solid to gaseous and liquid to gaseous phase transition produces larger amounts of heat. However, they are not generally applied due to the disadvantage of a larger change in volume and evaporation [67,73,80] making such storage systems more complex and unrealistic. Solid-to-solid LHS involves the rearrangement of crystalline form typically releasing a small amount of heat [67]. The application of solid-to-solid LHS has been proposed to overcome the problem associated with solid-to-liquid and other forms of PCM [81]. The solid-to-solid LHS material is simple to handle and cost-effective. Solid material does not require encapsulation or containment to eliminate leakage risk [81]. However, such a LHS material is an order of magnitude smaller in latent heat of fusion compared to other PCM forms during the transition process. The most common solid-to-solid LHS materials are metals and alloys. Such materials are suitable for use due to their smaller latent heat per unit mass [67,80].

The present work applies a solid-to-liquid-based LHS due to its advantages and the peculiarities involved in its application for wet central heating. The solid-to-liquid LHS system operates initially as an SHS to which the temperature of the solid PCM rises relating to the enthalpy of the system. Heat is transferred through conduction and convection when the storage material undergoes a phase change at constant temperature [66,81].

Figure 2.10 presents a schematic of the LHS operational principle. It can be observed that the melting process completes when the storage material undergoes a temperature change from solid to liquid. The storage material operates as a sensible solid initially at T_{solid} until the melting temperature T_m is reached, where the transformation occurs before it is further heated to T_{liquid} as a sensible liquid, after which evaporation occurs. The total heat stored is indicated by the addition of the sensible (solid and liquid) and latent heat. The total heat stored in the material, Q_{Total} , which is largely defined by its latent heat of fusion, is described by Equations (2.2) and (2.3) [67], where q_{Total} is the total heat per unit mass m , h_m the heat of melting and c_p the specific heat capacity of the storage material. Because of the larger values of heat of fusion due to the phase change, the heat of melting is much greater than the sensible heat and, therefore, has greater volumetric energy storage capacity compared to SHS material [67,79]. It is stressed that the PCM melting temperature depends on the thermo-physical properties and type of the LHS material applied. This is because of the high heat of fusion of various PCMs are retrieved during the phase change. Hence, the requirement to screen PCM is of paramount importance. Because of the nature of an LHS material undergoing phase change from solid to liquid and vice-versa during the melting and solidification processes respectively, providing the release of latent heat of fusion, PCMs are often applied for TES applications in building. However, this depends on the type of PCM selected for a particular application. PCM can be applied within the building fabric or in a heat exchanger system, with PCM in the annulus of a shell-and-tube heat exchanger for example.

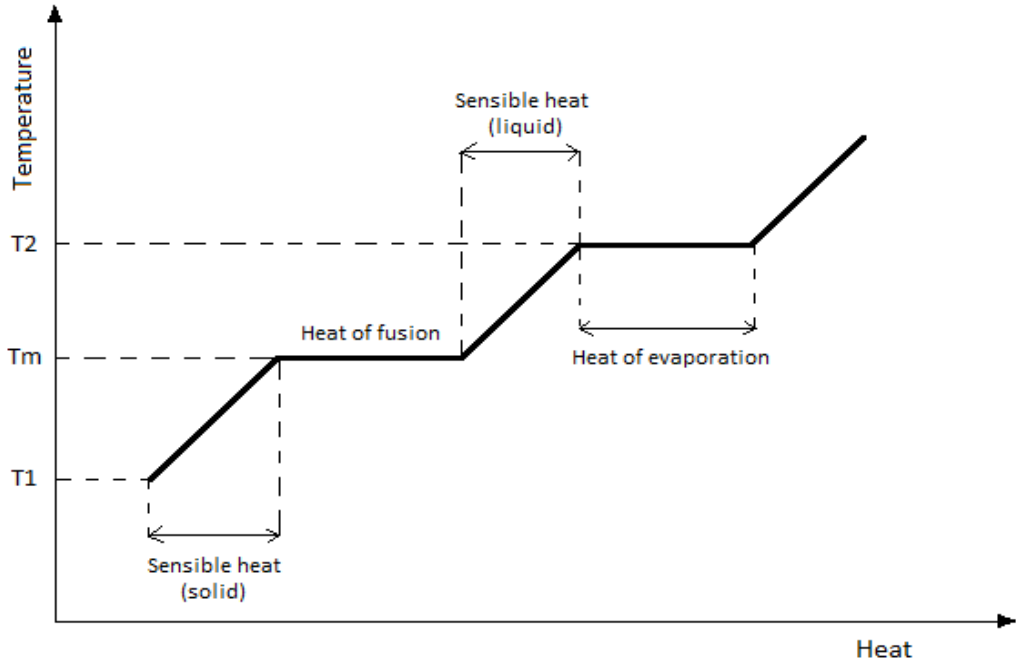


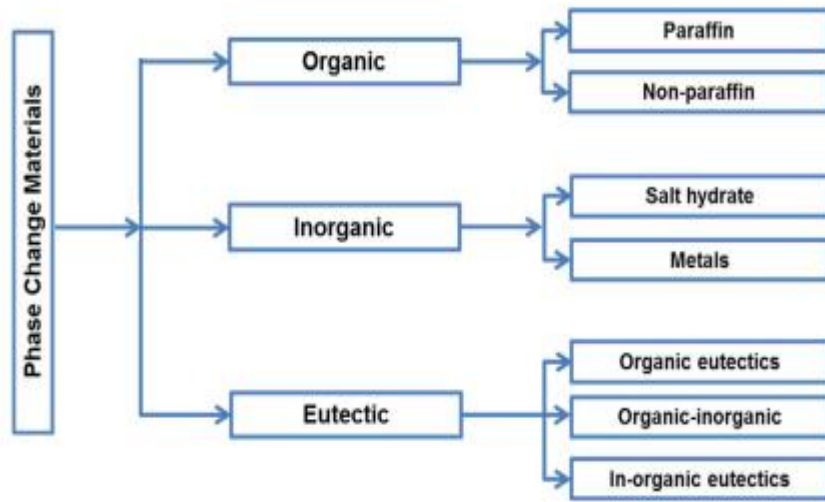
Figure 2.10: Phase transition as a function of heat addition [79].

$$Q_{Total} = Q_{(solid)} + Q_{latent} + Q_{liquid} = q_{Total} \cdot m \quad (2.2)$$

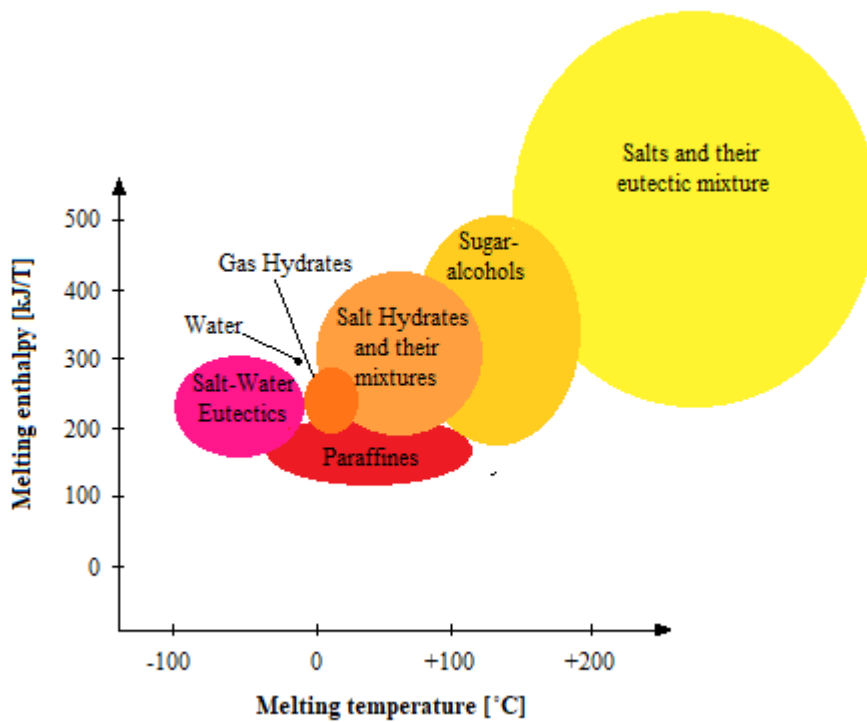
$$Q_{Total} = m \cdot c_{p,solid} (T_m - T_s) + m \cdot \Delta h_m + m \cdot c_{p,liquid} (T_l - T_m) \quad (2.3)$$

The heat absorbing and releasing characteristics of the PCM during transformation is an important requirement in the classification and application of solid-liquid-based PCM. This PCM characteristic has been exploited for various thermal storage applications. PCM is classified into organic, inorganic, and eutectics as summarised in Figure 2.11(a). This classification indicates various categories of PCM belonging to different groups such as paraffin and non-paraffin compounds, metallic PCM and alloys, salt hydrates, and eutectics.

Moreover, PCMs are also classified based on low, medium, and high melting temperatures [21,73] and melting enthalpies as illustrated in Figure 2.11 (b). This indicates the PCM's suitability for use in different operational temperature ranges. Such classification gives PCMs potential and capabilities for numerous TES applications.



(a)



(b)

Figure 2.11: Classification of PCM (a) material type [82] and (b) melting enthalpy and temperature [83].

Organic PCMs

Organic PCMs are characterised by good nucleation rate and no phase segregations. Organic PCM could melt and solidify over many cycles. This class of PCM offers the advantages of a larger fusion range with limited change in volume during phase transformation [79,84]. Organic PCMs are chemically stable, simple to use and free from supercooling. However, they are relatively expensive and characterised by low density [84]. The low thermal conductivity of most organic PCMs limits their use in thermal storage applications [84,85]. The organic PCMs are further categorised as paraffin and non-paraffin compounds [21,84,86].

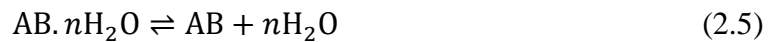
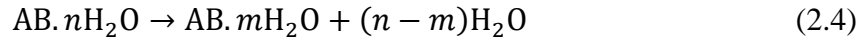
Paraffin wax is one of the most important organic PCMs and comprises a mixture of straight-chain n-alkanes, C_nH_{2n+2} , with n varying over a melting temperature range of 23°C to 67°C [87,88] for various thermal storage applications. The melting point and latent heat of fusion of the paraffin wax increases with an increase in the chain length [21,89]. Paraffin waxes are characterised by high latent heat storage capabilities [89]. The materials absorb and release heat under numerous cycles during phase transition. Paraffin waxes are, reliable, non-corrosive, less expensive, and available for wide-temperature applications [88,89].

Non-paraffin organic PCMs are the most abundant organic PCM types characterised by many different properties [21,79]. They include some compounds such as alcohol, esters, fatty acids, and glycol [21,73,90]. These organic PCMs are known for their TES applications. They are associated with high latent heat of fusion, flammability at high temperatures, non-toxic, low cost, low thermal conductivity, and low sub-cooling. They are chemically and thermally stable under many cycles [21,90].

Inorganic PCMs

Inorganic PCMs are compounds categorised as salt hydrates and metallic [20,84]. Inorganic PCMs are generally characterised by high melting temperatures [21,82]. However, they are highly corrosive and suffer from phase segregation, super-cooling, improper solidification, and high differences in their densities of solid and liquid states [91]. Most inorganic PCMs require a container to accommodate the expansion during melting. They are inexpensive and characterised by high storage densities, high latent heat and non-degradable melting enthalpies through cycling [84,92].

Salt hydrates are compounds containing alloys of inorganic salts (AB) with n k-mol water of crystallisation forming a typical solid material with the general formula $AB \cdot nH_2O$ [21,93]. The hydration and dehydration of salt compounds occur during the solid-liquid transition periodic melting process, to a hydrated salt with fewer moles of water as described by Equation (2.4) [21,93]. During the melting period, hydrated salt disintegrates into anhydrous salt and water as shown in Equation (2.5). This process is reversible upon heat withdrawal [21,67].



Because of the high latent heat of fusion per unit volume and relatively high thermal conductivity characteristics of salt hydrate, which is double compared to paraffin, they are often used in heat storage applications [21,94]. Hydrated salts are less corrosive, they are reported to be compatible with plastic containers [21,94]. However, their drawbacks are not limited to a low number of water molecules and water during solidification, spontaneity, incongruent melting, and super-cooling [21,67,95].

Metals and metal alloys possess high latent heat of fusion per unit volume compared to salt hydrates. They are associated with high thermal conductivity, eliminating other heat transfer enhancements, to improve heat conduction [95]. Metals and alloys are interesting inorganic PCMs used for TES applications at high temperatures. However, they have not been commonly considered LHS materials due to their elevated weight [80,95], high cost, and low melting enthalpy especially tin and lead metal alloys [21]. In addition, metallic alloys exhibit lower thermal conductivity compared to pure metals [96]. Safarian and Tangstand [97] compared binary and ternary aluminium-silicon alloys with commercial pure and ultra-pure aluminium. The thermal conductivity of aluminium alloys decreases with an increase in the concentration of silicon at a given temperature. In addition, Angadi et al. [98] indicated that the thermal conductivity of aluminium-silicon alloy is lower at higher temperatures for a given chemical composition. The addition of another metal to the alloy affects its thermal conductivity. Multiple combinations of PCM types such as metals or metal alloys give rise to eutectics.

High-Temperature Solid-solid PCM

In solid-solid PCMs, faster heat transfer occurs, with phase transition from crystalline to semi-solid polycrystalline structure, which further transforms into an amorphous phase [99]. This phase transition is perfectly reversible with reduced thermal degradation [99,100]. Solid-solid PCMs have several advantages over solid-liquid PCMs. They offer lower or no corrosiveness, low thermal expansion, large storage density, and are free from issues such as corrosion and supercooling [101].

Solid-solid PCMs have gained significant attention in thermal storage applications due to their advantages over solid-liquid PCMs, especially for high-temperature applications. Examples of high-temperature solid-solid PCMs are inorganic; sodium and lithium sulfates as well as their mixtures [101], other examples include metals such as titanium, copper, nickel and their alloys [102], organometallic; are mixtures of metals such as cobalt and zinc, polymeric materials such as cellulose, sorbitol, and polystyrene, and organic solid-solid PCMs often referred to as polyols [99].

In recent years, significant efforts have been made to develop high-performance solid-solid high-temperature PCMs. Recent studies [100,103,104] have demonstrated the development of various high-temperature solid-solid PCMs for thermal storage applications. One such class of PCMs is the ultrasonic performance high-temperature Ni-Mn-Ti PCMs, which was developed by Li et al [105]. These PCMs contain a high density of materials, which enhances their thermal conductivity and latent heat of martensitic phase transition. The transition occurs at a high-temperature range of 290–500°C and the PCMs can be easily fabricated and scaled up. The composition of the constituent metals can be adjusted to provide a solid-solid PCM that can be applied at different operating temperatures. Nishioka et al [104] developed Fe-based solid-solid PCM that exhibits high latent heat capacity. The Fe-based alloy was developed using a combination of crystallographic and magnetic transformations of the Fe. The Fe-based PCM is highly suitable for heat recovery from high-temperature exhaust gases. A high-temperature Solid-solid PCMs were prepared using a developed methodology [103], with a well-defined 3D main chain and alkyl side chain and can undergo radical polymerization to achieve controllable phase change temperature and ultrasonic thermal stability. The PCMs are highly resistant to heat erosion and

can withstand temperatures of up to 250°C without leakage or deformation. A kilogram-levelled preparation for engineering demand has been analysed through the simplest one-pot synthesis strategy. The phase change temperature of the solid-solid PCM has been modified to suit different applications such as battery management, building energy conservation, and waste heat recovery.

Liu et al [102] demonstrated the performance of a novel solid-solid PCM, high entropy alloys made of Ti-Zr-Hf-Co-Ni-Cu, for high thermal energy storage applications. The study indicates that the phase change temperature of the material can be accurately controlled between 290–470°C by regulating their compositions for various high-temperature TES applications. The study findings further indicated that combining the alloys of different elements with their unique phase transition temperature can produce cascaded solid-solid PCMs with higher energy storage capacity and improved charging and discharging rate of the system.

Eutectics

Eutectics are chemical compounds consisting of a mixture of two or more constituents that are organic, inorganic, or organic and inorganic to form a single crystalline that melt and freeze congruently [21,95]. The most important eutectics characteristic is its ability to melt and freeze without segregation. This is because they are formed as an intimate mixture of crystals [95]. Because of their good chemical and thermal stability, high heat capacity, negligible supercooling, and wide range of phase change temperatures, they are considered good materials for TES systems [96,97].

Table 2.4 presents the commercially available PCMs in the operating temperature range suitable for wet central heating applications. The application of LHS material in wet central heating has been relatively uncommon. However, the integration of a heat pump into wet central heating to charge a pre-sized TES system is a promising potential solution to satisfy the heating requirements of dwellings. Table 2.5 summarises the advantages and disadvantages of SHS and LHS materials. Investigations into the application of PCM-based TES in wet central heating are relatively scarce. Various studies [106–108] demonstrate the use of PCM-based TES for application in domestic hot water systems.

Table 2.4: Thermophysical properties of LHS materials against operating temperature for wet central heating applications.

PCM	Melting Temperature (°C)	Heat of Fusion (kJ/kg)	Specific Heat Capacity, solid/liquid (J/kg.K)	Density, solid/liquid (kg/m ³)	Thermal Conductivity (W/m.K)	Reference
RT58	53 - 59	160	2000	880/770	0.2	Gasia et al. [109]
Paraffin wax	55 - 60	141	5625	850/825	0.43	Juaifer et al. [110]
CrodaTherm53	51 - 55	226	----	- /829	0.28	Kuta et al. [111]
Dodecanoic acid	43.3 – 44.8	184	2400	930/850	0.16	Kabbara et al. [112]
Paraffin wax	54.3	184	2384/2440	833/775	0.15	Tripathi & Tomar [113]
NEPCM	58.3	196	2212	911	0.4	John et al. [114]
PCM A44	42.85 – 45.85	250	1800/2400	912/775	0.24	Pagkalos et al. [115]
Paraffin wax RT60	55 -61	160	2000	770	0.2	Mozafari et al. [116]
Urea-acetamide	53	224	1920/2660	1216	0.51	Da cunha & Eames [85]
PCM	57 - 61	185	2880/4190	1400/1290	0.54	De Gracia et al. [23]
Paraffin PCM	58.8	212	2341	855	0.39	John et al. [114]
Inorganic hydrated salt	48	210	2410/2410	1600/1666	0.45	Kelly et al. [28]
Paraffin wax	60	167	2100/2500	927/827	0.2	Tayssir et al. [117]
Organic PCM	41 - 44	250	2000	800/700	0.2	Baek and Kim [118]
Paraffin P116	46.5	210	2100/2500	817/786	---	Castro Flores et al. [119]
Stearic and palmitic acid	53	182	1720/2230	971	0.23	Da cunha & Eames [85]
MgSo4 7. H2O	49	202	1760/3310	1152/1208	---	Castro Flores et al. [119]
Paraffin wax	58 -59	190	2900	870/780	0.24	Vikas and Soni [120]
Sodium acetate 3 H2O	58	264	2700/3000	1450/1280	0.7	Tripathi & Tomar [113]
Paraffin wax RT50	45 - 51	168	2000	880/760	0.2	Seddegh et al. [121]

Table 2.5: Advantages and disadvantages of SHS and LHS materials [20,95,122].

TES Types	Typical Material	Advantages	Disadvantages
Sensible heat storage	Brick	Readily available	Low enthalpy
	Concrete	Abundant and low cost	Low energy density
	Granite	Simple in operation	Low storage density
	Rock	Good thermal stability	Large volume required.
	Sandstone		Seasonal overheating due to large mass
	Water		Large change in volume Operating at variable temperature
Latent heat storage	Paraffin and non-paraffin	High latent heat	High cost
	Metallics	High energy density	Low thermal conductivity
	Salt hydrates	High storage density	Low thermal stability under large number of cycles
	Water	Small volume required.	Subcooling and supercooling
		Small change in volume.	Phase segregation
		High phase change enthalpy	
		Operating at almost constant temperature	

A PCM-based TES for hot water systems was investigated [106]. An experimental and numerical investigations of a PCM storage tank were carried out under different operating scenarios. An integrated approach with analytical and numerical methods using paraffin wax as PCM (in cylindrical bottles) was used to model the tank. Figure 2.12 shows a schematic representation of a PCM-based hot water storage system.

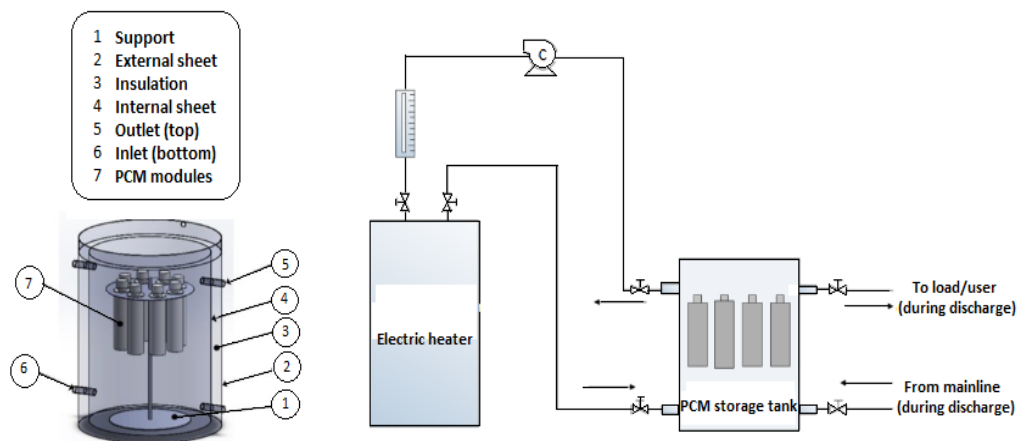


Figure 2.12: PCM-Based hot water storage system [106].

In the experimental study, an electric heater was applied for charging the tank using a 24-hour typical operating cycle under variable inlet conditions. The storage discharge was achieved at a constant flow rate or batch-wise. The efficient and cost-effective operation of the hot water system can be achieved during the period of low electricity tariff. Similarly, a double-pipe PCM-based solar water heating system has been proposed [107] for domestic heating. Figure 2.13 presents a schematic of the proposed system, which is charged by water that flows through the solar collector unit.

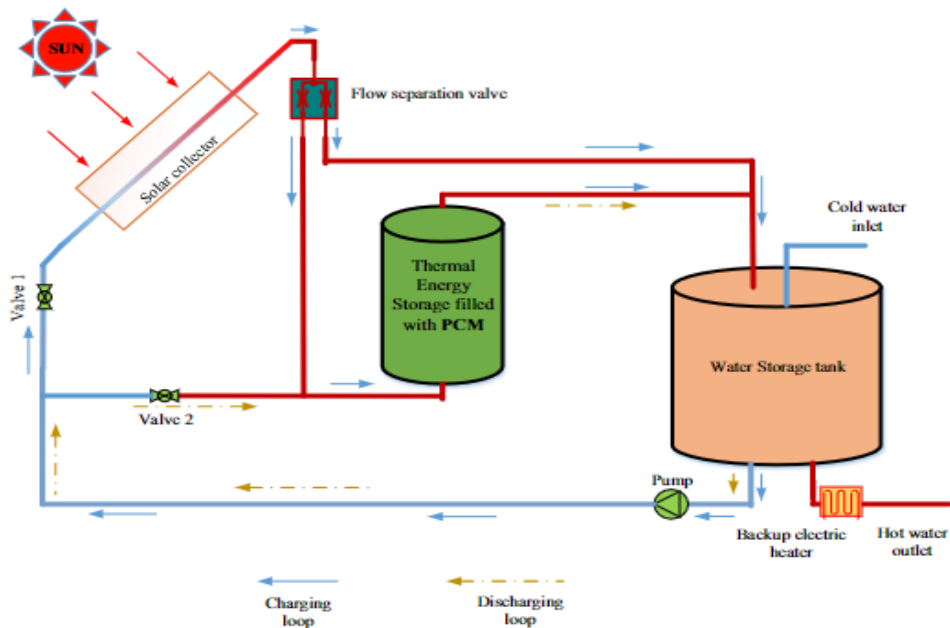


Figure 2.13: Schematic of PCM-based solar heating system [107].

A backup electric heater is applied to achieve the desired temperature. Different flow rates were applied for discharging the storage system until the output temperature was almost at ambient condition. The hot water flows from the tank to provide domestic heating.

2.3.3 TES Material Selection Criteria

The application of the LHS material as TES in wet central heating offers greater advantages compared to the SHS (see Table 2.5). This is due to the high LHS density and high latent heat of fusion characteristics extractable during the phase change from solid to liquid. Many researchers – e.g., Dincer, [78], Cardens and Leon [80], Abhat [88], Sharma et al. [95], and Castell and Sole [123] – proposed desirable prop-

erties such as thermodynamic, physical, chemical, and economic characteristics for considerations when selecting PCM as storage media. Muhammad [124] indicated the most important properties to be considered in the selection of PCM: reversible phase change with negligible sub-cooling and super-cooling, and compatibility with the container and other materials of the system. Other important considerations are the commercial availability of PCM within the operating temperature range, enthalpy requirement, and heat exchanger design suitable for wet central heating applications.

2.3.3.1 Operating Temperature and Enthalpy

The most desirable property to consider in the selection of PCM is the operating temperature range. In most cases, PCMs with melting temperatures in the range of 60°C to 80°C, matched to the operating temperature of a boiler are selected for residential heating. However, in the present work, where a heat pump is applied to charge the TES system, a suitable PCM melting temperature of 40°C to 55°C is selected to enable the effective and efficient operation of the heat pump-integrated TES solution. In this system, the heat stored is extracted when the LHS system undergoes the discharging process. This indicates that PCMs characterised by higher enthalpies and densities are required. This is because the enthalpy and density of PCMs determine the amount of energy to be stored per unit volume. However, in some cases, higher enthalpies are mostly preferred to the density [112].

2.3.3.2 Commercial Availability

The selection of a suitable PCM depends on the operational requirement of the application, in this case, wet central heating. This requirement determines whether PCM types are available in commercial quantity with the required operating temperature range and whether such PCM types are affordable. PCM of various types are obtainable in commercial quantity from various manufacturing companies. Table 2.6 lists some notable examples.

Table 2.6: Commercial manufacturers of PCM around the world.

Manufacturer	Country of Origin	Material Type	Official website
PCM Products	UK	Organic and Inorganic	www.pcmproducts.net [125]
Microtek Laboratories Ltd.	USA	Mostly organic	www.microteklabs.com [126]
Christopia Energy Systems	France	All PCM Types	www.cristopia.com [127]
Shanghai RU Entropy New Energy Technology Co., Ltd	China	All PCM types	www.pcmgel.com/about-ru-entropy/ [128]
Rubitherm Technologies GmbH	Germany	All PCM Types	www.rubitherm.eu [129]
Phase Change Solutions, Inc	USA	Mostly organic	www.phasechange.com [130]
PCM Energy P. Ltd	India	Mostly inorganic	www.pcmenergy.com [131]
Pure Temp LLC	USA	Mostly organic	www.puretemp.com [132]
Axiotherm GmbH	Germany	Organic and inorganic	www.axiotherm.de/en [133]

2.3.3.3 Heat Exchanger Design Requirements

It is important to design a storage device in a way that maximises the heat transfer rate. Consideration is given to the selection of a heat exchanger and components that are cost-effective, commercially available, and compatible with the TES material. The application of a suitable heat exchanger design with TES material based on its operating temperature range gives rise to a higher heat transfer rate between the heat exchanger and storage material during the charging and discharging processes [134–136]. Heat exchangers are designed to operate with direct or indirect contact between the storage material and HTF [67,123]. Various heat exchanger designs are applied for various TES material types. The most applied configurations are screw, shell-and-tube [137], spiral coil tube, and plate heat exchangers [111,138]. Figure 2.14 shows the various heat exchanger designs applied for PCM-based TES systems. Medrano et al. [135] investigated experimentally the performance of five commercial heat exchangers: double pipe, double pipe PCM graphite matrix, double pipe with fins, compact and plate heat exchangers using PCM (paraffin RT35) as the storage

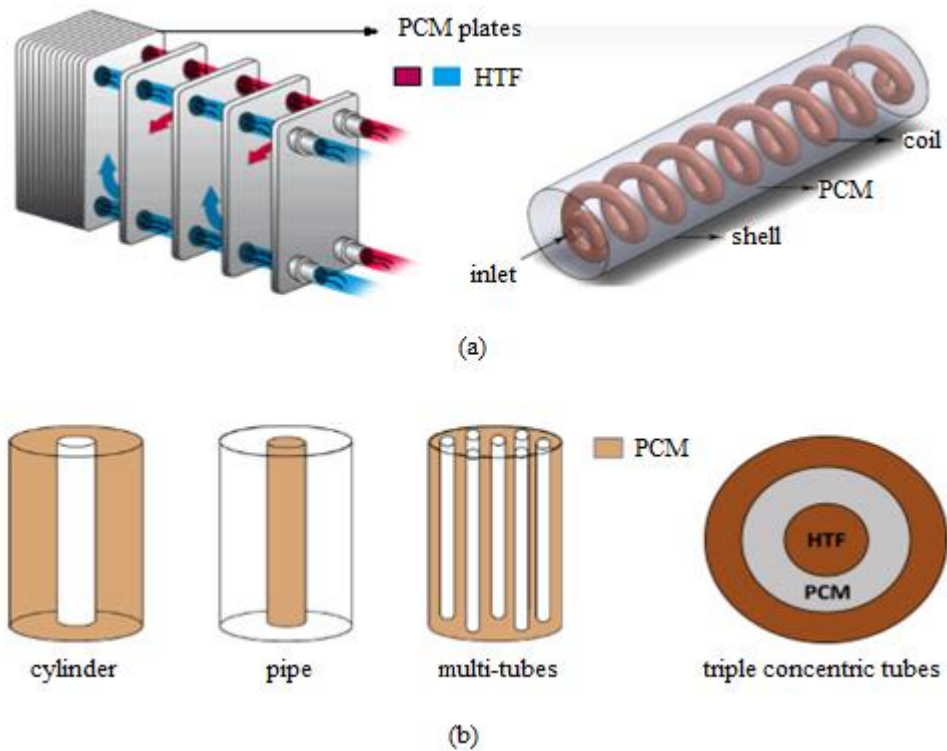


Figure 2.14: Schematic of PCM-based heat exchanger designs [134,138,139].

medium, and water as HTF. The five heat exchangers were compared based on evaluated average thermal power values. The results indicated that the double-pipe PCM graphite matrix and compact heat exchanger with an example shown (cylinder and plate model) produced values that better matched the requirements of real applications.

Kuta et al. [111] conducted a study on different heat exchanger designs applied for PCM-based TES tanks. This involved an experimental test carried out to analyse the performance of the PCM-based shell-and-tube TES tank for application in domestic heating and hot water. The results indicated that the proper selection of PCM and heat exchangers enables efficient performance of TES systems. Al-Abidi et al. [140] conducted a study of five PCM-based heat exchangers. The study results indicated that the shell-and-tube heat exchanger is the most promising storage technology. Much research has been conducted with analysis of various design and operating parameters that impact the performance of PCM-based heat exchangers [141–144].

Kalapala and Devanuri [134] described the design parameters that influence the performance of a heat exchanger: mass flow rate, HTF inlet temperature, direction of flow, flow orientation, number of tubes, and diameter of shell-and-tube. PCM-based heat exchangers are categorised into shell-and-tube and triple concentric tubes [134]. The shell-and-tube heat exchangers are further categorised into cylinder model, pipe model, and multi-tube model (Figure 2.14(b)). Many experimental and numerical studies that use the shell-and-tube heat exchanger design for PCM-based TES applications have been conducted [142–144].

A shell-and-tube heat exchanger is comprised of one or more circular tubes arranged parallel in a cylindrical shell [111,121,137]. Considering the cylinder model shown in Figure 2.14(b), the shell-and-tube heat exchanger is made up of HTF and PCM domains for the charging and discharging processes. In this type of heat exchanger, heat is transferred to the PCM in the annulus at the tube wall interface by the HTF that flows through the tube. This is well suited for application in wet central heating systems. In the present work, the cylinder model of the shell-and-tube heat exchanger design is virtually integrated with a heat pump for wet central heating application.

2.4 Heat pump Integrated TES Wet Central Heating

The technology of wet central heating involving the integration of a heat pump with a TES system as a retrofit measure, provides flexibility in the management and provision of space heating and hot water in dwellings. The technology involves adding a TES system to a heating network with a direct-mode heat pump wet central heating system. The heat pump-integrated TES system is similar in operation to the direct mode heat pump central heating. However, in the heat pump-integrated TES system, the heat pump does not completely provide heating directly to a dwelling. Instead, it supplies the heat required to charge the TES system, especially during off-peak periods to save cost. Figure 2.15 illustrates a schematic of wet central heating that involves a heat pump-integrated TES system. The TES system is charged by a heat pump operating at a constant output temperature as required for energy storage.

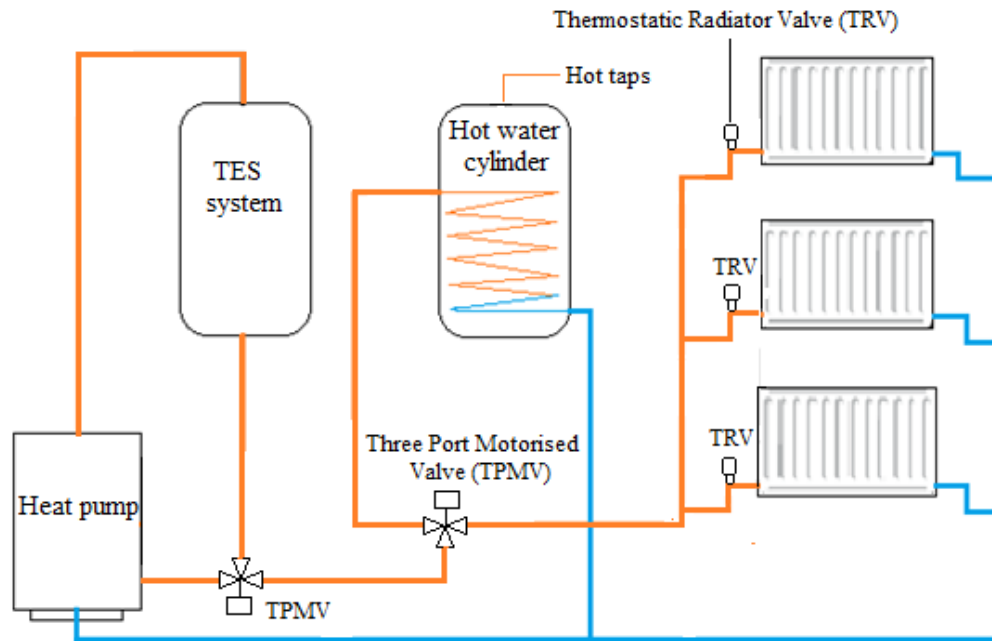


Figure 2.15: Schematic of a heat pump-integrated TES wet central heating system.

The pre-charged TES system is then discharged variably later to provide hot water and space heating during periods of potentially high electricity demand. Some tasks need to be undertaken to achieve effective and efficient operation of wet central heating systems in dwellings. For example, the requirement specification of the TES system needs to be determined using the target dwelling's heating demand profiles to *a priori* define the TES system's capacity required to meet the heat demand.

2.4.1 Potentials in Application of TES System

TES system is often used as a mechanism to overcome the mismatch between energy demand and supply. Using a heat pump-integrated TES reduces the system's operating costs as the storage system can be charged at a time of lower electricity tariff, i.e., during off-peak periods. The stored energy can be applied conveniently for later use especially at peak demand times when the electricity tariff is high. The use of a TES system in wet central heating gives the ability to provide thermal comfort in buildings by maintaining stable indoor temperature. However, the present work does not include an analysis of occupant comfort and convenience, when TES systems are applied. The procedure in future involving coupling of TES and building models could facilitate the evaluation of their impact on occupant comfort and convenience.

The low heat output characteristics of heat pumps especially under extreme cold weather conditions can be mitigated when the TES system is integrated with the required size to meet a dwelling's heat demand. In this case, the store sizing may involve the use of a store with a large capacity that always delivers the heat requirement for a dwelling. A TES system charged by a low or zero-carbon heat source (such as a heat pump utilising electricity derived from renewable sources) will support government policies to decarbonise the heat and electricity sectors. Such technologies provide flexibility in demand management that will be helpful to the operation of the electricity supply system.

2.4.2 Challenges in Application of TES System

The use of a heat pump as a source of heat for space heating is inevitably faced with problems when applied with a TES system in buildings. Most importantly, the capital, maintenance, and installation costs serve as the major challenges in the application of the system [43]. Some cost is incurred when replacing the TES material that will degrade over time. Further, the additional cost is incurred in the integration of the TES system into an existing wet central heating. Domestic heat pumps may not work efficiently at lower heat output compared to a gas-fired boiler. The application of larger or multiple TES systems and heat emitters as strategies to meet peak heat demand and mitigate the low output of heat pumps requires more space in a dwelling. Moreover, the application of this strategy causes additional capital and installation costs in the overall system and higher running and maintenance costs of the storage system in addition to the initial overall cost of the wet central heating system.

2.4.3 Reviews in Applications of Heat Pump TES Wet Central Heating

The application of heat pumps for dwelling heating is a technology that promotes the electrification of heating in buildings. The technology has the potential to reduce CO₂ and other emissions into the environment while ensuring thermal comfort in buildings. Heat pump technology offers greater efficiency and therefore, energy savings compared to other fossil fuel heating systems such as oil or gas boilers. The combination of TES with a heat pump system offers considerable potential for achieving greater energy efficiency and energy savings in buildings by utilising the possibilities for load-shifting during off-peak periods and flexibility in operation. The

integration of a heat pump with a TES system is promising as a potential technology to meet a dwelling's heating demand [14,16,145]. This indicates the advantage of heat pump integrated TES system application over the use of a direct mode of operation of heat pumps in meeting the heating requirements of dwellings.

Various studies have investigated the use of heat pump-integrated TES systems for dwelling heating. However, many of these studies [146–148] focused on the application of heat pump-integrated TES system technology specifically for district heating. Other applications of the heat pump-integrated TES system are found in industrial heating operations. An example of such applications is the studies by Arteconi et al. [149], Stampfli et al. [150] and Knudsen et al. [151]. Prendl et al. [152] studied design optimisation that utilises a simultaneous integration of a heat pump with two different TES systems by extending a method by Beck and Hofmann [153]. The approach provided energy savings in the two storage systems through heat recovery with the aid of the heat pump.

Heat pump-integrated TES system applications for dwelling heating have been studied by many researchers, mostly in new building applications. The technique is applied with a heat pump operating at a lower flow temperature using up-sized radiators to provide space heating. In addition, new houses are now built with better insulation. In a retrofit scenario, however, a heat pump is required to meet heating demand by providing water at higher temperatures suitable for the existing radiators. Moreover, significant sums of money are required to obtain a larger heat pump to deliver this heat, and this will incur higher operating costs for the electricity consumed by the heat pump. This prompted the concept underpinning the present project: to integrate a TES system to pre-store heat to fully satisfy the heat demand later. Investigations into such applications using heat pump-integrated TES systems for demand side management at the domestic level is still scarce [145,154]. More studies are required to explore the benefit of the heat pump-integrated TES system towards energy savings and emission reduction while maintaining the heat supply for existing dwellings. Furthermore, the practical implementation of this technique has not yet been studied. As summarised in Table 2.7, many publications have demonstrated this potential.

Table 2.7: Summary of studies utilising the application of heat pump-integrated TES technology for residential wet central heating.

Author	Study location	Heat pump capacity	Study/Methodology Applied	Summary of work conducted	Limitations
Le et al. [155]	UK	11 kW	TRNSYS simulations were used with a model that was validated against field trial results for retrofit evaluation.	Comparative performance and retrofit analysis of high-temperature ASHP with TES were investigated in different heating modes. The highest efficiency was attained with direct operation mode with a reduction in carbon emissions achieved.	The simulated results indicated the worst performance when continuous coupling of the heat pump and TES system was applied for house heating.
Facci et al. [15]	Three different climates of European cities		Graphical-based method, ASHP integrated TES system retrofit technology	A comparison of the performance of ASHP and TES with a gas boiler was conducted for residential buildings. An energy saving of 41% and 73% emission reduction with the heat pump integrated TES system compared with a gas boiler.	The load-shifting capabilities of the TES were analysed. However, the TES system was applied for limited hours at night to provide building heating.
Renaldi et al. [14]	Edinburgh, UK	Variable capacity (5-14 kW was considered)	Design and operational optimisation framework involving heat demand model.	The performance of the ASHP-TES system in the off-peak period was compared to conventional heating systems. Cost due to heat pump operation was reduced. Incentives enable competitiveness with conventional systems.	A heat pump-TES system was optimised to meet a dwelling's heat demand. However, a resistive backup heater was used to fulfil the house heat demand during cold winter days.
Niu et al. [17]		~ 1 kW	Experimental investigation for performance improvement of heat pump-TES system	The result indicated a dynamic balance in heat transfer between water and refrigerant with PCM interlayer. The PCM temperature, inlet, and outlet temperature difference fluctuates regularly at some balance point.	The PCM was applied as a buffer in the winter transition season. The energy stored in the PCM was used by the heat pump to meet space heating at night.

Table 2.7: Summary of studies utilising the application of heat pump-integrated TES technology for residential wet central heating (cont'd).

Author	Study location	Heat pump capacity	Study/Methodology Applied	Summary of work conducted	Limitations
Shah et al. [16]	UK	11 kW	Field trial performance test of heat pump integrated TES system for domestic heating.	A viable and efficient solution could be achieved in the operation of a heat pump-TES system at low storage temperature. Energy and CO ₂ savings were achieved with the heat pump-TES system in comparison with the gas boiler.	The heat pump partially met the dwelling's heating demand by charging the TES system, which was then used to fulfil a part of the heat demand.
Hirmiz et al. [145]		1 kW	Analytical and numerical performance predictions of heat pump-PCM TES for residential heating.	Numerical output results involving storage volume and average set point temperature, PCM fraction, peak duration, and system temperature were compared with analytical predictions.	A PCM thermal store was used for a part of the day (up to 6 hours) for load-shifting to offset the peak demand period in a detached dwelling.
Kelly et al. [28]	Glasgow, UK	10 kW	Annual performance evaluation using ESP-r simulation tool.	The performance of thermal storage buffering ASHP operation was studied. The results showed that augmenting the thermal buffer with 50% PCM halved the storage volume enabled effective load-shifting and maintained the space and hot water temperatures to the end-user	An enhanced thermal storage buffering was used. A large thermal buffer was needed for the load-shifting heat pump's operation to off-peak periods, to meet dwelling hot water and space heating requirements.
Lin et al. [156]	China	6 kW	Experimental/numerical investigation on the performance of ASHP system with latent heat thermal energy storage.	The heating performance of the ASHP system integrated with the latent heat thermal energy storage unit was investigated. Numerical analysis was conducted to further explore the charging and discharging characteristics of the storage unit.	An LHS system charged by a heat pump can theoretically provide space heating of a 78 m ² room for a limited period (2 hours) as opposed to daily load-shifting.

Le et al. [155] conducted a study to investigate the performance of a retrofitted, high-temperature ASHP and TES system with consideration of different system configurations. TRNSYS simulations were applied to model system configurations after the model was validated against field trial data. Two mid-terrace houses in Northern Ireland located at the Ulster University and built for experimental purposes were employed. To investigate the performance of the retrofitted system, the heat pump was operated in direct mode, storage mode, and combine mode. Figure 2.16 shows the schematic of the heat pump coupled with the TES system to achieve the operation of the wet central heating in these three modes.

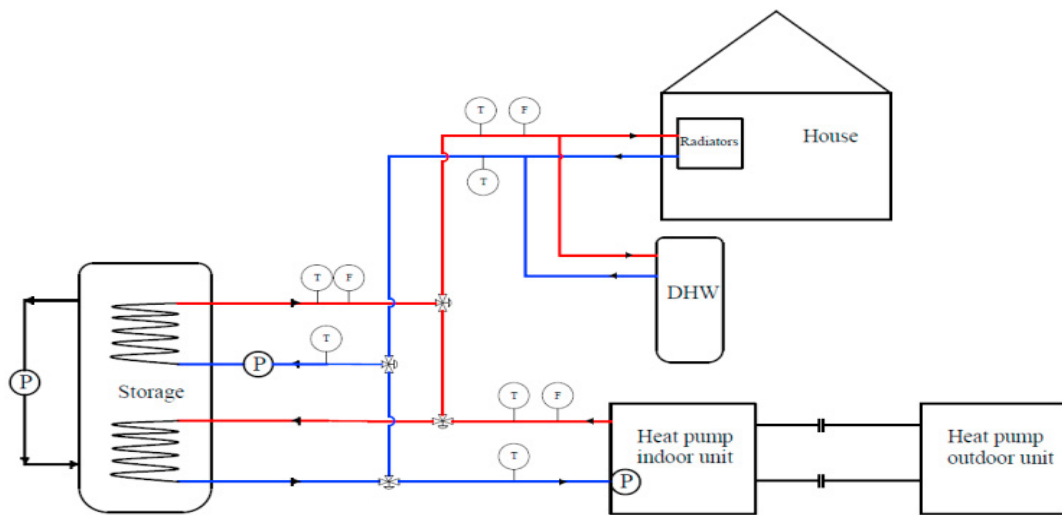


Figure 2.16: Schematic of heat pump-integrated TES wet central heating operating in different heating modes [155].

The simulated results indicated that the highest efficiency was achieved in direct mode operation. The heat pump coupled with the TES system recorded the worst performance. However, the operating costs have been reduced through carbon savings achieved by retrofit technology. Hirmiz et al. [145] investigated the performance of a heat pump-integrated PCM thermal storage for load-shifting in building demand-side management. The study focuses on integrating a TES system into a heat pump system to address increased CO₂ emissions during peak periods. The study presented a simplified analytical approach for sizing PCM-thermal storage to provide flexibility in managing building energy demand with heat pump application. The thermal performance of the PCM storage was evaluated using systems simulation and the simulation results compared with analytical predictions. The results showed more

than three-fold improvement in performance when using a thermal store with 75% PCM modules of 2 cm thickness, compared to a water-only storage operating at 10°C ΔT . When the appropriate storage volume was utilised, a residential household was sustained for a period of 2 to 6 hours. A similar study was conducted utilising a three-sleeve PCM heat exchanger designed with a heat pump operating under different weather conditions to improve the performance of the heating system at low ambient temperatures [17]. The system combined solar thermal and ASHP coupled through the triple heat exchanger to function into nine operating modes under different weather conditions to represent the operation of the system yearly. The study involved experimental analyses using a test rig established to investigate the time-varying operating characteristics of the integrated system. The experimental results show a dynamic balance in the heat transfer between water and refrigerant with PCM interlayer. However, the water temperature difference between the inlet and outlet of the evaporator and the PCM temperature fluctuates regularly around some balance points. Facci et al. [15] carried out a study to evaluate electricity-based heating involving smart integration of photovoltaics for heat pump TES system operation in residential applications. The study involved an investigation into the transformation of gas boilers to heat pumps powered by photovoltaics on one side and TES systems on the other side, for optimal performance of the heating system. Energy demand from a reference midrise apartment building was considered under three different climatic conditions. The assessment of four power plants based on energy cost and pollution potential was conducted for the analysis. A graphical method previously developed and validated was applied to analyse the performance of the power plants. Regarding the climatic conditions, the result indicated an energy savings of 41% and up to 78% reduction in carbon dioxide emission was achieved when the heat pump replaced the gas boiler.

Renaldi et al. [14] presented a design and operational optimisation model to assess heat pump-integrated TES system performance for dwelling heating in comparison with conventional heating systems. The model is comprised mainly of the heat demand design and operational parameters. The heating energy consumption, occupancy, and solar gain data were applied as input parameters for the heat demand model. The optimisation approach for residential heating involved the application of an op-

timal size and operational profile to save cost. The performance results indicated a higher capital and operational cost with direct mode heat pump operation compared to conventional heating systems. A representation of the operation of a heat pump-integrated TES system is illustrated in Figure 2.17.

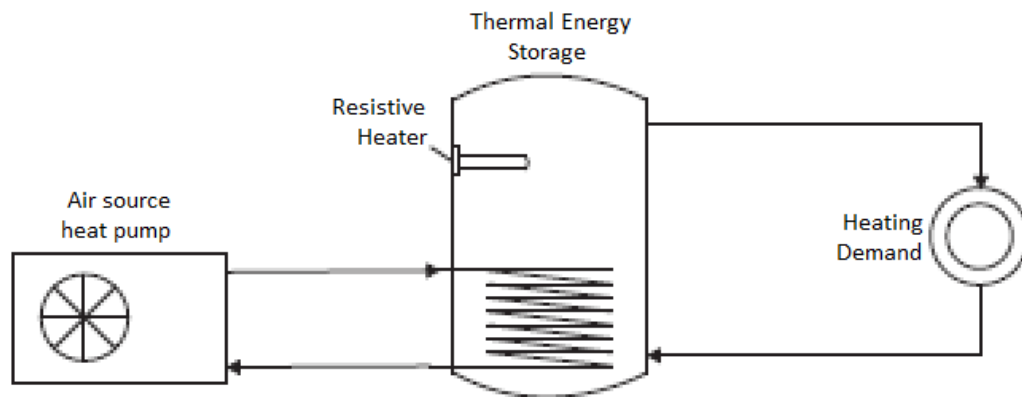


Figure 2.17: Model diagram of ASHP and TES tank with resistive backup heater for domestic wet central heating presented by Renaldi et al. [15].

However, the heat pump-integrated TES system operation in off-peak periods significantly reduces the operational cost. A detailed techno-economic analysis of ASHP combined with latent heat TES applied for space heating in China has been investigated [157]. In this study, developed mathematical models were used to evaluate the feasibility in the application of the proposed system from an energy, economic and environmental point of view. The proposed system was compared with a quasi-two-stage ASHP and other heating systems involving direct electric heating, coal-fired and wall-hanging gas boilers in Beijing, Harbin, Shanghai, and Shenyang of China. The results indicated that the heat pump of the quasi-two-stage and latent heat were suitable for space heating due to their energy-saving advantages and environmental protection capabilities. However, heat pump systems are associated with high initial and running costs compared to conventional heating systems. However, with the current government subsidy and incentives towards heat pump deployment and a discount towards obtaining units of latent heat TES system of up to 40%, the ASHP latent heat TES system will be of better choice in the severe cold regions of China [157]. Similar work has also been conducted by Shah et al. [16] involving a field trial study with a heat pump-integrated TES system in a domestic retrofit installation. The

heat pump operates to provide a flow temperature of 75°C as a direct way to replace boiler operation without the replacement of the existing heating systems. Two terrace houses that represent 28% of the Northern Ireland and UK housing stock were used in the trial. The heat pump integrated TES system was conditioned to operate in direct mode, storage mode, and combined mode to analyse the performance of the system. Figure 2.18 shows the schematic diagram for the application of the heating system in various operating modes.

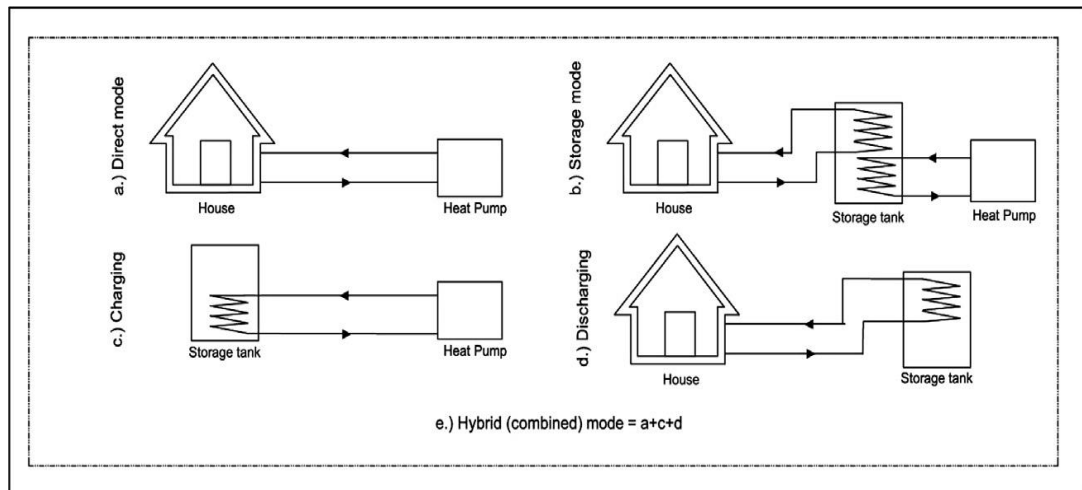


Figure 2.18: Schematic diagram of a high-temperature heat pump-integrated TES in various operating modes during the field trial test presented by Shah et al. [16].

The performance result indicated low efficiency with the storage mode operation due to a drop in COP because of the high flow temperature operation of the heat pump. However, higher heat output was obtained by the TES system due to the stored energy during the first heat call. This indicated that higher efficiency of the heat pump integrated TES system is achievable at low flow temperature for real house conditions. The suitability for a heat pump integrated TES system operation in a storage mode requires appropriate sizing to achieve better performance of the system.

The reviewed studies focused on the use of heat pump-integrated TES for wet central heating. The technology has proven to be effective in meeting the heating requirements of dwellings. However, current applications of this technology involve using the TES system for a limited period during the day to support the heat pump operation in heating dwellings. In this study, a pre-charged TES system charged by a heat

pump, is used to evaluate a thermal storage system's ability to fully meet the heat demand of a dwelling for the following day.

2.5 Next-day Heat Demand Profile Estimation

2.5.1 Introduction

The requirement specification for a TES system is obtained using dwelling heat demand profile. For any given dwelling, the yearly heating demand profile is scanned to determine the maximum daily energy requirement. This is then used to size the TES. In this work, a day-ahead heat demand profile is used to guide TES charging and discharging. The scheme is independent of how the heat demand profiles are derived. Various methods are available for the estimation of day-ahead heat demand profiles. Csoknyai et al. [158] indicated that a building's physical characteristics, location and technical system quality play a more important role in consumption than human factors in the case of heating and cooling. This is significant since every nation has housing stocks in which each house type has different physical and thermal properties. Dynamic building simulation software [159,160] provides a way to characterise a dwelling's heat demand profile. In the present work, the approach is used to emulate a day-ahead forecaster in a realistic manner to test the robustness of proposed TES/heat pump solutions. ESP-r, a building energy performance assessment tool, is used to simulate a common dwelling to obtain next-day heat demand profiles.

2.5.2 Estimation Approaches

Previous studies [160,161] have identified three main approaches to estimating a dwelling's day-ahead heat demand profile. These include an experimental or field trial, data-driven or statistical methods, and estimation using engineering modelling methods. Many projects have involved approaches that combine two or more of these methods, for example, Reynders Glen et al. [25] combined the statistical and engineering approach; Kelly and Cockroft [24] combined the field trial and engineering approach; and Wang and Mancarella [162] employed engineering modelling methods and data-driven approaches. These types of approaches are referred to as hybrid methods [160]. An example of this approach involves using multi-variable regression analysis and a machine learning algorithm to estimate heat demand profiles. Table 2.8 summarises the various approaches applied to estimate the next day's heat

Table 2.8: Studies involving prediction of next-day heat demand profiles.

Author	Approach	Methodology	Study conducted
Yao et al. [163]	Engineering methods	Use of thermal resistance network modeling technique	Daily heat demand profiles for space heating, hot water, and appliances were estimated for UK homes.
Watson et al. [164]	Field trial	Monitored data on heat pump electricity demand	Half-hour mean daily profiles of electricity demand of heat pumps were measured over a winter period in a field trial.
Reynders Glen et al. [25]	Hybrid involving statistical and engineering methods	The use of statistical black-box and grey-box model methodology	The day-ahead predictions of the thermal response of dwellings were analysed using the IDEAS package in Modelica.
De Rosa et al. [165]	Engineering methods	Application of TRNSYS and Energy-plus for building energy performance simulation	A simplified model was developed and implemented based on Matlab and Simulink. The tool was applied to predict the building energy demand.
Bunning et al. [166]	Statistical approach	Machine learning algorithm using artificial neural network	The next day building heat demand profile was predicted by artificial neural networks.
Ridley et al. [26]	Field trial	Monitored data on domestic heating gas consumption	A heat meter was applied to London dwellings. The heat demand profiles of space heating were estimated.
Allison et al. [167]	A hybrid field trial and engineering method	ESP-r simulation and monitored heat demand of building by a predictive controller	The next-day heat demand of building was monitored by the controller and compared with building simulation results.
Ruiz et al. [27]	Statistical approach using machine learning	Application of regression tree, support vector machine, and neural network	Every hour building energy was predicted using machine learning. Visual Monitoring Energy was used to predict energy consumption and expected expenditure in the future.

demand profiles. These approaches may be further classified as top-down and bottom-up. The top-down approach focuses on forecasting and predicting heat demand profiles based on historic hourly load data [168]. The approach applies to a relatively coarse scale of load data profiles. In the bottom-up approach, the heat demand profiles are generated through monitored, metered, or predicted building energy data. The application of building energy simulation to estimate the heat demand profile has advantages compared to the top-down approach [158,161,168]. This is because the building energy simulation provides a comprehensive and more accurate energy estimate due to its ability to model individual components such as the occupancy patterns, the building's physical and thermal properties and the use of HVAC systems to assess various scenarios. These factors may not have been accounted for, in the top-down approach as it relies on simplified models and generalised assumptions.

The hybrid approach can forecast and predict more accurate results. This is because it combines the application of two or more approaches to predict the heat demand profile [25,160]. However, hybrid methods may incur additional costs where field trials are involved. In addition, more time is required for the accurate prediction of heat demand profiles when two or more approaches are involved. The hybrid approach has been demonstrated using the statistical black-box and grey-box methods to estimate the heat demand profile. The black-box approach is like a grey-box method. The black-box approach focuses on the input and output relationship of the system. In this case, a statistical analysis is applied to define parameters that estimate a dwelling heating performance. However, the grey-box methods utilise building information to develop a mathematical model [25].

Reynders et al. [25] used grey-box and statistical black-box models that involve sets of differential equations that define building dynamics. The simulation was conducted to predict the next-day dwelling's heating temperature using the characteristics of the dwelling physical model. The dwelling's indoor temperature can be applied to estimate heat demand profiles. Day-ahead temperature predictions of high accuracy were applied with reduced-order models to optimise energy for heating and cooling and the integration of renewable energy sources. The input for the models includes measurements obtained for indoor temperature, heat flux, ambient temperature, radi-

ators' heat emission, internal gains, and solar gain. The simulations were conducted using the IDEAS library developed at KU-Leuven [25] based on the control volume method described by Beatens et al. [169]. The IDEAS library is implemented in Modelica to represent transient thermal processes based on the control volume. Allison et al. [167] developed and implemented a load-shifting predictive controller in a low-carbon house with an under-flow heating system. The controller predicted the next day's heating requirement of the house based on forecasted air temperature and solar radiation levels to achieve thermal comfort. Esp-r tool was used to model the test house and building energy performance simulations were conducted to estimate the heating charge required to maintain a temperature set point of 21°C for the next day. The monitored data showed that the predictive controller resulted in better thermal performance than the simulated results.

Among these methods, the experimental or field trial approach provides a more accurate estimation as it involves the use of physical building in a real situation. Hybrid methods have also been demonstrated to provide highly accurate results. This is because the method combines two or more approaches to predict the heat demand profiles. Hybrid approaches are expensive and time-consuming with more resources involved. The engineering modelling method is the most cost-effective and provides accurate results as evidenced by many researchers [170–172]. In this work, an engineering modelling approach is chosen to predict the next-day dwelling heat demand profile. The engineering modelling method involves the virtual implementation of experimental tests or field trials.

2.5.3 The Engineering Modelling Methods

Engineering methods have been extensively used by researchers to estimate day-ahead heating profiles. The approach utilises a mathematical model of a dwelling to simulate its performance realistically. Building design parameters such as insulation level, air permeability, thermal capacity, and material properties are imposed to estimate the heat demand profiles under changing weather conditions. Ferrari et al. [161] indicated that this approach can provide accurate estimations. Kelly et al. [28] used ESP-r to generate dwelling heat demand profiles for load shifting at a 1-minute time resolution. This was added to corresponding household electrical appliance demand

data to produce a total electrical demand profile for a single household. The approach was applied to develop energy demand profiles for 50 detached dwellings with hypothesised heat pump upgrades. The heat demand profile of a single-family dwelling has been estimated using building simulation through using TRNSYS [170]. The performance of the dwelling was assessed via a model comprising constructions, an HVAC system, control devices and use schedules. The 110 m² dwelling had four occupants. The heating energy demands of the dwelling were expressed as a function of the building type, size, construction materials, occupancy, and location.

De Rosa et al. [165] used TRNSYS and EnergyPlus to conduct simulations, with the predicted heating and cooling energy demands used to generate a simplified model based on a modified degree-days approach. The simplified model was implemented using Matlab and Simulink. Yao et al. [173] developed a program based on a heat flow resistance network method. The model was then applied to obtain daily heat demand profiles for four UK house types, including flats, detached, semi-detached, and mid-terraced dwellings [163]. The method was also applied to predict the daily breakdown of demand for appliances and domestic hot water. ESP-r was applied in the project to validate the simplified model.

2.5.3.1 Development of a Dwelling Model

It should be noted that the developed method can utilise heat demand profiles however obtained. Likewise, a demand profile can correspond to any dwelling type from any country, rendering the TES design procedure generally applicable. However, in this work, the ESP-r tool is applied to develop a dwelling model required to predict the next-day heat demand profile. The SHCS, as an example of a large, diverse estate, was used to identify dwelling types for processing in the project. The Scottish housing stock has the following characteristics.

- The stock is large with up to 2.5 million occupied dwellings [174].
- The stock is diverse with urban and rural settlements across the country.
- The stock is characterised by variations in the type, age, and size of dwelling.
- Table 2.9 shows the comprising archetypes.
- Table 2.10 shows the distribution of the stock by age and type.

Table 2.9: Scottish housing types SHCS [175].

House type	Characteristics
Detached	Free standing with no adjoining dwelling
Semi-detached	One other adjoining dwelling
Terraced	Forming part of a row with other adjoining dwellings
Tenement	Flats within a block with shared access
Four-in-block	Each flat in a block has its independent access
Tower block	Maisonettes and flats in a high-rise or multi-storey block
Conversion	Flats resulting from the conversion of a house or non-residential building

Table 2.10: Number of occupied dwellings (in thousands) and their percentage distribution by age band and type SHCS [174].

Dwelling age	Detached	Semi-detached	Terraced	Tenement	Other flats	Total
Pre-1919	94 [4]	60 [2]	71 [3]	208 [8]	54 [2]	486 [19]
1919 - 1944	50 [2]	72 [3]	36 [1]	35 [1]	83 [3]	277 [11]
1945 - 1964	52 [2]	145 [6]	171 [7]	83 [3]	74 [3]	525 [21]
1965 - 1982	124 [5]	117 [5]	169 [7]	92 [4]	54 [2]	556 [22]
Post - 1982	263 [10]	107 [4]	85 [3]	176 [7]	55 [2]	685 [27]
Total	584 [23]	500 [20]	531 [21]	595 [24]	319 [13]	2529 100%

Other highlights include the following.

- There were 3174 surveyed properties contributing to the statistical report published in 2021.
- The highest total number of dwellings of a single type is tenement flats at 24% (595,000). The highest total number of dwellings by age is 27% (685,000) contained in the post-1982 dwellings category.
- It can be deduced from
- Table 2.10 that the highest total number of dwellings by type and age band is in the post-1982 detached category at 10% (263,000).
- This indicated that most of the Scottish dwellings by type and age band are post-1982 detached categories. For this reason, the detached category is selected as a case study dwelling in this work, to integrate a thermal store. An example of a detached dwelling is illustrated in Figure 2.19.



Figure 2.19: Typical detached dwellings [176].

Figure 2.20 shows a typical detached dwelling wireframe which comprised the living room, kitchen, and bedroom with a total building floor area of 136 m² and volume of 448 m³ respectively based on the geometric data provided in [28].

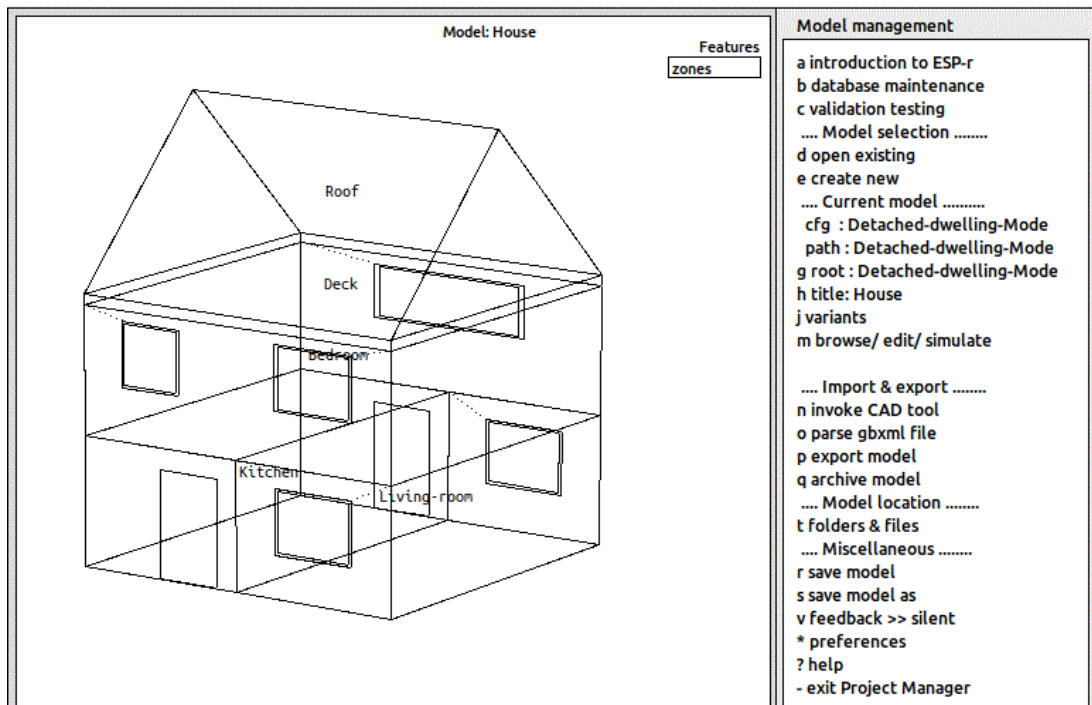


Figure 2.20: The thermal zone geometry of the detached dwelling model.

The dwelling was modelled using the ESP-r tool according to design parameter variations with an example established by Clarke et al. [177] and listed in Tables 2.11 and 2.12. ESP-r is designed to incorporate various building materials, construction, and systems. These include walls, roofs, floors, doors, windows, and controls that are bonded together based on the building design specifications. The building is considered a thermal zone that is affected by solar gain, air movement and casual gain from occupant, light, and equipment. The materials, properties, and construction used in the building are further elaborated in Chapter 4.

To assess the dwelling heating performance, an energy performance simulation will be conducted in the ESP-r. The next step is to predict the dwelling heat demand profile for the following day which will then be used to determine the requirement specification of the TES system. The procedure for predicting the next-day heat demand profiles of dwellings is explained in Chapter 3.

Table 2.11: Representative dwelling design parameter [177].

Design Parameter	Value	Comments
Window size:		
Large	10% of floor area	1981 Building Regulations
Small	25% of floor area	1997 Building Regulations
Insulation level:		
	<i>U</i> -value ($\text{Wm}^{-2} \text{K}^{-1}$):	
	wall floor roof ^{6c} :	
Poor	1.50, 0.86, 0.93	Pre 1965 ^a
Standard	0.60, 0.45, 0.35	1981 Building Regulations
High	0.30, 0.25, 0.16	2002 Building Regulations
Capacity level:		
	Effusivity ($\text{Jm}^{-2} \text{K}^{-1} \text{s}^{-1/2}$):	
Low	675	Timber
Medium	1095	Cavity wall
High	1285	Solid wall
Capacity Position:		
Inner		Internal
Outer		External
Air Permeability:		
	Air change rate:	
Poor	1.5	Typical
Standard	1.0	1997 Building Regulations
Tight	0.5	Indoor Environment & Health ^b

^aNo governing thermal regulation exists and therefore construction has minimal thermal insulation.

^bISBN 91-7257-025-3.

^cCorresponding *U*-values for single, double, and advanced glazing associated with windows.

Table 2.12: Scottish construction categories [177,178].

Category	%	Sub-category	Related house
Cavity wall brick/block	67	Cavity throughout—plastered on hard	Detached
		Hybrid—cavity dividing walls with single skin in-fill (brick, block, or cladding system) to front and rear—part plaster on hard/part lined.	Semi-detached Terraced Tenement/maisonette Four-in-block Conversion
			Detached
			Semi-detached
			Terraced Tenement/maisonette
Solid wall brick/block sand- stone whin/granite	23	Sandstone/whin/granite—strapped and lined	Detached
		Concrete block—plaster on hard	Semi-detached
		Concrete block—strapped and lined.	Terraced Tenement/maisonette
Non-traditional tim- ber concrete metal	10	Hollow concrete block—plastered on hard	Detached
		As above—strapped and lined.	Semi-detached
		Swedish timber or steel frame—not insulated	Terraced
		Swedish timber or steel frame—insulated	Tenement/maisonette
		No fines concrete—plaster on hard	Four-in-a-block
		As above—strapped and lined	Tower block
	Solid/in-situ concrete—plaster on hard		
	As above—strapped and lined.		

2.6 Chapter Summary

The operation of domestic wet central heating especially in dwellings has been studied with investigation of how the heating system works. The heating operation is delivered using either a gas-fired boiler or heat pump as the heat source. The different types of gas-fired boilers: open-vented, sealed systems, and sealed combi boiler systems used in dwelling wet central heating have been described. The sealed condensing boiler system has been the best and most used among all types. Heat pumps such as air, water, and ground source types are also used in dwelling wet central heating. Among all these types, the ASHP is the most widely used heat pump.

A literature review based on the application of heat pump wet central heating in dwellings has been conducted to analyse the system's performance. It was found that the heat pump systems applied in dwelling wet central heating operate at lower heat output compared to a gas/oil-fired boiler and a high cost of electricity is incurred in always running the system. This has prompted research into the alternative operation of heat pumps to deliver heat at higher COP and integration of heat pumps with the TES system to save the high cost of electricity.

Three methods used in storing thermal energy were reviewed: sensible, latent, and thermochemical heat storage. The THS methods are complex and still under research and developmental stages. Because of these barriers, sensible and latent heat storage methods are mostly considered for application in wet central heating. The SHS and LHS materials within the operating temperature for wet central heating are used. Heat generators such as heat pumps, solar and electric heaters are used to charge TES material. The TES material is discharged to provide heat demands in dwellings.

The application of LHS materials in wet central heating offers further advantages. LHS is associated with a small storage tank volume, high storage density, and high efficiency compared to the SHS systems. The high latent heat released during phase transition makes LHS materials more attractive for thermal storage applications in wet central heating. Various heat exchanger designs were investigated for an effective and efficient operation of the TES system. The cylinder model of the shell-and-tube heat exchanger design and commercially available PCMs; paraffin and inorganic salt in the operating temperature range for wet central heating were selected.

The solution to achieving better efficiency of the heat pump integrated TES system can be attributed to the appropriate sizing of the heating system and its application in dwelling wet central heating. The benefits and challenges in the application of the TES system especially during the off-peak period of heat pump operation in dwelling wet central heating have been analysed. Moreover, a literature review pertaining to the application of heat pump-integrated TES systems in dwelling wet central heating has been conducted to analyse the performance benefit of the use of TES systems in dwelling wet central heating. It was found that most past work focuses on the use of a TES system to fulfil a portion of the daily heating demand or as a buffer in the heating network. This contrasts with the present work, where the TES system is used to fully meet the dwelling's daily heat demand. In this study, the TES system is pre-charged to provide continuous space heating of the dwelling over the following 24-hour period before being pre-charged again.

Different techniques for the estimation of dwelling heat demand profiles were investigated, and the most suitable technique was identified. The most common methods used include experimental/field trials, statistical analysis, and engineering modelling.

Hybrids of these methods have also been explored to be highly accurate. However, they are costly and time-consuming. The experimental/field trial approach provides more accurate results as it involves physical building models in a real-world situation to evaluate building energy performance. This method can be expensive because it requires access to real buildings to measure their energy performance and estimate heating requirements over a certain period.

The engineering modelling method is selected to predict the dwelling's next-day heat demand profiles. This method offers the most cost-effective and accurate estimations. The engineering modelling method involves a virtual implementation of the experimental or field trial approach by considering the building's characteristics, material properties and usage patterns under varying weather conditions in a building energy simulation tool. A detached dwelling was identified and developed in the ESP-r to predict the dwelling's next-day heat demand profiles. A step-by-step procedure for conducting this work is explained in Chapter 3.

3 Research Procedure

3.1 Introduction

This chapter details a step-by-step guide to conduct this work. The guide serves as a procedure for assessing the load-shifting capabilities of a TES system pre-charged by a domestic heat pump to fully meet a dwelling's space heating demand. The most important and initial task is to determine the requirement specification of the TES system (step 1). First, a dwelling heat demand profile is established. Various methods can be applied to this end [170,179], as described in the literature review (Chapter 2). The most applied methods are experimental/field trials, statistical analysis, and engineering modelling [180,181]. The next-day dwelling's heat demand profiles are obtained and integrated to determine the required capacity of the TES system for a discrete period. The information on the storage capacity would be used to obtain the correct design and sizing of the TES system required to meet the dwelling's next-day heat demand profile (step 2). However, a suitable TES material and heat exchanger design configuration is needed before this. A study has been conducted in Chapter 2, and the TES material and heat exchanger design suitable for wet central heating was selected for the storage assessment. In addition, the procedure also involves a guide for TES model development, verification and validation using a similar study that has been analysed (step 3). The TES system design and sizing information is used to create a CFD model of the thermal storage vessels incorporating the heat exchanger design and storage material, to produce the required output from the storage system at discharge time. The TES model is applied for numerical solutions to determine the thermal behaviour and characteristics of the storage system during the charging and discharging processes (step 4). Charge-time simulations are then conducted using a domestic heat pump flow rate and temperature with the specification of initial and boundary conditions. Simulations for the TES system charging are initiated until the storage system is fully charged or the next-day heating charge required of a dwelling is achieved. At discharge time, HTF flow control that involves varying the inlet mass flow rate and temperature is used to obtain storage output that matches the dwelling's heat demand. In situations where the TES system is unable to fulfil the heat demand, the TES system is resized, and charge and discharge simulations are repeated. Figure

3.1 shows the procedure flow chart indicating the various tasks that need to be undertaken, to achieve the study's objectives. The procedure is applied to assess the heat pump-integrated TES system's capability to provide the output requirement to match

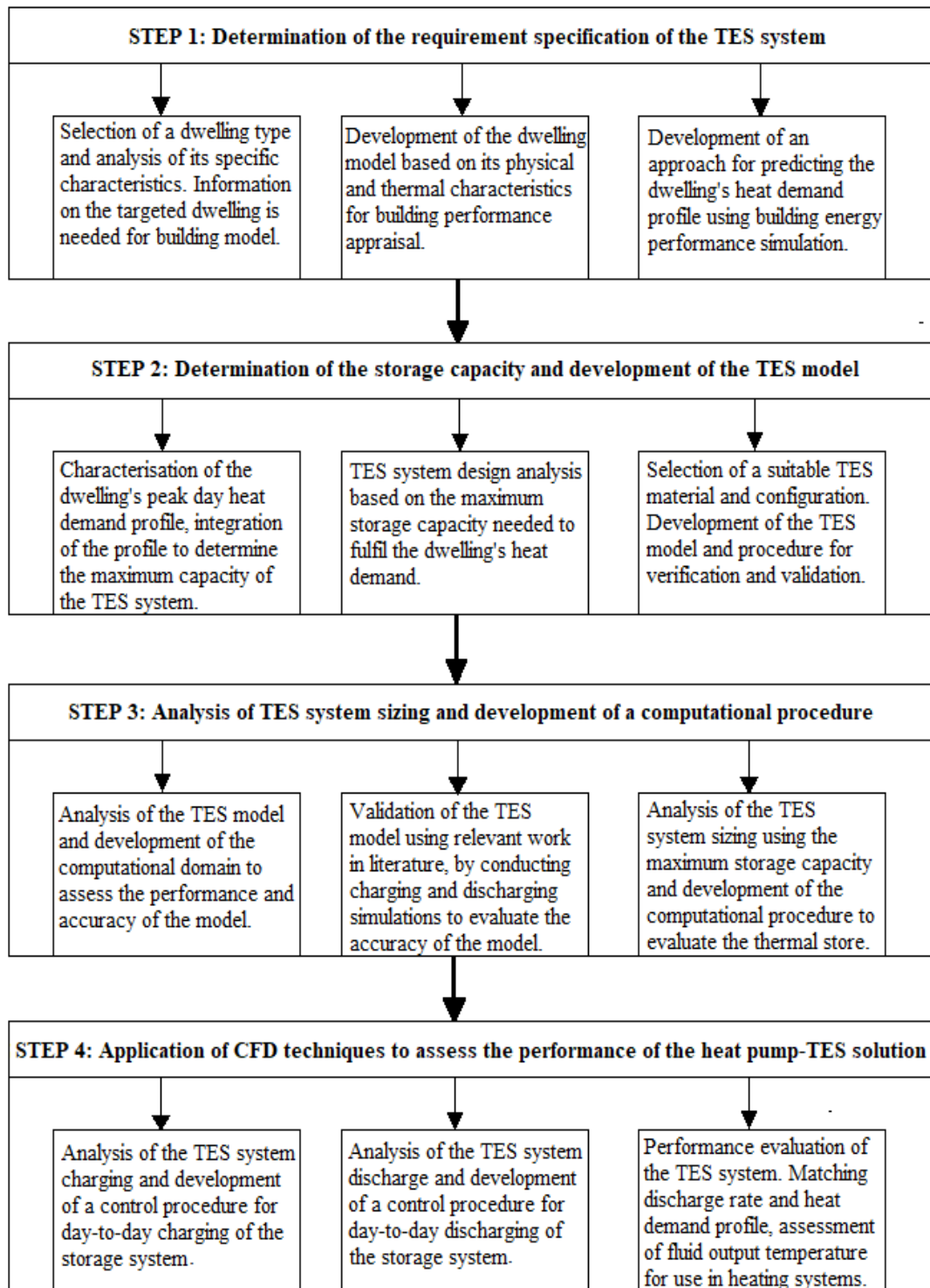


Figure 3.1: Procedure flow chart.

a dwelling's heat demand over any period. The procedure can be implemented in real-world scenarios by utilising the heat demand of any dwelling type located anywhere in the world. In practice, a predictive charge/discharge controller can be applied to guide the operation of the TES system. The charge controller would have access to the next day's heat demand estimate [167]. This would probably be based on a simple algorithm used for charging remotely controlled storage heaters [182], to obtain a heating charge for the next day. The discharge controller modulates the mass flow rates to match the load.

The methodology provides an overview of how the study is conducted, utilizing dynamic models of the thermal store and building to evaluate the system's performance. In this work, there is no attempt to dynamically couple the two models. Instead, a simple model is introduced to act as the linkage between the TES and dwelling heating system. The following steps further elaborate on how the study's methodology is implemented to evaluate the overall system performance.

STEP 1 involves an analysis of the dynamic building model. A common dwelling type is selected and information about the dwelling is used to develop the dwelling model. An approach is devised to estimate the dwelling's next-day heat demand profile (potentially repetitively throughout the heating season). In this study, a dynamic building simulation tool, ESP-r, is employed to obtain the dwelling's heat demand profile.

STEP 2 requires a study to analyse the thermal storage model, which includes the selection of an appropriate storage medium and suitable heat exchanger configuration, as well as the development of a procedure to validate the thermal store model. This step also involves analysing the TES system design and determining the maximum storage capacity based on the dwelling's peak daily heat demand.

STEP 3 involves validating the thermal storage model to assess its accuracy and reliability for use in wet central heating systems. In this step, an analysis is performed to replicate experimental work found in the literature, which is used to validate the storage model. This step also includes a demonstration of the sizing process for the TES

system (based on either the peak demand or a percentage of the peak) to evaluate its performance.

STEP 4 describes the application of the CFD model to simulate the charging and discharging processes of the TES system to analyse its performance. This step involves a model to serve as the linkage between the thermal storage and dwelling model. In this work, the linkage is achieved by transforming the radiator inlet temperature (i.e. the TES supply temperature) to a radiator outlet temperature (i.e. the TES inlet temperature) as a function of the known dwelling heat load prevailing at the time. In this way the TES discharge rate is adjusted to match the dwelling's heat demand throughout the day.

3.2 Determine the TES System Requirement Specification

Day-ahead dwelling heat demand profiles are obtained to establish the TES system energy charge requirement. Dwellings can be decomposed into different categories [175], with varying heat demands due to variations in their characteristics such as form and fabric, systems and control, and weather context. The analysis of dwelling categories was conducted in Chapter 2, detached dwelling was chosen from the Scottish housing stock for further study. Day-ahead heat demand profiles of the different dwelling types are obtained by engineering modelling methods, statistical analysis or using monitored data available from the literature [161,183], to determine the storage system's requirement. In this work, a dwelling heat demand profile is determined by an engineering modelling method using the ESP-r simulation tool. It is always important to ensure the quality of the model to predict the heat demand profile accurately. The accuracy of the simulation model is ensured by utilising standard parameter values to predict the heat demand of the detached dwelling. ESP-r has been extensively validated [184], and is proven to be reliable for predicting building heat demand. The dwelling's peak daily heat demand profile (as will be shown in Figure 4.4) is processed to estimate the required TES system's capacity that can meet the next-day heat demand.

3.3 Determine the TES System Size and Capacity

Integration of a dwelling's next-day heat demand profile gives the amount of energy that should be stored (charge side), while the hourly heat demands define the discrete discharges throughout the following day. The capacity information is applied using the appropriate heat exchanger design and TES material (which can be found in Table 6.1) for storage sizing. This is important because it determines the storage system size required to meet the next-day dwelling's heat demand. The TES system capacity defines the amount of heat to be charged and discharged from the storage system within a specified period. The charge/discharge time is important in determining the effectiveness and efficiency of the storage system in meeting the dwelling's heat demand. In the present work, the TES size and capacity are determined by the number of PCM elements equivalent to the maximum 24-hour energy demand of a dwelling.

3.4 Develop the TES Model and Computational Procedure

The TES system consists of vertical cylindrical enclosures (PCM elements) arranged in parallel in a container is illustrated, see Figure 6.2. The PCM elements are identical and have the same size, capacity, and storage medium. In this case, the capacity of the TES system is obtained by multiplying the capacity of a single PCM element by the number of PCM elements in the storage system. The TES system is sized using the dwelling's peak heat demand. In this study, a 2D axisymmetric geometry of the PCM element is used to model the TES system. The axisymmetric 2D domain of the storage element is used because it allows easy visualisation, facilitates meshing and reduces computational time. The CFD model is used to evaluate the performance of the storage system that comprises the heat exchanger, PCM and HTF, during charging and discharging for effective system's operation.

3.4.1 Analyse TES Components

The cylinder model of a shell-and-tube heat exchanger is adopted for the storage element as this configuration has proven to be the best design to achieve good heat transfer performance in wet central heating applications [22,111]. The cylinder model of the storage element comprises an HTF section described as the tube and a PCM section located in the annulus. The HTF (here water) flows through the tube to transfer heat through conduction at the tube wall to charge and discharge the PCM in the

annulus. It is assumed that there is no fouling to ensure the effectiveness of the heat exchanger. A preliminary study is conducted to investigate the compatibility of the heat exchanger with the HTF and PCM applied within their operating range to achieve greater performance of the system. An example of investigations involving heat exchanger compatibility is described in [185].

3.4.2 Set out the HTF and TES Material Section

The geometry of the PCM element is analysed to determine its capacity for use in a replica that represents the complete TES system. This defines the storage volume that gives the required capacity of the TES system suitable for domestic wet central heating applications. The geometry of the PCM element is established with a pipe diameter of 22 mm (commonly used in most dwellings) for HTF flow and a shell diameter of 80 mm that encloses the PCM over a length of 1 m. The schematic diagram of the storage element is presented in Figure 7.2. A preliminary study is conducted to determine the PCM type that can produce the required capacity of the TES system by the given dimensions that define the storage volume. This enables the development of an axisymmetric 2D geometry of the storage element, encompassing the HTF domain, the PCM domain and the shell-and-tube walls. The 2D axisymmetric domain is converted into a discretised form, as required for CFD simulation, to validate and analyse the dynamic performance of the storage system.

3.4.3 Validate the TES System Model

To determine whether the storage system can meet the heat demand of a dwelling, the TES model's performance accuracy is assessed using a similar model. The TES model, which consists of the PCM, water, and shell-and-tube heat exchanger sections is applied to validate the storage model. An experimental test of a similar storage model available in the literature [186] is emulated using CFD software, Fluent. The thermophysical properties of the storage material with the initial and boundary conditions used in the experimental test, are implemented to simulate the model. The governing equations including continuity, momentum, and energy, are solved using the finite volume method. The accuracy of the TES model is verified by comparing the storage temperature variation with that of the reported work during the charging and discharging processes as evident in many studies [186–189]. The validity of the stor-

age model is judged by analysing the variation of the storage system's HTF outlet temperature and the average PCM temperature at different locations over time and comparing it with the experimental data and numerical results of Longeon et al. [186]. A comprehensive analysis of the TES model validation procedure is presented in Chapter 5.

3.4.4 Discretise the TES System CFD Domain

CFD techniques are applied to analyse the thermal performance and behaviour of the storage element representing the TES system. The 2D axisymmetric geometry of the storage element is discretised into a computational domain with 11,000 cells in the HTF and 28,000 cells in the PCM domains to investigate the performance of the TES system. The CFD Fluent software is applied to obtain the mesh domain (Figure 6.4). The computational domain represented by the mesh cells of a small control volume is applied to solve the continuity, momentum, and energy equations in the domain, to evaluate the thermal performance of the storage system when subjected to simulations. A preliminary study is carried out to investigate the methods for achieving a high-quality meshing. Careful consideration is given to examine the mesh quality, to ensure good performance of the TES system. A detailed procedure that was followed to achieve a high-quality mesh of the storage CFD domain is described in [13].

3.5 Assess the Heat pump-integrated TES System's Performance

3.5.1 Set-up Simulation

Before conducting simulations for charging and discharging the storage element, the accuracy of the CFD Fluent melting and solidification model is investigated and the results of the CFD solution are compared with the experimental data and numerical results of Longeon et al. [186]. The CFD domain of the storage element is discretised based on the mesh size used for validation. The discretised domain of the storage element is applied with the initial and boundary conditions, and thermophysical properties of the PCM to assess the performance of the heat pump-integrated TES system. The heat exchanger wall and its thermophysical properties are specified, coupled with the PCM and HTF and set for conduction heat transfer. The semi-implicit method for pressure linked equation (SIMPLE) algorithm is applied for the pressure-velocity coupling, a least square cell-based gradient and pressure staggering option

(PRESTO) for the pressure correction equation and spatial discretisation, the first-order upwind scheme is used for the momentum and energy equations, and the Boussinesq approximation for the effect of density variation in the CFD Fluent for charging and discharging simulations. Chapter 7 gives a description of the simulations set up for the charging and discharging the storage element.

3.5.1.1 Boundary and Initial Conditions

The boundary condition for the tube wall, which comprises the surfaces adjacent to the PCM and HTF domains, is defined as coupled energy transfer with no-slip shear thermal conditions. A heat flux thermal condition is specified at the outer wall adjacent to the PCM, while the top and bottom walls of the storage element are set as adiabatic to simplify the analysis. A constant inlet mass flow rate and temperature are set as the inlet conditions for the HTF domain during charging. In contrast, variable inlet mass flow rates and temperatures are used during discharging of the TES system. The computational domain of the storage element is set at an initial temperature of 36°C to simulate the charging, and 60°C for the discharging of the TES system.

3.5.2 Charge TES System

Simulations for the charging process are conducted with heat transfer through conduction and convection for the melting of PCM in the storage system. The computational domain is set at a reference temperature of 36°C for charging which is approximately the stabilised temperature of the system after discharging. A domestic heat pump with properties suitable for wet central heating is virtually implemented in the CFD Fluent software for simulation. The process of how the storage system is charged is illustrated in Figure 7.1. A 7kW heat pump with mass flow rates of 0.24 kg/s and 0.33 kg/s at a constant flow of 60°C is virtually applied to charge the storage element within a specified period to store the energy required for the next day. Day-ahead charging of the thermal store results in a suitable storage size and takes advantage of the lower night tariff. This approach allows for efficient storage charging during off-peak hours through (potentially) the integration of renewable energy sources, ensuring that the dwelling's heating demand is met effectively. This makes it a practical option for managing heating needs in residential settings. Storing for a shorter period reduces the required storage size but increases operational costs due to

the daytime operation of heat pumps. The PCM, which is at a lower temperature, absorbs heat at the HTF wall until it is completely melted such that the heat stored can be retrieved to deliver the heat output needed to meet the dwelling's heat demand upon discharging the TES system.

3.5.3 Discharge TES System

The pre-charged TES system is discharged to extract the stored energy from the storage system. Simulations for storage system discharge, are conducted using a flow of water at a lower temperature compared to the storage medium [190]. The required heating power output is extracted during discharging using variable HTF inlet flow control. A schematic diagram that describes the storage discharge is presented (see Figure 7.10). The TES system is set at a reference temperature of 60°C assuming a full charge of the thermal storage is achieved. The radiator return temperatures (TES inlet temperature) are determined from the (variable) HTF temperature and mass flow rate from the thermal store and the known heat demand. As a function of the TES state, a controller then determines the new temperature and mass flow rate supplied of the HTF supplied to the radiator. The TES system is conditioned to discharge using HTF inlet mass flow rates that are comparably lower to the ones used for the charging process, depending on the heat output requirement at various time steps during discharging. The procedure is carried out to match the TES heat output to the dwelling heat demand while obtaining a useful hot water return temperature. An analysis of the TES system's performance based on the delivered heat and HTF temperature output is given in Chapter 7.

3.5.4 Match Heat Demand and Power Output Profiles

Simulations are conducted to discharge the storage system in a manner to obtain the storage power output that matches the heat demand profile of a given dwelling. In practice, a proportional/integral/derivative (PID) controller can be used to ensure this match. In this work, an expression for the HTF inlet mass flow rate is applied to predict the TES power output during a given period. The time-variant HTF inlet control conditions used in discharging the storage system are necessary due to variations in the heating load with time. The TES power output is predicted using frequent control of the HTF inlet mass flow rate and temperature during the discharging process to

extract the sensible heat from the storage system. However, the HTF inlet control is applied after a longer successive period for the latent heat extraction to ensure a close match. The sensible heat is extracted at 0–6h and 16–24h and latent heat between the period 6–16h during the storage discharge. A detailed analysis for comparison of the TES power output and dwelling heat demand profiles is presented in Figure 7.20.

3.6 Chapter Summary

The procedure followed to accomplish the study's objectives is summarised as follows:

- Determine the requirement specification of the TES system. This involves obtaining the next-day dwelling's heat demand profile and integrating it to define the maximum capacity and size of the TES system.
- Select an appropriate heat exchanger design configuration and a suitable thermal storage medium based on the operational characteristic of a domestic heat pump wet central heating. This has been conducted in Chapter 2.
- Develop a TES model and apply CFD techniques to validate its accuracy and assess its thermal performance. In addition, create a computational procedure and discretise the CFD domain of the TES system.
- Set up simulations using the computational domain of the TES system with the specification of the thermophysical properties of the storage components, and the initial and boundary conditions for charging and discharging, to evaluate the performance of the storage system as in real-life situations.
- Conduct simulations using the operational characteristics (the mass flow rate and temperature) of a domestic heat pump to charge the TES system and analyse the thermal behaviour and performance characteristics of the storage system during the charging process.
- Conduct simulations to discharge the TES system in a manner that predicts the storage power output matching the dwelling heat demand profile while achieving a useful fluid outlet temperature during the discharging period.

- Analyse the performance of the heat pump integrated TES system solution by comparing the storage power output with the dwelling heat demand profile and justify the implication of the HTF output temperature for the performance of heating systems in dwellings.

4 Generation of a Test Heat Demand Profile

4.1 Introduction

To effectively integrate TES into a heat pump system and evaluate the load-shifting possibilities in residential buildings, it is crucial to predict the detached dwelling's heat demand profile required to accurately size the TES system. This will enhance the system's ability to respond to heat demand in buildings. This chapter presents a study to estimate the next-day heat demand profile of the dwelling, which is necessary to analyse the capacity of the TES system. The engineering modelling method is used to predict the next-day heating load of the detached dwelling. Considering various socio-economic parameters relating to the lifestyle, health status or family situation of households, different occupancy patterns lead to diverse heat demands across household types. Cuerda et al. [191] studied the full-day energy demand profile of a detached house that could be applied to sick or elderly individuals living indoors due to cultural attitudes or unfavourable climate conditions. The study analysed the impact of users' occupancy patterns obtained from standard occupancy profiles with full occupancy throughout the day on weekdays and weekends. The all-day full occupancy pattern is exemplified in the study conducted by Yao and Steemers [192], where the household could be a family with a minor child to care for, or retired couples and singles who require continuous full-day space heating, especially during severe winter conditions. In this work, a full-day occupancy is assumed for a three-person household, indicating the house is occupied and constantly requires heating for 24 hours. This type of occupancy pattern is not commonly found in UK dwellings. However, this study examines the full-day continuous heating pattern to assess the performance of the TES system. Considering that different dwellings have varying heat demand profiles; continuous or intermittent. The selection of a continuous heating profile corresponds to a worst-case scenario in terms of the total energy to be stored. The procedure is adaptable to any heat demand profile from a dwelling, ensuring flexibility in its use to demonstrate the thermal store performance using its maximum capacity. This suggests that the heat demand based on different heating patterns could be extracted from the full-day continuous heating scenario. This study involves the generation of a profile for a common type of dwelling to demonstrate

the TES system sizing. Therefore, the study analyses the full-day heat demand profile of the detached dwelling, to determine the capacity of the TES system. In this work, the peak heat demand of the detached dwelling will be used to size the TES system. Various factors such as the building's thermal characteristics, internal air temperature control, orientation, local climate and internal heat gains from occupancy and equipment [192] are considered in the building energy performance assessment to analyse the dwelling's heating load requirements. The developed detached dwelling model (refer to Figure 2.20) is used in the ESP-r tool to conduct the building energy performance simulation to predict the heat demand profile. The task involves the simulation of the dwelling model through a heating season to predict daily heat demand. In this way, it is possible to obtain the dwelling's peak day heat demand profile (worst case) weather condition. The peak daily heat demand profile is then used to determine the maximum storage capacity required to size the TES, and subsequently define the TES system pre-charge and later draw-off. This analysis followed the process as summarised in Figure 4.1 to determine the detached dwelling's peak day heat demand profile.

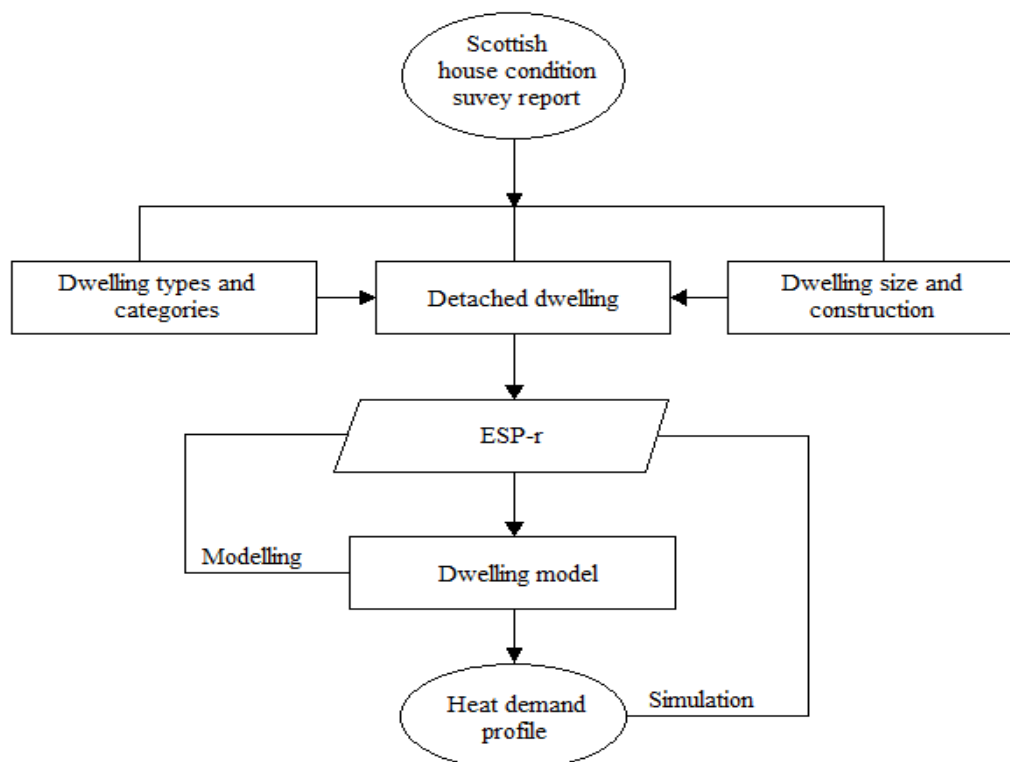


Figure 4.1: Determination of heat demand profile using ESP-r.

4.2 Determination of Dwelling Heat Demand Profile

To obtain a dwelling's heat demand profile, information on the target housing type needs to be obtained. For the present project, it was necessary to identify a dwelling that is common to a large housing stock. A detached dwelling was selected, and its defining parameters were used to construct the corresponding ESP-r model. The dwelling model is a typical detached house that comprises the thermal zone that defines the room space. The zone volume is bounded by surfaces made of various construction material types. ESP-r is distributed with comprehensive construction, material and optical database files that contain ready-to-use entities and templates for practitioners [193]. The files hold common entity data of various properties such as absorptivity, conductivity, density, emissivity, specific heat and solar transmission, reflection, and absorptivity available at different incident angles [193,194].

The dwelling was modelled with constructions that comprised an external wall of bricks typical of 1990 and UPVC frames used for windows. The present work focuses on the electrofitting of an existing dwelling and part of the requirement is to obtain the heat demand profile of a dwelling and use it to define the capacity of a TES system. This study does not account for hot water use in the detached dwelling, and the thermal store is not sized to meet this additional demand. However, it demonstrates the sizing procedure based on the dwelling's space heating demand. Sizing that includes hot water demand should be tackled in future work. The building model was designed with a double-layer glazing north-south oriented window. Table 4.1 lists the construction properties of the detached dwelling. The construction properties (U-values) used in modelling the detached dwelling are based on the standard U-values of the building elements provided in the SAP [195]

Table 4.1: Characteristics of the building construction.

Fabric element	U-value (W/m²K)	Area (m²)
Glazing	2.2	28
External walls	0.41	134
Ground floor	0.14	68
Upper floor ceiling	0.32	68
Average air change rate (air-changes-per-hour)		0.5

4.2.1 ESP-r Building Energy Simulation

The ESP-r building simulation tool allows users to assess the energy and environmental performance of a building and its energy systems over a specified period, such as a day, week, or year. It calculates all the energy and mass transfer processes underpinning building performance [28], using a mathematical model that represents possible energy flow path and their interactions within building envelopes to emulate reality. The simulator consists of parts related to the different domains such as conduction, convection and radiation heat exchanges, fluid flows networks, air movement, HVAC and control systems, and occupant behaviour. The building or plant system is made discrete by placing nodes at point of interest representing homogeneous and non-homogeneous physical volumes [30]. These control volumes correspond to thermal zones that consist of boundary surfaces, construction elements, room air, plant and renewable energy components. The nodes bounded by a region are in thermodynamic contact and conservation equations are applied to represent the transfer of energy, mass and momentum. The entire sets of equations are solved simultaneously for successive time steps using time series weather data and control to calculate future variables such as energy exchanges, fluid flows, and temperature evolution as a function of prevailing boundary conditions [30]. In the present work ESP-r is applied to predict the dwelling's heat demand profile. Prior to conducting simulation, the following parameters and boundary conditions are defined and specified in the simulation tool.

4.2.1.1 Weather data

ESP-r is distributed with extensive weather data for various locations worldwide. A weather data file in ESP-r contains yearly data held at hourly (or greater) frequency. The weather parameters comprise dry bulb temperature ($^{\circ}\text{C}$), direct and diffuse solar radiation (W/m^2), relative humidity (%), wind direction ($^{\circ}$), wind speed (m/s) and atmospheric pressure (mbar). The weather data can be augmented by format conversions applied to data from other sources [193]. Weather data for Aberdeen, which is already incorporated within the system was used for the building energy performance assessment. Aberdeen is a port city in the northeast of Scotland at latitude 57.15 N and longitude 2.09 W . This location was selected because the lowest-ever temperature recorded was in Aberdeenshire [196], and so was used to assess the performance

of the TES system. Note that other weather conditions, including anticipated future climate, can be readily incorporated into the procedure based on climate projection models or weather generators for specific locations.

4.2.1.2 Occupancy Characteristics

The detached house is designed for a three-person household with occupants present throughout the day. This means that the house is occupied and active 24 hours a day, where no differences are considered between weekdays and weekends [197]. The occupants were assumed to be sleeping between 22:00–6:00h and other spaces, the living room and kitchen were occupied for the rest of the day. The internal heat gain corresponds to the heat generated by the occupants, lighting and equipment. The ESP-r tool is distributed with schedules to define such internal heat gain profiles. Sensible and latent heat gains of 75W and 55W per person, with a 30% reduced gain during sleeping were set, with 2W/m² for lighting and 450W for equipment based on standard values from the CIBSE guide [197] were assumed.

4.2.1.3 Control and Operational Schedules

The ESP-r tool consists of different networks within the building, corresponding to ventilation, electrical and HVAC systems. An airflow schedule for the dwelling set an infiltration of 0.5 air changes per hour throughout the day. This value is the average air change rate used in the model and is typically applied in standard dwelling assessments [28,195] for air tightness. The built-in HVAC system in the ESP-r is applied to provide a maximum sensible heating input of 1kW to maintain a set point air temperature of 21°C typical for the Scottish [198] and UK [199] housing stock for thermal comfort. The building energy performance analysis is performed with the magnitude and time-varying casual gains from occupants, lighting and equipment set using average values and corresponding information defined in [197]. The Aberdeen weather data was specified and the November to March winter case assessment period [193], was used for the building performance simulation to identify daily heat demand throughout the heating season. When assessing the heating load, it is best practice to account for thermal bridging. Thermal bridges affect building performance, and there are various techniques to address them in building models. For instance, ESP-r has the capability to model thermal bridging explicitly, by modelling

3D heat flows effects, or by imposing factors that amplify construction conduction. In this work, a detailed thermal bridging analysis has not been carried out. However, the simplest approach was adopted by applying the SAP [195] default U-value of $0.15 \text{ W/m}^2\text{K}$, multiplied by the total area (m^2) of the building's external elements. The building performance simulations were conducted over 150 days at 15-minute time steps to predict the dwelling's heat demand profile.

An ESP-r simulation is conducted to assess the heating performance of the detached dwelling throughout the heating season. Factors such as ambient conditions, building characteristics, solar radiation, occupant behaviour, internal gains, and heating system efficiency primarily influence the energy required to maintain indoor thermal comfort. The simulated daily average heat demand and the prevailing ambient temperature over the heating season are presented in Appendix I. The analysis of the seasonal heat demand pattern shows the day with peak heat demand. Figures 4.2 and 4.3 illustrate the seasonal ambient temperature and the simulated heat demand pattern of the detached dwelling during the heating season.

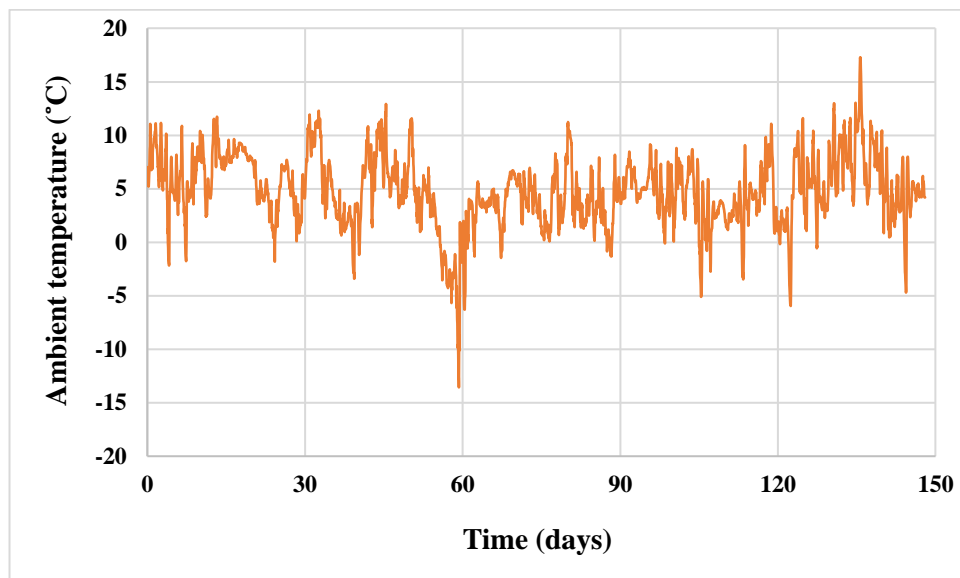


Figure 4.2: Variation of dry-bulb temperature during a typical winter scenario (November to March).

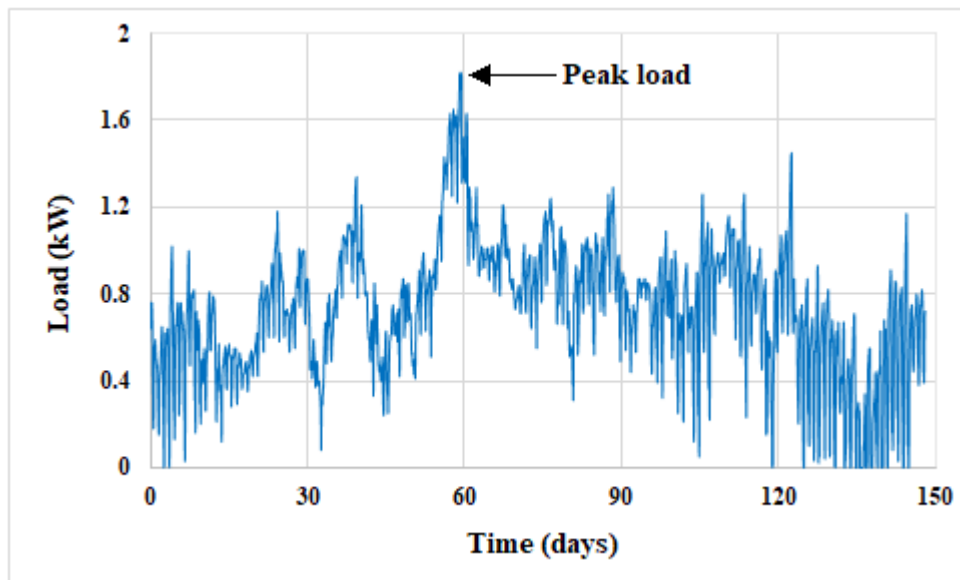


Figure 4.3: Seasonal heat demand profile of the detached dwelling for the typical winter scenario (November to March).

The seasonal heat demand pattern of the detached dwelling was analysed to extract the peak daily heat demand during the heating season. The day with the peak load (kW) corresponds to the maximum energy demand (kWh), which occurs on 28 December as depicted in the seasonal demand profile and outlined in Appendix I. This analysis determines the thermal storage size needed to meet the peak daily heat demand, indicating the sizing approach to be applied, to ensure that the next-day's heating demand throughout the season can be met using the same thermal store size.

The seasonal heat demand profile can be used to determine the storage capacity for other representative periods. However, determining the storage system's maximum capacity based on the peak day heat demand enables a single TES system to meet the dwelling's daily heating needs. Figure 4.4 presents the simulated peak day heat demand profile of the detached dwelling. The peak day heat demand is used to assess the performance of the TES system in fulfilling the space heating needs.

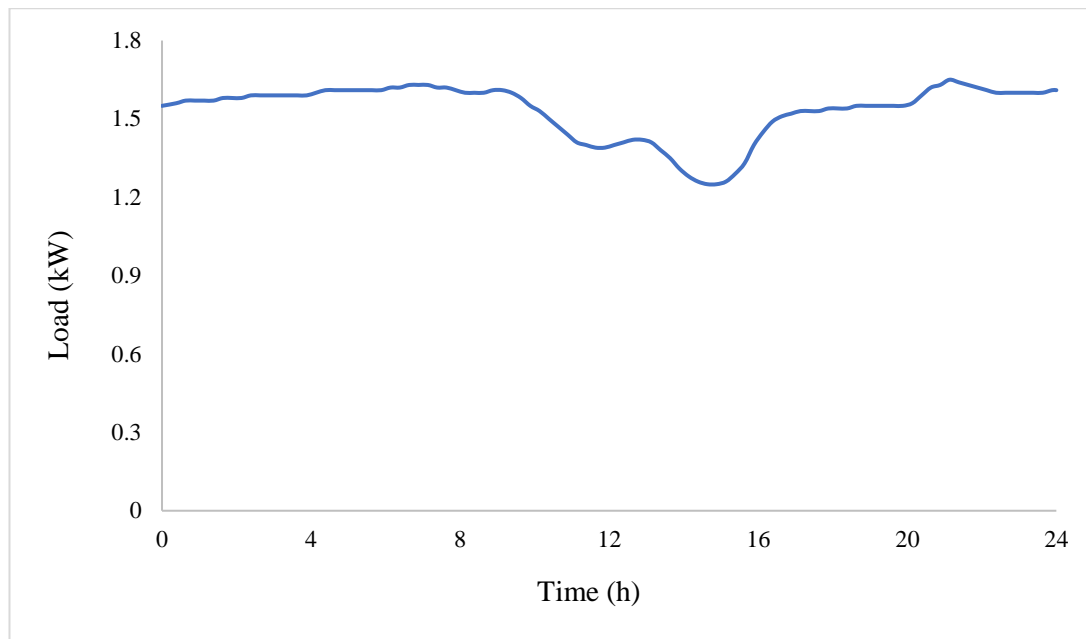


Figure 4.4: Peak day heat demand profile of the detached dwelling.

The results of the building energy performance simulation indicated a heat demand of 37-kWh for the peak day. Note that the profile generated is for one of the most numerous types of houses in the Scottish housing stock and the approach to sizing is adaptable to other housing types. The estimated space heating demand of the dwelling represents the total energy required over 24 hours to maintain the space air set point temperature to achieve thermal comfort. The estimated heat demand was calculated using standard parameters for occupancy, internal heat gain, infiltration and precise weather data. ESP-r has been extensively validated for predicting a building's heat demand. Strachan et al. [184] summarised the validation efforts applied to ESP-r. Clarke et al. [200] developed a methodology applied to ESP-r for the calibration/validation of a building's heating and cooling loads. ESP-r contributed to BESTEST, an IEA initiative that established a benchmark for evaluating the quality of energy simulation programs [201]. The benchmark has been integrated into ASHRAE standard 140. This study emphasizes in obtaining a dwelling space heating demand which is then used to determine the size and capacity of the TES system required to assess its performance for load-shifting capabilities. Chapter 6 provides a detailed analysis of how to size the TES system. The TES system is first validated to ascertain its accuracy for use in wet central heating. The validation analysis is presented in Chapter 5.

4.3 Chapter Summary

A study was conducted to predict the heat demand profile of a detached dwelling for the next day using building energy simulation. The ESP-r tool was utilised to simulate the building, considering the parameters and boundary conditions such as infiltration, weather data and occupancy characteristics. Heating control was implemented to maintain the air space set point temperature, and the occupancy characteristics including the internal heat gain due to occupancy, lighting, and equipment, as well as the weather data, were defined and integrated using the control and operational schedules of the ESP-r simulation tool. The initial step involved conducting a building energy performance simulation to analyse the seasonal heat demand of the detached dwelling and identify its peak heat demand. This analysis assisted in determining the dwelling's peak day heat demand for further investigation. Subsequently, further simulation was conducted to predict the detached dwelling's peak day heat demand profile. The simulation results showed 37-kWh for the peak day heat demand of the detached dwelling. The generated profile is for one of the most numerous types of houses in the Scottish housing stock and the approach to sizing is adaptable to other housing types. The predicted peak heat demand of the dwelling will be utilised to size the TES system. This procedure is general and can be used to determine the size and capacity of the TES system required to meet the next-day heat demand profile for any dwelling with forecasted heat demand. However, at this stage, it is important to verify and validate the TES model to ensure its accuracy and performance for use in the dwelling's wet central heating. These tasks are analysed in Chapter 5.

5 Numerical Modelling and Simulation of LHS System

5.1 Introduction

Several experimental and numerical studies involving latent heat thermal storage systems [79,121,202–204] have been carried out with modelling for melting and solidification in a shell-and-tube cylindrical enclosure. However, most of these studies were conducted either for melting or solidification only. Other studies combine analysis for melting and solidification of latent heat thermal storage systems experimentally [202,205] and numerically [204,206] or both [186,188,207]. The thermal performance of cylindrical enclosures may differ due to differences in their orientation. In a vertical cylindrical enclosure, regardless of the shell diameter, the nature of the transport phenomena is the same [188]. This implies that the shell-tube ratio does not affect the performance of LHS systems. Figure 5.1 presents the geometrical configuration of a vertical shell-and-tube heat exchanger. The geometrical configuration of a cylindrical enclosure is usually assessed by the length-to-diameter ratio (L/D). Most studies conducted for the melting and solidification of LHS in cylindrical enclosures used an aspect ratio of less than 21 for low and medium-temperature applications [186,188,208,209]. However, in practice, larger aspect ratios are used depending on the design requirements for the thermal storage applications.

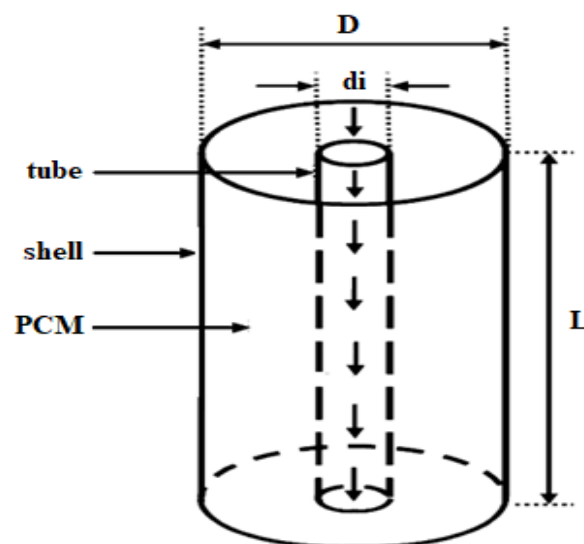


Figure 5.1: Schematic diagram of a vertical shell-and-tube heat exchanger

Pal et al. [208] used an L/D of less than 21 to investigate complex flow and the thermal performance pattern for a baffled and un-baffled shell-and-tube heat exchanger. Hussain and Jabbar [209] investigated, experimentally and numerically, the natural convection heat transfer through a fluid-saturated porous media in an inclined cylindrical enclosure using an L/D of less than 12. The results of the investigation showed that the heat transfer rate in a cylindrical enclosure increases with an increase in the Raleigh number, amplitude, time, and angle of inclination to the horizontal. However, Seddegh et al. [121,206] indicated that the heat transfer characteristics of the LHS material in vertical shell-and-tube cylindrical enclosures differ when compared based on thermal conduction heat transfer analysis. The conduction and convection heat transfer model of the LHS material shows significant heat transfer performance compared to a pure conduction model during the charging process. However, during the discharging process, natural convection in the PCM is insignificant in the heat transfer performance of the system [121,186]. Because of natural convection in the latent heat storage region of a cylindrical enclosure, the heat transfer rate depends on the geometrical configuration of the system during the charging process [210,211]. Other factors that influence the heat transfer rate during the charging and discharging of an LHS is the orientation of the cylindrical enclosure [212,213]. A comparison in the heat transfer characteristics of LHS material in the vertical and horizontal shell-and-tube heat exchanger is illustrated in Figure 5.2. The position of the cylindrical

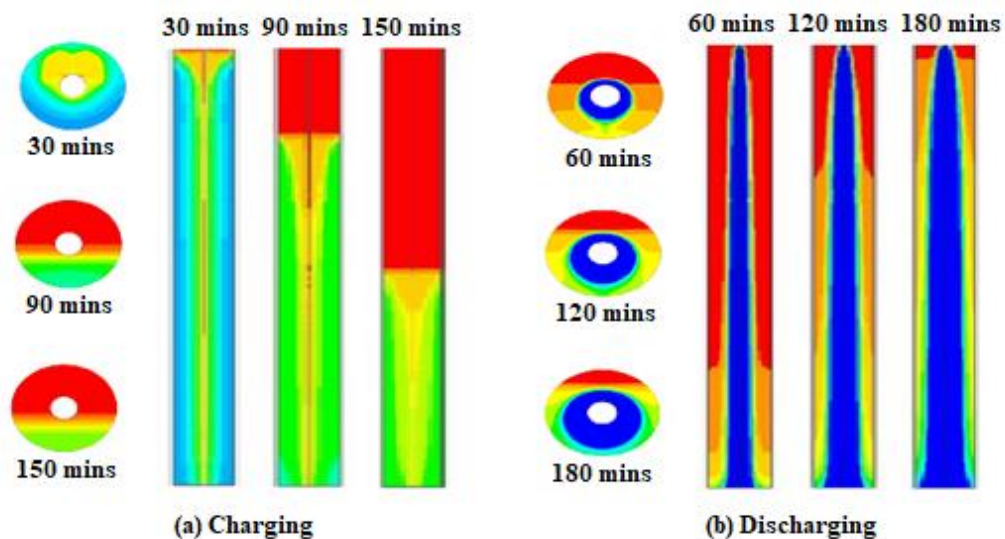


Figure 5.2: Heat transfer characteristics in the vertical and horizontal heat exchangers during charging and discharging of LHS materials [121].

enclosure, either vertical as preferred in this work or horizontal during charging and discharging, provides different heat transfer performance [121]. The heat transfer rate in the vertical cylindrical enclosure during charging remains almost constant compared to the horizontal unit. This is due to the constant circulation region that remains the same during charging. In this work, modelling, and simulation of a phase change LHS element is conducted using a melting and solidification model implemented in the Fluent CFD program. The experimental and numerical results of Longeon et al. [186] are used to validate the CFD model for predicting the thermal performance characteristics of the TES system. This analysis is crucial for ensuring the accuracy of the TES system's performance in wet central heating to fulfil the space heating requirements of the considered detached dwelling.

5.2 Phase Change Heat Transfer Modelling

Modelling of a phase change LHS system involves a complicated process that considers the solid-liquid interface during the charging and discharging processes. Melting and solidification of LHS are characterised by unique physical properties involving the moving boundary that separates the solid and liquid regions [214]. The solid-liquid phase consists of different transport properties making the phase change modelling complex due to the presence of buoyancy-driven motion in the liquid region driven by natural convection and volumetric expansion. The heat transfer phenomena that occur between the PCM and HTF also contributed to the system's complexity [215,216].

5.2.1 Numerical Modelling

Phase change occurs when latent heat is absorbed or released by the thermal storage system without a temperature change. This condition occurs during the melting and solidification process through conduction only when the PCM is solidified or conduction and convection [121,186,216]. The solution to such problems was first provide by Steffan and is generally regarded as a classical Steffan problem [79,95]. A temperature-dependent thermophysical property of the material is applied by approximating it to a constant temperature or through the phase change temperature interval [79,95]. The solution is obtained numerically with consideration to the difference in PCM thermal properties in separate regions of the solid and liquid phases. In these

phenomena, the domain of interest lies in the moving interface between the solid and liquid regions [214,217]. The thermal property of the solid is assumed constant. However, natural convection may be induced when the solid and liquid phases have variable densities [213,214,218]. To numerically solve the phase change problem, two approaches are typically employed: variable and fixed-grid methods.

5.2.1.1 Variable Grid Method

This is applied to solve phase change problems with the calculation domain defined by the interface between the solid and liquid regions. The technique involves tracking the phase change interface at grid points at each time step [219,220]. The method is accomplished through front-tracking or front-fixing methods. With front tracking, the moving boundary location is calculated at each time step [219,221] via a variable time-step solution. In the front-fixing method, the moving front is tracked and fixed by introducing a new space variable [221]. The variable grid method is based on treating the computational domain of solid and liquid phases separately using separate equations that are solved by the energy balance at the interface between the solid and liquid regions [219–221]. The variable grid method interface equation is given by [79,95].

$$\lambda\rho\left(\frac{ds(t)}{dt}\right) = k_s\left(\frac{\delta T_s}{\delta t}\right) - k_l\left(\frac{\delta T_l}{\delta t}\right) \quad (5.1)$$

where λ is the latent heat of fusion, ρ the density of the material phase, s the phase front of the PCM, k_s and k_l the solid and liquid phase thermal conductivities, and T_s and T_l the solid and liquid phase temperatures [79].

5.2.1.2 Fixed Grid Method

In this method, the phase change is characterised by interface position. This implies that there is no interface tracking, indicating that the fixed grid method is useful in describing the continuous properties of phase change processes [222]. An advantage of the fixed grid is that it is simple to implement numerically and yields more accurate results than the variable grid method [223,224]. The phase change characterisation is achieved by phase fraction-based models that utilise a simple computational domain involving a single set equation applied to the entire domain that comprises

the continuity and momentum equations [222]. This method involves a phase change occurring within a small temperature range.

The solution to the phase change problem requires an equation that satisfies the characteristics involving non-linear latent heat evolution at the phase change interface [224]. The latent heat is applied in the sets of equations using an enthalpy function [222,224]. The governing equation for enthalpy-based formulation for solid-liquid phase conduction and vice-versa can be established based on the constant thermo-physical properties using Equation (5.2), where H is the total volumetric enthalpy at the phase change interface [220].

$$\frac{\partial(\rho H)}{\partial t} + \nabla \cdot (\rho V H) = \nabla \cdot (k \nabla T) \quad (5.2)$$

The total volumetric enthalpy is applicable to phase change phenomena using effective heat capacity or enthalpy formulation, involving the source term-based method [220,225].

The Effective Heat Capacity Method

This method involves the approximation of the latent heat capacity of PCM over a temperature interval during phase change processes [226]. The method operates between the melting and solidification when heat is gained or released by the PCM by an additional heat capacity during phase change using a temperature function [79,226]. The temperature-dependent effective heat capacity of the PCM is defined by Equation (5.3), which is represented as a function of the latent heat of fusion during phase change processes:

$$H = \int_{T_s}^{T_l} C_{eff} \partial T, \quad C_{eff} = \begin{cases} C_p & \text{if } T_s < T < T_s \\ \frac{\lambda}{T_s - T_l} + C_p(T_l), & \text{if } T_l \leq T \leq T_s \end{cases} \quad (5.3)$$

where C_{eff} is the effective heat capacity, λ the latent heat of fusion, and T_s and T_l the solid and liquid temperature of the PCM [79]. Effective heat capacity methods have not been widely used in solving phase change problems.

Enthalpy Function Method

The enthalpy function as the name implies involves the representation of enthalpy as a function of the temperature of phase change [121,227]. In this case, the PCM latent heat of fusion is expressed in terms of temperature, accounted as an enthalpy function that sums up the sensible and latent heat energy (Equation (5.4)), where the sensible heat energy is given by Equation (5.5) and liquid fraction, f , in the solid-liquid region by Equation (5.6) [79,121,227].

$$H(T) = h(T) + \lambda f(T) \quad (5.4)$$

$$h(T) = \int_{T_s}^{T_l} C_p dT \quad (5.5)$$

$$f = \begin{cases} 0 & \text{if } T < T_{solid} \\ 1 & \text{if } T > T_{liquid} \\ \frac{T - T_{solid}}{T_{liquid} - T_{solid}} & \text{if } T_{solid} < T < T_{liquid} \end{cases} \quad (5.6)$$

Substituting Equation (5.6) into Equation (5.2), and assuming the phase change material density is constant, the governing equation becomes:

$$\frac{d\rho h_{pcm}(T)}{dt} = \nabla (k\nabla h_{pcm}) - \rho_{pcm}\lambda \frac{\delta f}{\delta t}. \quad (5.7)$$

The advantage of a variable grid over a fixed grid method is that the former has a better prediction of flow phenomenon and position of the phase change interface. However, the variable grid method uses larger sets of equations requiring more computing resources. [221,222]. There is no explicit condition that needs to be satisfied at the interface between solid and liquid (i.e., the mushy zone). The fixed grid enthalpy method can spot the positions of two boundaries using the temperature field [221]. Therefore, the thermophysical properties of PCM are readily evaluated since the temperature can be determined at every point in the system [79,121]. In a fixed

grid, a single energy equation applies to all phases; solid, liquid and the mushy zone. In this study, the fixed grid method is applied to solve the phase change problem and assess the performance accuracy of the TES system. This method is chosen due to its significant advantages over the variable grid method.

5.3 CFD Modelling, Verification and Validation

In the present work, the modelling for melting and solidification of an LHS material in a shell-and-tube cylindrical enclosure is conducted using the melting and solidification model in the CFD Fluent software following the model validation against the experimental data and numerical solutions published by Longeon et al. [186].

5.3.1 The CFD Model

The fixed grid enthalpy-based formulation method for melting and solidification was applied to modelling a vertical cylindrical enclosure. In this approach, there is no interface tracking because the phase change is characterised by interface position. The phase change interface is indicated by a mushy zone, which separates the solid and liquid regions. The mushy zone is modelled as a porous zone with a liquid fraction that lies between 0 and 1, where 0 is solid and 1 represents PCM in the liquid state. The energy equation in terms of the total volumetric enthalpy and temperature is given in Equation (5.8) and is then solved.

$$\frac{\partial(\rho H)}{\partial t} + \nabla \cdot (\rho V H) = \nabla \cdot (k \nabla T) + S \quad (5.8)$$

The total volumetric enthalpy H is the sum of the sensible enthalpy h and latent enthalpy ΔH (Equation (5.9)) at a reference temperature at any point in the system described by Voller and Prakash [228]. The latent enthalpy is zero when the PCM is completely solid or liquid, f has been defined in Equation (5.6). The latent heat is represented as a function of temperature (Equation (5.10)). This applies to cases where melting of the PCM occurs at a single temperature point or over a range of temperatures. The sensible heat is represented as described in Equation (5.11).

$$H = h + \Delta H \quad (5.9)$$

$$\Delta H = f(T) \quad (5.10)$$

Substituting h and ΔH in Equation (5.8), where h_{ref} is the enthalpy at the reference temperature for which $T_{ref} = 25^\circ\text{C}$ and a function of temperature. The source term S used in the enthalpy-based formulation is defined in Equation (5.12) [217,229].

$$h = h_{ref} + \int_{T_{ref}}^T C_p \partial T \quad (5.11)$$

$$S = \frac{\partial(\rho\Delta H)}{\partial t} + \nabla \cdot (\rho V \Delta H) \quad (5.12)$$

5.3.1.1 Boussinesq Approximation

To solve problems of buoyancy-driven flows that occur due to variations in the PCM densities, the fluid density is specified as a function of temperature. A constant fluid density is applied in all terms of the governing equation except the buoyancy term [121]. The buoyancy effect is modelled with approximations represented in terms of the reference density ρ_o and volumetric thermal expansion coefficient β_o described in Equation (5.13) [121,217], where ΔT is the difference between the reference and cell temperature.

$$\rho = \rho_o(1 - \beta_o \Delta T) \quad (5.13)$$

The variation in density between the solid and liquid phases might affect the structure of the PCM used. However, there is not much effect on heat transfer [33]. The Boussinesq approximation has been widely applied for the solution of natural convection in the analysis of various LHS systems [121,186,217].

In this study, the experimental and numerical results of Longeon et al. [186] is used to validate the TES model. The analysis aimed to replicate the experimental test conducted to evaluate the thermal performance accuracy and reliability of the TES model that will be applied to meet the space heating demand of the detached dwelling. The experimental test section is modelled and implemented in Fluent CFD software for charging and discharging simulations to validate the TES model. The simulation results are then compared with the numerical solution of Longeon et al. [186].

5.3.2 Experimental Set-up

Figure 5.3 shows a schematic of an experimental setup presented by Longeon et al. [186]. The HTF inlet and outlet are attached to 2 K-type thermocouples that record the flow temperature. The HTF is regulated by a micro pump coupled with a Coriolis flowmeter to maintain the flow rate. 48 K-types 0.5 mm calibrated thermocouples are distributed at different angles (0° to 270°) at point D and radial positions a, b and c through points A-G. However, only point D is considered here for validation. This is because the location of point D is about the centre of the cylindrical enclosure. Any point above or below D provides similar thermal characteristics. However, this depends on the HTF injection configuration applied.

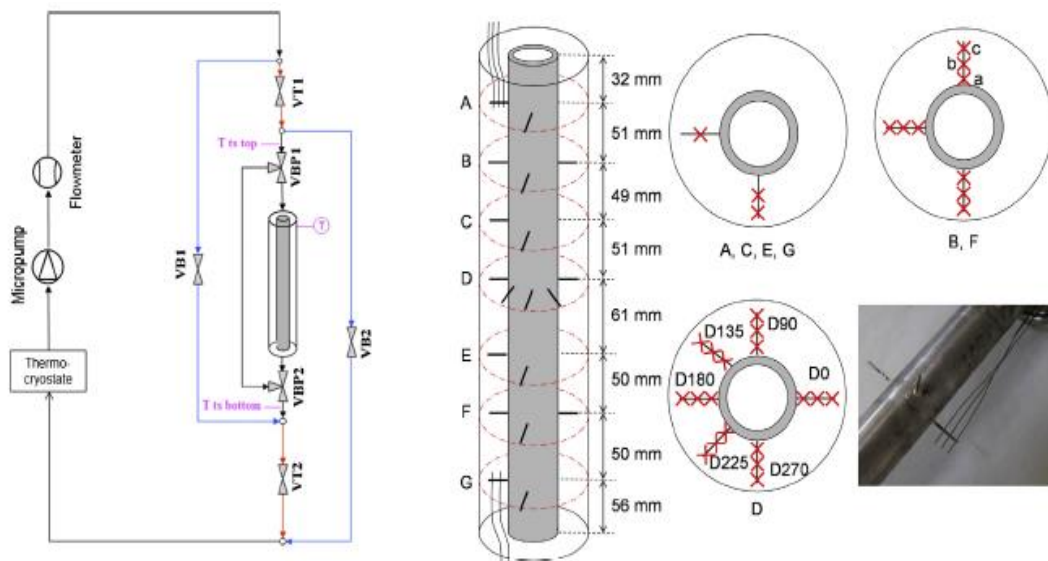


Figure 5.3: The experimental set-up for melting and solidification of the annular PCM conducted by Longeon et al. [186].

Table 5.1 presents the angular and radial positions of thermocouples at point D, which is located 217 mm from the bottom of the vertical cylindrical enclosure.

Table 5.1: Specification for the point D thermocouple positions a, b and c.

Position	a	b	c
Angular position (degree)	0	90	135
Radial position (mm)	3.3	6.6	9

Figure 5.4 illustrate the experimental test section involving geometry and boundary conditions applied for the validation using the CFD melting and solidification model. The vertical cylindrical enclosure is composed of two cylinders with 480g of PCM filled in the annulus. The outer cylinder is made up of Plexiglas with an inner diameter of 44 mm and a tube made of stainless steel, having an inner diameter of 15 mm with a thickness of 2.5 mm. The length of the entire system is 400 mm. The HTF is injected at a velocity of 0.01 m/s from the top (VT1 and VT2 open) and bottom (VB1 and VB2 open) configurations for charging and discharging respectively.

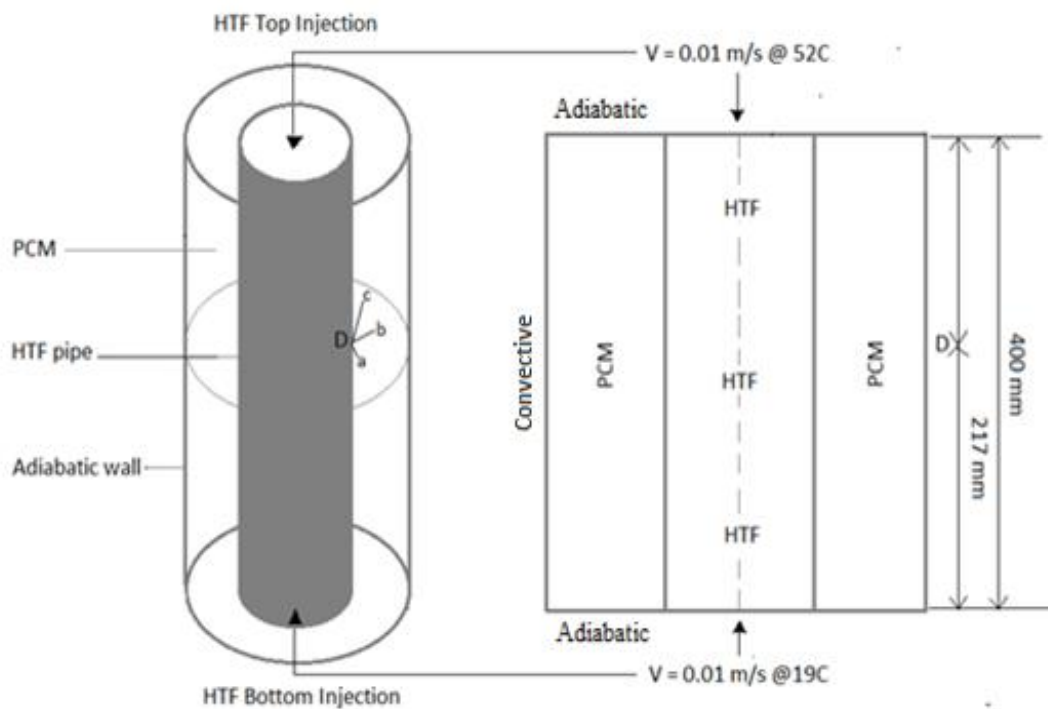


Figure 5.4: Geometry and boundary condition of the test section.

5.3.3 Numerical Procedure and Verification

The experimental section is modelled in Fluent as a 2D axisymmetric geometry as shown in Figure 5.5(a). The melting and solidification of the PCM in the vertical cylindrical enclosure is conducted using the modelled geometry of the 2D axisymmetric domain presented which comprises both outer and inner pipes enclosed by the PCM and the HTF as illustrated.

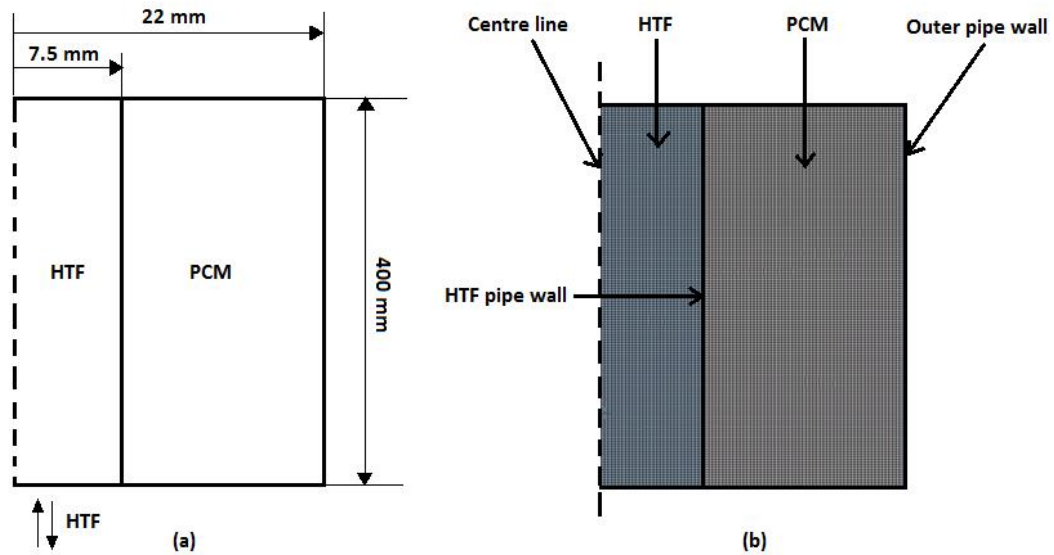


Figure 5.5: Schematic diagram of the axisymmetric geometry and computational domain applied in the Fluent model for validation.

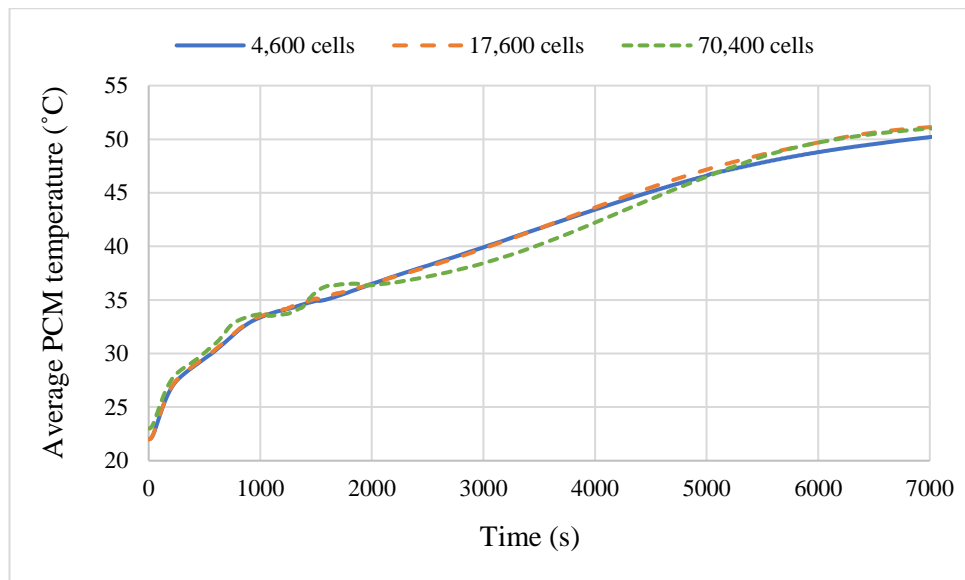
The PCM and HTF were drawn and meshed with pipe wall thermal resistance modelled in 1D conduction through the walls. Figure 5.5(b) illustrates part of the mesh applied for the charging and discharging of the PCM in the annulus. Fluent allows the specification of wall thermophysical properties and boundary conditions in each dialogue box. A heat flux thermal condition was set at the outer pipe wall, with the top and bottom walls set as adiabatic, and the HTF pipe wall (tube wall), specified as coupled energy transfer condition. It is likely there is a small heat loss in the experiment as the phase change range was close to the ambient temperature to avoid high heat loss without insulating the test section. The semi-implicit pressure-linked equation algorithm was used for pressure-velocity coupling. A least square cell-based gradient and pressure staggering option for the pressure correction equation spatial discretization was applied. The first-order upwind scheme was used for the momentum and energy equations. A convergence criterion of 10^{-6} was considered for the energy residual values and 10^{-3} for all other variables. The transient simulation was run using a laminar model. The PCM density was assumed to be constant and the effect of density variation due to natural convection was taken into consideration by the Boussinesq approximation. The HTF inlet boundary condition was applied for the simulation. Table 5.2 presents the thermophysical properties of the PCM used in the experiment.

Table 5.2: Thermophysical properties of paraffin RT35 [186].

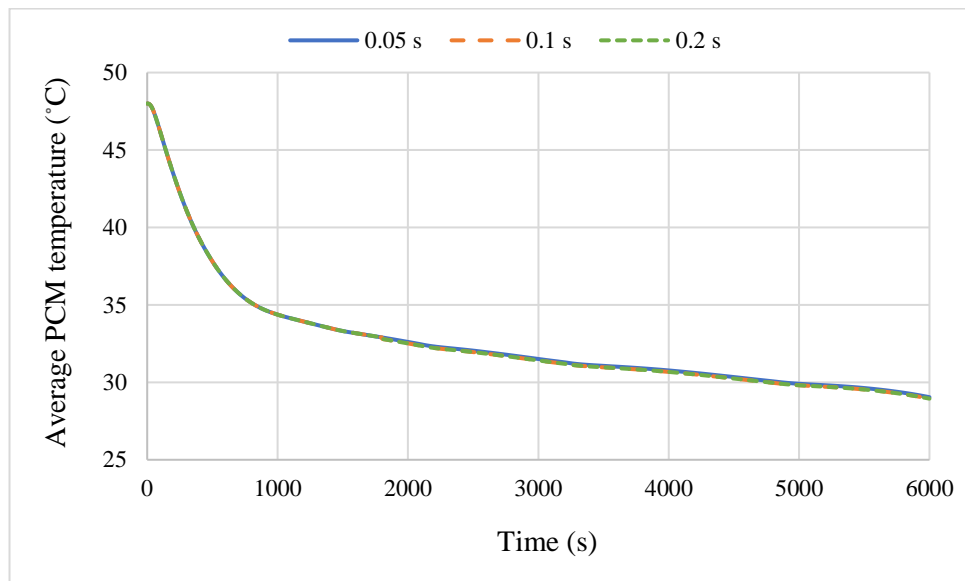
Properties	Paraffin RT35 data
Melting temperature (°K)	308
Kinematic viscosity (m ² /s)	3.3 x 10 ⁻⁶
Latent heat of fusion (kJ/kg)	168
Density of PCM, solid (kg/m ³)	880
Density of PCM, liquid (kg/m ³)	760
Thermal conductivities (W/mk)	0.2
Thermal expansion coefficient (1/K)	0.001
Specific heat capacity of PCM, solid (J/kg K)	1800
Specific heat capacity of PCM, liquid (J/kg K)	2400

5.3.3.1 Grid and Time Step Dependency Study

A preliminary study was conducted to examine the grid and time step in order to ensure the accuracy and reliability of the CFD solution in predicting the thermal characteristics and overall performance of the storage model during charging and discharging cycles. Simulations were conducted using different grid sizes and time steps to determine the best convergence of the computational grid. The computational domain was analysed using three meshes of 4,600 cells, 17,600 cells and 70,400 cells to determine the optimal mesh size for the analysis. The computational grid consisting of 17,600 cells was well-suited to yield accurate results under the least computational time. To obtain the best time step that can provide accurate results, three timesteps of 0.05s, 0.1s and 0.2s were simulated. It was found that the 0.2s time step gave the best results with the least computational time (although there were no significant results differences between the simulated time steps). The results reveal that the solution accuracy improves with finer grid resolution and smaller time steps. However, an optimal balance between the time step and grid resolution ensures accuracy and efficiency in simulation. The computational grid consisting of 17,600 cells and a time step of 0.2s was subsequently used to validate the storage model with charging and discharging simulations. Figure 5.6 presents a detailed comparison of different meshes and time step sizes.



(a)



(b)

Figure 5.6: Average PCM temperature against time for (a) different meshes and (b) convergence time steps.

5.3.4 Validation of the Numerical Methodology

5.3.4.1 Validation with Experimental Results

To validate the CFD numerical model against the experimental data of Longeon et al. [186], simulations are conducted for charging and discharging the PCM in the vertical enclosure using the computational grid size of 18,045 nodes and 17,600 cells at a time step of 0.2s. The simulation was set with the specification of first-order implicit transient formulation. The input data required to run the CFD software for validating the thermal storage model are summarized in Appendix IIA. The simulation considers the following assumptions.

- Material volume expansion is neglected.
- Both solid and liquid phases are homogenous and isotropic.
- Change in the PCM property within the porous zone is assumed to be linear.
- Variation in density due to natural convection has been taken into consideration by the Boussinesq approximation.

The vertical cylindrical enclosure was set at a reference temperature of 22°C. The HTF with a flow velocity of 0.01 m/s at 52°C was injected at the top of the vertical cylindrical enclosure for melting of the PCM as performed in the experiment. A charging simulation is conducted and the modes of heat transfer during the charging process are conduction and convection. The PCM melts as it absorbs heat at the interface of the HTF pipe wall through conduction. In this process, natural convection plays a major role in the melting process.

Figure 5.7 compares the liquid fraction between the CFD solution and the experimental results during the charging process. The blue and white colour section of the cylindrical enclosure (liquid fraction is 0) shows that the PCM is in the solid phase, while the red and colourless parts (liquid fraction is 1) indicate melted PCM. The PCM is solid at zero seconds where the tube was completely white before charging. However, during the charging process, the PCM melts continuously about 90% as shown at 30,000 timesteps with the remaining solid PCM settled at the bottom of the vertical enclosure. It can be observed that the shape and magnitude of the PCM liquid fraction in the annular gap for the CFD solution and experimental results are similar. This shows that the two results exhibit similar thermal performance behaviour.

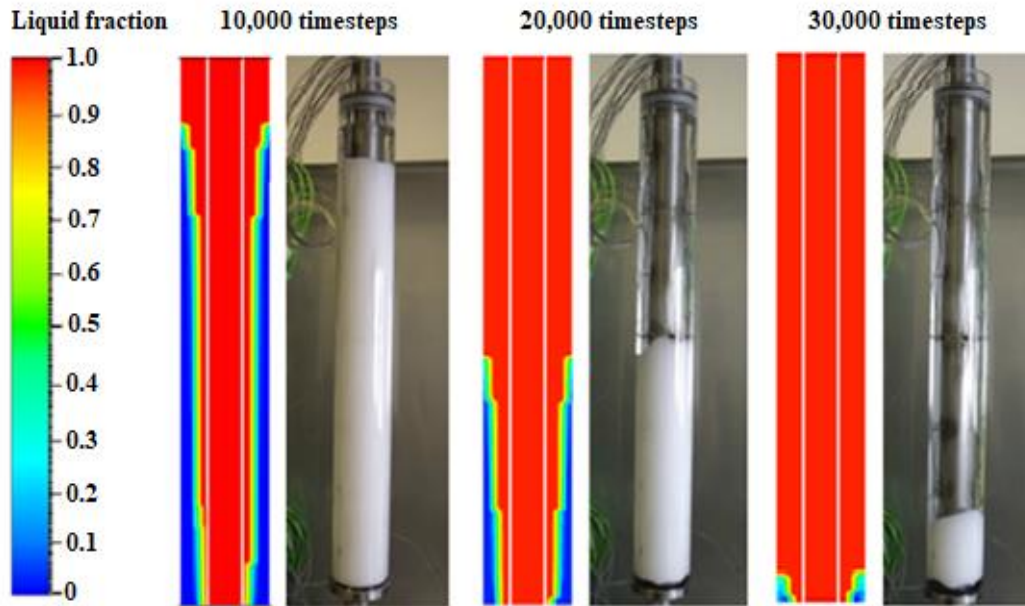


Figure 5.7: Contour of PCM liquid fraction for the CFD solution (left) and the experimental results of Longeon et al. [186] (right) during charging with top HTF injection.

Figure 5.8 presents the temperature variations for the selected angular and radial positions at point D during the charging process. It can be observed that a similar relationship between the CFD solution and experimental results can be depicted during the charging process. However, there is a slight variation in the temperature profiles. The temperature at the various locations for the CFD solution is higher than those obtained experimentally when the PCM is solid. This is because of the PCM liquid density used throughout the simulation. The solid PCM's heat capacity is lower causing a higher rise in temperature. In addition, heat is lost through the cylindrical wall due to imperfect insulation around the point where the thermocouples are attached to the heat exchanger. Practically, it is impossible to provide perfect insulation around the wall of the PCM container to prevent such heat loss [229]. The accuracy of the storage model is further assessed by comparing the fluid outlet temperature from the CFD solution with the experimental data during the charging process. The HTF outlet temperature profile obtained from the CFD solution exhibits a pattern similar to the experimental data as shown in Figure 5.9.

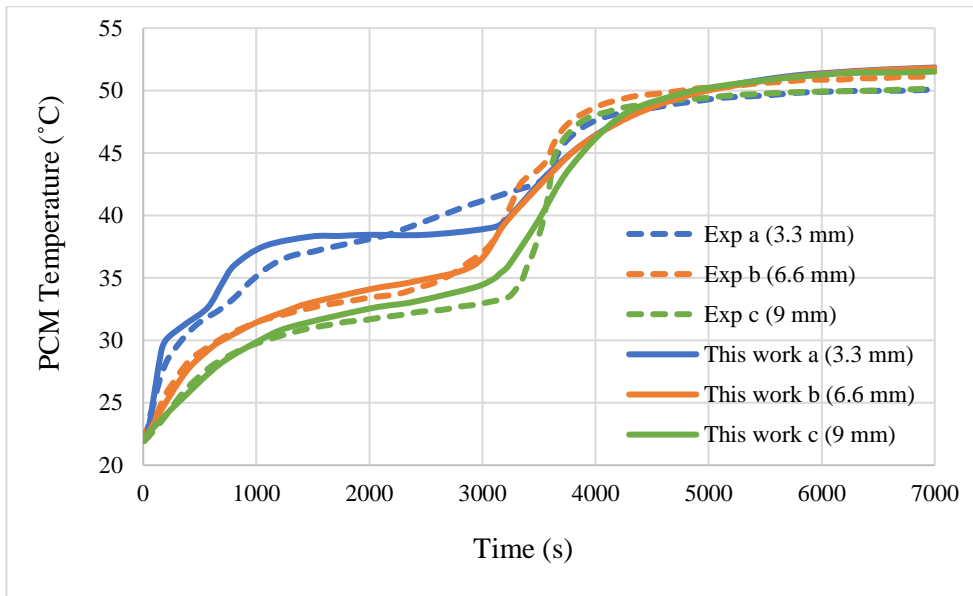


Figure 5.8: Temperature variations of the radial points a, b, and c, at axial position D of the CFD solution and the experimental results of Longeon et al. [186] during charging with top HTF injection.

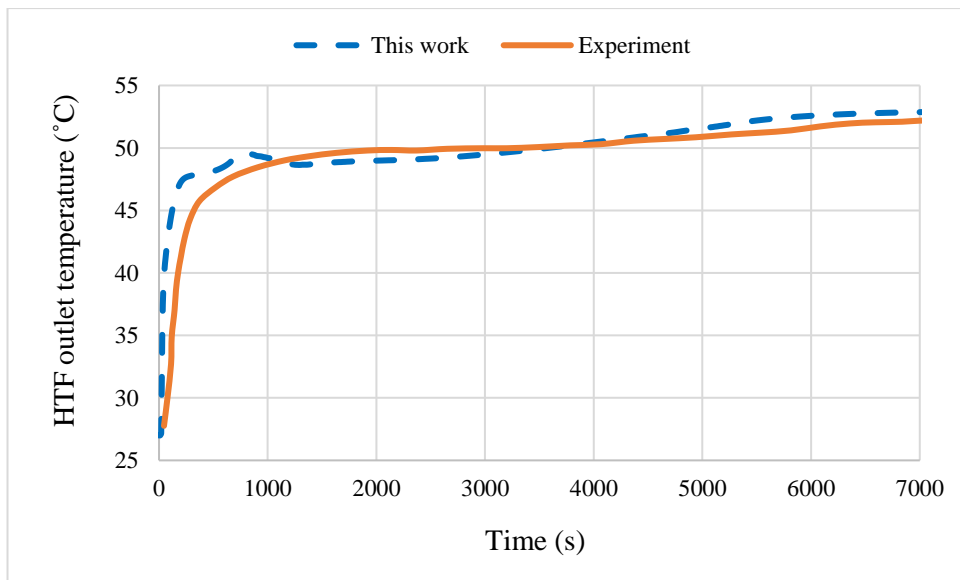


Figure 5.9: Variation of the HTF outlet temperature of the CFD solution and the experimental results of Longeon et al. [186] during charging process.

Simulation for the PCM solidification was conducted using an HTF flow of 0.01 m/s at 19°C specified at boundary conditions at a reference temperature of 48°C. The solidification of the PCM is slow compared to melting. This is because, during the discharging process, conduction heat transfer is dominant. The PCM solidifies by releasing heat to the HTF at the wall interface through the process. The PCM start to solidify at the bottom of the vertical enclosure due to variations in density.

Figures 5.10 and 5.11 show the comparison of the temperature profiles at the selected locations and the fluid outlet temperature between the CFD solution and the experimental results. The temperature profiles of the CFD solution are consistent with the experimental results. However, minor discrepancies are observed in the results. Longeon et al. [186] indicated that the discrepancies in the numerical and experimental results during discharging were due to the difference between the specific heat capacity for melting and solidification. This is because paraffin behaves differently during melting and solidification processes (the hysteresis effect) [186]. During solidification, the PCM is initially in a liquid state. However, as the PCM start to solidify, its density varies. The density of the PCM in the liquid state, during phase transformation and in the solid state are different. These phenomena may not be accurately captured in the CFD simulation, which can cause slight errors in the results.

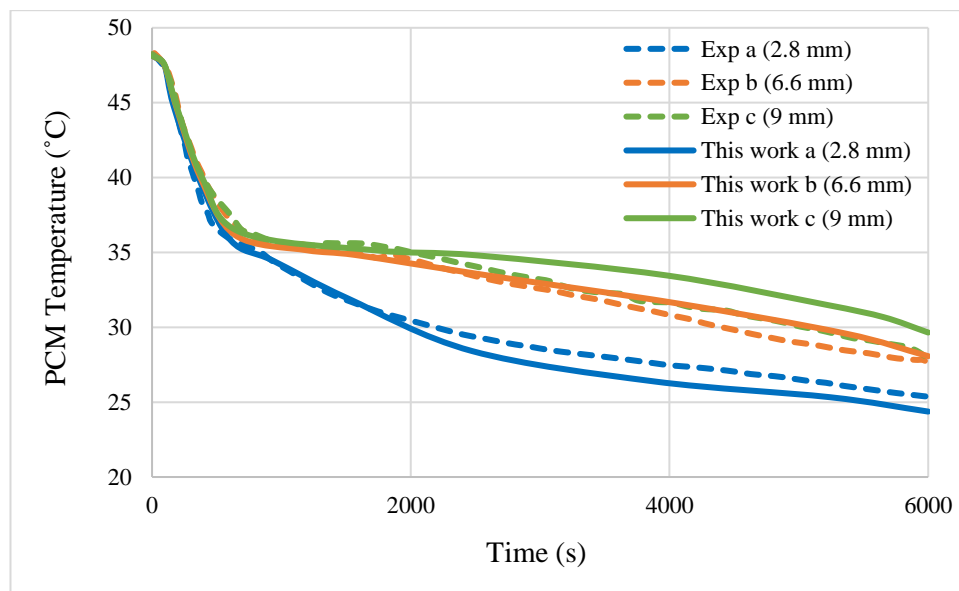


Figure 5.10: Temperature variations of the radial points a, b, and c, at axial position D of the CFD solution and the experimental results of Longeon et al. [186] during discharging with bottom HTF injection.

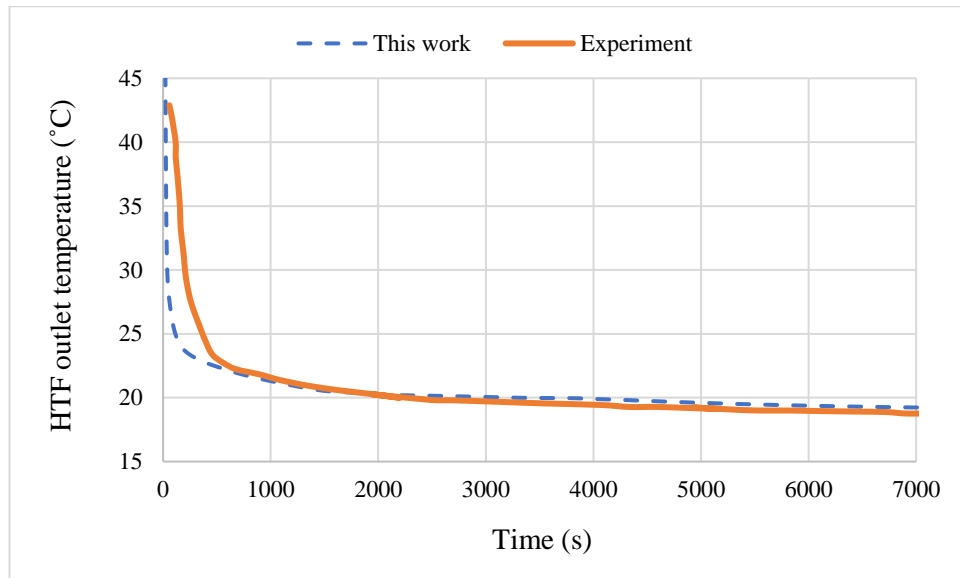


Figure 5.11: Variation of the HTF outlet temperature of the CFD solution and the experimental results of Longeon et al. [186] during the discharging process.

Statistical analysis is conducted to assess the performance accuracy of the TES model for use within wet central heating to meet the detached dwelling’s space heating demand. The statistical analysis compares the HTF outlet temperature and the PCM temperature profiles at the selected points a, b and c, between the CFD model and the experimental data for the charging and discharging processes. The statistical parameters which include the maximum error (Max E), mean absolute error (MAE) and root mean square error (RMSE) were estimated to analyse the accuracy of the storage model. Table 5.3 presents the error statistics confirming the model's accuracy.

Table 5.3: Calculated statistical parameters at the selected points (validation).

Process	Location (mm)	Max. E (°C)	MAE (°C)	RMSE (°C)
Charging	a (3.3)	2.46	1.13	1.33
	b (6.6)	2.17	0.53	0.73
	c (9.4)	1.64	0.89	1
	Outlet	0.92	0.41	0.51
Discharging	a (2.8)	1.12	0.52	0.67
	b (6.6)	1.81	0.85	1.02
	c (9)	2.08	0.96	1.11
	Outlet	0.1	0.05	0.06

A maximum variation of 0.92°C and 2.46°C was calculated for the fluid outlet temperature and temperature profiles at the selected points between the CFD results and experimental data. The analysis results indicate that the CFD solution closely agrees with the experimental results.

A study was conducted to examine the rate of energy transfer at the tube and shell walls of the heat exchanger during the charging process. In the experiment by Longeon et al. [186], the tube was modelled as a coupled energy transfer condition, while the outer shell wall was exposed to the environment, indicating a convective heat transfer. In this study, a heat flux thermal condition was applied to the shell wall to investigate the heat transfer rate at the outer wall during charging. The CFD simulation results indicate that the heat transfer rate at the outer shell wall is significantly lower than at the tube wall. This difference is attributed to the lower temperature gradient between the PCM and the outer wall, where conduction-dominated heat transfer occurs. In contrast, the heat transfer at the tube wall is much higher due to the combination of conduction and enhanced convection within the tube, driven by a larger temperature gradient and direct contact with the HTF. During the charging process, an average heat transfer rate of 16W was observed at the tube wall and 0.9W at the outer shell wall of the heat exchanger. Figure 5.12 illustrates the comparison of the heat transfer rates at the tube and shell walls of the heat exchanger.

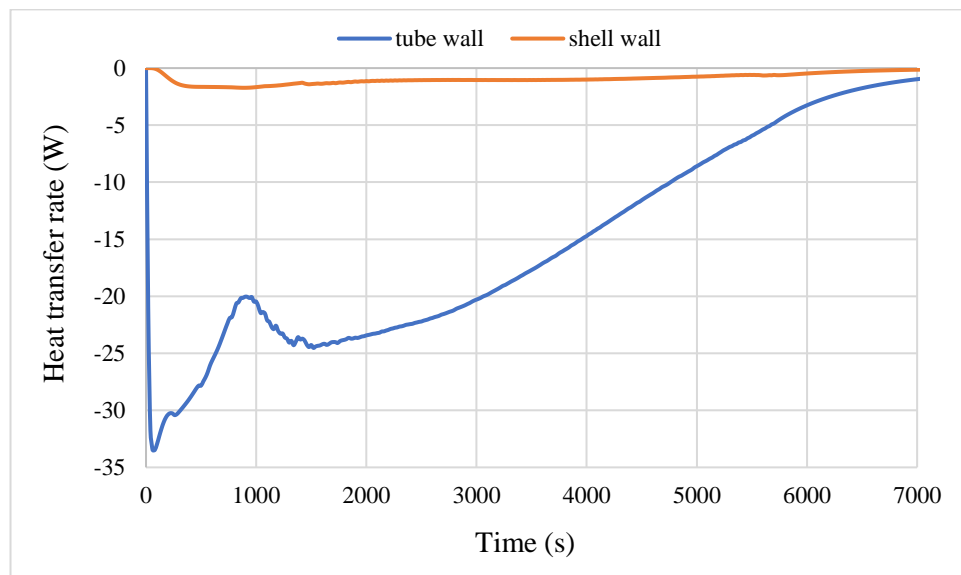


Figure 5.12: Variation of heat transfer rates at the tube and shell wall during charging process.

The relatively small heat transfer at the outer shell wall compared to the tube wall can therefore be ignored to simplify the TES system analysis. This enables the performance analysis of the TES system by assuming the container that houses the thermal storage elements is insulated and treated as a controlled volume.

5.3.4.2 Comparison of the CFD Solution with Numerical Results

The 2D axisymmetric geometry of the experimental test section has been modelled numerically by Longeon et al. [186]. The geometry of the vertical cylindrical enclosure comprised the tube domain in which the HTF flows for charging and discharging the PCM, the annular domain that houses the PCM, and the shell-and-tube walls through which heat is transferred. The CFD model was validated with the experimental data. However, the CFD model used in this work is compared with the numerical model of Longeon et al. [186] to further assess the consistency and accuracy of the two numerical models. In this case, separate simulations are conducted for charging and discharging the PCM by considering the difference in the radial positions of the selected points a, b and c in the vertical enclosure used in the numerical model. The temperature contours and temperature profiles for the CFD solution are compared with the numerical results during the charging and discharging processes.

Figure 5.13 illustrates the temperature contours for the Fluent CFD solution and the numerical results during charging with top HTF injection configuration. It is noticeable that the PCM temperature is observed to gradually increase from 22°C to 52°C as it melts during the charging process. This is due to conduction heat transfer at the wall of the HTF, causing variations in PCM densities and inducing natural convection. The charging process continues until the PCM is almost completely melted as shown at 30,000 time steps. The temperature contours of the CFD solution and the numerical results are similar, demonstrating a close match between the two results.

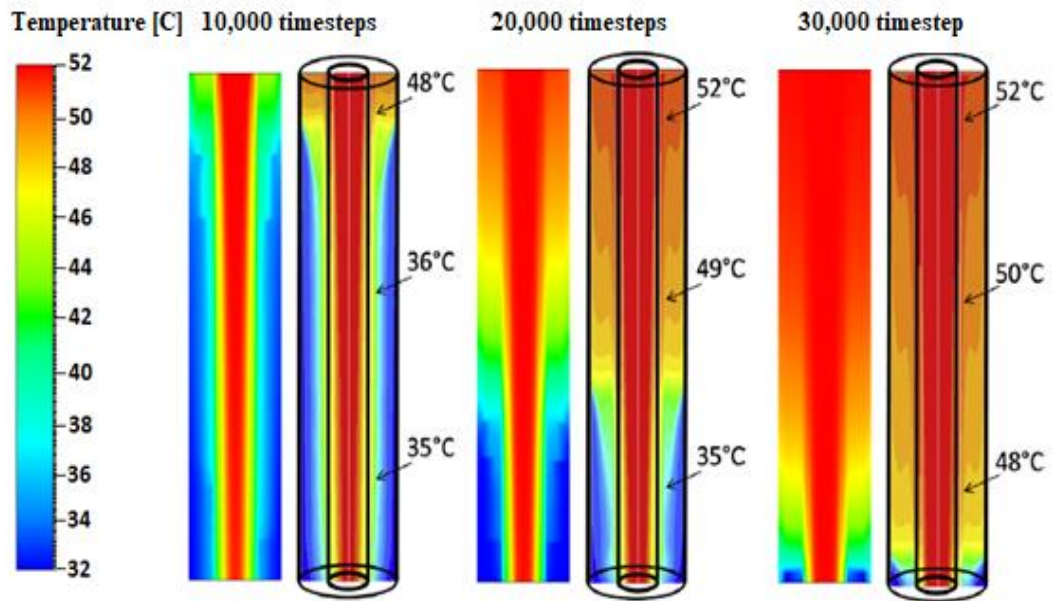
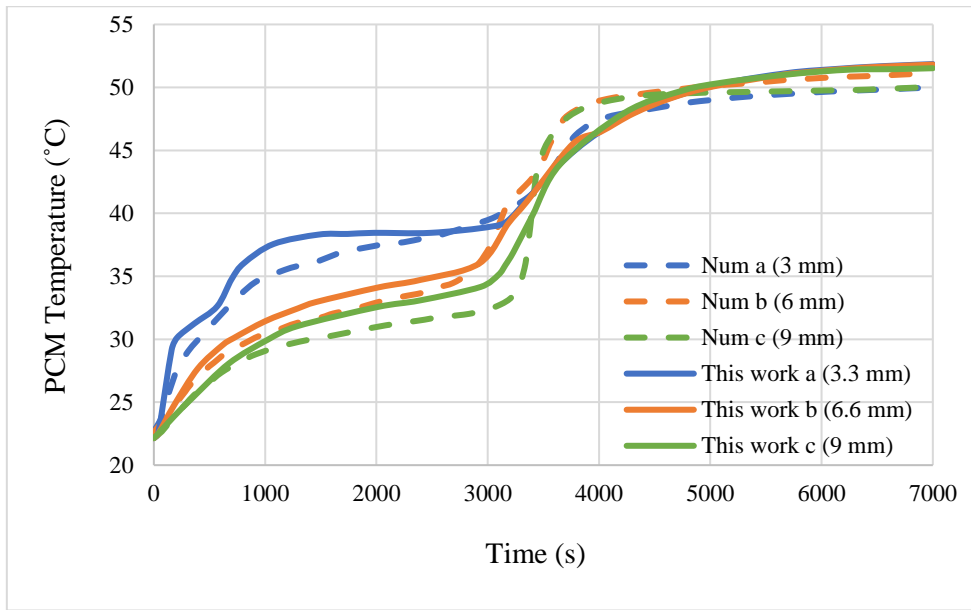
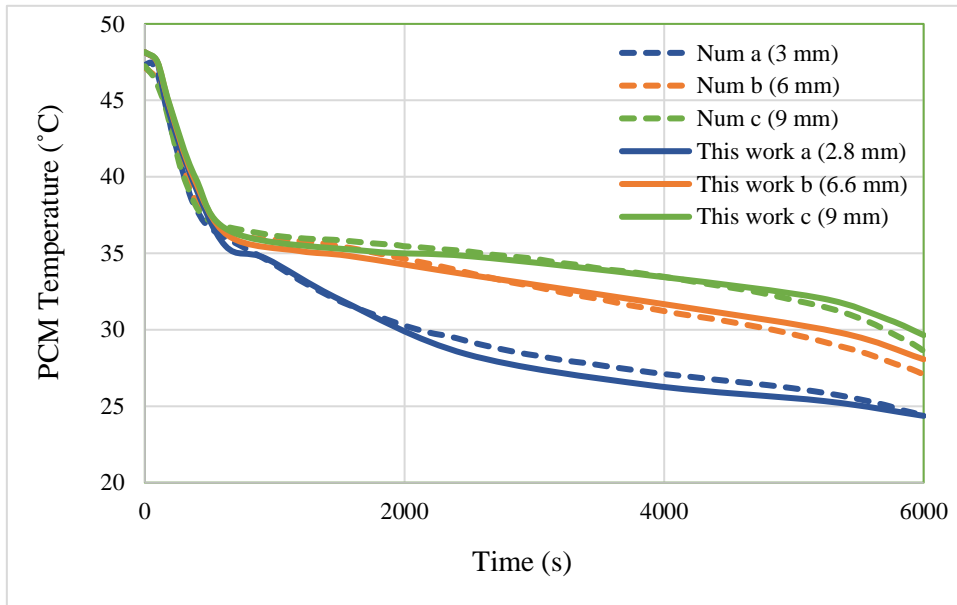


Figure 5.13: Temperature contours of the CFD solution (left) and the numerical results of Longeon et al. [186] (right) during charging with top HTF injection.

Figure 5.14 shows the temperature variations at the different locations within the cylindrical enclosure during charging and discharging with top and bottom HTF injection configurations. The initial temperature of the heat exchanger was 22°C , indicating that the PCM was solid before charging. However, upon charging, the PCM conducts heat to store the sensible heat until it reaches the melting point (35°C) where the latent heat is stored. The PCM temperature continues to increase above the melting point until it is completely melted at about 52°C while storing the sensible heat in the liquid PCM. The solidification of the PCM in the cylindrical enclosure is conducted at an initial temperature of 48°C same as for the model validation. The main mode of heat transfer in this process is conduction. The discharging process continues until the PCM is solidified. It can be observed that the temperature profiles for the two numerical results during the charging and discharging processes are similar.



(a)



(b)

Figure 5.14: Temperature variations of the radial points a, b, and c, at axial position D for the CFD solution and the numerical results of Longeon et al. [186] during (a) charging and (b) discharging process.

Statistical analysis was conducted to determine the variations between the CFD solution and the numerical results, using the PCM temperature profiles at the selected points. Table 5.4 shows the statistical parameters obtained for the charging and discharging processes. The analysis results show that the CFD solution closely matches the numerical results. However, a maximum error of 2.63°C was calculated between

Table 5.4: Calculated statistical parameters at the selected points.

Process	Location (mm)	Max. E (°C)	MAE (°C)	RMSE (°C)
Charging	a (3)	2.35	1.17	1.32
	b (6)	2.31	0.86	1.01
	c (9)	2.63	1.23	1.46
Discharging	a (3)	1.43	0.41	0.58
	b (6)	1.11	0.67	0.72
	c (9)	1.58	1.04	1.12

the two numerical models. The trend in the variations between the CFD results and the experimental and numerical results can be attributed to many factors such as the uncertainties in the measured thermophysical properties for example, the specific heat data recorded in the experiment. The specific heat data obtained in the experimental test conducted by Longeon et al. [186] was recorded only during the melting process and this may cause a larger difference between the simulation and experiment [186]. The thermocouple positions, and the impact it may have on the phase transformation during the melting and solidification of the PCM in the annular gap. In addition, heat losses, boundary conditions and assumptions used in the simulations can contribute to the observed variations [230].

The observed maximum discrepancy between the CFD solution and the experimental and numerical results is very close to the 2°C variation reported by Alam et al. [189] who validated the CFD model of the vertical cylindrical enclosure using the same experimental data. This indicates that the Fluent melting and solidification model is an acceptable representation of the configurations considered in this work and can reliably and accurately predict the thermal characteristics and dynamic performance of the TES system.

5.4 Chapter Summary

Modelling of phase change-based LHS is characterised as a complex phenomenon that requires an understanding of transport properties such as buoyancy-driven flows caused natural convection, volumetric expansion, and heat transfer processes. Two approaches: the variable and fixed grid methods used in solving heat transfer in phase change were analysed. The variable grid methods have a better prediction of the flow phenomenon and the position of the phase change interface. However, a fixed grid is the most applied method due to its advantages including a relatively easy solution, no explicit conditions need to be satisfied within the mushy zone, and the method can differentiate two boundaries using a temperature field.

The fixed grid enthalpy-based method of melting and solidification model in the Fluent was validated against experimental results available in the literature and compared with numerical results. The experimental test section of Longeon et al. [186] was modelled in 2D axisymmetric geometry that comprised the shell-and-tube walls, PCM and HTF domain. The CFD model used paraffin RT35 in the vertical cylindrical enclosure which is the PCM used in the experiment during the charging and discharging processes. Simulations were conducted on the melting and solidification of the paraffin in the vertical enclosure to validate the storage model and assess its performance. The fluid outlet temperature, temperature contours and temperature profiles of the CFD solution and the experimental and numerical results of Longeon et al. [186] were compared during the charging and discharging processes.

Statistical analysis was used to evaluate the variation in the fluid outlet temperature and PCM temperature profiles at different positions between the models. A maximum error of 0.92°C was found between the CFD solution and the experiment results. Furthermore, maximum errors of 2.46°C and 2.63°C were observed in the temperature profiles between the CFD solution with the experimental and numerical results. The results indicate that the CFD solution is in close agreement with the experimental and numerical results. The discrepancies in the experimental and numerical results may be because of the difference in the heat capacity of melting and solidification as indicated in the numerical model. The validated TES model will be applied to simulate the charge and discharge of the TES system and obtain the heat output

required to meet the detached dwelling's heat demand. However, the TES system needs to be sized first, and the sizing procedure is explained in Chapter 6.

6 Thermal Energy Storage System

6.1 Introduction

This chapter analyses the TES system, which comprised the cylinder model shell-and-tube heat exchanger and PCM. The TES system is being studied to determine how it can best fulfil the space heating requirements of the detached dwelling with wet central heating. The analysis involves determining the TES system's capacity based on the dwelling's heat demand and providing accurate information for sizing the storage system. The chapter also outlines the procedure for sizing the TES system, which is crucial as the heat demand through a heating season varies, requiring different heating charges and discharges to meet the space heating demand of the dwelling. The study further presents the design and development of the TES model based on the size and capacity of the storage system obtained, as well as the discretization of the CFD domain for performance evaluation.

6.2 Determination of the TES System Capacity

The maximum TES capacity (kWh) required to accommodate all possible next-day demands is obtained by integrating the peak day heat demand profile, while the energy to be stored before any 'next-day' commences is obtained by integrating each daily profile in day-ahead mode. Different storage capacities would be required at various times of the year throughout the heating season. The operational robustness of any TES design can be assessed only by using the peak heat demand profile to size the store and then only part-charging the store on non-peak days. The building energy simulation results indicated a peak day heat demand of 37-kWh for the detached dwelling. The simulated dwelling heat demand was obtained from the peak day extracted from the heating season profile analysed. However, for the pursuit of this work, indicating the procedure can be applied to any known dwelling heat demand, the detached dwelling peak day heat demand obtained is applied as an example of application to determine the TES system's capacity. Allison et al. [194] developed an approach that utilised simulated heat demand of buildings to predict the required TES system capacities that can be applied to support load-shifting capabilities. In this work, the approach developed by Allison et al. [194] has been adapted to obtain the

maximum TES system capacity required to meet the detached dwelling's heat demand loads. The approach involves reshaping the dwelling's peak day heat demand data obtained from the building energy simulations into equal segments with time steps that correspond to a certain period of desired load shifting. The required storage capacity (kWh) for example, of the dwelling's designed heat demand for each q -th segment through the heat demand profile for 24 hours was obtained by integrating the peak day heat demand profile (approximately 2509 cells) in the segments illustrated in Figure 6.1.

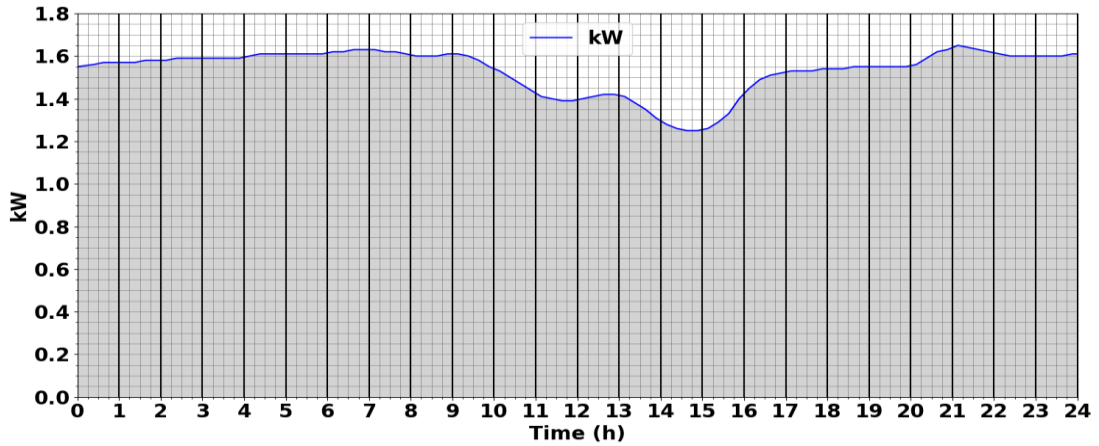


Figure 6.1: Discretised segmented diagram of a dwelling peak day heat demand profile.

Each cell in the segments represents 0.05×0.25 kWh of heat storage through a 24-hour scan to produce a storage capacity of 37-kWh. This analysis determines the required storage capacity for the detached dwelling's peak day heat demand and any other day heat demand through the heating season falls under this curve. Equation (6.1) describes the expression applied to determine the required TES capacity where n_{seg} is the number of segments in the 24-hours, i is the i -th time step in the simulation. E_{Dem} and E_{Loss} are the simulated building heat demand and storage energy losses (kWh), and q is the time segment [194]. In this approach, the maximum storage capacity of the TES system was used to determine energy losses in the storage system at each time step.

$$Q_{\text{tes},q} = \sum_{i=1}^{n_{\text{seg}}} E_{\text{Dem}}[i] + \sum_{i=1}^{n_{\text{seg}}} E_{\text{Loss}}[i] \quad (6.1)$$

This was applied to ensure all heat demands are met under all circumstances during the period of operation, with the assumption that the maximum storage capacity is required to meet the thermal demand load during the time segment q when the storage system is perfectly insulated. Storage heat loss analysis was conducted by Allison et al. [194] and the result of the analysis indicated that around 5% per day worst-case loss rate was appropriate for heat storage materials that include heavy-weight concrete, hot water, magnetite brick, and paraffin (C₂₈), and geometries such as tanks or the storage material integrated into building fabrics. In this regard, the required storage size for each q -th segment presented in Equation (6.1) has been transformed into the following:

$$Q_{tes,q} = (1.05) \sum_{i=1}^{n_{seg}} E_{Dem}[i]. \quad (6.2)$$

Equation (6.2) was applied in this work to obtain the TES system's capacity required to meet the peak day heat demand profile of the detached dwelling. The equation can also be applied to any other dwelling types to which their heat demands (kWh) per day are known. The calculated maximum TES system's capacity needed to meet the peak day heat demand of the detached dwelling and any other day through the heating season is 39-kWh. This value is used to define the size of the TES system.

6.3 The TES System Size and Configuration

The cylinder model of the shell-and-tube heat exchanger was selected for the TES system element with PCM in the annulus and HTF flowing through the tube at a relatively high temperature to charge and a low temperature to discharge the storage system. The shell-and-tube heat exchanger is applied to achieve a uniform heat transfer to the storage material. The TES system configuration has been designed to consist of several vertical shell-and-tube PCM elements that are commercially available. The PCM elements are designed with the same size, capacity, and thermophysical properties, and heat flux thermal condition is applied to the external wall as in a real sense, this study assesses the capability of the TES system to fulfil the detached dwelling's space heating requirement. The approach proposed in this work assumes passing the HTF through parallel tubes. Since all tubes are identical, a single storage element is

used for the analysis to simplify the model. An example of the approach utilising an HTF injection through parallel identical tubes has been demonstrated by Fang et al. [231] and Morisson et al. [232], with detailed models of heat transfer and fluid flow provided for the reported numerical solutions. Table 6.1 presents the dimensions and geometrical properties of the PCM elements within the TES system configuration. Figure 6.2 shows a schematic diagram of a typical TES system with the symmetric domain of the PCM element applied. The TES system contains 61 PCM elements. However, the size of the TES system is defined by the type of PCM applied.

Table 6.1: Geometric characteristics and configuration of the dwelling's TES system.

Configuration of TES System	Material/Dimension (mm)
Diameter of the TES system	Depends on No. of PCM elements
TES system material type	Steel
Shell-and-tube material type	Copper
The thickness of the shell-and-tube diameter	1
Tube/Inner diameter of PCM element (d_i)	22
Shell/Outer diameter of PCM element (d_o)	82
Length of the PCM element in the container	1000

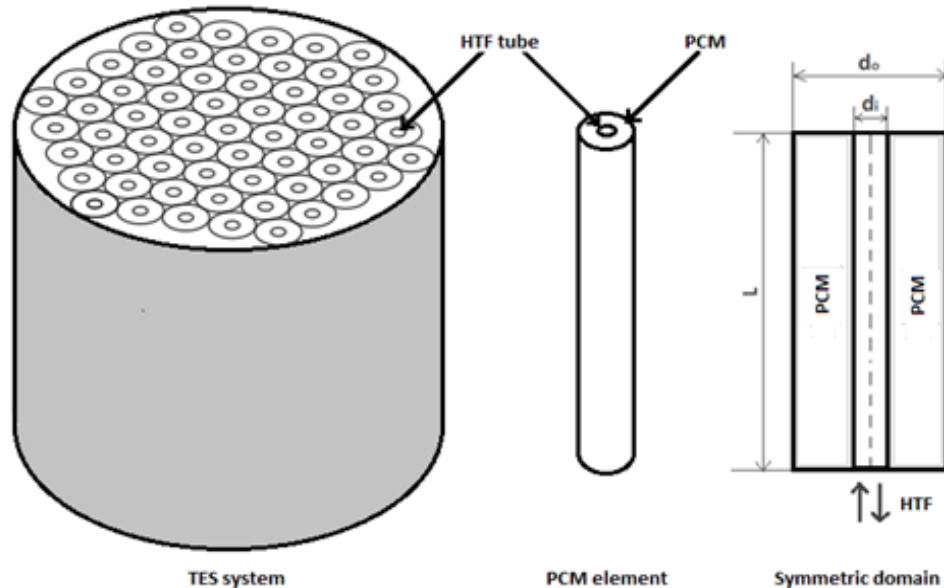


Figure 6.2: Schematic diagram of the TES system with symmetric PCM element domain.

Two PCM types, paraffin–PCM1 and inorganic hydrated salt–PCM2, were selected based on their latent heat TES potential (see Table 2.4). Investigations are conducted to analyse the TES system size using the PCMs. The PCMs were selected because of their high energy density, commercial availability, cost-effectiveness and higher latent heat of fusion compared to other types operating at a medium temperature range. The PCMs have been chosen to demonstrate their effectiveness for use in the TES system. It is important to note that, the PCMs are used to size the TES system based on the 39-kWh storage capacity. The TES system for the detached dwelling is designed to deliver the heat output required to meet the dwelling’s heat demand.

The TES system for the dwelling is designed with an n -number of storage elements. Table 6.2 presents the thermophysical properties of the selected PCM. The value of ‘ n ’ was then determined for the dwelling. The geometrical properties of the storage element and thermophysical properties of the paraffin and inorganic hydrated salt were applied to determine the total capacity (kWh) of a single storage element. The storage system size for the dwelling is determined by scaling up the PCM element capacity. The storage capacity for the single storage element is obtained using Equation (6.3) where m is the mass of the PCM in the annular gap, Q_{PCM} the total capacity (kWh) and h_m the PCM latent heat of fusion as presented in Table 6.2.

Table 6.2: Thermophysical properties of the PCM.

Properties	PCM1 [115]	PCM2 [28]
Melting temperature (K)	315.85 – 318.85	321
Dynamic viscosity (kg/m s)	7×10^{-3}	---
Latent heat of fusion (kJ/kg)	250	210
Density of PCM, solid (kg/m ³)	912	1600
Density of PCM, liquid (kg/m ³)	775	1666
Thermal conductivity (W/m K)	0.24	0.45
Specific heat capacity of PCM, solid (J/kg K)	1800	2410
Specific heat capacity of PCM, liquid (J/kg K)	2400	2410

$$m = \rho V, \quad Q_{PCM} = Q_{solid} + Q_{liquid} + h_m \quad (6.3)$$

To size a TES system, the obtained storage capacity (kWh) required for the detached dwelling is divided by the total capacity (kWh) of a single storage element obtained using the thermophysical properties of the PCM. This provides information on the minimum number of storage elements required by the TES system. Hence, the TES system is sized by the number of storage elements in the TES system.

With consideration to the corresponding storage capacity (kWh) obtained for the detached dwellings, the volume and number of storage elements of the thermal store needed for the detached dwelling were determined using the thermophysical properties of the PCMs. The thermophysical properties of the PCMs were applied to analyse the sizing of the storage system based on different PCMs considering the operating temperature of the TES system to provide heating assuming energy is stored or released at a temperature range of 36 to 60°C. The characteristics of the TES system for the detached dwelling were determined as follows:

- The TES system of 39-kWh capacity requires 107 storage elements, equivalent to a storage size of 0.75 m³, using the PCM1 as the storage medium for the detached dwelling.
- The TES system of 39-kWh capacity requires 84 storage elements, equivalent to a storage size of 0.61 m³, using the PCM2 as the storage medium for the detached dwelling.

The number of PCM elements needed for the dwelling's TES system is greater when PCM1 thermophysical properties are used. As a result, a larger TES system size is required. This shows that PCM2 has a higher energy density compared to PCM1. Therefore, this allows the use of a small-size TES system. This indicates that selecting PCMs with higher storage density enables better sizing of TES systems for wet central heating applications. In this case, PCM2 offers greater advantages than PCM1 in terms of performance and space constraints in buildings. Therefore, PCM2, the inorganic hydrated salt, will be used to size the TES system and evaluate the performance of the storage system in fulfilling the detached dwelling's heat demand.

6.4 TES System Sizing

The TES system sizing is achieved using the peak capacity of the storage system. The calculated maximum storage capacity of 39-kWh is applied to meet the space heat demands of the detached dwelling. The TES system sizing does not account for hot water use in the detached dwelling. However, the storage system is sized to fulfil each-day space heat demand of the dwelling throughout the heating season. The sizing approach uses a single thermal store that is sized based on the peak day heat demand or a percentage of the peak day heat demand. The dwelling's heating charge needed for lower demand days can be achieved by part-charging the thermal store or having a quantized store that can be charged to different levels to fulfil the heating needs. This implies that the sizing based on the peak storage capacity allows the TES system to be partially charged to a percentage of this capacity to meet the dwelling's heat demand for any given day. This approach ensures that the heating charge can be obtained to fulfil the daily space heating demand of the detached dwelling.

An investigation into a similar approach for sizing a TES system as part of a cooling system in building has been carried out [233]. The peak daily integrated coil load which occurs during periods of severe weather was used to determine the storage capacity. A significant component of the peak daily coil load was obtained based on the accumulated energy that was stored in the building materials and furnishings, during the period when the building is not cooled. However, in this study the TES system is sized based on the maximum storage capacity obtained from the peak day heat demand of the detached dwelling predicted using ESP-r building energy simulation.

To further demonstrate the sizing techniques, two days; day x and day y are randomly selected from the heating season analysed in Chapter 4. The boundary conditions, operational schedules, and all other parameters used to determine the next-day heat demand pattern of the detached dwelling are applied for building energy performance simulation. The ESP-r building energy simulation was conducted, and the detached dwelling's heat demands for the two days were obtained. The corresponding storage capacities required to meet the detached dwelling's heat demands for day x and day y were determined based on the method used to obtain the peak capacity of the TES system. The calculated storage capacities are 29-kWh and 33-kWh, representing the

charges needed by the TES system for the two days to meet the heating demands of the detached dwelling. The required heating charge for each day is smaller and can adequately fit into the peak heating charge. Figure 2 illustrates the sizing technique used in this study. The heating charge needed for days x and y, represented by the area under the curves fits well within the heating charge needed for the peak day.

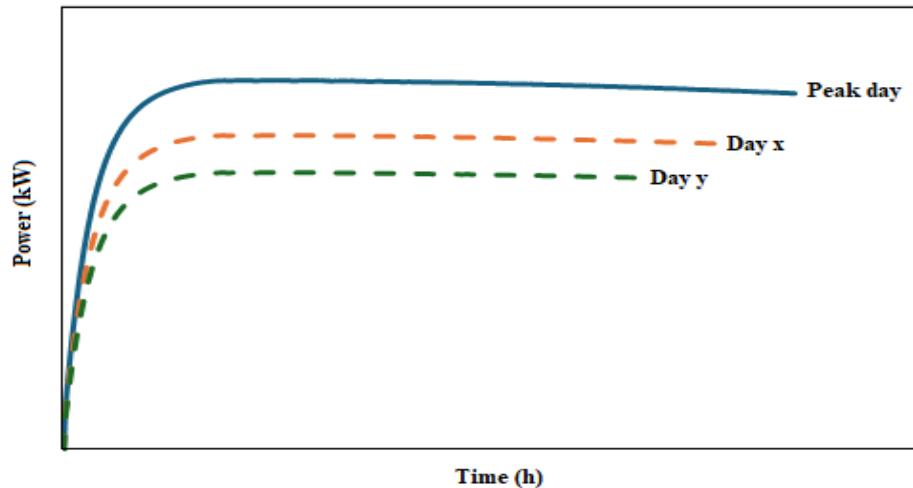


Figure 6.3: Characteristics of the TES system sizing.

It is clear from the analysis that the TES system can adequately contain the heating charge for days x and y, as well as for all other days through the heating season. In a real situation, the TES system needs to be charged daily. Although, the analysis does not detail on how the day x and day y heating charges are acquired. However, it does demonstrate the method applied in sizing the storage system. It is important to note that the daily heat demand may vary throughout the heating season, which means that the heating charge required by the TES system will also differ.

To obtain the daily heating charge needed other than the peak day, the TES system is charged to a certain percentage to achieve the necessary charge that adequately fulfils the dwelling's heat demand. This method may utilise a predictive controller to determine the required daily heating charge, as demonstrated by Allison et al. [167], where the next day's heating charge of a house is predicted based on forecast air temperature and solar radiation levels. In this study, the robustness of the solution is justified by charging the TES system to the maximum storage capacity to obtain the heating charge needed to meet the peak heat demand of the detached dwelling.

6.5 CFD Modelling of the TES System

This study uses a single storage element to model the TES system. This is because the PCM elements are identical and are assumed to deliver the same output capacity. This allows a single storage element to be modelled as a replica of the others and its capacity is multiplied by the number of the storage elements in the TES system. The storage element is designed with an aspect ratio (L/D) of 12, containing the inorganic hydrated salt placed in the annular gap. The HTF (water) flows through the tube to charge and discharge the storage element.

Considering the geometry of the storage element presented in Figure 6.2, a 2D axisymmetric model is developed to analyse the performance of the TES system. Figure 6.4 presents the schematic of the 2D axisymmetric geometry and computational domain of the storage system. The HTF pipe thickness of 1mm is used in the model. The 2D computational domain that comprised the HTF section (tube) and PCM section (annular gap) has been discretised with a fine mesh (equivalent to that applied for the TES model validation). This produces a mesh of 11,000 cells in the HTF and 28,000 cells in the PCM domains respectively. The 2D axisymmetric meshed domain of the storage element illustrated in Figure 6.4, is applied to conduct simulations for charging and discharging of the TES system. A domestic heat pump with a capacity

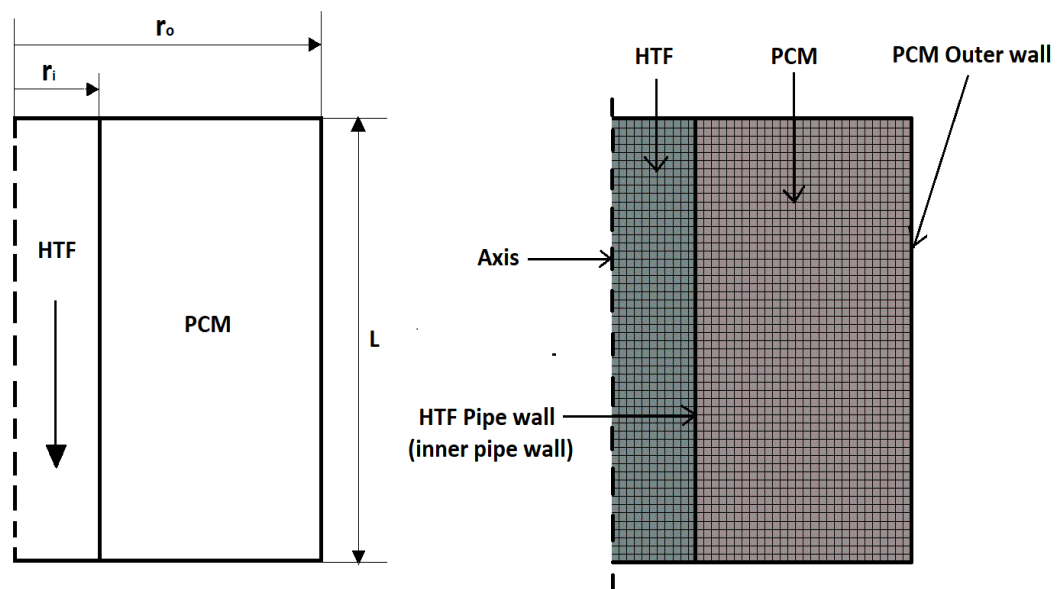


Figure 6.4: The axisymmetric geometry and part of the discretised mesh domain of the storage element.

matched to the operational requirement for wet central heating is applied to charge the PCM element. In practice, the storage element can be charged using any type of domestic heat pump. Investigations into the application of various heat pumps such as air, water, and ground sources in charging TES systems for domestic heating have been demonstrated elsewhere [14,16,145,234]. The pre-charged TES system is discharged to determine the heat output that matches the detached dwelling's heat demand. Appendix IIB summarizes the input data required to run the TES system's CFD model.

6.6 Chapter Summary

The study outlined the procedure to determine the TES system capacity based on the simulated heat demand of the detached dwelling. The simulated peak heat demand (kWh) was used to analyse the energy loss in the storage system and to determine the maximum storage capacity needed to meet the heat demands of the detached dwelling. The analysis of the storage system energy loss was carried out and a 5% worst-case energy loss per day was used to determine the TES system capacity.

The maximum storage capacity was used to size the TES system. The storage system was designed to fulfil the peak heating charge therefore, the TES system can be applied to meet the heating requirements of the dwelling for any day. The size of the TES system was assessed using paraffin and inorganic hydrated salt as storage mediums. Inorganic hydrated salt, having a higher storage energy density and requiring fewer storage elements than paraffin, was chosen to evaluate the TES system's performance. A PCM-based storage medium with a greater latent heat of fusion and storage energy density is favoured for TES applications.

The cylinder model of the shell-and-tube heat exchanger was selected as the suitable TES system configuration for the application of wet central heating. The single storage element that comprised the vertical cylindrical enclosure was modelled using a 2D axisymmetric domain. The 2D axisymmetric domain was discretised with a fine mesh to enable the charging and discharging of the storage element. The CFD model is now ready to use, to study the dynamic performance of the storage system during charging and discharging to meet the heating requirements of the detached dwelling.

7 Thermal Energy Storage System Performance Evaluation

7.1 Introduction

This chapter presents a study that examines the performance of the TES system during its charging and discharging cycles. The TES system model developed is evaluated to determine its thermal performance for application in wet central heating systems, aiming to fulfil the space heating needs of a detached dwelling. The analysis involves using a domestic heat pump with size characterised by its compatibility with wet central heating, to charge the TES system and to discharge it, ensuring the necessary heat output is available to meet the dwelling's heating demands. The study investigates the performance of the TES system using Fluent, CFD software. The characteristics of the domestic heat pump, including the mass flow rate and flow temperature, are incorporated into Fluent simulations. This is to charge the TES system with a heating equivalent necessary to meet the dwelling's heat demand and to assess the storage system's thermal performance. A sensitivity analysis of the charging rate is conducted to evaluate the performance of the TES system during the charging process. This analysis examines the impact of varying the HTF mass flow rate and the use of top and bottom HTF injection configurations on the TES system's charging rate. The analysis includes using the Fluent techniques to discharge the TES system, utilising the necessary mass flow rate and temperature to deliver storage heat outputs that align with the dwelling's peak heat demand profile and achieve a suitable outlet temperature for radiators to fulfil the space heating needs of the dwelling.

A domestic heat pump with mass flow rates [235] suitable for charging the TES systems is applied to analyse the TES system's thermal performance. The domestic heat pump can provide a continuous hot water flow at various temperatures without problem [236]. The heat pump flow rate is determined by its operating capacity and temperature difference between flow and return. The heat pump operates with an HTF mass flow rate that can be obtained using Equation (7.1) where Q_{HP} is the heat pump capacity (kW), \dot{m} the mass flow rate (kg/s), C_p the specific heat capacity (J/kgK) and ΔT the temperature difference between flow and return.

$$\dot{m} = Q_{HP}/C_p(\Delta T) \quad (7.1)$$

To charge the TES system independent of any dwelling, the mass flow rate and temperature of a domestic heat pump are utilised. The heat pump operates to determine the extent to which the TES system is charged with consideration of the period required to achieve full charging. The TES system is discharged to extract the power output that matches the detached dwelling's heat demand profile. The thermal behaviour of the TES system during the charging and discharging processes is described. This showcases the operational ability of the TES system in real situations.

7.2 TES System Charging

In this work, the operation of a 7kW domestic heat pump is emulated using the CFD techniques to provide hot water flow at a relatively high HTF velocity for charging the TES system. Figure 7.1 presents the schematic diagram describing the heat pump integrated TES system configured to operate in offline mode to charge the TES system. The heat pump is virtually applied to continuously provide hot water of 60°C at maximum and minimum mass flow rates of 0.24 kg/s and 0.33 kg/s respectively through the tube until the TES system is a fully charged within a specified period. The temperature and mass flow rates are representative of a typical ASHP [237]. The temperature and mass flow rates are applied to conduct a limited sensitivity analysis, by examining the TES system's charge rate over a specified timeframe to assess the solution's performance. The study analyses the thermal behaviour and dynamic performance of the TES system during the charging process.

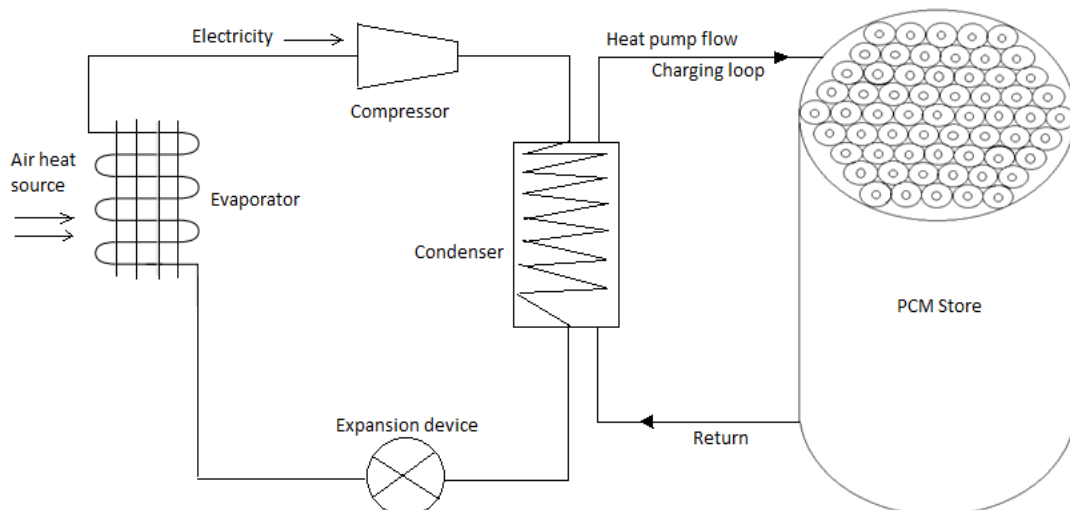


Figure 7.1: Schematic diagram of heat pump charging a TES system.

The analysis involves examining the energy stored in the TES system and assessing its state of charge based on the mass flow rates to evaluate the charging rate of the storage system. Simulations for charging the storage system are carried out to provide the flow requirement needed to charge the TES system for wet central heating. An example of an application involving varying the mass flow rates of a heat pump to charge the TES system is demonstrated in the analysis. As discussed in the previous chapter, the TES system was modelled using a single storage element. The 2D computational domain of the storage element presented in Figure 6.4 is applied to simulate the charging of the TES system and analyse its state of charge to store the heating charge required to fulfil the heating needs of the detached dwelling.

Figure 7.2 illustrates the storage element geometry represented with a 2D symmetry that shows the positions of points A, B, and C, located at 250 mm, 500 mm, and 750 mm respectively along the length of the storage element, with a radial distance of 26 mm about the centre of the PCM in the annulus. These points are defined at the given radial and axial dimensions to analyse the TES system's performance by predicting the temperature in the storage system at the various locations during charging and discharging with top and bottom HTF injection configurations.

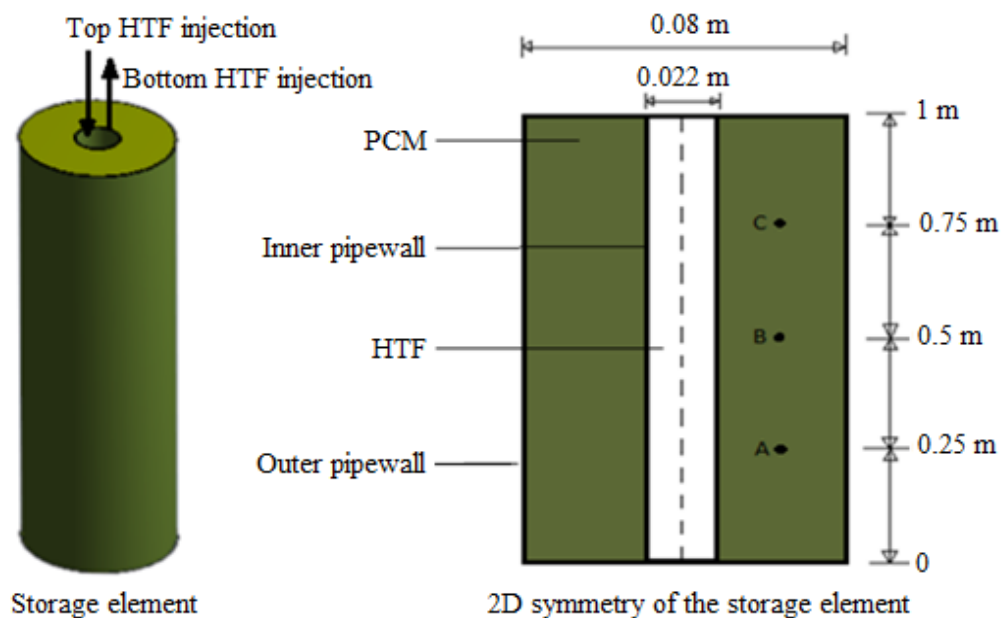


Figure 7.2: Schematic diagram of the single storage element.

A study has been conducted to determine the rate at which the TES system can be charged faster with top and bottom HTF injection configurations. The computational domain of the storage element was set at an initial temperature of 25°C (PCM is solidified) for simulation to analyse the TES system's charging performance. In a real sense, the initial temperature may be greater because the system is considered a control volume when the storage system is well-insulated. A constant HTF inlet mass flow rate of 0.33 kg/s with a flow temperature of 60°C was set at the boundary condition. This indicates a relatively very high HTF velocity is applied to ensure an almost constant wall temperature for the system's efficient operation during the charging process. The simulation runs until a full storage system charge is achieved.

The simulation results for the preliminary investigations are presented by comparing the temperature contour between the top and bottom HTF injection configurations as shown in Figure 7.3. When charging the storage system via top HTF injection, the PCM melting front descends in a vessel shape through the annular region. This is due to the natural convection that arises once a sufficient layer of the PCM has melted. The upper portion of the vertical enclosure melts initially causing the heated liquid PCM to flow downward within the annular space. With bottom HTF injection, the melting front advances counter to gravitational force; hot liquid PCM ascends to melt

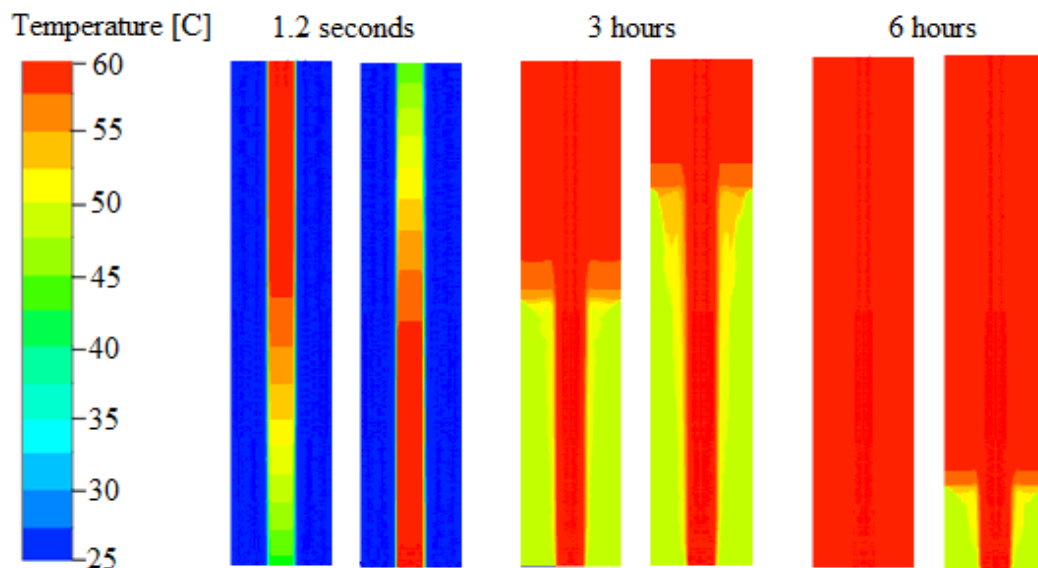


Figure 7.3: Variation of temperature contour of the storage element during charging with a top (left) and bottom (right) HTF injection of 0.33 kg/s at 60°C.

the upper PCM layer and natural convection induced to intensify the melting process. The storage system exhibits similar characteristics at the beginning of the charging process. However, a more rapid charge of the TES system is evident when utilising the top HTF injection. This occurs due to the buoyancy force in the direction of the HTF flow which makes the convection process faster. Notably, with the top HTF injection, the storage system achieves full charge in approximately 6 hours. In comparison, the bottom HTF injection, charges about 80% of the storage element within the same time frame. This demonstrates that the top HTF injection method is more efficient and enables a quicker charging process than the bottom HTF injection method.

Figure 7.4 illustrates the state of charge for the TES system comparing the average PCM temperature in the scenarios where the HTF is injected from the top and bottom of the storage system at a flow temperature of 60°C. Initially, a rapid increase in the TES system's state of charge, is attributed to the significant temperature change during the storage of the PCM's sensible heat. As the process nears completion, the rate of charge increase diminishes due to the reduced temperature differential between the HTF and PCM. However, a close correlation between the storage charge rate indicated by the percentage of average PCM temperature for the top and bottom HTF injection configurations can be depicted.

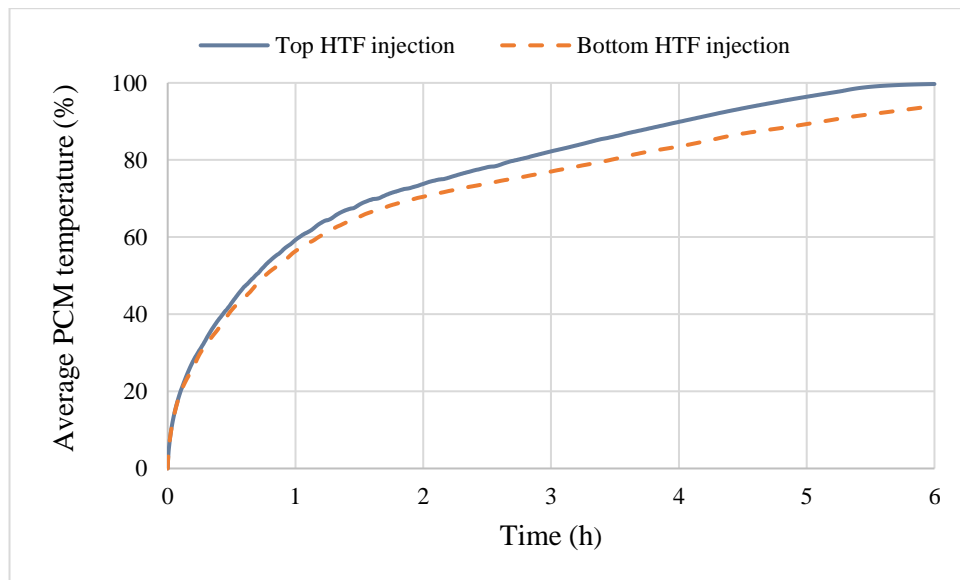


Figure 7.4: Variation of average PCM temperature during charging with top and bottom HTF flow of 0.33 kg/s at 60°C.

Using statistical analysis, a 5.1% variation was observed using the root mean square (RMS) of the average PCM temperature between the top and bottom injection methods. The study by Longeon et al. [185] recommends the top HTF injection during the charging process and the bottom during discharging. This is because the storage system is easily manageable during partial charging as most heat accumulates at the upper section. Consequently, the stored energy can conveniently be retrieved through bottom-charging [186]. In the present work, the top HTF injection configuration is considered for charging the TES system. This suggests that the storage system discharge should be conducted using the bottom HTF injection configuration.

7.2.1 TES System Charging Control Procedure

To enable an efficient and effective TES system charging required to store the heating charge needed by the dwelling for the next day, a simplified control system is proposed in the charging network. Day-ahead charging of the TES system enables appropriate storage size by incorporating weather forecasts and occupancy patterns to predict the heating charge needed by the dwelling. As soon as the charging starts, a control signal with information on the energy stored by the TES system over a time interval is sent to the controller. This process is continuous until the total energy stored adequately matches the predicted heat demand of the dwelling. In this condition, a successful TES system charging is achieved. Hence the charging stops. The day-to-day TES system charging control procedure is summarised in Figure 7.5.

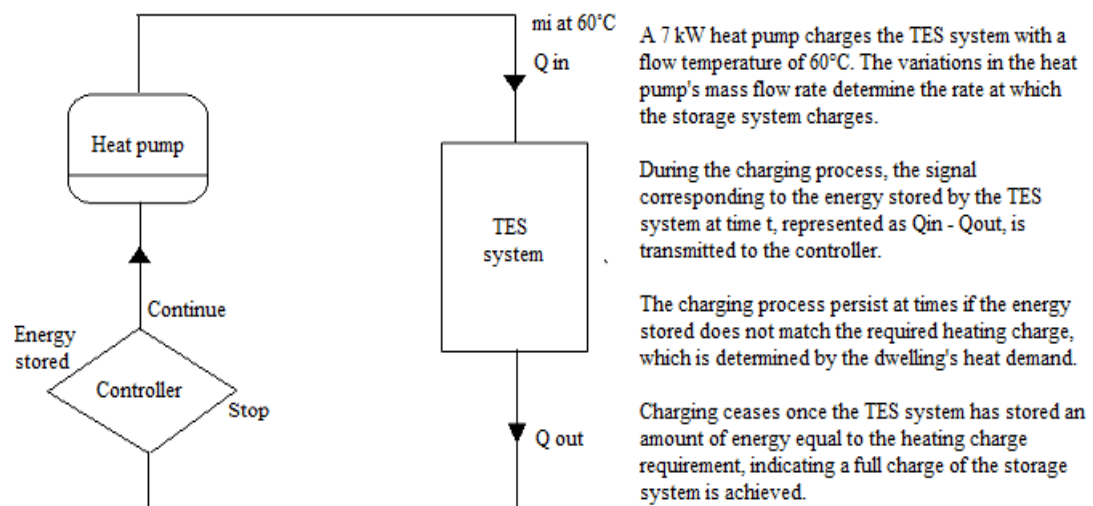


Figure 7.5: Schematic of a day-to-day TES system charging control.

The charging control procedure can be applied to obtain the required heating charge for the dwelling's heat demands throughout the heating season. The specific enthalpy of the PCM, corresponding to its average temperature, is used to calculate the total energy stored in the system at any given time. The stored energy is determined by multiplying the specific enthalpy with the PCM's mass as expressed in Equation (7.2) where $Q(t)$ represents the energy stored (in joules) in the TES system, m is the mass of the PCM (in kg), and $h(t)$ is the specific enthalpy (in J/kg) of the PCM at time t .

$$Q(t) = m \cdot h(t) \quad (7.2)$$

This technique offers a means to measure the energy stored as the PCM experiences temperature variations and possible phase transitions, which are crucial for the performance of the TES system. The specific enthalpy of the storage unit indicated by the PCM temperature at a particular time is obtained in the Fluent simulation and used to quantify the energy stored in percentages that determine the TES system state of charge. In this scenario, 0% (36°C) and 100% (60°C) represent the minimum and maximum storage system charge levels respectively. A full charge is achieved when the PCM is in a liquid state, which signifies that the temperature of the PCM at time t is equal to or higher than the HTF inlet temperature. The TES system's state of charge at time t can be determined using Equation (7.3) [238].

$$State\ of\ Charge\ (T) = \begin{cases} 100 & T_i \geq T_{inlet} \\ \int_{T_i}^{T_l} \frac{cp(T)dT}{\Delta hi} \times 100\% & T_{ref} \leq T_i \leq T_{inlet} \\ 0 & T_i < T_{ref} \end{cases} \quad (7.3)$$

The energy stored (%) is calculated by the integral of the enthalpy at a specific time, divided by the PCM's total enthalpy. In this study, the heating charge required by the detached dwelling is stored when the TES system reaches full capacity. Under this condition, the TES system is 100% charged, indicating a successful heating charge is obtained for the dwelling. This is evidenced by correlating the operation condition to the charging rate, where the state-of-charge of the TES system is 100% at the end of various charging cycles, using the differing heat pump mass flow rates. Consequently, the TES system is deemed to be fully charged. This condition ensures that the

TES system operates efficiently to effectively meet the heat demand of the dwelling. The state of charge of the TES system is analysed to predict its performance under different heat pump mass flow rates. The extended operation of heat pumps can minimise start and stop cycles leading to lower energy loss and the system can achieve a more stable and energy-efficient performance while effectively meeting the thermal needs of the dwelling. The maximum and minimum heat pump mass flow rates and mean values are used to simulate the charging of the storage system. A limited sensitivity analysis is carried out to study the system performance and ensure efficient and effective charging of the TES system is achieved in a specified time. Simulations are then conducted using the established heat pump mass flow rates to explore how fast or slow the TES system can be charged. This analysis highlights the thermal behaviour of the storage system under varying charging rates.

Figure 7.6 shows the TES system's state of charge at varying heat pump mass flow rates. It can be depicted that the storage system is charged to its maximum capacity (100%) at the end of the charging process for the various heat pump mass flow rates. This indicates that, despite the differences in flow rates, the TES system successfully reaches full charge under each condition, however, at different charging times. The analysis demonstrates the system's ability to store the maximum thermal energy regardless of the mass flow rates used during the charging process.

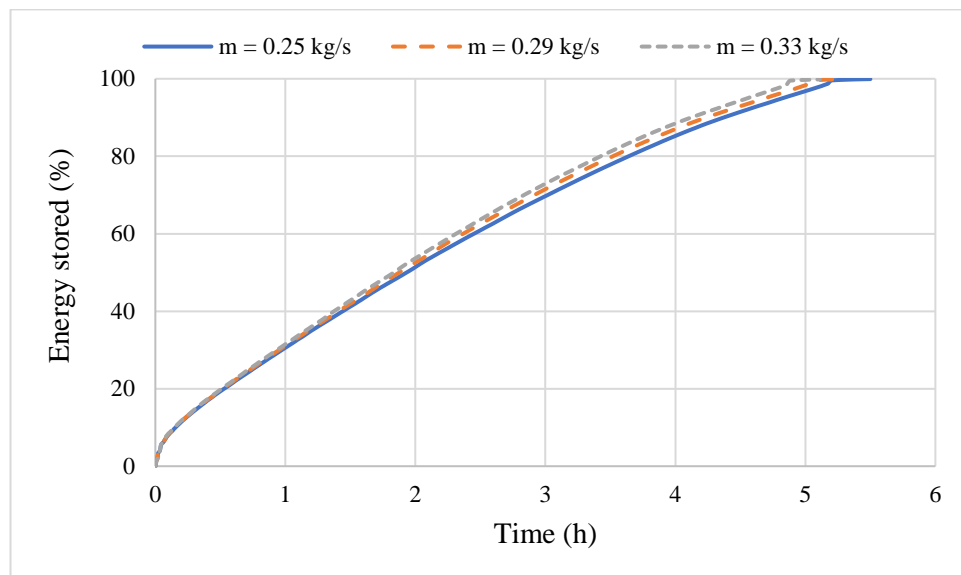
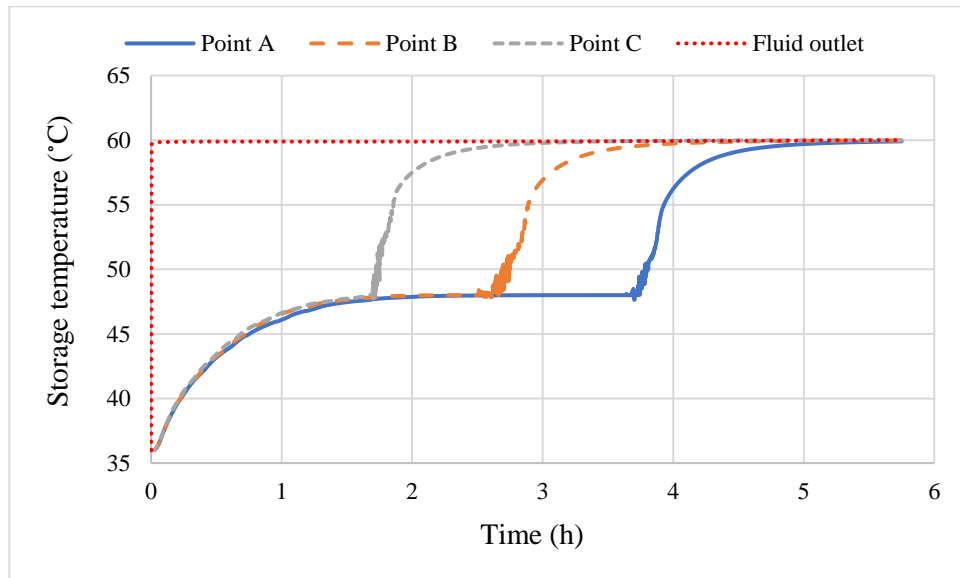


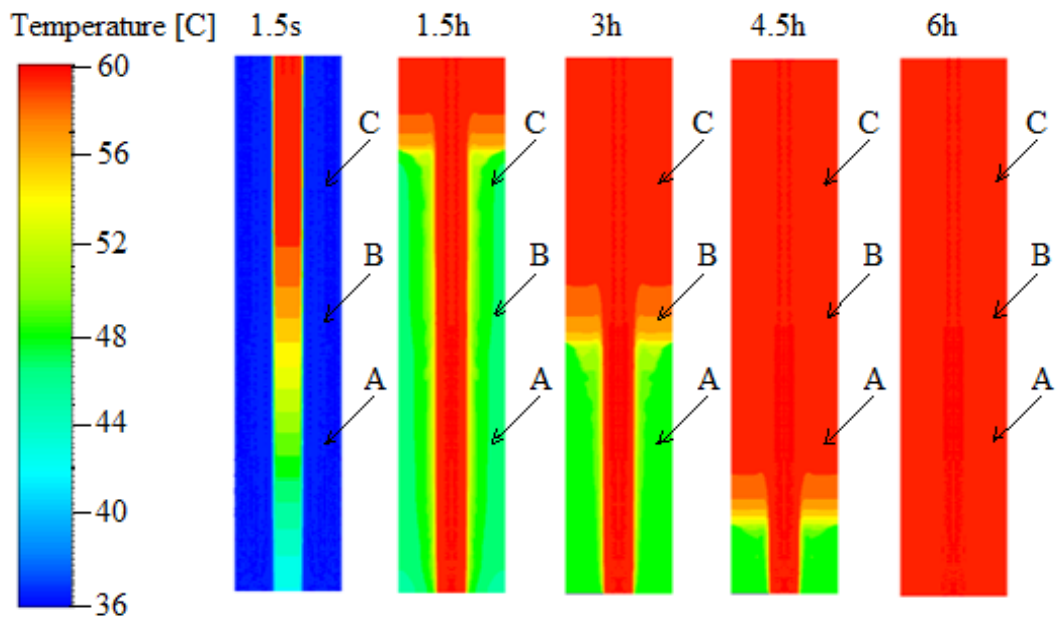
Figure 7.6: State of charge of the TES system at different mass flow rates for the charging process.

Moreover, the analysis results indicate that a higher mass flow rate of the heat pump leads to faster charging of the storage system. This is because the convective heat transfer is enhanced by allowing more heat to be stored in the TES system in a shorter time. The HTF has less time to exchange heat within the system and this might reduce the temperature difference between the HTF inlet and outlet, hence the thermal storage efficiency can be reduced. In this case, an optimal mass flow rate can balance the fast charging with energy efficiency and heat transfer effectiveness.

Figures 7.7–7.9 depict the evolution of temperature contours within the storage element over time, alongside the temperature profiles at the specific points A, B, and C within the storage system. These visual representations provide insights into the thermal characteristics of the TES system under real operating conditions. It is evident that the temperature of the storage system varies over time, as demonstrated by the increase in its temperature from 25°C at the beginning to 60°C at the end of the charging process. However, the fluid temperature in the tube remained largely unchanged during the charging process. This is attributed to the high HTF velocity, which helps maintain nearly constant wall temperatures as the HTF spends less time within the tube. Consequently, the temperature difference between the HTF and the inner tube wall remains minimal. In contrast, at lower velocities, the HTF remains in contact with the storage medium for a longer duration, allowing more heat transfer and resulting in a greater temperature change. The alignment of the temperatures at various points in the system with the fluid outlet temperature at the end of the charging cycles to 60°C indicates that the system has been effectively charged. The consistent temperature profile across the different locations within the TES system further supports this conclusion, confirming the full charge. Additionally, the temperature contours and profiles at these points closely match the inlet HTF temperature further validating the full charge of the TES system. Following this successful charging, the TES system is then discharged to obtain heat output that matches the peak day heat demand of the detached dwelling. The analysis of the TES system's fluid output temperature and its implications for the performance of heating systems (radiators) is conducted to demonstrate its effectiveness in real-world applications.

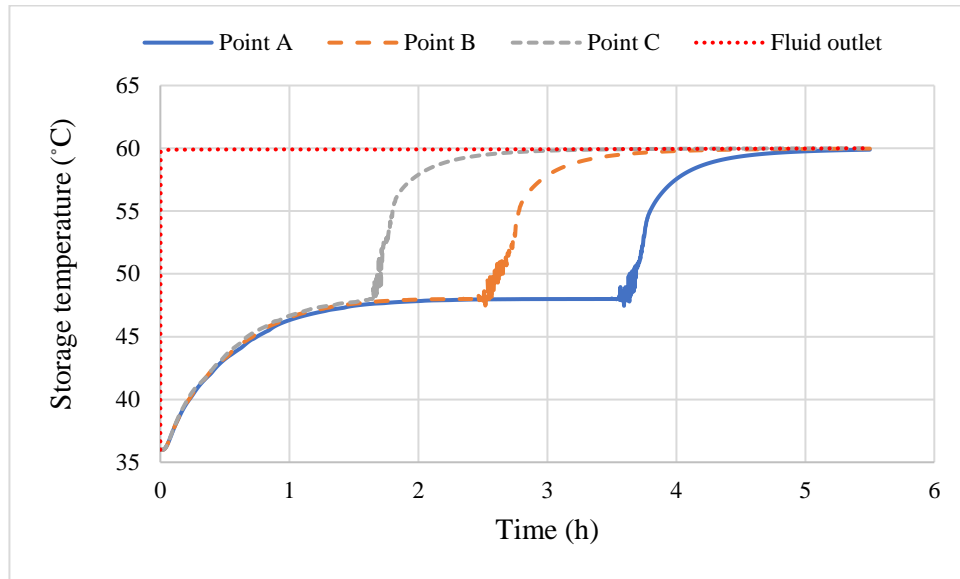


(a)

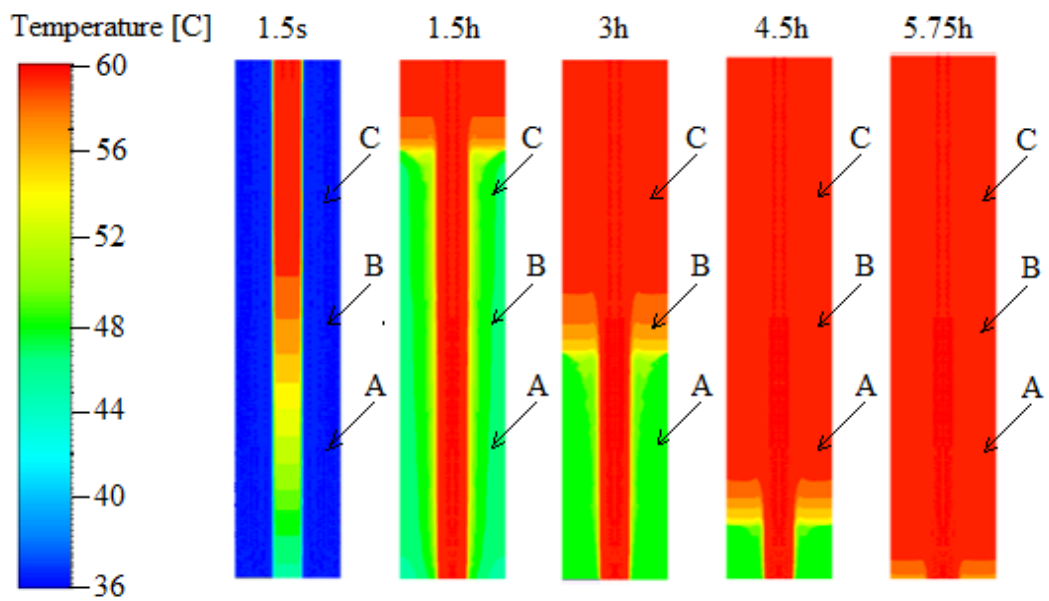


(b)

Figure 7.7: Variation of TES system: (a) temperature at points A, B, C and outlet and (b) temperature contour of the storage element over time during the charging process for an HTF flow of 0.25 kg/s at 60°C.

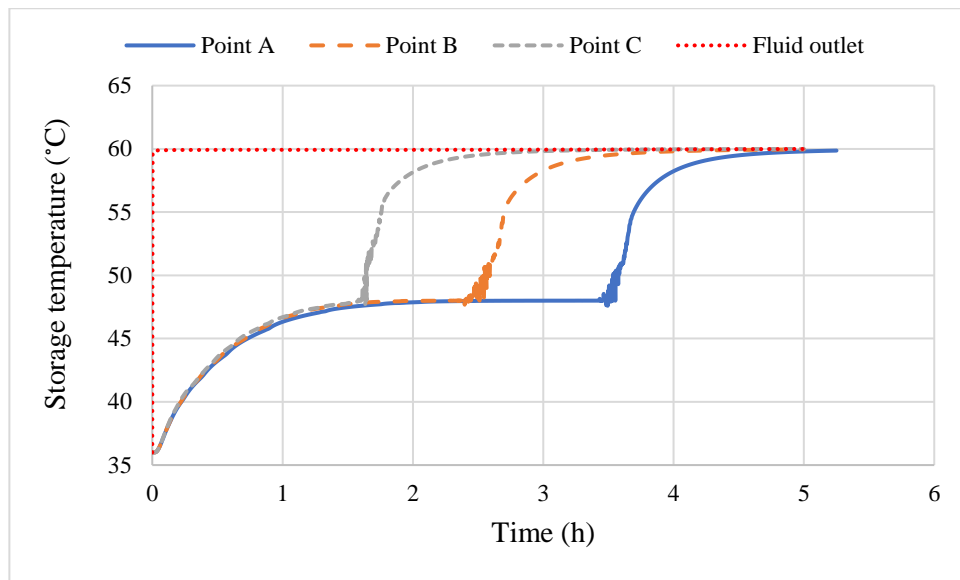


(a)

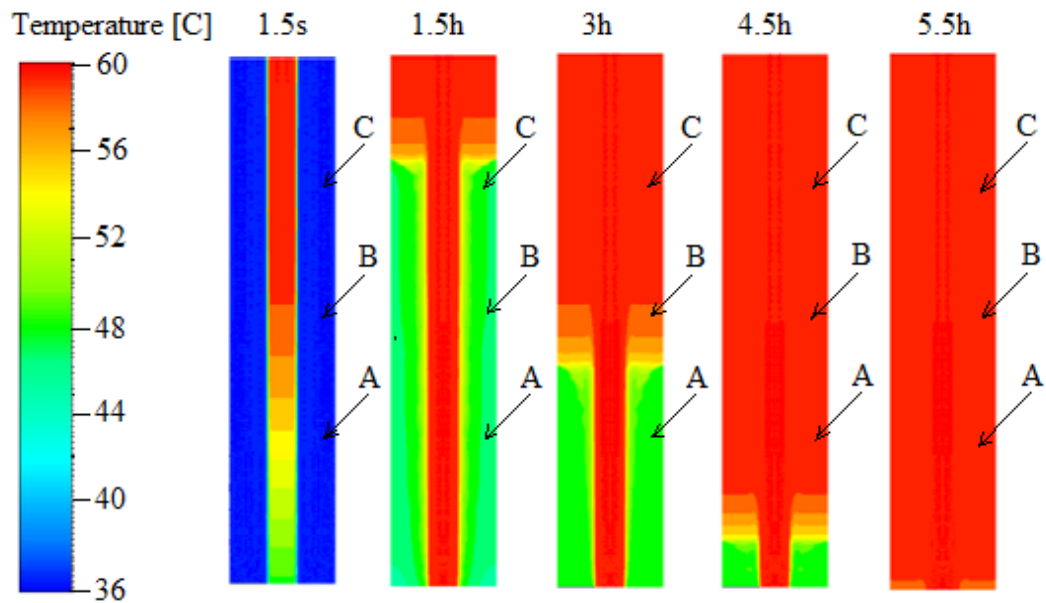


(b)

Figure 7.8: Variation of TES system: (a) temperature at points A, B, C and outlet and (b) temperature contour of the storage element over time during the charging process for an HTF flow of 0.29 kg/s at 60 °C.



(a)



(b)

Figure 7.9: Variation of TES system: (a) temperature at points A, B, C and outlet and (b) temperature contour of the storage element over time during the charging process for an HTF flow of 0.33 kg/s at 60°C.

7.3 TES system Discharging

The pre-charged TES system is discharged the following day to extract heat at varying levels throughout the day, to fulfil the day with peak heat demand of the detached dwelling. This indicates that the TES system can be strategically discharged to meet the dwelling's heat requirements on any given day during the heating season. This integration ensures that the pre-charged TES system efficiently supplies heat to the dwelling as needed, to maintain thermal comfort within the building. The TES system discharges using a time-variant inlet water flow maintained at a suitable flow temperature for domestic wet central heating. This approach ensures that the discharge matches the dwelling's peak (or any other) day heat demand profile at specific discrete times by controlling the flow rate and temperature according to the demand throughout the discharging cycle so that the system efficiently meets the dwelling's heating needs. An example of a discretised heat demand profile, which outlines the heating requirements at various intervals during the day, has been detailed in Chapter 6. The pre-charged TES system discharges with a circulating water flow, to extract energy for the dwelling's heating needs. Figure 7.10 presents a schematic diagram describing the TES system's discharging process. The diagram illustrates how the TES system integrates with the dwelling's heating system to meet the space heating requirements.

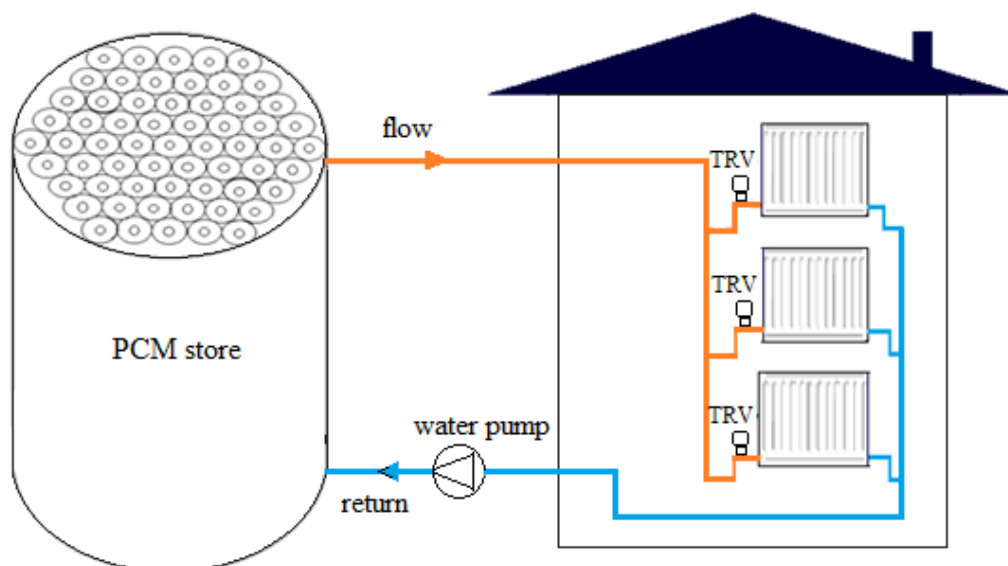


Figure 7.10: Schematic of TES system discharging heat to a dwelling.

A study is conducted to investigate a suitable water return temperature from dwelling heating systems utilising a domestic heat pump flow for space heating. An appropriate heating system for example, a radiator water return temperature is established and used as the inlet fluid boundary condition necessary for discharging the storage system to extract the heat output. Most studies utilised a temperature difference (ΔT) of less than 20°C between the flow and return fluid temperatures in wet central heating. However, the return fluid temperature depends on a variety of factors such as radiator design, flow properties the thermal output required and other variables that impact the system's efficiency [239] through the heating period.

In the study conducted by Kelly and Cockroft [24], ΔT in the range of about $10\text{--}20^{\circ}\text{C}$ was observed between the flow and return temperatures in field trials and utilised in building energy simulations for assessing ASHP retrofitted in dwellings. The study by Kelly et al. [28] also confirms this, for the field trial and building energy simulation conducted for the assessment of ASHP load-shifting performance. Lin et al. [240] examined the performance of ASHP integrated with LHS materials to improve system performance in cold regions through experimental and numerical modelling. An initial ΔT of about 20°C between the flow and return was used to assess the storage system's efficiency during discharge. This aligns with the common practice for ΔT between flow and return, often considered optimal for balancing efficiency and effective heat extraction. In real-world applications, the temperature differential between the flow and return fluid in wet central heating is not constant. Instead, it varies over time to match the thermal load during the heating process.

7.3.1 Determination of Radiator Fluid Outlet Temperature.

It is important to develop a method to assess the connection between the TES system and the radiator to analyse the performance of the system to meet the space heating needs of the detached dwelling, as it would in a real situation. This analysis demonstrates the linkage between the storage output and radiator operation, determining the radiator fluid outlet temperature, which serves as the fluid inlet temperature for discharging the TES system. In this work, no attempt is made to model the dynamic coupling between the thermal storage model and the dwelling model. Instead, the connection is established via a simplified model as represented by Equation (7.4),

based on TES output data from the CFD analysis and the known heat demand profile of the detached dwelling. The radiator return temperature can be calculated by rearranging Equation (7.4) into Equation (7.5), where T_r is the radiator return temperature ($^{\circ}\text{C}$), T_f is the temperature ($^{\circ}\text{C}$) of the hot water flowing to the radiator from the store, \dot{m} is the mass flow rate (kg/s), and \dot{Q} is the load (kW) needed to maintain the room temperature in the dwelling. The mass flow rate and temperature applied to the

$$Q = \dot{m} \cdot C_p (T_f - T_r) \quad (7.4)$$

$$T_r = T_f - \frac{Q}{\dot{m} \cdot C_p} \quad (7.5)$$

radiator, are obtained from the CFD analysis of the storage discharge, while \dot{Q} represents the heating load for each timestep, derived from the predicted heat demand profile of the detached dwelling. In this analysis, the mass flow rate and temperature at each timestep from the CFD analysis are known, and extracting the load from the radiator determines the outlet temperature, which is then supplied to the thermal storage system for the next discharge segment. An example application is conducted to determine the radiator outlet temperature at discrete points over time from the heat demand profile of the detached dwelling, as presented in Figure 7.11.

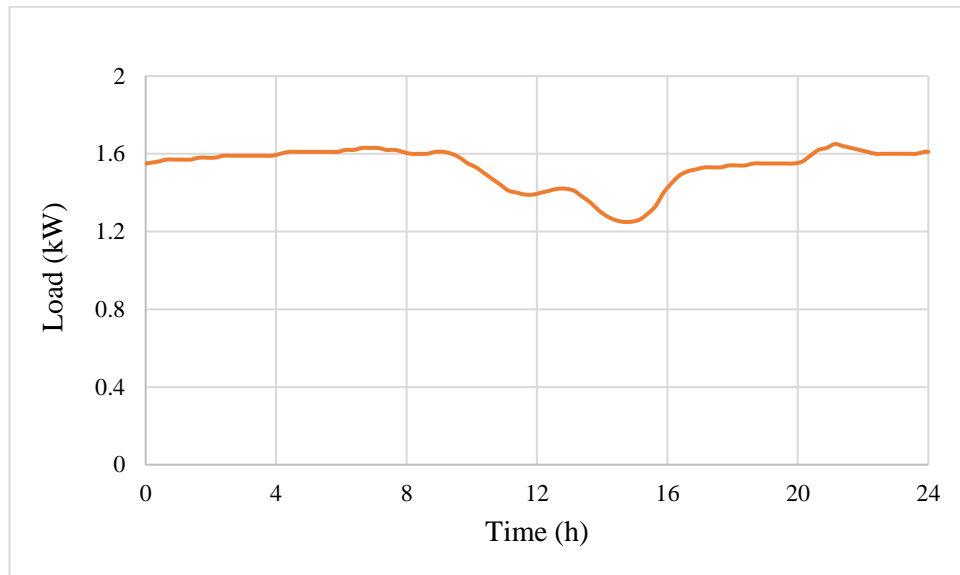


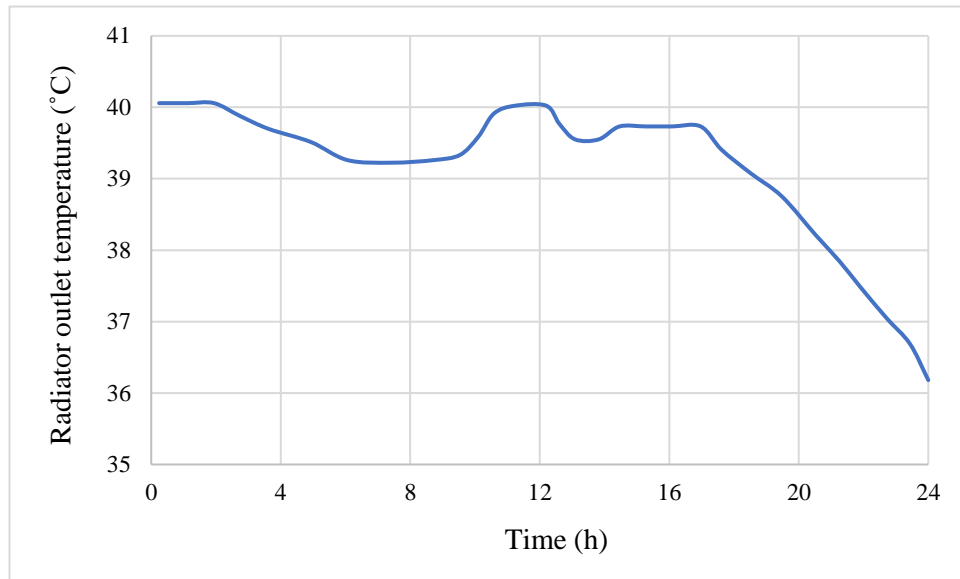
Figure 7.11: Variation in the detached dwelling's heating load over time.

Upon discharging, this process provides a new thermal storage return temperature to the radiator, which produces a new radiator outlet temperature that returns to discharge the storage system, continuing as a cycle. Considering the heating load profile presented in Figure 7.11, at 4:00 hours, the demand profile indicates that 1.6 kW is required to fulfil the space heating needs. According to the results reported (refer to Figure 7.17), the CFD analysis of the thermal storage provides a mass flow rate of 0.029 kg/s and a temperature of 52°C to meet the heating load. Using Equation (7.5), when the heat is extracted, a radiator outlet temperature of 39°C is obtained, which is then used as the inlet water temperature to discharge the TES system at the next time interval.

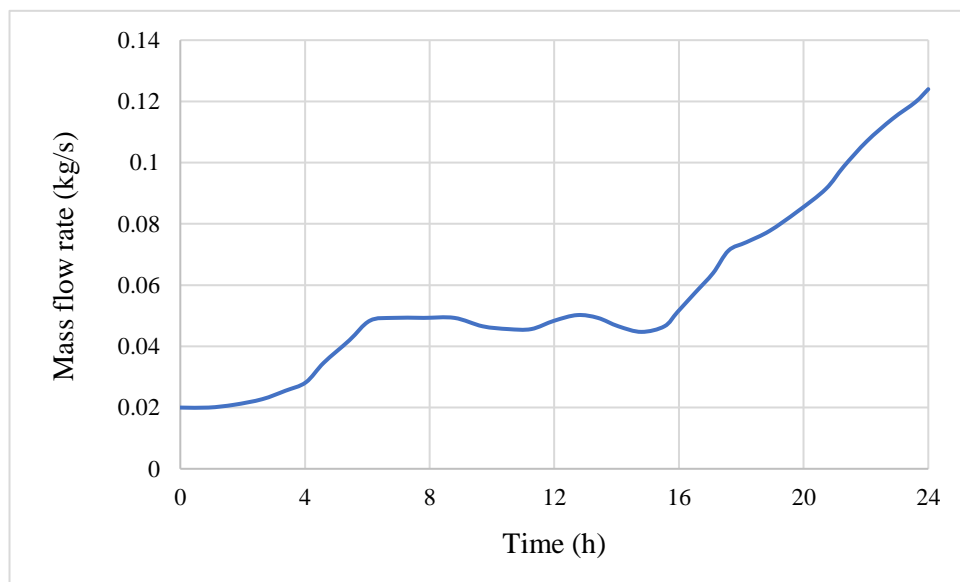
Referring to the example heating load profile, a previous time step calculation for the thermal storage return temperature of 47°C (Figure 7.17), with a mass flow rate of 0.047 kg/s obtained from the CFD analysis, is applied to match the heating load of 1.4 kW at 12:00 hours. The heating load is extracted from the thermal storage return, and a radiator outlet temperature of 40°C is determined using the Equation (7.5). Unlike the previous example, where sensible heat extraction caused a rapid decrease in the storage return temperature, in this case, the heat is extracted at the phase change temperature, resulting in an almost constant thermal storage output temperature.

The situation is different later in the day, for example, at 20:00 hours, when sensible heat is extracted from the storage system. At this point, the flow temperature drops drastically as the phase change is complete, requiring an increase in the mass flow rate to deliver the heat output of 1.55 kW. The TES system is then required to be discharged with a mass flow rate of 0.085 kg/s at a flow temperature of 43°C, which becomes the inlet to the radiator model. Equation (7.5) is then used, and 38.5°C is determined as the new radiator return temperature after heating load extraction, and this continues through the heating period having variable flow return properties from the radiator and the TES system at different time intervals. The challenge here is to ensure that the variable-speed heat pump can cope with the variation in the mass flow rates used to match the heating load. This issue should be explored in a future study. Figure 7.12 presents the radiator return temperature as applied to discharging

the TES system to fulfil the new space heating need of the dwelling – and the new mass flow rate as determined from the CFD analysis.



(a)



(b)

Figure 7.12: Variation of (a) radiator fluid return temperature and (b) mass flow rate during discharging of the TES system.

7.3.2 TES System Discharging Control Procedure

The heat extracted at successive intervals during discharging determines the state of discharge of the TES system. The heat output can be derived using a smart control system, like the one proposed for charging the storage system. Here, the heat output is continuously retrieved while meeting the dwelling heat demand at a time interval during the discharging process. This condition of operation provides information on the TES system's state of discharge at a given time. The process continues until the TES system discharge matches the dwelling's peak day heat demand.

However, a percentage charge and discharge of the peak case can be applied for lower demands. The controller modulates the mass flow rate and temperature to predict the heat output needed to fulfil the dwelling's space heating demand. A higher mass flow rate means more fluid passes through the thermal store absorbing more heat and discharging the system more rapidly. For example, using a slightly warmer HTF at 40°C might vary the heat extraction rate compared to using an HTF at 35°C.

The proposed thermal store discharge control system operates with water circulating using a mass flow rate of 0.02–0.12 kg/s at a temperature of 36–40°C and discharges the TES system to obtain heat output. The heat output is determined by the rate at which energy is extracted from the storage system, represented as $Q_{out} - Q_{in}$, and transmitted to the controller at a discrete time, throughout the discharging process. The discharge of the TES system persists at any given time when the total energy extracted from the thermal store does not meet the heat demand of the dwelling adequately. The discharge of the TES system ceases once the extracted energy completely meets the heat demand of the dwelling. The control system can be applied to the heating network to meet the detached dwelling's any-day heat demand. To conduct the discharge simulations, the entire CFD domain of the TES model is initialised at a uniform temperature of 60°C. This indicates that the TES system is fully charged with the heat required before the discharging process begins. An inlet HTF mass flow rate ranging from 0.02–0.12 kg/s at a radiator return temperature of 36–40°C is specified in the boundary condition at discrete time intervals to fulfil the space heating needs. Simulations are performed to discharge the TES system by controlling the HTF inlet mass flow rate and the return temperature from the radiator to align the

heat output with the peak day heat demand profile of the detached dwelling over time. An example of a CFD code to discharge the TES system at discrete time intervals is presented in Appendix III. A day-to-day TES system discharge control procedure is summarised in Figure 7.13.

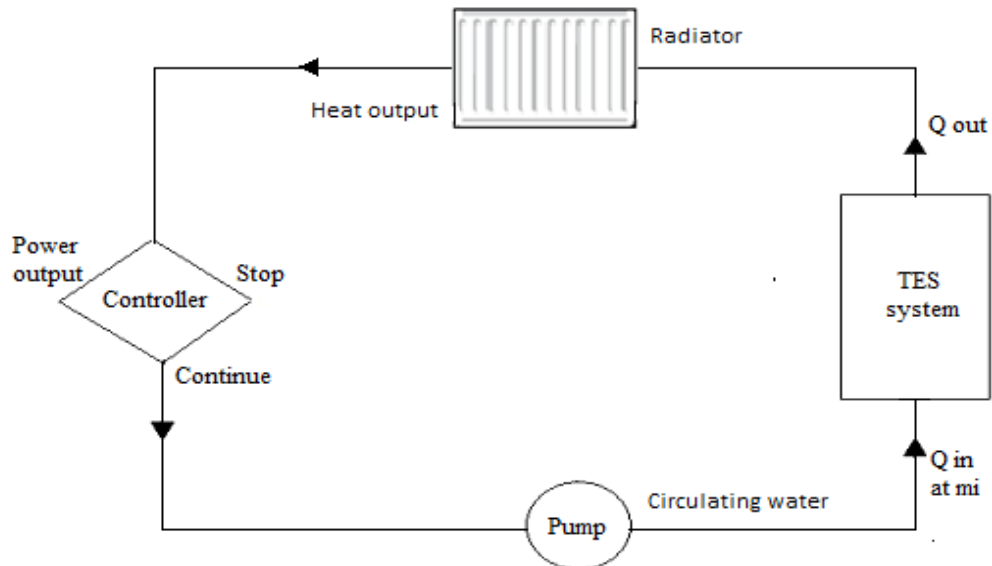
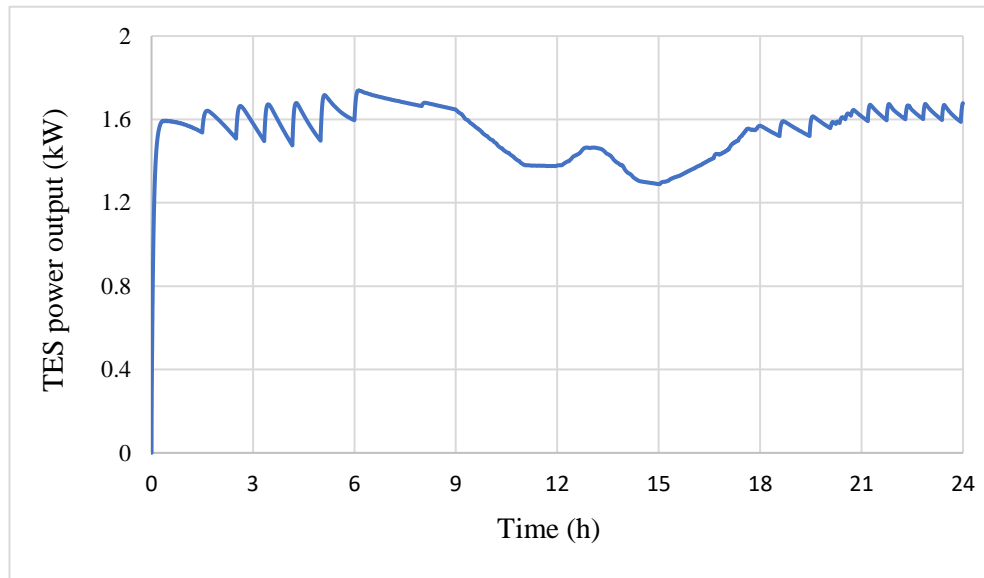


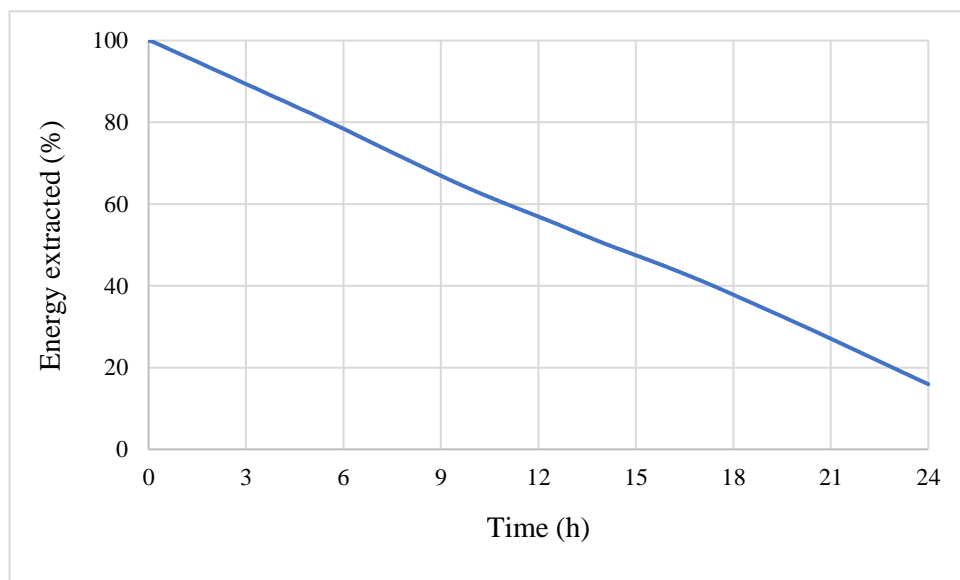
Figure 7.13: Schematic of a day-to-day TES system discharging control.

Figure 7.14 illustrates the variation in the rate at which energy is extracted and the state of discharge over time to meet the heat demand of the dwelling. The energy extracted during the TES system discharge is analysed at discrete time intervals to depict the operation of the storage system in a real sense. The state of discharge of the TES system ascertains the total energy extracted during the discharging cycle. The analysis of the storage discharge revealed that the energy extraction led to an 85% depletion of the TES system. The correlation between the energy extracted and the TES system state of discharge demonstrates that the TES system is operational, and the extracted energy corresponds to the heat needs of the dwelling. The discharge analysis indicates the TES system was not depleted to its minimum. This is because the TES system's capacity is predicated on using the maximum storage capacity, which achieves a full charge at the maximum stored energy and is used as the reference point for discharging the storage system. However, the analysis further indicated that the TES system is adequately discharged. The energy extracted sufficiently meets the heating requirements of the detached dwelling. This analysis confirms that

the TES system can be charged and discharged at a specific capacity to meet the heat demand of the dwelling on any given day, since the storage system has adequately fulfilled the heating needs for the day with the peak heat demand.



(a)



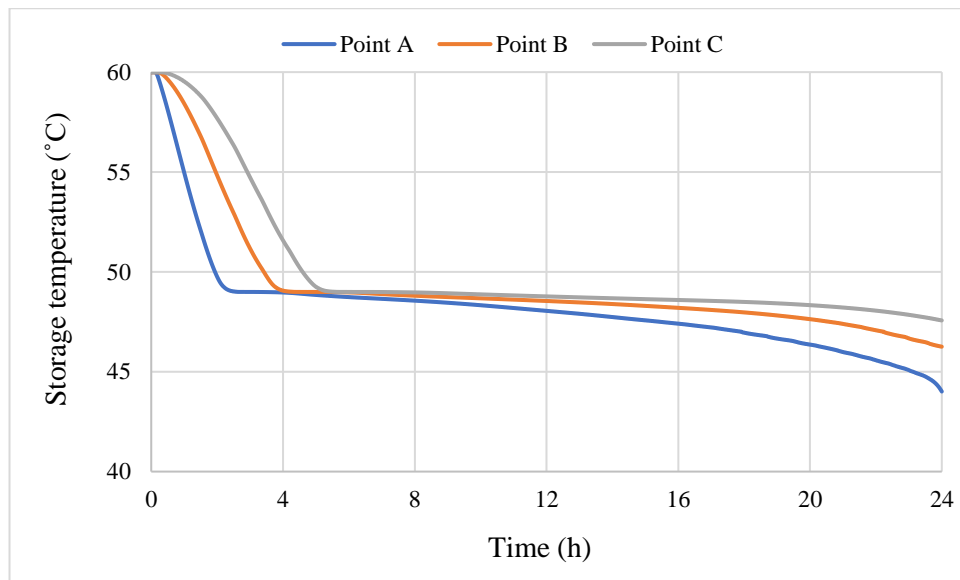
(b)

Figure 7.14: Variation of TES: (a) power output and (b) state of discharge over time during discharging with water flow of 0.02–0.12 kg/s at 36–40 °C.

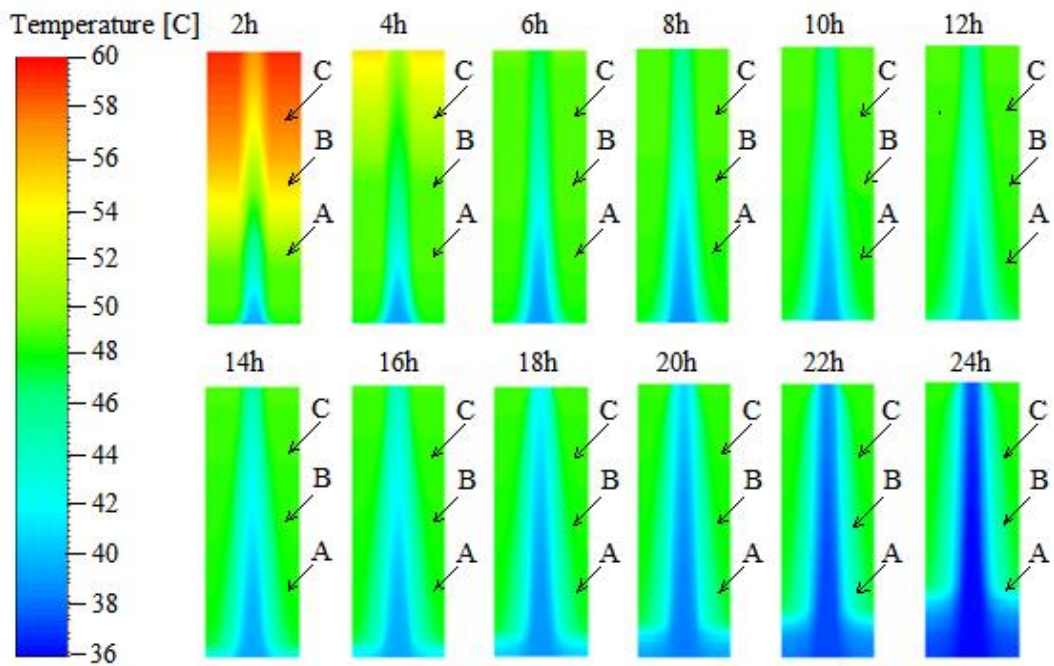
Figure 7.15 present the temperature evolution at various positions within a storage element and the temperature contour variations throughout. The graphics illustrate the dynamic performance of the storage system during the discharging process, highlighting how temperature changes over time. Before the discharging the TES system, the initial temperature of the storage element was set to 60°C, indicating that the system was fully charged and had stored the maximum possible energy requirement. However, as the discharging process commenced, the temperature in the thermal store decreased from 60°C to 48°C while extracting the sensible heat stored. The storage system maintained an almost constant temperature of 48°C for a longer period indicating the extraction of the latent heat stored. This decrease in temperature depicted by the temperature contours is reflected in the temperature profiles at the various points within the storage system, indicating the gradual release of the stored energy while matching the heat demand of the dwelling during the storage discharge.

The temperature contour in the storage element exhibited similar thermal characteristics to the temperature profiles observed at various positions. The temperature contour revealed that Point C maintained a higher temperature as compared to the other points. This is because most of the heat energy is concentrated in the upper section of the storage system. The temperature profiles at various positions further confirm this phenomenon, demonstrating the correlation between these profiles and the temperature contours within the storage system. The dynamic performance of the TES system, as indicated by the analysis of the temperature contours and temperature profiles, reflects the operation of the storage system.

This analysis shows that the TES system is effectively discharged to provide the heat output required to meet the detached dwelling's heat demand. To assess the performance of the TES system, an analysis of the system's output is conducted to determine its capability to meet the heating needs of the detached dwelling. The performance analysis will evaluate whether the TES system is a reliable and efficient solution by comparing its output to the actual heating demands, thereby assessing its suitability for real-world applications.



(a)



(b)

Figure 7.15: Variation of TES (a) temperature at points A, B, C and (b) temperature contour of the storage element over time during discharging with water flow of 0.02–0.12 kg/s at 36–40 °C.

7.4 Analysis of TES System Output

7.4.1 TES Power Output

The performance of the TES system is analysed by matching the power output from the system with the detached dwelling's peak day heat demand profile. This analysis assesses the capability of the TES system to fulfil the space heating requirements of the dwelling. Figure 7.16 illustrates the analysis of matching the TES power output with the dwelling's peak heat demand profile. The TES system is discharged by modulating the HTF mass flow rate and temperature to extract the required heat outputs at discrete time periods. The energy extracted from the storage discharge is determined by multiplying the discharge rate by 24 hours, corresponding to the area under the power output profile. A total heat output of 37.44-kWh was used to match the peak heat demand of the detached dwelling. It can be observed that the TES discharge rate and the detached dwelling's peak day heat demand profile exhibit a similar pattern. To further investigate the relationship between the two profiles, a statistical analysis is conducted to determine the correlation between the TES power output and the dwelling's heat demand profile. The degree of match between the TES power output and the dwelling's heat demand is quantified using the Pearson correlation coefficient. A correlation coefficient of 70-100% indicates a very strong match, 50-70% represents a strong match, and 30–50% reflects a moderate match.

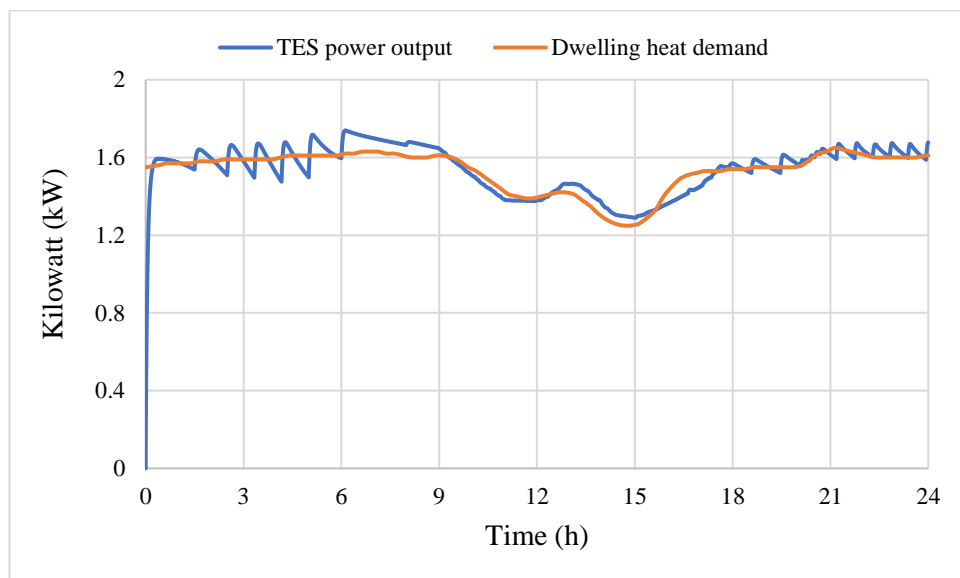


Figure 7.16: Comparison of the TES power output and the detached dwelling's peak day heat demand profile

The analysis shows a 94% correlation, indicating a very strong match between the TES power output and the dwelling's heat demand profile. The discharge rates for the TES system were obtained at an average of 1.56 kW and a peak of 1.73 kW. These rates represent the necessary average and maximum output for radiators to operate efficiently and ensure thermal comfort in the detached dwelling. The minimal difference of 0.17 kW between the peak and mean discharge rates indicates that the radiators for this case, particularly if oversized, may be sufficient. This small variance signifies that the system experiences minimal demand fluctuations, implying that substantially larger radiators may not be required.

The peak and mean discharge rates are within the standard radiator output capacity as defined by EN 442-2 [241], and the output level aligns with the typical range for residential heating applications, as noted by Liu et al. [242], for providing space heating in dwellings with average insulation and standard room sizes. Based on this analysis, the performance of the TES system has been demonstrated by successfully matching its power output with the detached dwelling's heat demand profile. It is evident that the heat extracted from the TES system during discharge closely matched the heat demand of the detached dwelling.

7.4.2 TES System Output Temperature

Figure 7.17 illustrates the variation in the storage fluid's output temperature during the TES system discharge, which meets the space heating requirements of the detached dwelling. The fluid's output temperature decreases from 60°C to 40°C while thermal energy is extracted from the storage system during the discharge cycle. At the beginning of the TES system discharge, a higher fluid output temperature is observed, which is attributable to the full storage charge. However, the fluid output temperature quickly decreases from 60°C to 48°C and then to 40°C, due to the extraction of sensible heat from both the solid and liquid within the storage system. Heat is extracted at an almost constant temperature of approximately 48°C, indicating the release of melting enthalpy from the TES system during discharging. The descending temperature profile reflects the thermal energy depletion as the stored heat is extracted. The rate at which temperature declines indicates how quickly the stored energy is consumed, potentially influenced by the dwelling's heating load.

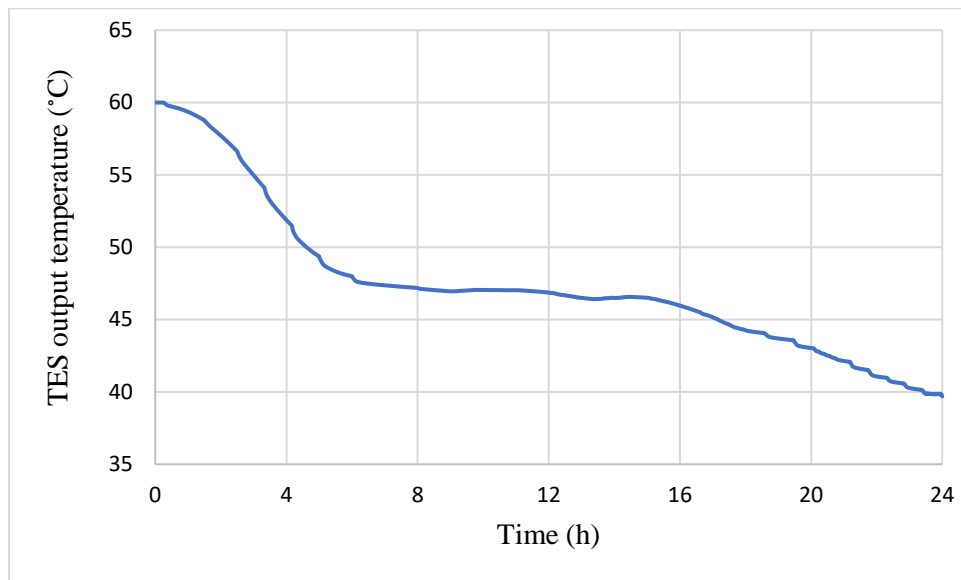


Figure 7.17: Variation of TES system fluid output temperature during discharging with water flow of 0.02–0.12 kg/s at 36–40 °C.

The TES system’s output temperature of 60–40°C is well within the operating range for low-temperature radiators, designed to work efficiently under these conditions. While the heat output is lower than in higher-temperature systems, low-temperature radiators can still provide adequate heating, particularly in well-insulated buildings. When the TES system provides water at 60°C at the beginning of the discharge cycle, the radiators will operate efficiently and produce a high heat output. This higher temperature maximises the temperature differential between the radiator surface and the room air around 21°C, leading to effective heat transfer and faster room heating. As the discharge progresses and the storage output temperature decreases, the radiators' heat output diminishes. This reduced temperature differential results in less heat being emitted into the room, which could slow down heating and potentially make it difficult to maintain the desired indoor temperature, especially during colder periods. However, low-temperature heating systems (e.g., underfloor heating or radiators designed for lower temperatures) would cope better with the declining output.

The key implications include the need for larger or more radiators to meet heating demands and the potential for consistent, energy-efficient operation in the radiators of existing dwellings. Overall, with a proper system design, the 60–40°C output temperature, can result in a comfortable and energy-efficient heating solution. Effective

control strategies are essential to manage the varying output temperatures from the TES system. Weather compensation controls, thermostatic radiator valves (TRVs), or smart home systems can help optimize radiator performance and maintain comfort as the fluid output temperature decreases.

7.5 Chapter Summary

This chapter examined the performance characteristics of the TES system to assess its ability to satisfy the space heating needs of an example dwelling. The analysis demonstrated the process of charging the TES system, utilising heat pump characteristics to store the necessary maximum heating charge to meet the dwelling's peak day heat demand. A full charge of the TES system was accomplished, and its thermal performance was analysed by observing the variation in storage temperature indicated by temperature contour and temperature profile throughout the charging process. The amount of heat stored at discrete times was utilised to determine the state of charge of the TES system throughout the charging cycle.

The extraction of heat output was achieved by modulating the fluid inlet mass flow rate and temperature at discrete time intervals during the discharging process. The rate of heat energy extraction through the process was used to determine the state of discharge of the TES system, and the variation in the temperature of the storage system indicated the operation of the TES system while fulfilling the dwelling's heat demand. It was observed that frequent changes in the fluid mass flow rate were required during sensible heat extraction to match the dwelling's heat demand profile.

The performance of the TES system was evaluated by matching the storage output to the peak day heat demand profile of the dwelling and determining the appropriateness of the fluid output temperature for use in residential radiators. A total of 37.44-kWh of heat, with peak and average discharge rates of 1.73 kW and 1.56 kW respectively, was utilised to meet the space heat demand of the dwelling. These peak and average discharge rates fall within the standard output capacity of radiators, aligning with the typical range for residential heating applications. The results indicated that the TES system is compatible with standard radiator systems used in dwellings, typically designed to operate efficiently with outputs in this range. This compatibility

indicates that the TES system can be integrated into existing dwelling heating systems without the need for major modifications or upgrades to the radiators. The TES system discharge with fluid output at a temperature range of 60°C to 40°C directly impacts radiator performance and overall heating comfort. While the radiators will perform well at the higher end of this range (60°C), their heat output diminishes as the temperature drops to 40°C. This can lead to challenges in maintaining consistent indoor temperatures, especially in poorly insulated spaces or during peak heat demand. To mitigate these effects, radiators may need to be larger or designed for low-temperature operation, energy efficiency measures implemented (to reduce the heating load), and advanced control strategies employed to optimise the system's performance and maintain comfort throughout the discharge cycle.

8 Conclusions, Limitations of the Study and Future Work

8.1 Introduction

This chapter presents the conclusions drawn from the study, outlining the key findings and their implications. It also discusses the limitations encountered during the research and highlights areas where further investigation could enhance the understanding and application of the findings.

8.2 Conclusions

Various PCMs in the operating temperature range for wet central heating were analysed. The PCMs were screened based on the commercial availability, melting temperature and enthalpy, and heat exchanger design type. The inorganic hydrated salt was selected as the PCM, with water as the HTF. The selection of inorganic hydrated salt as PCM provided sufficient energy storage capacity and efficient heat transfer due to their high latent heat and appropriate melting temperature for wet central heating applications. The shell-and-tube heat exchanger configuration was selected for TES design as it has been demonstrated to be an effective and efficient configuration entailing fluid flow heat exchange.

The TES system, featuring multiple identical storage elements of the cylindrical shell-and-tube heat exchanger model, stands out as the optimal thermal storage technology for wet central heating applications. Its efficiency in heat transfer to the storage medium during both the charging and discharging phases is a key advantage. The capacity of the storage elements is determined by the type of PCM used in the configuration, the size of the storage system for any given dwelling depends on the number of storage elements. Thus, the sizing of the TES system is contingent upon the quantity of storage elements used.

The engineering modelling method was utilised to estimate the next-day heat demand for the detached dwelling. The dwelling was modelled using the ESP-r program, and simulations were conducted over the heating season using the building's physical and thermal characteristics and other parameters relating to occupancy and weather patterns. From the outcome the dwelling's peak day heat demand profile was obtained

to inform the TES system capacity required to fulfil the space heating requirement of the dwelling.

The introduction of the phase change model in CFD Fluent commercial software has simplified the application of LHS models. The phase change model was validated against experimental data and numerical solution provided by Longeon et al. [186] for the melting and solidification of paraffin RT35 in a vertical cylindrical shell-and-tube heat exchanger. The comparison utilised the variation of the fluid outlet temperature and PCM temperature profiles at various positions in the storage system between the CFD solution and the experimental and numerical results. The analysis of the fluid outlet temperature and the PCM temperature profiles demonstrated a strong correlation with the experimental data, and the results achieved were consistent with those derived from numerical solutions.

The TES system sizing was determined using a day with the peak heat demand of the dwelling, which was extracted from the heating season profile. The predicted dwelling's peak day heat demand was used to ascertain the storage system's capacity. The TES system, designed for peak day heat demand, can be used to meet the space heating needs for any day throughout the heating season assuming a full charge was achieved. The TES system sizing was demonstrated by discharging the storage system to meet the peak day heat demand of the detached dwelling. This indicates that the TES system can fulfil any day heat demand of the detached dwelling through the heating season when the required heating charge is stored.

The TES model, consisting of a 2D axisymmetric domain, was developed in the Fluent CFD tool to assess the TES system's performance. The 2D axisymmetric domain, comprising mainly the HTF and PCM sections, was discretised for performance simulation. The 2D computational domain was used to analyse the thermal behaviour and characteristics of the storage system during the charging and discharging phases. The thermal behaviour and attributes of the TES system during the charging and discharging processes were analysed.

The Fluent simulation employed a typical domestic heat pump's mass flow rates and supply temperature to charge the TES system. The storage system's performance was

evaluated through a limited sensitivity analysis, which involved charging the TES system virtually using a heat pump with a flow of 60°C at varying mass flow rates. A preliminary study analysed the charging performance of the storage system using top and bottom HTF injection methods. The top HTF injection method demonstrated faster charging due to the induced buoyancy force along the direction of the HTF.

The TES system charging simulation was conducted by injecting the HTF at the top, ensuring an almost constant wall temperature due to the high HTF velocity. The simulation results indicated a realistic change in the temperature of the thermal store from 36°C to 60°C as confirmed by temperature contours and temperature profiles at different positions in the storage system. This consistency indicates that the TES system reached full charge by the end of the charging cycle, as confirmed by the state of charge of the TES system.

The simulation of the TES system discharge utilised a bottom HTF injection method, circulating water at relatively low mass flow rates was used to extract the stored heat. The storage component was maintained at a reference temperature of 60°C. This signifies the fully charged state of the thermal store. A variable inlet mass flow rate and temperature of the HTF (radiator return), ranging from 0.02 to 0.12 kg/s and 36-40°C respectively, were used to discharge the TES system. By controlling the circulating water's mass flow rate and temperature at specific time intervals, the storage heat output was obtained and used to evaluate the performance of the TES system.

The TES system's performance was assessed by matching the discharge rate with the detached dwelling's peak day heat demand profile. The power output obtained from the TES system discharge adequately matched the dwelling's peak heat demand profile. The storage power output is consistent with the standard output capacity of radiators used in residential heating. Statistical analysis with the Pearson correlation coefficient was used to analyse the matching rate between the TES power output and dwelling peak heat demand profile. The calculated Pearson correlation coefficient of 94% indicated a strong correlation between the two profiles.

The performance of the TES system was further evaluated by assessing the fluid output temperature for its suitability in providing thermal comfort in dwellings with un-

derfloor heating systems and radiators. The fluid output indicated a decrease in temperature from 60°C to 40°C due to the heat extraction during the discharge process. The fluid output temperature can present challenges in maintaining indoor thermal comfort when standard radiators are used, as the temperature decreases towards the end of the heating cycle. This could necessitate the use of larger or additional radiators to heat the space adequately. However, the fluid output temperature can work well with underfloor heating systems and radiators designed for low-temperature use.

To conclude the research, the heat pump integrated TES system sizing procedure is summarised as follows:

- Select a dwelling and develop a building model that accurately predicts the characteristics of the dwelling. The goal is to conduct a building performance appraisal.
- Use an appropriate building energy performance simulation tool and simulate it to determine the dwelling's daily heat demand through a heating season.
- Identify the dwelling's peak heat demand and use it to size the TES system. The dwelling's daily heat demand may vary throughout the heating season. In this case, the TES is sized using the dwelling's peak daily heat demand.
- Determine the TES system's capacity using the predicted peak heat demand. The TES system's configuration (heat exchanger design) must have been selected and the size (volume) is determined by the storage capacity.
- Use appropriate CFD techniques to model and validate the TES system. The performance of the storage model is evaluated to determine the accuracy of the TES system for application in wet central heating systems.
- Charging the TES system. Apply a representative heat pump's mass flow rate and temperature to simulate the charging of the TES system and store the required heating charge.
- Discharging the TES system and assessing its performance by matching the power output with the dwelling's peak heat demand profile and evaluating the fluid output temperature's suitability for use in radiators or underfloor heating systems to ensure thermal comfort.

8.3 Contributions to Knowledge

Various studies have implemented using heat pump-integrated TES systems to meet the space heating requirements of residential buildings. These studies focused on the application of TES systems to fulfil the space heating needs of dwellings for a fraction of the day. In most cases, TES systems are used as buffers to support the direct operation of heat pumps, unlike the indirect approach used in this study.

This thesis contributes to knowledge by developing and applying a procedure for sizing a heat pump-integrated TES system for wet central heating. This methodology has been utilized to assess the feasibility of using the TES system for load-shifting capabilities in residential settings. The assessment shows the application of building performance simulations and CFD techniques to evaluate the TES system's performance in fulfilling the space heating demand of a dwelling throughout the day. Additionally, the thesis further contributes to knowledge by developing a day-to-day control procedure for charging and discharging the TES system to meet the heating requirements of residential buildings.

This study contributes by developing a detached dwelling model and analysing building energy performance using the ESP-r tool to determine the peak-day heat demand profile. This profile was crucial for accurately sizing the TES system, ensuring the capability to meet the dwelling's next-day heating needs. The study demonstrates the application of CFD Fluent software to model the TES system design, specifically focusing on the charging process, which incorporates the heat pump's mass flow rate and temperature. Additionally, the study models the discharging process to assess the extraction of heat output, providing critical insights into the system's performance during discharging of the TES system.

The study further showcases the analysis of evaluating the performance of the TES system through a detailed assessment of the storage output. Specifically, the study matches the TES power output with the next-day (here peak day) heat demand profile of a detached dwelling, ensuring the system's capability to meet the anticipated heating needs. The fluid output temperature was analysed to assess its suitability for

integration into heating systems, providing valuable insights for optimizing TES-based space heating solutions.

8.4 Limitations of the Study

This study developed a procedure for sizing a heat pump-integrated TES system as a substitute for a conventional gas-fired domestic heating boiler. The procedure was used to assess the feasibility of using a TES system to meet the next-day space heating needs of an example dwelling. The load-shifting capability of the TES system was assessed by analysing the regulation of a pre-charged store's output to meet the heating requirement of the dwelling. Some limitations of the study can be highlighted as follows.

The study focused on space heating demand and did not include domestic hot water. This suggests that hot water demand needs to be addressed separately, potentially leading to an additional heating cost for the dwelling. Furthermore, the assessment of the TES system's capability was based on the maximum storage capacity determined using the peak-day heat demand profile of the detached dwelling, and heat demand profiles for other dwelling types, geographical locations and times of year were not considered. The study employed simplified assumptions such as uniform material properties, specific weather boundary conditions, and focused on a single storage element within the bundle of elements comprising a TES. This approach may limit the model's accuracy in real-world scenarios, where conditions are more variable and complex. Additionally, the study does not integrate the CFD model with a building simulation model to account for dynamic discharge/usage interactions, thereby emulating the system's operation under real-world conditions. The assessment of the TES system's capability was conducted by scaling up the capacity of a single storage element for charging and discharging with HTF flow from the inner tube surface area. Further, the study used inorganic hydrated salt, which may have inherent limitations, such as phase instability and supercooling and does not include an analysis for the overall effectiveness of the thermal store. The use of other PCMs was beyond the scope of this study, limiting the understanding of potential alternatives. HTF flow from both the inner and outer surface areas of the storage element could be utilized to enhance the charging and discharging performance. Finally, while a techno-

economic analysis is necessary when implementing any solution, it was not possible to consider the cost implications of using the proposed system in wet central heating system applications.

8.5 Recommendations for Future Work

This section explores an avenue for further improvement in the study by addressing the limitations and expanding the scope of the analysis. Future research can provide valuable insights into optimising the heat pump integrated TES system technology. To further expand and improve this methodology, the study offers the following recommendations for future work.

- The study's findings were based on using the CFD techniques and building energy simulations to assess the load-shifting capability of the TES system. Conducting field tests in a real residential setting would provide a detailed understanding of the practical challenges and benefits of the TES system while evaluating its performance.
- Future research should develop a more sophisticated dynamic building model that includes space heating and hot water demands to assess the performance of the TES system under diverse scenarios.
- Expanding the scope by testing with different dwelling types, heat demand profiles, and a wider range of geographical locations would provide valuable insights to assess the TES system's capability in meeting the heating needs of various dwellings.
- Future studies should explore the effectiveness index of the thermal store and investigate advanced or alternative PCMs with enhanced characteristics, such as phase stability and higher enthalpies, to improve the performance of the TES system leading to greater efficiency and expanded applications.
- Conducting a study on the long-term durability of the thermal store to assess the degradation of the PCM under multiple charge and discharge cycles, can

provide valuable information for system maintenance and energy efficiency over extended periods.

- Exploring the use of advanced and smart control systems that utilize real-time data from weather forecasts and occupancy patterns to optimize the charging and discharging process, allows for evaluating the solution's performance in real-world scenarios.
- Future research should focus on enhancing the overall heat transfer rate of the TES system by considering the heat transfer from both the inner and outer surface areas of the storage element. This would lead to a faster and more efficient heat transfer process, particularly when rapid charging and discharging of the TES system are required.
- Conducting a techno-economic analysis of the heat pump-integrated TES system would provide comprehensive insights into the economic viability of the solution, helping to inform decision-making regarding its application.

References

- [1] Chiara Delmastro and Olivia Chen. Buildings - Energy System - IEA 2023. <https://www.iea.org/energy-system/buildings> (accessed September 22, 2023).
- [2] Francois Briens and Rafael Martinez-Gordon. Buildings-related energy demand for heating and share by fuel in the Net Zero Scenario, 2021-2030 – Charts – Data & Statistics - IEA 2022.
- [3] Calderón C, Underwood C, Yi J, Mcloughlin A, Williams B. An area-based modelling approach for planning heating electrification. *Energy Policy* 2019; 131:262–80. <https://doi.org/10.1016/j.enpol.2019.04.023>.
- [4] Foxon TJ, Pearson PJG. 9 The UK low carbon energy transition Prospects and challenges. *Carbon Governance, Climate Change and Business Transformation*, 2014, p. 158–74.
- [5] Hesselink LXW, Chappin EJJ. Adoption of energy efficient technologies by households – Barriers, policies and agent-based modelling studies. *Renewable and Sustainable Energy Reviews* 2019; 99:29–41. <https://doi.org/10.1016/j.rser.2018.09.031>.
- [6] Fawcett Tina. The future role of heat pumps in the domestic sector. 2011.
- [7] Strategy Committee I. Decarbonising heat in homes Seventh Report of Session 2021-22 Report, together with formal minutes relating to the report. 2022.
- [8] Holmes G, Hay R, Davies E, Hill J, Barrett J, Style D, et al. Acknowledgements Other members of the Secretariat who contributed to this report 2019.
- [9] Department for Business E and IS (BEIS). Domestic Heat Distribution Systems: Evidence Gathering. Final Report BEIS Research Paper Number: 2021/015. 2021.
- [10] Committee on Climate Change (CCC). Net Zero the UK’s contribution to stopping global warming Committee on Climate Change. 2019.
- [11] Committee on Climate Change (CCC). The Sixth Carbon Budget. 2020.
- [12] Bagarella G, Lazzarin R, Noro M. Sizing strategy of on off and modulating heat pump systems based on annual energy analysis. *International Journal of Refrigeration* 2016; 65:183–93. <https://doi.org/10.1016/j.ijrefrig.2016.02.015>.
- [13] Ansys Fluent Tutorial Guide, 2019 R1 15317 (2019) 673-713 2018.

- [14] Renaldi R, Kiprakis A, Friedrich D. An optimisation framework for thermal energy storage integration in a residential heat pump heating system. *Appl Energy* 2017; 186:520–9. <https://doi.org/10.1016/j.apenergy.2016.02.067>.
- [15] Facci AL, Krastev VK, Falcucci G, Ubertini S. Smart integration of photovoltaic production, heat pump and thermal energy storage in residential applications. *Solar Energy* 2019; 192:133–43. <https://doi.org/10.1016/j.solener.2018.06.017>.
- [16] Shah NN, Wilson C, Huang MJ, Hewitt NJ. Analysis on field trial of high temperature heat pump integrated with thermal energy storage in domestic retrofit installation. *Appl Therm Eng* 2018; 143:650–9. <https://doi.org/10.1016/j.applthermaleng.2018.07.135>.
- [17] Niu F, Ni L, Yao Y, Yu Y, Li H. Performance and thermal charging/discharging features of a phase change material assisted heat pump system in heating mode. *Appl Therm Eng* 2013; 58:536–41. <https://doi.org/10.1016/j.applthermaleng.2013.04.042>.
- [18] Ding Y, Riffat SB. Thermochemical energy storage technologies for building applications: a state-of-the-art review. *International Journal of Low-Carbon Technologies* 2013; 8:106–16. <https://doi.org/10.1093/ijlct/cts004>.
- [19] Kant K, Pitchumani R. Advances and opportunities in thermochemical heat storage systems for buildings applications. *Appl Energy* 2022; 321:119299. <https://doi.org/10.1016/j.apenergy.2022.119299>.
- [20] Zhang H, Baeyens J, Cáceres G, Degrève J, Lv Y. Thermal energy storage: Recent developments and practical aspects. *Prog Energy Combust Sci* 2016; 53:1–40. <https://doi.org/10.1016/j.pecs.2015.10.003>.
- [21] Sarbu I, Sebarchievici C. A Comprehensive Review of Thermal Energy Storage. *Sustainability* 2018; 10:191. <https://doi.org/10.3390/su10010191>.
- [22] Cabeza LF, Ibáñez M, Solé C, Roca J, Nogués M. Experimentation with a water tank including a PCM module. *Solar Energy Materials and Solar Cells* 2006; 90:1273–82. <https://doi.org/10.1016/j.solmat.2005.08.002>.
- [23] de Gracia A, Oró E, Farid MM, Cabeza LF. Thermal analysis of including phase change material in a domestic hot water cylinder. *Appl Therm Eng* 2011; 31:3938–45. <https://doi.org/10.1016/j.applthermaleng.2011.07.043>.

- [24] Kelly NJ, Cockroft J. Analysis of retrofit air source heat pump performance: Results from detailed simulations and comparison to field trial data. *Energy Build* 2011; 43:239–45. <https://doi.org/10.1016/j.enbuild.2010.09.018>.
- [25] Reynders Glen, Nuytten Thomas, Saelens Dirk. Robustness of Reduced-Order Models for Prediction and Simulation of the Thermal Behavior of Dwellings. *Proceedings of BS2013: 13th Conference of International building Performance Simulation Association, Chambery, France., 2013*, p. 660–7.
- [26] Ridley I, Clarke A, Bere J, Altamirano H, Lewis S, Durdev M, et al. The monitored performance of the first new London dwelling certified to the Passive House standard. *Energy Build* 2013; 63:67–78. <https://doi.org/10.1016/j.enbuild.2013.03.052>.
- [27] Ruiz LGB, Pegalajar MC, Molina-Solana M, Guo Y-K. A case study on understanding energy consumption through prediction and visualization (VIMOEN). *Journal of Building Engineering* 2020; 30:101315. <https://doi.org/10.1016/j.jobe.2020.101315>.
- [28] Kelly NJ, Tuohy PG, Hawkes AD. Performance assessment of tariff-based air source heat pump load shifting in a UK detached dwelling featuring phase change-enhanced buffering. *Appl Therm Eng* 2014; 71:809–20. <https://doi.org/10.1016/j.applthermaleng.2013.12.019>.
- [29] SevernWye Energy Agency. A guide to wet central heating systems Heating & hot water fact sheet 1 SevernWye energy advice. 2016.
- [30] Clarke J. *Energy Simulation in Building Design*. Routledge; 2007. <https://doi.org/10.4324/9780080505640>.
- [31] Simic K, T’Jollyn I, Faes W, Borrajo Bastero J, Laverge J, De Paepe M. Modelling of a gas-fired heating boiler unit for residential buildings based on publicly available test data. *Energy Build* 2021; 253:111451. <https://doi.org/10.1016/j.enbuild.2021.111451>.
- [32] - International Energy Agency I. *World Energy Outlook Special Report the Future of Heat Pumps*. 2022.
- [33] Association of Plumbing and Heating Contractors. *Understanding central heating systems*. n.d.

- [34] Hamworthy Heating. Sealed central heating systems and open vented heating systems 2022.
- [35] Energy Saving Trust. CE30 - Domestic heating by gas. 2008.
- [36] Microgeneration Certification Scheme. Domestic Heat Pumps A Best Practice Guide. 2018.
- [37] Energy Saving Trust. In-depth Guide to heat Pumps-Heating your homes 2022.
- [38] The European Parliament and the Council of the European Union. Directive (EU) 2018/2001 of the European Parliament and the Council of 11 December 2018 on the promotion of the use of energy from renewable sources (recast) (Text with EEA relevance) 2018.
- [39] Bell M, Gault A, Thompson M, Hill J, Joffe D, Taro Hallworth included, et al. Other members of the Secretariat who contributed to this report: A number of organisations and individuals for. 2016.
- [40] Rosenow J, Gibb D, Nowak T, Lowes R. Heating up the global heat pump market 2022. <https://doi.org/10.1038/s41560-022-01104-8>.
- [41] Gibb Jan Rosenow Samuel Thomas D, Malinowski Alexia Ross M, Graham P. A policy toolkit for global mass heat pump deployment Global Buildings Performance Network. 2022.
- [42] Ambrose J. What are heat pumps and why is the UK government pushing them? The Guardian Newspaper 2021.
- [43] Sky News.org. How to apply for heat pump grant: The new Government £5,000 boiler replacement scheme explained 2021.
- [44] Government H. Heat and Buildings Strategy 2021.
- [45] Arteconi A, Hewitt NJ, Polonara F. Domestic demand-side management (DSM): Role of heat pumps and thermal energy storage (TES) systems. *Appl Therm Eng* 2013; 51:155–65.
<https://doi.org/10.1016/j.applthermaleng.2012.09.023>.
- [46] Caird S, Roy R, Potter S. Domestic heat pumps in the UK: user behaviour, satisfaction and performance. *Energy Efficiency* 2012; 5:283–301.
<https://doi.org/10.1007/s12053-012-9146-x>.
- [47] The Energyshop. Compare Energy Prices per kWh across the UK 2023.

- [48] Carbon Emission Calculator. Carbon Emissions Calculator Scotland Carbon emissions from heating systems renewable Heating Ground Source Heat Pumps | Renewable Cooling 2023. https://www.icax.co.uk/Carbon_Emissions_Calculator_Heating_UK.html (accessed September 25, 2023).
- [49] Elementenergy. Development of trajectories for residential heat decarbonisation to inform the Sixth Carbon Budget. 2021.
- [50] Carroll P, Chesser M, Lyons P. Air Source Heat Pumps field studies: A systematic literature review. *Renewable and Sustainable Energy Reviews* 2020; 134:110275. <https://doi.org/10.1016/j.rser.2020.110275>.
- [51] European Heat pump Association. EHPA_market_report_2023_Executive-Summary. 2023.
- [52] Zhang Q, Zhang L, Nie J, Li Y. Techno-economic analysis of air source heat pump applied for space heating in northern China. *Appl Energy* 2017; 207:533–42. <https://doi.org/10.1016/j.apenergy.2017.06.083>.
- [53] Amirirad A, Kumar R, Fung AS, Leong WH. Experimental and simulation studies on air source heat pump water heater for year-round applications in Canada. *Energy Build* 2018; 165:141–9. <https://doi.org/10.1016/j.enbuild.2018.01.052>.
- [54] Zhang Y, Ma Q, Li B, Fan X, Fu Z. Application of an air source heat pump (ASHP) for heating in Harbin, the coldest provincial capital of China. *Energy Build* 2017; 138:96–103. <https://doi.org/10.1016/j.enbuild.2016.12.044>.
- [55] Touchie MF, Pressnail KD. Testing and simulation of a low-temperature air-source heat pump operating in a thermal buffer zone. *Energy Build* 2014; 75:149–59. <https://doi.org/10.1016/j.enbuild.2014.02.015>.
- [56] Stamatellos G, Zogou O, Stamatelos A. Energy Performance Optimization of a House with Grid-Connected Rooftop PV Installation and Air Source Heat Pump. *Energies (Basel)* 2021; 14:740. <https://doi.org/10.3390/en14030740>.
- [57] Kelly JA, Fu M, Clinch JP. Residential home heating: The potential for air source heat pump technologies as an alternative to solid and liquid fuels. *Energy Policy* 2016; 98:431–42. <https://doi.org/10.1016/j.enpol.2016.09.016>.

- [58] Liang C, Zhang X, Li X, Zhu X. Study on the performance of a solar assisted air source heat pump system for building heating. *Energy Build* 2011; 43:2188–96. <https://doi.org/10.1016/j.enbuild.2011.04.028>.
- [59] Parameshwaran R, Kalaiselvam S, Harikrishnan S, Elayaperumal A. Sustainable thermal energy storage technologies for buildings: A review. *Renewable and Sustainable Energy Reviews* 2012; 16:2394–433. <https://doi.org/10.1016/j.rser.2012.01.058>.
- [60] Mahon H, O'Connor D, Friedrich D, Hughes B. A review of thermal energy storage technologies for seasonal loops. *Energy* 2022; 239:122207. <https://doi.org/10.1016/j.energy.2021.122207>.
- [61] Hesaraki A, Holmberg S, Haghghat F. Seasonal thermal energy storage with heat pumps and low temperatures in building projects—A comparative review. *Renewable and Sustainable Energy Reviews* 2015; 43:1199–213. <https://doi.org/10.1016/j.rser.2014.12.002>.
- [62] Arteconi A, Hewitt NJ, Polonara F. State of the art of thermal storage for demand-side management. *Appl Energy* 2012; 93:371–89. <https://doi.org/10.1016/j.apenergy.2011.12.045>.
- [63] Ibrahim Alghamdi Christian Bach Jeffrey D Spitler KK, Ibrahim K, Alghamdi KI, Bach CK, Spitler JD. Water-Based Thermal Energy Storage for Heating and Air-Conditioning Applications in Residential Buildings: Review and Preliminary Study. n.d.
- [64] Soares N, Costa JJ, Gaspar AR, Santos P. Review of passive PCM latent heat thermal energy storage systems towards buildings' energy efficiency. *Energy Build* 2013; 59:82–103. <https://doi.org/10.1016/j.enbuild.2012.12.042>.
- [65] Gohar Gholamibozanjani MF. A Comparison between Passive and Active PCM Systems Applied to Buildings. *Thermal Energy Storage with Phase Change Materials*. First Edition, CRC Press; 2021.
- [66] Cabeza LF, Martorell I, Miró L, Fernández AI, Barreneche C, Cabeza LF, et al. Introduction to thermal energy storage systems. *Advances in Thermal Energy Storage Systems*, Elsevier; 2021, p. 1–33. <https://doi.org/10.1016/B978-0-12-819885-8.00001-2>.

- [67] Bauer T, Steinmann W-D, Laing D, Tamme R. Thermal Energy Storage Materials and Systems. *Annual Review of Heat Transfer* 2012; 15:131–77. <https://doi.org/10.1615/AnnualRevHeatTransfer.2012004651>.
- [68] Alva G, Lin Y, Fang G. An overview of thermal energy storage systems. *Energy* 2018; 144:341–78. <https://doi.org/10.1016/j.energy.2017.12.037>.
- [69] Garg HP, MSC, BAK. *Solar Thermal Energy Storage*. First Edition. Dordrecht: D. Reidel Publishing Company; 1985.
- [70] Anandan SS, Sundarababu J. A comprehensive review on mobilized thermal energy storage. *Energy Sources, Part A: Recovery, Utilization, and Environmental Effects* 2021:1–24. <https://doi.org/10.1080/15567036.2021.1942331>.
- [71] de Gracia A, Cabeza LF. Phase change materials and thermal energy storage for buildings. *Energy Build* 2015; 103:414–9. <https://doi.org/10.1016/j.enbuild.2015.06.007>.
- [72] Sadineni SB, Madala S, Boehm RF. Passive building energy savings: A review of building envelope components. *Renewable and Sustainable Energy Reviews* 2011; 15:3617–31. <https://doi.org/10.1016/j.rser.2011.07.014>.
- [73] Pielichowska K, Pielichowski K. Phase change materials for thermal energy storage. *Prog Mater Sci* 2014; 65:67–123. <https://doi.org/10.1016/j.pmatsci.2014.03.005>.
- [74] Sang Le T, Hieu Le T, Tuan Pham M, Chi Minh city H. A review of the indirect solar dryer with sensible heat storage mediums. *Journal of Mechanical Engineering Research and Developments* 2021; 44:131–40.
- [75] Alva G, Liu L, Huang X, Fang G. Thermal energy storage materials and systems for solar energy applications. *Renewable and Sustainable Energy Reviews* 2017; 68:693–706. <https://doi.org/10.1016/j.rser.2016.10.021>.
- [76] Wu M, Li M, Xu C, He Y, Tao W. The impact of concrete structure on the thermal performance of the dual-media thermocline thermal storage tank using concrete as the solid medium. *Appl Energy* 2014; 113:1363–71. <https://doi.org/10.1016/j.apenergy.2013.08.044>.
- [77] Pinel P, Cruickshank CA, Beausoleil-Morrison I, Wills A. A review of available methods for seasonal storage of solar thermal energy in residential applica-

- tions. *Renewable and Sustainable Energy Reviews* 2011; 15:3341–59. <https://doi.org/10.1016/j.rser.2011.04.013>.
- [78] Dincer I, RMA. *Thermal Energy Storage, Systems and Applications*. Newyork: 2002.
- [79] Jerol Soibam. *Numerical Investigation of a Phase Change Materials (PCM) heat exchanger*. Norwegian University of Science and Technology, 2017.
- [80] Cárdenas B, León N. High temperature latent heat thermal energy storage: Phase change materials, design considerations and performance enhancement techniques. *Renewable and Sustainable Energy Reviews* 2013; 27:724–37. <https://doi.org/10.1016/j.rser.2013.07.028>.
- [81] Raj CR, Suresh S, Bhavsar RR, Singh VK, Govind KA. Influence of fin configurations in the heat transfer effectiveness of Solid solid PCM based thermal control module for satellite avionics: Numerical simulations. *J Energy Storage* 2020; 29:101332. <https://doi.org/10.1016/j.est.2020.101332>.
- [82] Mohamed SA, Al-Sulaiman FA, Ibrahim NI, Zahir MdH, Al-Ahmed A, Saidur R, et al. A review on current status and challenges of inorganic phase change materials for thermal energy storage systems. *Renewable and Sustainable Energy Reviews* 2017; 70:1072–89. <https://doi.org/10.1016/j.rser.2016.12.012>.
- [83] Crespo A, Barreneche C, Ibarra M, Platzer W. Latent thermal energy storage for solar process heat applications at medium-high temperatures – A review. *Solar Energy* 2019; 192:3–34. <https://doi.org/10.1016/j.solener.2018.06.101>.
- [84] Souayfane F, Fardoun F, Biwole P-H. Phase change materials (PCM) for cooling applications in buildings: A review. *Energy Build* 2016; 129:396–431. <https://doi.org/10.1016/j.enbuild.2016.04.006>.
- [85] Pereira da Cunha J, Eames P. Thermal energy storage for low and medium temperature applications using phase change materials – A review. *Appl Energy* 2016; 177:227–38. <https://doi.org/10.1016/j.apenergy.2016.05.097>.
- [86] Tyagi VV, Buddhi D. PCM thermal storage in buildings: A state of art. *Renewable and Sustainable Energy Reviews* 2007;11:1146–66. <https://doi.org/10.1016/j.rser.2005.10.002>.

- [87] Akgün M, Aydın O, Kaygusuz K. Experimental study on melting/solidification characteristics of a paraffin as PCM. *Energy Convers Manag* 2007; 48:669–78. <https://doi.org/10.1016/j.enconman.2006.05.014>.
- [88] Abhat A. Low temperature latent heat thermal energy storage: Heat storage materials. *Solar Energy* 1983; 30:313–32. [https://doi.org/10.1016/0038-092X\(83\)90186-X](https://doi.org/10.1016/0038-092X(83)90186-X).
- [89] Reza Vakhshouri A. Paraffin as Phase Change Material. Paraffin - an Overview, IntechOpen; 2020. <https://doi.org/10.5772/intechopen.90487>.
- [90] Rathore PKS, Shukla SK. Enhanced thermophysical properties of organic PCM through shape stabilization for thermal energy storage in buildings: A state-of-the-art review. *Energy Build* 2021; 236:110799. <https://doi.org/10.1016/j.enbuild.2021.110799>.
- [91] Junaid MF, Rehman Z ur, Čekon M, Čurpek J, Farooq R, Cui H, et al. Inorganic phase change materials in thermal energy storage: A review on perspectives and technological advances in building applications. *Energy Build* 2021; 252:111443. <https://doi.org/10.1016/j.enbuild.2021.111443>.
- [92] Casini M. *Smart Buildings: Advanced Materials and Nanotechnology to Improve Energy-Efficiency and Environmental Performance*-384 pages. 2016.
- [93] Xie N, Huang Z, Luo Z, Gao X, Fang Y, Zhang Z. Inorganic Salt Hydrate for Thermal Energy Storage. *Applied Sciences* 2017; 7:1317. <https://doi.org/10.3390/app7121317>.
- [94] Purohit BK, Sistla VS. Inorganic salt hydrate for thermal energy storage application: A review. *Energy Storage* 2021;3. <https://doi.org/10.1002/est2.212>.
- [95] Sharma A, Tyagi VV, Chen CR, Buddhi D. Review on thermal energy storage with phase change materials and applications. *Renewable and Sustainable Energy Reviews* 2009; 13:318–45. <https://doi.org/10.1016/j.rser.2007.10.005>.
- [96] Wang Z, Wang H, Yang M, Sun W, Yin G, Zhang Q, et al. Thermal reliability of Al-Si eutectic alloy for thermal energy storage. *Mater Res Bull* 2017; 95:300–6. <https://doi.org/10.1016/j.materresbull.2017.07.040>.
- [97] Safarian J, Tangstad M. Phase change materials for high-temperature operation. *Ultra-High Temperature Thermal Energy Storage, Transfer and Conver-*

- sion, Elsevier; 2021, p. 85–111. <https://doi.org/10.1016/B978-0-12-819955-8.00004-1>.
- [98] Angadi BM, Hiremath CR, Reddy AC, Hyderabad J, Katti IV V, Kori SA. Studies on the Thermal Properties of Hypereutectic Al-Si Alloys by Using Transient Method. vol. 2. 2014.
- [99] Fallahi A, Guldentops G, Tao M, Granados-Focil S, Van Dessel S. Review on solid-solid phase change materials for thermal energy storage: Molecular structure and thermal properties. *Appl Therm Eng* 2017; 127:1427–41. <https://doi.org/10.1016/j.applthermaleng.2017.08.161>.
- [100] Raj CR, Suresh S, Bhavsar RR, Singh VK. Recent developments in thermo-physical property enhancement and applications of solid solid phase change materials. *J Therm Anal Calorim* 2020; 139:3023–49. <https://doi.org/10.1007/s10973-019-08703-w>.
- [101] Bayon A, Liu M, Sergeev D, Grigore M, Bruno F, Müller M. Novel solid–solid phase-change cascade systems for high-temperature thermal energy storage. *Solar Energy* 2019; 177:274–83. <https://doi.org/10.1016/j.solener.2018.10.085>.
- [102] Liu G, Li S, Song C, Liu Z, Du J, Xie X, et al. High-entropy Ti-Zr-Hf-Ni-Cu alloys as solid-solid phase change materials for high-temperature thermal energy storage. *Intermetallics (Barking)* 2024; 166:108177. <https://doi.org/10.1016/j.intermet.2023.108177>.
- [103] Xiao C, Li S, Zhu S, Zhang G, Yang X. Series of solid-solid phase change materials with ultra-high thermal stability and controllable phase change temperature: kilogram-leveled preparation and application investigation. *J Energy Storage* 2021; 36:102405. <https://doi.org/10.1016/j.est.2021.102405>.
- [104] Nishioka K, Suura N, Ohno K, Maeda T, Shimizu M. Development of Fe Base Phase Change Materials for High Temperature Using Solid–Solid Transformation. *ISIJ International* 2010; 50:1240–4. <https://doi.org/10.2355/isijinternational.50.1240>.
- [105] Li S, He L, Lu H, Hao J, Wang D, Shen F, et al. Ultrahigh-performance solid-solid phase change material for efficient, high-temperature thermal energy

- storage. *Acta Mater* 2023; 249:118852.
<https://doi.org/10.1016/j.actamat.2023.118852>.
- [106] Carmona M, Rincón A, Gulfo L. Energy and exergy model with parametric study of a hot water storage tank with PCM for domestic applications and experimental validation for multiple operational scenarios. *Energy Convers Manag* 2020; 222:113189. <https://doi.org/10.1016/j.enconman.2020.113189>.
- [107] Mahfuz MH, Anisur MR, Kibria MA, Saidur R, Metselaar IHSC. Performance investigation of thermal energy storage system with Phase Change Material (PCM) for solar water heating application. *International Communications in Heat and Mass Transfer* 2014; 57:132–9.
<https://doi.org/10.1016/j.icheatmasstransfer.2014.07.022>.
- [108] Reddy RM, Nallusamy N, Reddy KH. Experimental Studies on Phase Change Material-Based Thermal Energy Storage System for Solar Water Heating Applications. *Journal of Fundamentals of Renewable Energy and Applications* 2012; 2:1–6. <https://doi.org/10.4303/jfrea/R120314>.
- [109] Gasia J, Diriken J, Bourke M, Van Bael J, Cabeza LF. Comparative study of the thermal performance of four different shell-and-tube heat exchangers used as latent heat thermal energy storage systems. *Renew Energy* 2017; 114:934–44. <https://doi.org/10.1016/j.renene.2017.07.114>.
- [110] Juaifer HJA, AbdulAmeer SA, Mahdi JA. Exploration of a plate heat exchanger utilising a phase change material: an experimental and computational study. *IOP Conf Ser Mater Sci Eng* 2021; 1067:012104.
<https://doi.org/10.1088/1757-899X/1067/1/012104>.
- [111] Kuta M, Matuszewska D, Wójcik TM. Designs of PCM based heat exchangers constructions for thermal energy storage tanks – examples and case study for selected design. *E3S Web of Conferences* 2018; 70:01010.
<https://doi.org/10.1051/e3sconf/20187001010>.
- [112] Kabbara M, Groulx D, Joseph A. A parametric experimental investigation of the heat transfer in a coil-in-tank latent heat energy storage system. *International Journal of Thermal Sciences* 2018; 130:395–405.
<https://doi.org/10.1016/j.ijthermalsci.2018.05.006>.

- [113] Tripathi S, Tomar A. CFD Analysis and Melting Performance of PCMs in two-dimensional sphere. *International Research Journal of Engineering and Technology* 2017.
- [114] Wilson John MR, Mamidi T, Subendran S, Ganapathy Subramanian LR. Experimental investigation of low-temperature latent heat thermal energy storage system using PCM and NEPCM. *IOP Conf Ser Mater Sci Eng* 2018; 402:012197. <https://doi.org/10.1088/1757-899X/402/1/012197>.
- [115] Pagkalos C, Dogkas G, Koukou MK, Konstantaras J, Lymperis K, Vrachopoulos MGr. Evaluation of water and paraffin PCM as storage media for use in thermal energy storage applications: A numerical approach. *International Journal of Thermofluids* 2020;1–2:100006. <https://doi.org/10.1016/j.ijft.2019.100006>.
- [116] Mozafari M, Lee A, Cheng S. Simulation Study of Solidification in the Shell-And-Tube Energy Storage System with a Novel Dual-PCM Configuration. *Energies (Basel)* 2022; 15:832. <https://doi.org/10.3390/en15030832>.
- [117] Tayssir M, Eldemerdash SM, Sakr RY, Elshamy AR, Abdellatif OE. Experimental investigation of melting behavior of PCM by using coil heat source inside cylindrical container. *Journal of Electrical Systems and Information Technology* 2017; 4:18–33. <https://doi.org/10.1016/j.jesit.2016.10.008>.
- [118] Baek S, Kim S. Analysis of Thermal Performance and Energy Saving Potential by PCM Radiant Floor Heating System based on Wet Construction Method and Hot Water. *Energies (Basel)* 2019; 12:828. <https://doi.org/10.3390/en12050828>.
- [119] Flores JFC, Espagnet AR, Chiu JNW, Martin V, Lacarrière B. Techno-economic assessment of active latent heat thermal energy storage systems with low-temperature district heating. *International Journal of Sustainable Energy Planning and Management* 2017; 13:5–18. <https://doi.org/10.5278/ijsepm.2017.13.2>.
- [120] Chauhan V. Simulation of Melting Process of a Phase Change Material (PCM) using ANSYS (Fluent). 2017.
- [121] Seddegh S, Wang X, Henderson AD. A comparative study of thermal behaviour of a horizontal and vertical shell-and-tube energy storage using phase

- change materials. *Appl Therm Eng* 2016; 93:348–58.
<https://doi.org/10.1016/j.applthermaleng.2015.09.107>.
- [122] Zhang S, Feng D, Shi L, Wang L, Jin Y, Tian L, et al. A review of phase change heat transfer in shape-stabilized phase change materials (ss-PCMs) based on porous supports for thermal energy storage. *Renewable and Sustainable Energy Reviews* 2021; 135:110127.
<https://doi.org/10.1016/j.rser.2020.110127>.
- [123] Castell A, Solé C. Design of latent heat storage systems using phase change materials (PCMs). *Advances in Thermal Energy Storage Systems*, Elsevier; 2015, p. 285–305. <https://doi.org/10.1533/9781782420965.2.285>.
- [124] Muhammad MD. Development of a cascaded latent heat storage system for parabolic trough solar thermal power generation. Cranfield University, 2014.
- [125] PCM Product Ltd n.d. <https://www.pcmproducts.net/> (accessed October 3, 2023).
- [126] Phase Change Materials - Microtek Labs. n.d.
- [127] Cristopia: Thermal energy storage solution - Thermofin n.d.
<https://thermofin.net/products/cristopia-thermal-energy-storage/> (accessed October 2, 2023).
- [128] RU Entropy - China 1st Authority PCM Manufacturer n.d.
<http://www.pcmgel.com/about-ru-entropy/> (accessed October 2, 2023).
- [129] Rubitherm GmbH n.d. <https://www.rubitherm.eu/> (accessed October 2, 2023).
- [130] Products – BioPCM® – Phase Change Solutions n.d.
<https://phasechange.com/products-biopcm/> (accessed October 2, 2023).
- [131] Phase Change Material Products Manufacturers - Green House Electronic AC n.d. <https://www.pcmenergy.com/products/general.htm> (accessed October 2, 2023).
- [132] Global Authority on Phase Change Material® - PureTemp n.d.
<https://puretemp.com/> (accessed October 2, 2023).
- [133] Axiotherm PCM - products | Axiotherm GmbH - Innovative thermal storage systems n.d. <https://www.axiotherm.de/en/produkte/axiotherm-pcm/> (accessed October 2, 2023).

- [134] Kalapala L, Devanuri JK. Influence of operational and design parameters on the performance of a PCM based heat exchanger for thermal energy storage – A review. *J Energy Storage* 2018; 20:497–519.
<https://doi.org/10.1016/j.est.2018.10.024>.
- [135] Medrano M, Yilmaz MO, Nogués M, Martorell I, Roca J, Cabeza LF. Experimental evaluation of commercial heat exchangers for use as PCM thermal storage systems. *Appl Energy* 2009; 86:2047–55.
<https://doi.org/10.1016/j.apenergy.2009.01.014>.
- [136] Pakalka S, Valančius K, Streckienė G. Experimental comparison of the operation of PCM-based copper heat exchangers with different configurations. *Appl Therm Eng* 2020; 172:115138.
<https://doi.org/10.1016/j.applthermaleng.2020.115138>.
- [137] Ibrahim Albanna Noorah Khaled Altamimi Reem Ahemed Abuhamra M. Design of Heat Exchanger for Thermal Energy Storage Using High Temperature Phase Change Material. n.d.
- [138] Ahmadi R, Hosseini MJ, Ranjbar AA, Bahrampoury R. Phase change in spiral coil heat storage systems. *Sustain Cities Soc* 2018; 38:145–57.
<https://doi.org/10.1016/j.scs.2017.12.026>.
- [139] Nurhan Adil Ozturk. Institute of Natural and Applied Sciences PhD Thesis. Investigation of Flow Characteristics in Heat Exchangers of Various Geometries Department of Mechanical Engineering Adana. 2006.
- [140] Al-Abidi AA, Bin Mat S, Sopian K, Sulaiman MY, Lim CH, Th A. Review of thermal energy storage for air conditioning systems. *Renewable and Sustainable Energy Reviews* 2012; 16:5802–19.
<https://doi.org/10.1016/j.rser.2012.05.030>.
- [141] Prieto MM, González B, Granado E. Thermal performance of a heating system working with a PCM plate heat exchanger and comparison with a water tank. *Energy Build* 2016; 122:89–97.
<https://doi.org/10.1016/j.enbuild.2016.03.078>.
- [142] Tay NHS, Belusko M, Bruno F. Experimental investigation of tubes in a phase change thermal energy storage system. *Appl Energy* 2012; 90:288–97.
<https://doi.org/10.1016/j.apenergy.2011.05.026>.

- [143] Chow T-T, Lyu Y. Numerical analysis on the advantage of using PCM heat exchanger in liquid-flow window. *Appl Therm Eng* 2017; 125:1218–27. <https://doi.org/10.1016/j.applthermaleng.2017.07.098>.
- [144] Khan LA, Khan MM. Role of orientation of fins in performance enhancement of a latent thermal energy storage unit. *Appl Therm Eng* 2020; 175:115408. <https://doi.org/10.1016/j.applthermaleng.2020.115408>.
- [145] Hirmiz R, Teamah HM, Lightstone MF, Cotton JS. Performance of heat pump integrated phase change material thermal storage for electric load shifting in building demand side management. *Energy Build* 2019; 190:103–18. <https://doi.org/10.1016/j.enbuild.2019.02.026>.
- [146] Sorknæs P. Simulation method for a pit seasonal thermal energy storage system with a heat pump in a district heating system. *Energy* 2018; 152:533–8. <https://doi.org/10.1016/j.energy.2018.03.152>.
- [147] Todorov O, Alanne K, Virtanen M, Kosonen R. A method and analysis of aquifer thermal energy storage (ATES) system for district heating and cooling: A case study in Finland. *Sustain Cities Soc* 2020; 53:101977. <https://doi.org/10.1016/j.scs.2019.101977>.
- [148] Siddiqui S, Macadam J, Barrett M. The operation of district heating with heat pumps and thermal energy storage in a zero-emission scenario. *Energy Reports* 2021; 7:176–83. <https://doi.org/10.1016/j.egy.2021.08.157>.
- [149] Arteconi A, Ciarrocchi E, Pan Q, Carducci F, Comodi G, Polonara F, et al. Thermal energy storage coupled with PV panels for demand side management of industrial building cooling loads. *Appl Energy* 2017; 185:1984–93. <https://doi.org/10.1016/j.apenergy.2016.01.025>.
- [150] Stampfli JA, Atkins MJ, Olsen D, Wellig B, Walmsley TG, Varbanov PS, et al. Sustainable Process Integration Laboratory (SPIL) View project Total Site Heat Integration for low and high temperature industrial clusters. View project. *Chem Eng Trans* 2018;70. <https://doi.org/10.3303/CET1870151>.
- [151] Knudsen BR, Rohde D, Kauko H. Thermal energy storage sizing for industrial waste-heat utilization in district heating: A model predictive control approach. *Energy* 2021; 234:121200. <https://doi.org/10.1016/j.energy.2021.121200>.

- [152] Prendl L, Schenzel K, Hofmann R. Simultaneous integration of heat pumps and different thermal energy storages into a tightened multi-period MILP HENS superstructure formulation for industrial applications. *Comput Chem Eng* 2021; 147:107237. <https://doi.org/10.1016/j.compchemeng.2021.107237>.
- [153] Beck A, Hofmann R. A Novel Approach for Linearization of a MINLP Stage-Wise Superstructure Formulation. *Comput Chem Eng* 2018; 112:17–26. <https://doi.org/10.1016/j.compchemeng.2018.01.010>.
- [154] Le K, Huang M, Shah N, MacArtain P, Byrne R, Hewitt N. High Temperature Air Source Heat Pump Coupled with Thermal Energy Storage: An Analysis of Demand-Side Management Designed for Flattening the Grid Demand 2018.
- [155] Le KX, Huang MJ, Shah N, Wilson C, Artain P Mac, Byrne R, et al. High Temperature Air Source Heat Pump Coupled with Thermal Energy Storage: Comparative Performances and Retrofit Analysis. *Energy Procedia* 2019; 158:3878–85. <https://doi.org/10.1016/j.egypro.2019.01.857>.
- [156] Lin Y, Fan Y, Yu M, Jiang L, Zhang X. Performance investigation on an air source heat pump system with latent heat thermal energy storage. *Energy* 2022; 239:121898. <https://doi.org/10.1016/j.energy.2021.121898>.
- [157] Yu M, Li S, Zhang X, Zhao Y. Techno-economic analysis of air source heat pump combined with latent thermal energy storage applied for space heating in China. *Appl Therm Eng* 2021; 185:116434. <https://doi.org/10.1016/j.applthermaleng.2020.116434>.
- [158] Csoknyai T, Legardeur J, Akle AA, Horváth M. Analysis of energy consumption profiles in residential buildings and impact assessment of a serious game on occupants' behavior. *Energy Build* 2019; 196:1–20. <https://doi.org/10.1016/j.enbuild.2019.05.009>.
- [159] Swan LG, Ugursal VI. Modeling of end-use energy consumption in the residential sector: A review of modeling techniques. *Renewable and Sustainable Energy Reviews* 2009; 13:1819–35. <https://doi.org/10.1016/j.rser.2008.09.033>.
- [160] Fumo N. A review on the basics of building energy estimation. *Renewable and Sustainable Energy Reviews* 2014; 31:53–60. <https://doi.org/10.1016/j.rser.2013.11.040>.

- [161] Ferrari S, Zagarella F, Caputo P, D'Amico A. Results of a literature review on methods for estimating buildings energy demand at district level. *Energy* 2019; 175:1130–7. <https://doi.org/10.1016/j.energy.2019.03.172>.
- [162] Wang H, Mancarella P. Towards sustainable urban energy systems: High resolution modelling of electricity and heat demand profiles. 2016 IEEE International Conference on Power System Technology, IEEE; 2016, p. 1–6. <https://doi.org/10.1109/POWERCON.2016.7754005>.
- [163] Yao R, Steemers K. A method of formulating energy load profile for domestic buildings in the UK. *Energy Build* 2005; 37:663–71. <https://doi.org/10.1016/j.enbuild.2004.09.007>.
- [164] Watson SD, Lomas KJ, Buswell RA. How will heat pumps alter national half-hourly heat demands? Empirical modelling based on GB field trials. *Energy Build* 2021; 238:110777. <https://doi.org/10.1016/j.enbuild.2021.110777>.
- [165] De Rosa M, Bianco V, Scarpa F, Tagliafico LA. Heating and cooling building energy demand evaluation; a simplified model and a modified degree days approach. *Appl Energy* 2014; 128:217–29. <https://doi.org/10.1016/j.apenergy.2014.04.067>.
- [166] Bünning F, Heer P, Smith RS, Lygeros J. Improved day ahead heating demand forecasting by online correction methods. *Energy Build* 2020; 211:109821. <https://doi.org/10.1016/j.enbuild.2020.109821>.
- [167] Allison J, Cowie A, Galloway S, Hand J, Kelly NJ, Stephen B. Simulation, implementation and monitoring of heat pump load shifting using a predictive controller. *Energy Convers Manag* 2017; 150:890–903. <https://doi.org/10.1016/j.enconman.2017.04.093>.
- [168] Heiple S, Sailor DJ. Using building energy simulation and geospatial modeling techniques to determine high resolution building sector energy consumption profiles. *Energy Build*, vol. 40, 2008, p. 1426–36. <https://doi.org/10.1016/j.enbuild.2008.01.005>.
- [169] Baetens R, De Coninck R, Van Roy J, Verbruggen B, Driesen J, Helsen L, et al. Assessing electrical bottlenecks at feeder level for residential net zero-energy buildings by integrated system simulation. *Appl Energy* 2012; 96:74–83. <https://doi.org/10.1016/j.apenergy.2011.12.098>.

- [170] Gesteira LG, Uche J, de Oliveira Rodrigues LK. Residential Sector Energy Demand Estimation for a Single-family Dwelling: Dynamic Simulation and Energy Analysis. *Journal of Sustainable Development of Energy, Water and Environment Systems* 2021;9:1–18.
<https://doi.org/10.13044/j.sdewes.d8.0358>.
- [171] Neu O, Oxizidis S, Flynn D, Finn D. Utilising Time of Use Surveys to Predict Domestic Hot Water Consumption and Heat Demand Profiles of Residential Building Stocks. *British Journal of Environment and Climate Change* 2016; 6:77–89. <https://doi.org/10.9734/BJECC/2016/18188>.
- [172] Kelly N, Cowie A, Flett G. Assessing the ability of electrified domestic heating in the UK to provide unplanned, short-term responsive demand. *Energy Build* 2021; 252:111430. <https://doi.org/10.1016/j.enbuild.2021.111430>.
- [173] Yao R, Baker N, Mcevoy M. A Simplified Thermal Resistance Network Model for Building Thermal Simulation. *Canadian Conference on Building Energy Simulation, 2000, 2000*, p. 1–6.
- [174] SHCS. *Scottish House Condition Survey: 2021 Key Findings An Experimental Statistics Publication for Scotland*. 2023.
- [175] Scottish Government T. *A National Statistics publication for Scotland Scottish House Condition Survey: 2017 Key Findings*. 2018.
- [176] Saint Property Services. *What is a Detached House-Benefit of a Detached House* n.d. <https://wcdn.co/media/1000/1000/f3897fa4-12fe-43aa-8d14-50a52c0496c7.jpg> (accessed October 18, 2024).
- [177] Clarke JA, Johnstone CM, Kondratenko I, Lever M, McElroy LB, Prazeres L, et al. Using simulation to formulate domestic sector upgrading strategies for Scotland. *Energy Build* 2004; 36:759–70.
<https://doi.org/10.1016/j.enbuild.2004.01.034>.
- [178] A CJ, M JC, A SP, Executive S, Johnstone C. *Application of a Building Energy Performance System to Assess Domestic Sector Upgrading Strategies for Scotland. Proceedings of the World Renewable Energy Congress: Innovation in Europe Regional Meeting.*, 2005.

- [179] Good N, Zhang L, Navarro-Espinosa A, Mancarella P. High resolution modeling of multi-energy domestic demand profiles. *Appl Energy* 2015; 137:193–210. <https://doi.org/10.1016/j.apenergy.2014.10.028>.
- [180] Aragon V, James PAB, Gauthier S. The influence of weather on heat demand profiles in UK social housing tower blocks. *Build Environ* 2022; 219:109101. <https://doi.org/10.1016/j.buildenv.2022.109101>.
- [181] Leiria D, Johra H, Marszal-Pomianowska A, Pomianowski MZ. A methodology to estimate space heating and domestic hot water energy demand profile in residential buildings from low-resolution heat meter data. *Energy* 2023; 263:125705. <https://doi.org/10.1016/j.energy.2022.125705>.
- [182] Fell M. The Radio Teleswitch: An historical perspective on the roll-out of domestic load control. In: *Proceedings of the 9th International Conference on Energy Efficiency in Domestic Appliances and Lighting (EEDAL'17)* EU Publications: Irvine, CA, USA (2018) 2018.
- [183] Farhami N, Bozorgian A, Farhami N, Bozorgian A. Factors Affecting Selection of Tubes of Heat Exchanger. 2011.
- [184] Strachan PA, Kokogiannakis G, Macdonald IA. History and development of validation with the ESP-r simulation program. *Build Environ* 2008; 43:601–9. <https://doi.org/10.1016/j.buildenv.2006.06.025>.
- [185] Nomura T, Tsubota M, Oya T, Okinaka N, Akiyama T. Heat storage in direct-contact heat exchanger with phase change material. *Appl Therm Eng* 2013; 50:26–34. <https://doi.org/10.1016/j.applthermaleng.2012.04.062>.
- [186] Longeon M, Soupart A, Fourmigué J-F, Bruch A, Marty P. Experimental and numerical study of annular PCM storage in the presence of natural convection. *Appl Energy* 2013; 112:175–84. <https://doi.org/10.1016/j.apenergy.2013.06.007>.
- [187] Hosseini MJ, Ranjbar AA, Sedighi K, Rahimi M. A combined experimental and computational study on the melting behavior of a medium temperature phase change storage material inside shell and tube heat exchanger. *International Communications in Heat and Mass Transfer* 2012; 39:1416–24. <https://doi.org/10.1016/j.icheatmasstransfer.2012.07.028>.

- [188] Seddegh S, Joybari MM, Wang X, Haghghat F. Experimental and numerical characterization of natural convection in a vertical shell-and-tube latent thermal energy storage system. *Sustain Cities Soc* 2017; 35:13–24.
<https://doi.org/10.1016/j.scs.2017.07.024>.
- [189] Alam T, Bacellar D, Ling J, Aute V. Numerical Study and Validation of Melting and Solidification in PCM Embedded Heat Exchangers with Straight Tube, 2021.
- [190] Seddegh S, Wang X, Joybari MM, Haghghat F. Investigation of the effect of geometric and operating parameters on thermal behavior of vertical shell-and-tube latent heat energy storage systems. *Energy* 2017; 137:69–82.
<https://doi.org/10.1016/j.energy.2017.07.014>.
- [191] Cuerda E, Guerra-Santin O, Sendra JJ, Neila González FcoJ. Comparing the impact of presence patterns on energy demand in residential buildings using measured data and simulation models. *Build Simul* 2019; 12:985–98.
<https://doi.org/10.1007/s12273-019-0539-z>.
- [192] Yao R, Steemers K. A method of formulating energy load profile for domestic buildings in the UK. *Energy Build* 2005; 37:663–71.
<https://doi.org/10.1016/j.enbuild.2004.09.007>.
- [193] Jon William Hand. *Strategies for Deploying Virtual Representations of the Built Environment*. Glasgow, University of Strathclyde: 2018.
- [194] Allison J, Bell K, Clarke J, Cowie A, Elsayed A, Flett G, et al. Assessing domestic heat storage requirements for energy flexibility over varying time-scales. *Appl Therm Eng* 2018; 136:602–16.
<https://doi.org/10.1016/j.applthermaleng.2018.02.104>.
- [195] BRE. *The Government’s Standard Assessment Procedure for Energy Rating of Dwellings*. 2012 Edition. 2013.
- [196] Prior J, Kendon M. The UK winter of 2009/2010 compared with severe winters of the last 100 years. *Weather* 2011; 66:4–10.
<https://doi.org/10.1002/wea.735>.
- [197] CIBSE. *Design methodology for the assessment of overheating risk in homes*. Chartered Institution of Building Services Engineers; 2017.
- [198] *Technical Handbook - Domestic* 2017.

- [199] Shipworth M, Firth SK, Gentry MI, Wright AJ, Shipworth DT, Lomas KJ. Central heating thermostat settings and timing: building demographics. *Building Research & Information* 2010; 38:50–69. <https://doi.org/10.1080/09613210903263007>.
- [200] Clarke JA, Strachan PA, Pernot C. *An Approach to the Calibration of Building Energy Simulation Models*. n.d.
- [201] Energy System Research Unit (ESRU). *Overview of ESP-r capabilities A research-oriented tool for integrated energy simulation*. Glasgow: 2024.
- [202] Wang Y, Wang L, Xie N, Lin X, Chen H. Experimental study on the melting and solidification behavior of erythritol in a vertical shell-and-tube latent heat thermal storage unit. *Int J Heat Mass Transf* 2016; 99:770–81. <https://doi.org/10.1016/j.ijheatmasstransfer.2016.03.125>.
- [203] Raul AK, Bhavsar P, Saha SK. Experimental study on discharging performance of vertical multitube shell and tube latent heat thermal energy storage. *J Energy Storage* 2018; 20:279–88. <https://doi.org/10.1016/j.est.2018.09.022>.
- [204] Riahi S, Saman WY, Bruno F, Belusko M, Tay NHS. Comparative study of melting and solidification processes in different configurations of shell and tube high temperature latent heat storage system. *Solar Energy* 2017; 150:363–74. <https://doi.org/10.1016/j.solener.2017.04.061>.
- [205] Joybari MM, Seddegh S, Wang X, Haghghat F. Experimental investigation of multiple tube heat transfer enhancement in a vertical cylindrical latent heat thermal energy storage system. *Renew Energy* 2019; 140:234–44. <https://doi.org/10.1016/j.renene.2019.03.037>.
- [206] Seddegh S, Wang X, Henderson AD. Numerical investigation of heat transfer mechanism in a vertical shell and tube latent heat energy storage system. *Appl Therm Eng* 2015; 87:698–706. <https://doi.org/10.1016/j.applthermaleng.2015.05.067>.
- [207] Chen G, Sun G, Jiang D, Su Y. Experimental and numerical investigation of the latent heat thermal storage unit with PCM packing at the inner side of a tube. *Int J Heat Mass Transf* 2020; 152:119480. <https://doi.org/10.1016/j.ijheatmasstransfer.2020.119480>.

- [208] Pal E, Kumar I, Joshi JB, Maheshwari NK. CFD simulations of shell-side flow in a shell-and-tube type heat exchanger with and without baffles. *Chem Eng Sci* 2016; 143:314–40. <https://doi.org/10.1016/j.ces.2016.01.011>.
- [209] Hussain IY, Jabbar NA. *Natural Convection Heat Transfer in Cylindrical Enclosure of Porous Media with Periodic Boundary Conditions*. vol. 65. 2013.
- [210] Kirincic M, Trp A, Lenic K. Influence of natural convection during melting and solidification of paraffin in a longitudinally finned shell-and-tube latent thermal energy storage on the applicability of developed numerical models. *Renew Energy* 2021; 179:1329–44. <https://doi.org/10.1016/j.renene.2021.07.083>.
- [211] Han G-S, Ding H-S, Huang Y, Tong L-G, Ding Y-L. A comparative study on the performances of different shell-and-tube type latent heat thermal energy storage units including the effects of natural convection. *International Communications in Heat and Mass Transfer* 2017; 88:228–35. <https://doi.org/10.1016/j.icheatmasstransfer.2017.09.009>.
- [212] Sari A, Kaygusuz K. Thermal performance of palmitic acid as a phase change energy storage material. *Energy Convers Manag* 2002; 43:863–76. [https://doi.org/10.1016/S0196-8904\(01\)00071-1](https://doi.org/10.1016/S0196-8904(01)00071-1).
- [213] Dhaidan NS, Khodadadi JM. Melting and convection of phase change materials in different shape containers: A review. *Renewable and Sustainable Energy Reviews* 2015; 43:449–77. <https://doi.org/10.1016/j.rser.2014.11.017>.
- [214] Ziskind G. Modelling of heat transfer in phase change materials (PCMs) for thermal energy storage systems. *Advances in Thermal Energy Storage Systems*, Elsevier; 2015, p. 307–24. <https://doi.org/10.1533/9781782420965.2.307>.
- [215] Tian Y, Zhao CY. A numerical investigation of heat transfer in phase change materials (PCMs) embedded in porous metals. *Energy* 2011; 36:5539–46. <https://doi.org/10.1016/j.energy.2011.07.019>.
- [216] Yang L, Jin X, Zhang Y, Du K. Recent development on heat transfer and various applications of phase-change materials. *J Clean Prod* 2021; 287:124432. <https://doi.org/10.1016/j.jclepro.2020.124432>.

- [217] Memon A, Mishra G, Gupta AK. Buoyancy-driven melting and heat transfer around a horizontal cylinder in square enclosure filled with phase change material. *Appl Therm Eng* 2020; 181:115990.
<https://doi.org/10.1016/j.applthermaleng.2020.115990>.
- [218] Gupta SC. *The Classical Stefan Problem: Basic Concepts, Modelling and Analysis with quasi-analytical solutions and methods* (Vol. 45). Elsevier. 2018.
- [219] Sadoun N, Si-Ahmed E-K, Colinet P, Legrand J. On the boundary immobilization and variable space grid methods for transient heat conduction problems with phase change: Discussion and refinement. *Comptes Rendus Mécanique* 2012; 340:501–11. <https://doi.org/10.1016/j.crme.2012.03.003>.
- [220] Hu H, Argyropoulos SA. Mathematical modelling of solidification and melting: a review. *Model Simul Mat Sci Eng* 1996; 4:371–96.
<https://doi.org/10.1088/0965-0393/4/4/004>.
- [221] Sultana KR, Dehghani SR, Pope K, Muzychka YS. Numerical techniques for solving solidification and melting phase change problems. *Numerical Heat Transfer, Part B: Fundamentals* 2018;73:129–45.
<https://doi.org/10.1080/10407790.2017.1422629>.
- [222] Nazi Ehms JH, De Césaró Oliveski R, Oliveira Rocha LA, Biserni C, Garai M. Fixed Grid Numerical Models for Solidification and Melting of Phase Change Materials (PCMs). *Applied Sciences* 2019; 9:4334.
<https://doi.org/10.3390/app9204334>.
- [223] Voller VR, Swaminathan CR, Thomas BG. Fixed grid techniques for phase change problems: A review. *Int J Numer Methods Eng* 1990; 30:875–98.
<https://doi.org/10.1002/nme.1620300419>.
- [224] Ma Z, Zhang Y. Solid velocity correction schemes for a temperature transforming model for convection phase change. *Int J Numer Methods Heat Fluid Flow* 2006; 16:204–25. <https://doi.org/10.1108/09615530610644271>.
- [225] Reichl C, Both S, Mascherbauer P, Emhofer J. Comparison of Two CFD Approaches Using Constant and Temperature Dependent Heat Capacities during the Phase Transition in PCMs with Experimental and Analytical Results. *Processes* 2022; 10:302. <https://doi.org/10.3390/pr10020302>.

- [226] Iten M, Liu S, Shukla A. Experimental validation of an air-PCM storage unit comparing the effective heat capacity and enthalpy methods through CFD simulations. *Energy* 2018; 155:495–503.
<https://doi.org/10.1016/j.energy.2018.04.128>.
- [227] Kousha N, Hosseini MJ, Aligoodarz MR, Pakrouh R, Bahrampoury R. Effect of inclination angle on the performance of a shell and tube heat storage unit – An experimental study. *Appl Therm Eng* 2017; 112:1497–509.
<https://doi.org/10.1016/j.applthermaleng.2016.10.203>.
- [228] Voller VR, Prakash C. A fixed grid numerical modelling methodology for convection-diffusion mushy region phase-change problems. *Int J Heat Mass Transf* 1987; 30:1709–19. [https://doi.org/10.1016/0017-9310\(87\)90317-6](https://doi.org/10.1016/0017-9310(87)90317-6).
- [229] Zeneli M, Nikolopoulos A, Karellas S, Nikolopoulos N. Numerical methods for solid-liquid phase-change problems. *Ultra-High Temperature Thermal Energy Storage, Transfer and Conversion*, Elsevier; 2021, p. 165–99.
<https://doi.org/10.1016/B978-0-12-819955-8.00007-7>.
- [230] Parsa N, Kamkari B, Abolghasemi H. Enhancing thermal performance in shell-and-tube latent heat thermal energy storage units: An experimental and numerical study of shell geometry effects. *International Communications in Heat and Mass Transfer* 2024; 154:107398.
<https://doi.org/10.1016/j.icheatmasstransfer.2024.107398>.
- [231] Fang Y, Niu J, Deng S. Numerical analysis for maximizing effective energy storage capacity of thermal energy storage systems by enhancing heat transfer in PCM. *Energy Build* 2018; 160:10–8.
<https://doi.org/10.1016/j.enbuild.2017.12.006>.
- [232] Morisson V, Rady M, Palomo E, Arquis E. Thermal energy storage systems for electricity production using solar energy direct steam generation technology. *Chemical Engineering and Processing: Process Intensification* 2008; 47:499–507. <https://doi.org/10.1016/j.cep.2007.01.025>.
- [233] Carroll WL, BBE, DD, KR, AB, EJ and WF. *Thermal Energy Storage System Sizing*. Berkeley, USA: 1989.
- [234] Huang C, Wei W, Sun Y, Wang W, Li Z, Wang S, et al. Energy saving and peak load shifting performance of tail water source heat pump integrated with

- large-scale thermal storage pool space heating system in technology park. *Energy Convers Manag* 2023; 287:117032.
<https://doi.org/10.1016/j.enconman.2023.117032>.
- [235] OMNIE Ltd. Heat pump pipe sizing. 2023.
- [236] Marek Miara. Fraunhofer ISE: Are heat pumps able to deliver sufficiently high temperatures in the heating circuit? Episode 2 of Heat Pumps in Existing Buildings: Why the Maximum Required Temperature Is Not the Decisive Factor 2021.
- [237] Screwfix Direct Ltd. LG Therma V R32 S Series 7kW Air-Source Heat Pump Kit 225Ltr n.d. <https://www.screwfix.com/p/lg-therma-v-r32-s-series-7kw-air-source-heat-pump-kit-225ltr/323kh> (accessed September 11, 2024).
- [238] Bastida H, De la Cruz-Loredo I, Ugalde-Loo CE. Effective estimation of the state-of-charge of latent heat thermal energy storage for heating and cooling systems using non-linear state observers. *Appl Energy* 2023; 331:120448.
<https://doi.org/10.1016/j.apenergy.2022.120448>.
- [239] Lämmle M, Bongs C, Wapler J, Günther D, Hess S, Kropp M, et al. Performance of air and ground source heat pumps retrofitted to radiator heating systems and measures to reduce space heating temperatures in existing buildings. *Energy* 2022; 242:122952. <https://doi.org/10.1016/j.energy.2021.122952>.
- [240] Lin Y, Fan Y, Yu M, Jiang L, Zhang X. Performance investigation on an air source heat pump system with latent heat thermal energy storage. *Energy* 2022; 239:121898. <https://doi.org/10.1016/j.energy.2021.121898>.
- [241] EN-442-1. Radiators and convectors. Technical specifications and requirements. CEN Brussels: 2014.
- [242] Liu Z, Xu W, Li Z, Zhang L, Li J, Li A, et al. Research on heating performance of heating radiator at low temperature. *Journal of Building Engineering* 2021; 36:102016. <https://doi.org/10.1016/j.job.2020.102016>.

Appendices

Appendix I: Analysis of the Building Simulation Model Results.

Table AI.1: Daily average ambient temperature for Aberdeen and heat demand of the detached dwelling throughout the heating season (November to March).

Days	Amb. Temp (°C)	Heat demand (kWh)	Days	Amb. Temp (°C)	Heat demand (kWh)	Days	Amb. Temp (°C)	Heat demand (kWh)
1	7.45	13.03	41	2.58	23.62	81	6.75	18.64
2	9.38	9.48	42	7.89	16.52	82	7.64	13.82
3	7.35	10.58	43	6.27	15.24	83	3.84	19.17
4	5.64	11.91	44	8.31	13.10	84	2.65	21.84
5	4.22	14.28	45	9.41	10.20	85	2.81	22.98
6	4.97	14.22	46	8.44	11.46	86	4.09	20.24
7	6.32	12.41	47	5.70	16.08	87	3.95	21.51
8	2.69	18.13	48	5.91	15.74	88	3.09	22.38
9	5.94	14.25	49	4.77	18.46	89	0.46	26.27
10	7.52	11.61	50	6.73	16.98	90	3.01	24.62
11	8.13	10.90	51	8.46	13.12	91	4.63	19.64
12	4.13	16.82	52	3.56	19.16	92	4.84	18.86
13	8.26	12.52	53	4.30	19.99	93	7.27	15.46
14	9.09	9.32	54	4.44	19.08	94	5.91	16.54
15	7.30	11.86	55	3.21	22.15	95	4.35	20.12
16	8.22	11.30	56	0.44	27.62	96	5.04	20.06
17	8.42	11.06	57	-1.93	33.34	97	7.16	16.20
18	8.92	10.69	58	-3.81	36.73	98	5.61	16.77
19	8.57	10.70	59	-3.41	36.53	99	4.13	17.85
20	7.80	12.07	60	-3.65	36.68	100	2.89	20.85
21	6.17	14.45	61	1.78	31.82	101	4.31	18.28
22	4.56	17.55	62	-1.41	31.66	102	4.90	16.39
23	4.79	18.28	63	2.94	25.91	103	5.66	14.64
24	2.61	21.24	64	3.19	24.89	104	5.03	18.03
25	1.82	22.71	65	3.64	23.34	105	6.76	13.93
26	6.06	18.25	66	3.55	23.07	106	3.49	15.08
27	6.93	15.96	67	4.24	22.37	107	0.34	22.16
28	4.83	17.48	68	2.93	23.10	108	1.74	19.27
29	2.31	21.36	69	1.16	26.19	109	1.88	20.79
30	3.85	20.93	70	5.35	21.74	110	3.08	22.46
31	8.94	14.47	71	6.32	18.90	111	3.06	23.39
32	9.46	11.43	72	5.70	18.97	112	1.89	25.24
33	11.08	7.62	73	3.97	21.34	113	3.24	22.07
34	5.61	13.73	74	4.89	20.13	114	3.20	20.33
35	6.17	15.37	75	4.30	20.15	115	2.42	20.44
36	4.07	18.92	76	2.37	23.16	116	4.20	19.30
37	2.15	23.40	77	1.27	26.02	117	4.01	20.40
38	1.96	25.35	78	1.99	26.98	118	5.23	18.22
39	2.26	25.08	79	6.29	20.14	119	6.57	13.27
40	1.00	25.79	80	2.28	23.41	120	8.45	8.59

Cont'd.			Cont'd			Cont'd		
Days	Amb. Temp. (°C)	Heat demand (kWh)	Days	Amb. Temp. (°C)	Heat demand (kWh)	Days	Amb. Temp. (°C)	Heat demand (kWh)
121	1.97	18.39	131	5.73	13.71	141	7.08	6.52
122	1.61	21.49	132	8.04	9.71	142	4.61	10.21
123	1.23	22.97	133	8.27	10.26	143	2.67	13.00
124	0.90	23.84	134	8.63	7.41	144	3.70	12.87
125	8.47	12.45	135	8.32	7.77	145	4.13	12.40
126	6.53	11.53	136	7.95	8.50	146	2.37	13.13
127	4.86	12.61	137	13.03	2.31	147	4.55	14.98
128	6.64	10.92	138	6.58	4.33	148	4.74	15.35
129	3.94	12.07	139	8.25	5.61	149	4.97	15.26
130	3.82	13.03	140	8.18	6.58			

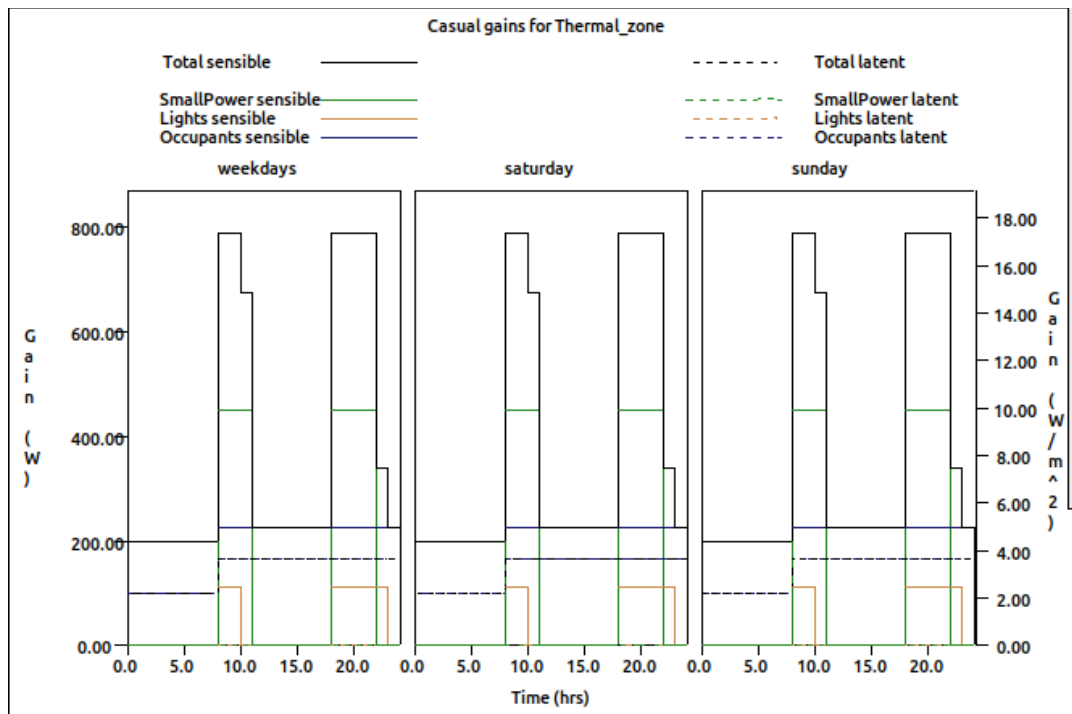


Figure AI.1: Occupant casual gain profile of the detached dwelling estimated over a 24-hour period.

Appendix II: Input Data for CFD Simulation

Appendix IIA: Input Data for CFD Model Validation

Geometric and mesh data of the CFD model

Parameter	Value	Unit	Description
Shell diameter	0.044	m	Diameter of the shell.
Tube outer diameter	0.02	m	Outer diameter of the heat exchanger tube.
Tube inner diameter	0.015	m	Inner diameter of the heat exchanger tube.
Tube length	0.4	m	Length of the heat exchanger.
PCM thickness in shell	0.024	m	Radial thickness of PCM layer.
Number of mesh elements	17,600	-	Total computational cells for the domain.
Mesh type	Rectangle	-	Type of mesh used for discretization.

Material properties of PCM and HTF

Material	Property	Value	Unit	Description
PCM	Density (ρ), solid/liquid	880/760	kg/m ³	Density of the PCM.
PCM	Specific heat (c_p), solid/liquid	1800/2400	J/(kgK)	Specific heat capacity
PCM	Thermal conductivity (k)	0.2	W/(mK)	Thermal conductivity of PCM
PCM	Kinematic viscosity (ν)	3.3×10^{-6}	m ² /s	Viscosity of PCM
PCM	Latent heat (h_m)	168,000	J/kg	Latent heat of fusion
PCM	Melting temperature	35	°C	Phase change temperature
HTF	Density (ρ)	998.2	kg/m ³	Density of water.
HTF	Specific heat (c_p)	4186	J/(kgK)	Specific heat capacity of water
HTF	Thermal conductivity (k)	0.6	W/(mK)	Thermal conductivity of water

Boundary and Operating Conditions.

Charging Simulations			
Parameter	Value	Unit	Description
HTF inlet velocity	0.01	m/s	Velocity of the heat transfer fluid.
HTF inlet temperature	52	°C	Temperature of water at the inlet.
HTF outlet pressure	1	atm	Pressure at the outlet boundary.
Reference temperature	22	°C	Initial temperature of the system.
Shell wall temperature	Heat flux	-	Convective boundary condition for the shell.
Discharging Simulations			
Parameter	Value	Unit	Description
HTF inlet velocity	0.01	m/s	Velocity of the heat transfer fluid.
HTF inlet temperature	19	°C	Temperature of water at the inlet.
HTF outlet pressure	1	atm	Pressure at the outlet boundary.
Reference temperature	48	°C	Initial temperature of the system.
Shell wall temperature	Heat flux	-	Convective boundary condition for the shell.

Solver and Simulation Settings

Parameter	Value	Unit	Description
Simulation type	Transient	-	Charging and discharging are time-dependent.
Solver type	Pressure-based	-	Solver for incompressible flow.
Melting/solidification model	Enabled	-	For phase change of PCM.
Laminar model	Re =271	-	Laminar model used for HTF flow
Gravity	9.81	m/s ²	Gravitational acceleration for buoyancy.
Time step	0.2	s	Time step size for transient simulation.
Convergence criteria	10 ⁻⁶	-	Residual threshold for continuity and energy.

Appendix IIB: Input Data for CFD Simulation of the TES System

Geometric and mesh data of the TES system

Parameter	Value	Unit	Description
Shell diameter	0.082	m	Diameter of the shell.
Tube outer diameter	0.024	m	Outer diameter of the heat exchanger tube.
Tube inner diameter	0.022	m	Inner diameter of the heat exchanger tube.
Tube length	1	m	Length of the heat exchanger.
PCM thickness in shell	0.028	m	Radial thickness of PCM layer.
Number of mesh elements	39,000	-	Total computational cells for PCM and HTF domain.
Mesh type	Rectangle	-	Type of mesh used for discretization.

Material properties of PCM and HTF

Material	Property	Value	Unit	Description
PCM	Density (ρ), solid/liquid	1600/1666	kg/m ³	Density of the PCM.
PCM	Specific heat (c_p), solid/liquid	2410/2400	J/(kgK)	Specific heat capacity
PCM	Thermal conductivity (k)	0.45	W/(mK)	Thermal conductivity of PCM
PCM	Kinematic viscosity (ν)	-	m ² /s	Viscosity of PCM
PCM	Latent heat (h_m)	210,000	J/kg	Latent heat of fusion
PCM	Melting temperature	48	°C	Phase change temperature
HTF	Density (ρ)	998.2	kg/m ³	Density of water.
HTF	Specific heat (c_p)	4186	J/(kgK)	Specific heat capacity of water
HTF	Thermal conductivity (k)	0.6	W/(mK)	Thermal conductivity of water

Boundary and Operating Conditions.

Charging Simulations			
Parameter	Value	Unit	Description
HTF inlet velocity	0.64/0.88	m/s	Velocity of the heat transfer fluid.
HTF inlet temperature	60	°C	Temperature of water at the inlet.
HTF outlet pressure	1	atm.	Pressure at the outlet boundary.
Reference temperature	25/36	°C	Initial temperature of the system.
Shell wall temperature	Heat flux	-	Convective boundary condition for the shell.
Discharging Simulations			
Parameter	Value	Unit	Description
HTF inlet velocity	Variable	m/s	Velocity of the heat transfer fluid.
HTF inlet temperature	Variable	°C	Temperature of water at the inlet.
HTF outlet pressure	1	atm.	Pressure at the outlet boundary.
Reference temperature	60	°C	Initial temperature of the system.
Shell wall temperature	Heat flux	-	Convective boundary condition for the shell.

Solver and Simulation Settings

Parameter	Value	Unit	Description
Simulation type	Transient	-	Charging and discharging are time-dependent.
Solver type	Pressure-based	-	Solver for incompressible flow.
Melting/solidification model	Enabled	-	For phase change of PCM.
Laminar/turbulent model	Variable	-	Laminar/turbulent model used for HTF flow
Gravity	9.81	m/s ²	Gravitational acceleration for buoyancy.
Time step	0.2	s	Time step size for transient simulation.
Convergence criteria	10 ⁻⁶	-	Residual threshold for continuity and energy.

Appendix III: CFD Code for Variant Inlet HTF Mass Flow Rate

The following code for the inlet HTF mass flow rate is compiled in the Fluent UDF to determine the TES system power output that meets the detached dwelling's heat demand. The code was applied in time intervals to accurately predict the power output required to match the dwelling heat demand profile.

```
#include "udf.h"

DEFINE_ON_DEMAND(WriteData)
{
int surface_thread_id= 7;
FILE* fp;
real total_area=0.0;
real total_pres_a=0.0;
real Temp = 0.0;
real area[ND_ND];

face_t face;
Thread* thread;
```

```

Domain* domain;
domain = Get_Domain(1);

thread = Lookup_Thread(domain,surface_thread_id);

begin_f_loop(face,thread)
{
F_AREA(area,face,thread);
total_area += NV_MAG(area);
total_pres_a += NV_MAG(area)*F_T(face,thread);
}
end_f_loop(face,thread)

Temp = total_pres_a/total_area;

printf("Average Temperature %f \n",Temp);
printf("Area %f \n",total_area);

fp = fopen("temperature.txt","w");
fprintf(fp,"%f",Temp);
fclose(fp);
}

DEFINE_PROFILE(VelocityUDF, thread, position)
{
int density = 998;
float A = 0.00038;
int CP = 4200;
int TIn = 310;
int Q = 25;
real M_in;
FILE *fp;
float temp;
face_t f;
real t = CURRENT_TIME;; /*Atual timestep size*/

////////////////////////////////////
fp = fopen("temperature.txt","r");
fscanf(fp, "%f", &temp); /* read one value per line */
fclose(fp); /*close file*/
////////////////////////////////////

M_in = Q / (CP * (temp - TIn));

begin_f_loop(f, thread)
{
F_PROFILE(f, thread, position) = -M_in;
}
end_f_loop(f, thread)
}

```